APPENDIX A

Pretest Analysis Results

APPENDIX A

Pretest Analysis Results

Figure A.1 – A.15	S1(H+V)
Figure A.16 – A.30	S2(H+V)

Notes

1. The test data in this appendix are provided by the Nuclear Power Engineering Corporation (NUPEC) and are based on reports to the Ministry of International Trade and Industry (MITI) of Japan. The tests were performed by NUPEC at Tadotsu Engineering Laboratory, located in Tadotsu, Japan. No modifications or changes were made to the recorded test results.

   Information about the tests was provided by NUPEC, under an agreement between the U.S. Nuclear Regulatory Commission (NRC) and MITI. The terms and conditions of the technical exchange and general cooperation agreement between the NRC and the Agency of National Resources and Energy of MITI in the field of nuclear regulatory matters and nuclear safety research are given in the agreement "Collaboration on Concrete Containment Vessels (CCV) Seismic Proving Test Program and Information Exchange between USNRC and NUPEC."

2. Damage accumulates in the finite element analyses, so any residual force, strain, or displacement from the previous analysis is the starting point for the next analysis. Figures A.16 – A.30 include residual effects from the previous analysis.

3. See Figure 2.14 for location of reporting points.

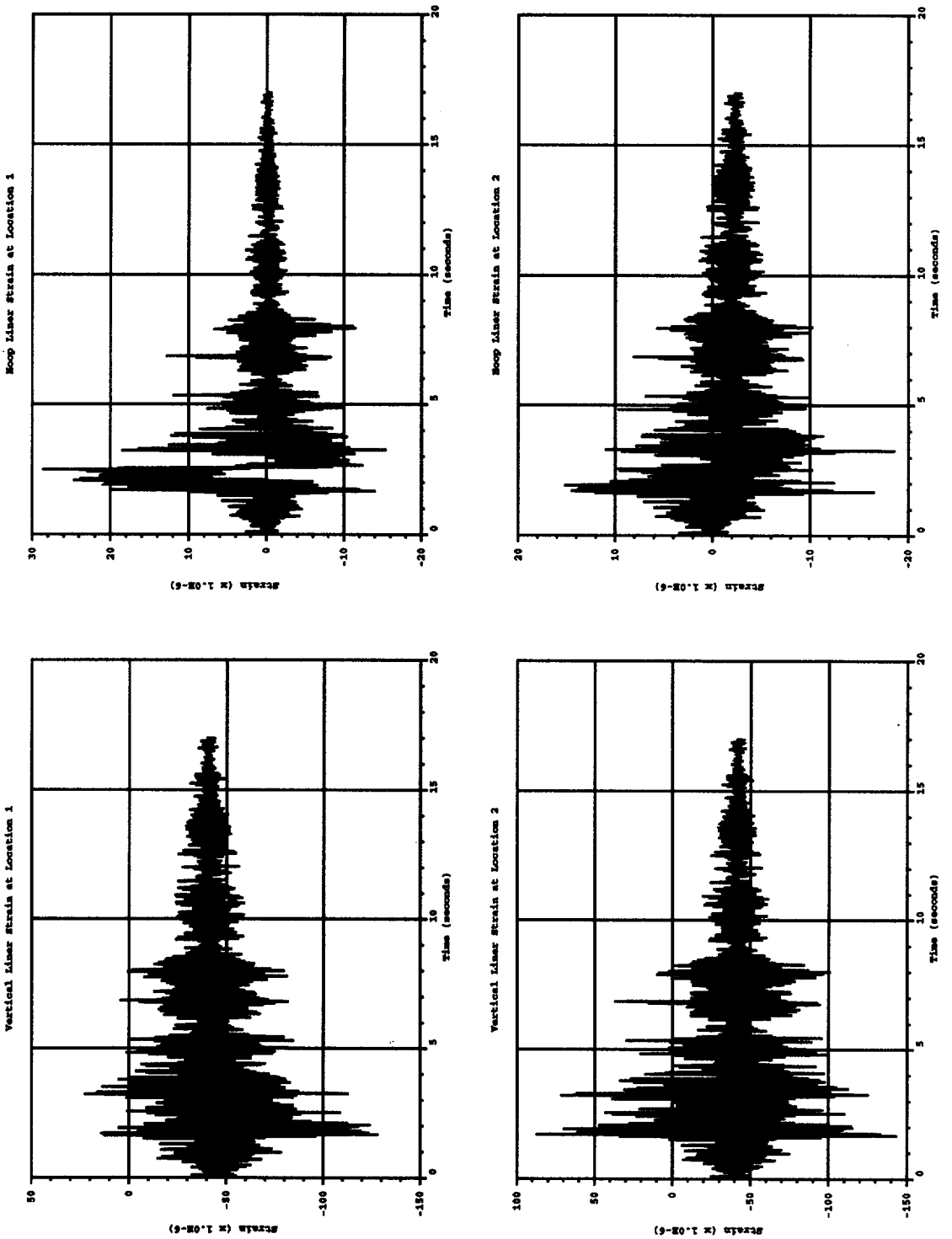

Figure A.1 Liner strains for RCCV under S1(H+V)

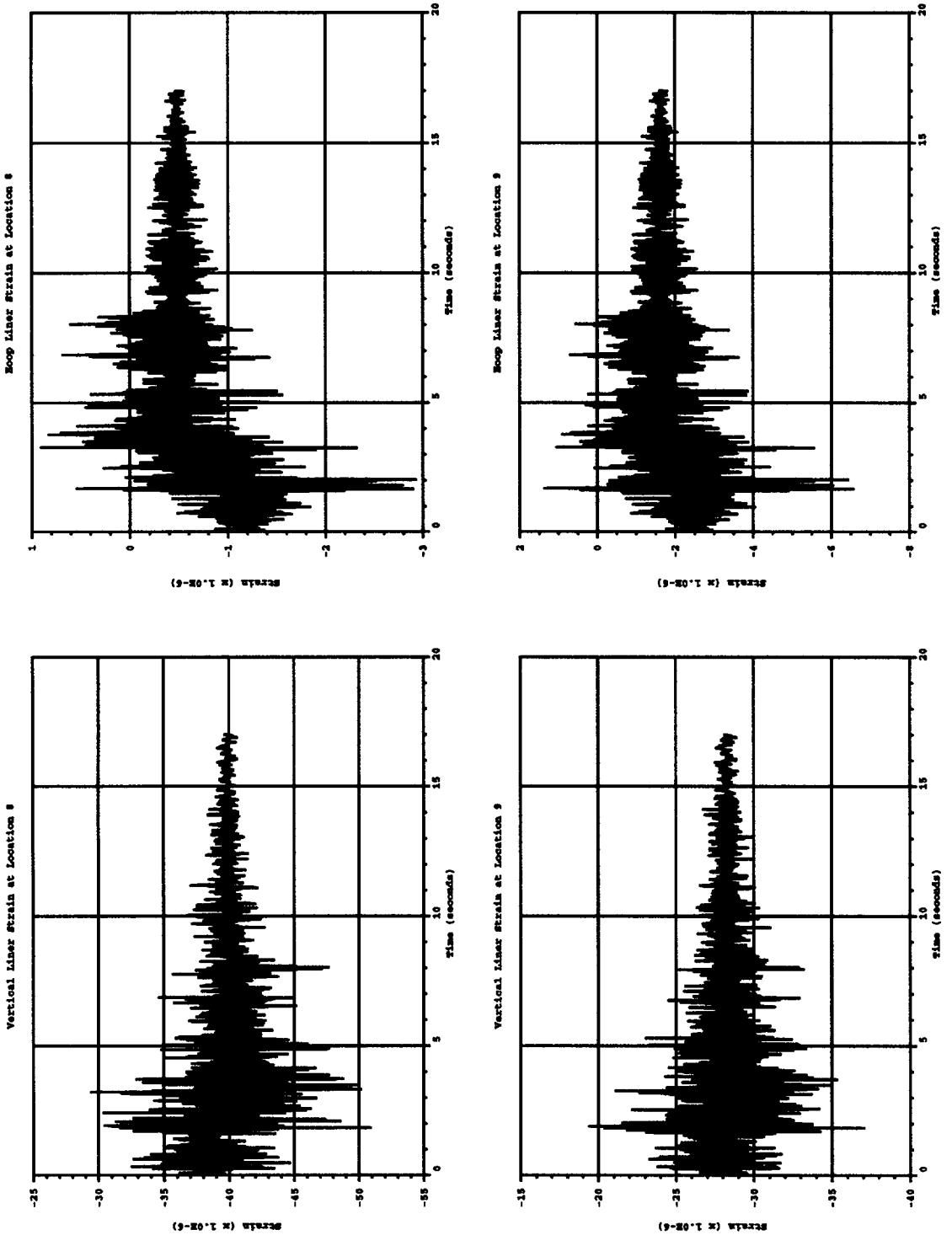

Figure A.2 Liner strains for RCCV under S1(H+V)

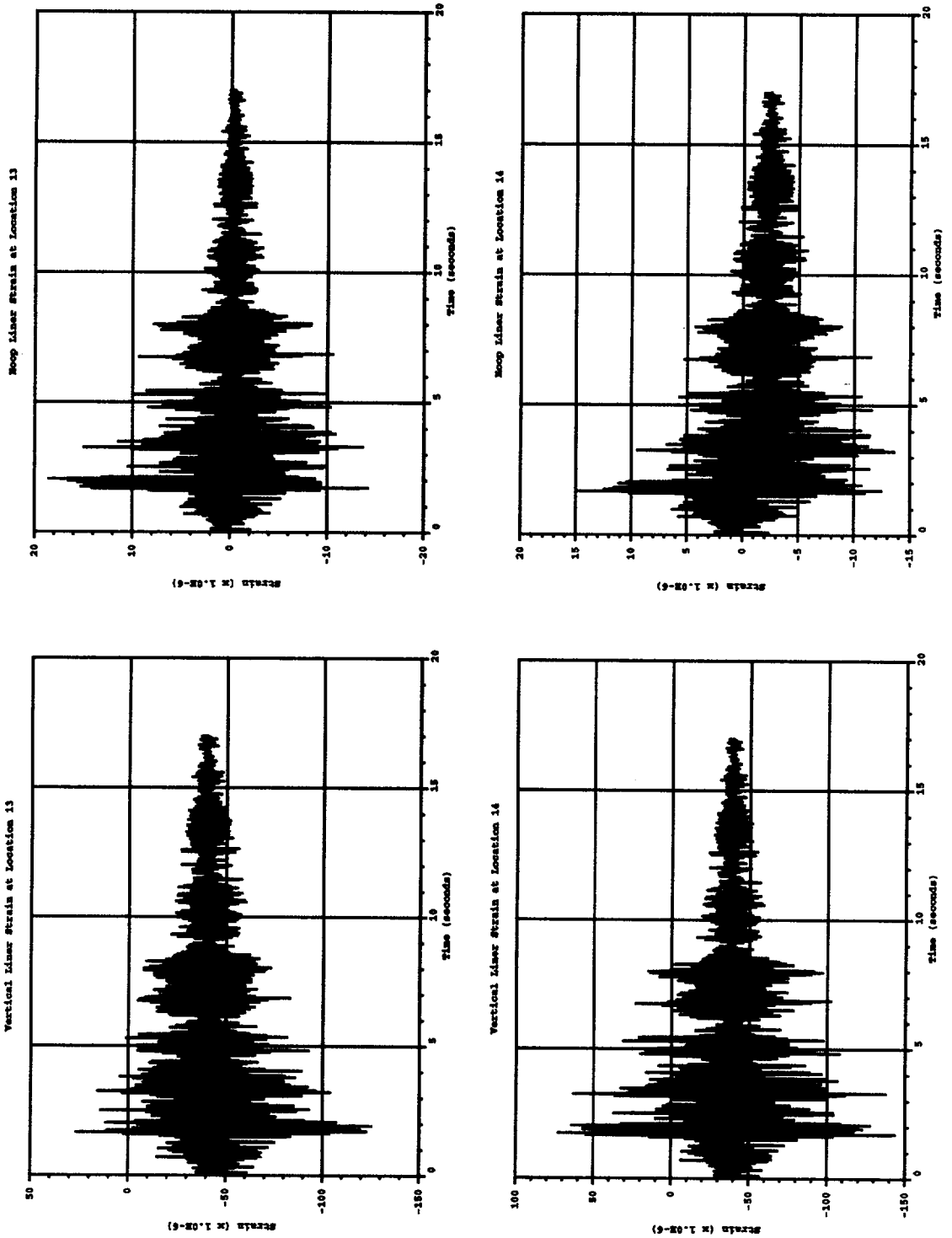

Figure A.3 Liner strains for RCCV under S1(H+V)

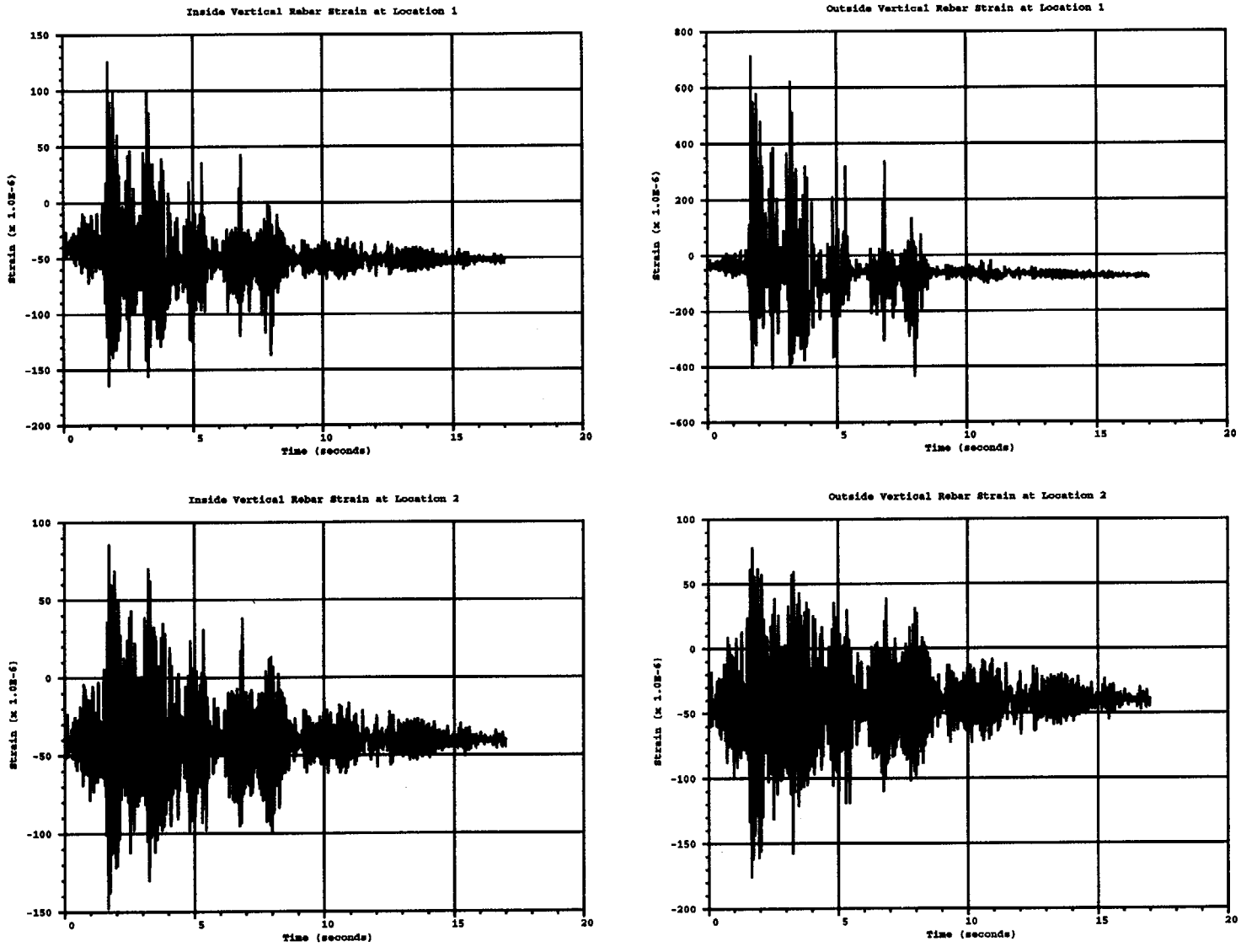

Figure A.4 Vertical rebar strains for RCCV under S1(H+V)

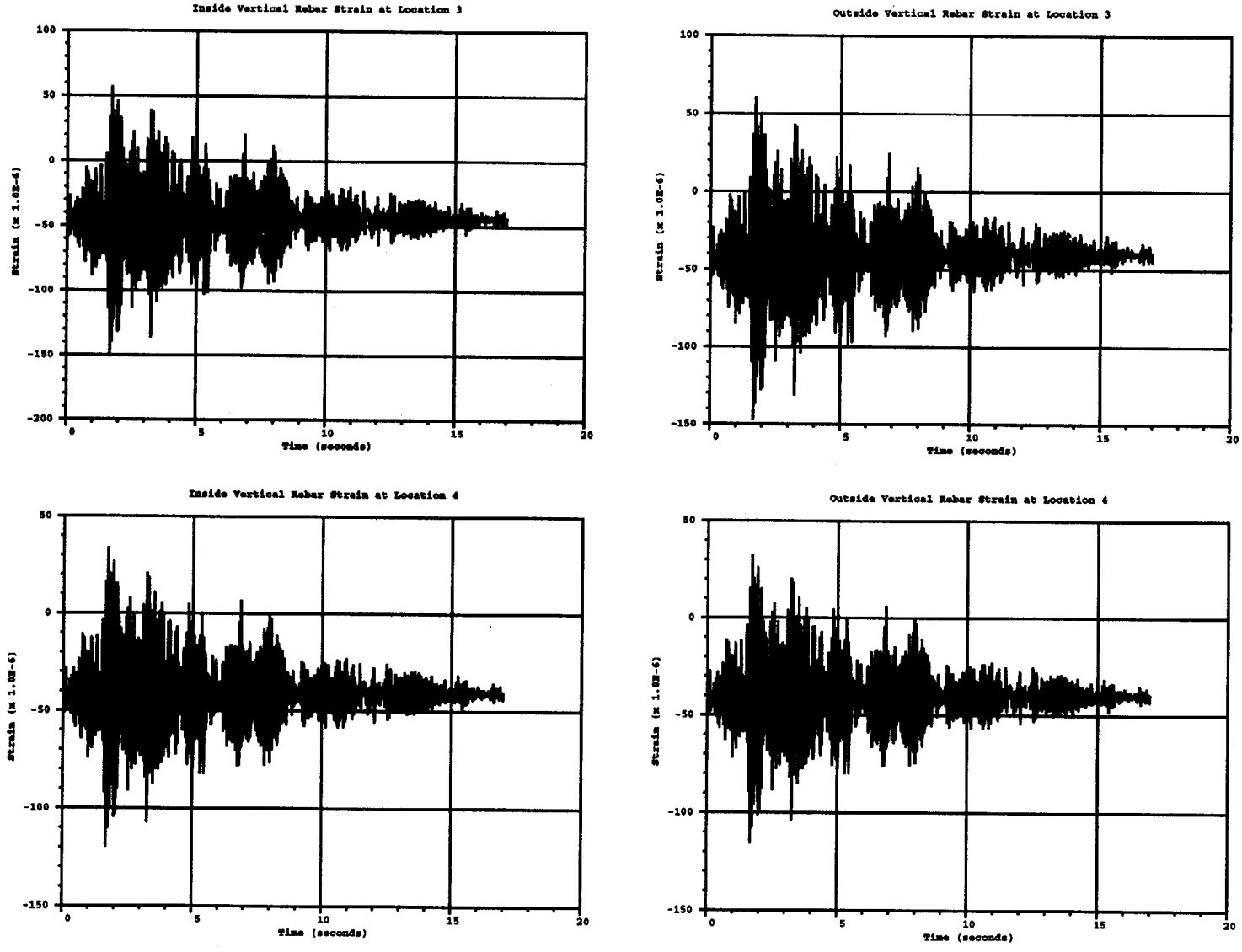

Figure A.5 Vertical rebar strains for RCCV under S1(H+V)

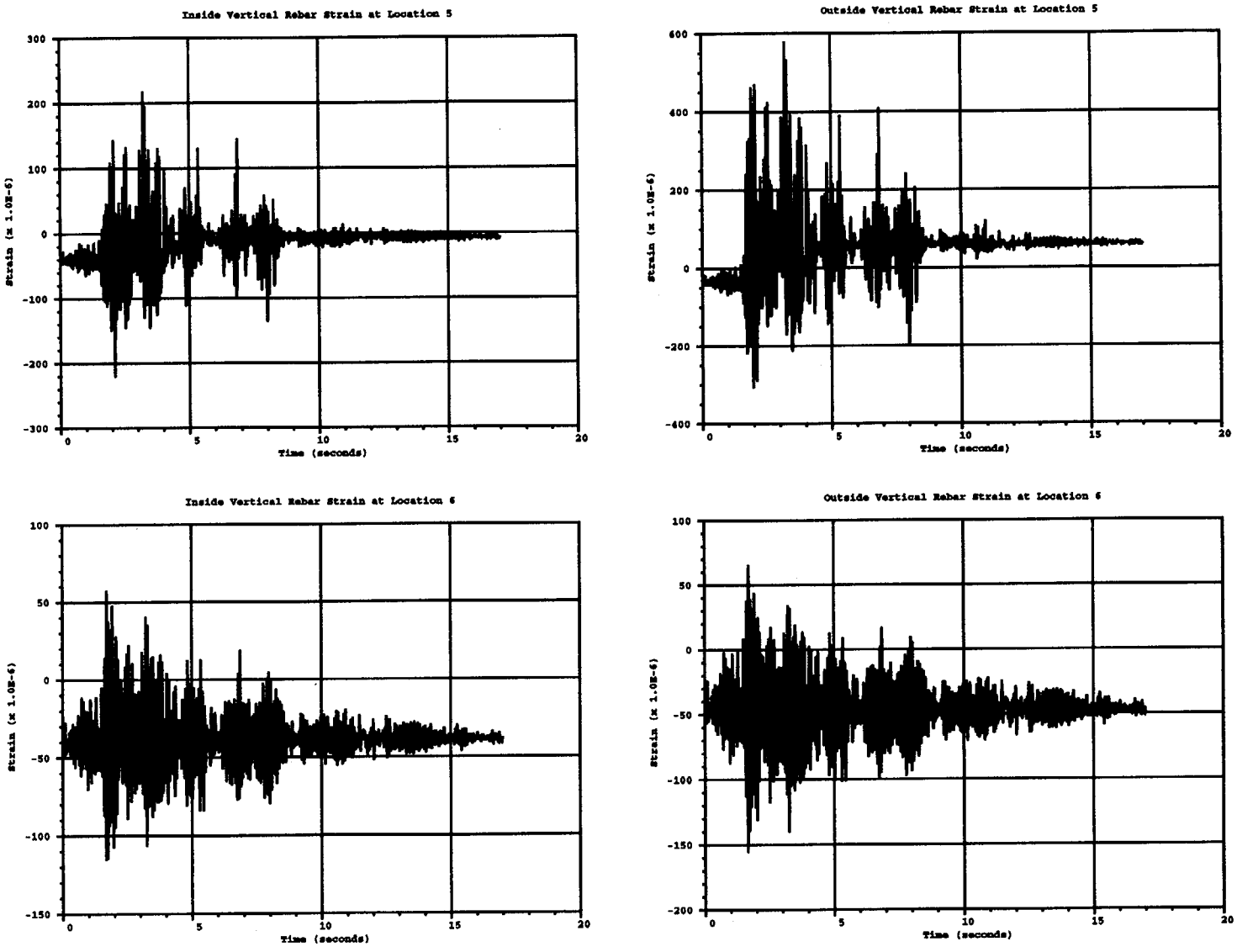

Figure A.6 Vertical rebar strains for RCCV under S1(H+V)

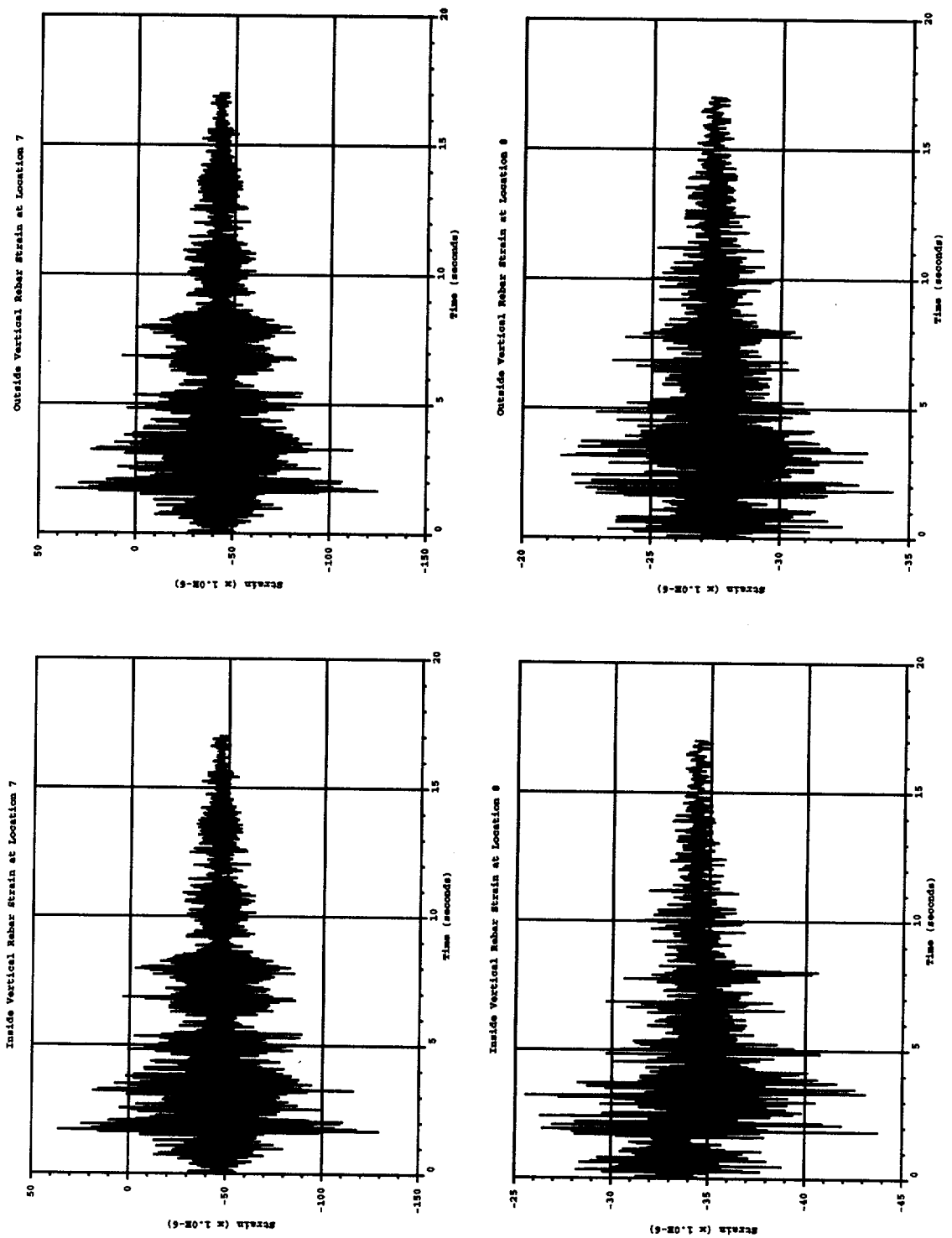

Figure A.7 Vertical rebar strains for RCCV under S1(H+V)

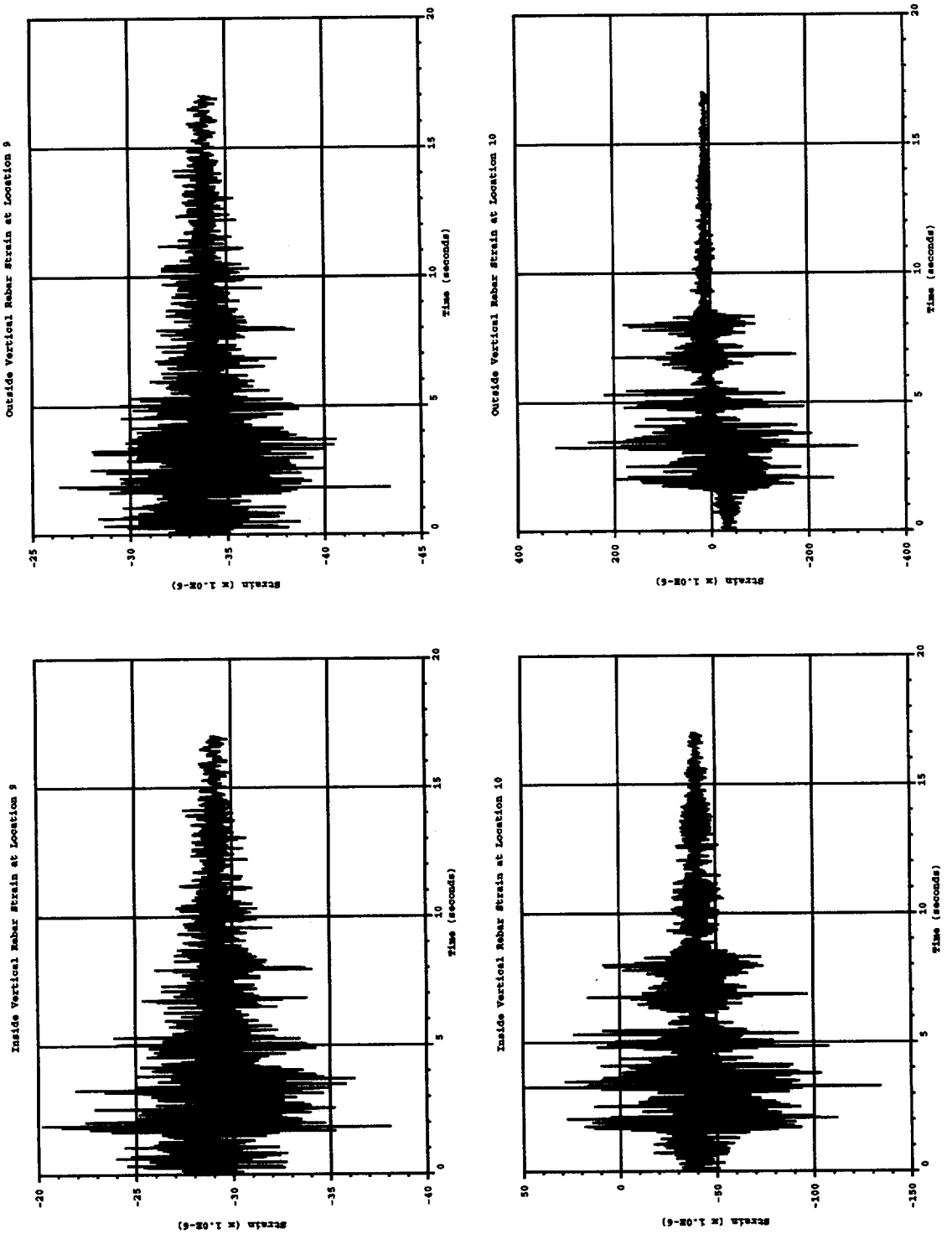

Figure A.8 Vertical rebar strains for RCCV under S1(H+V)

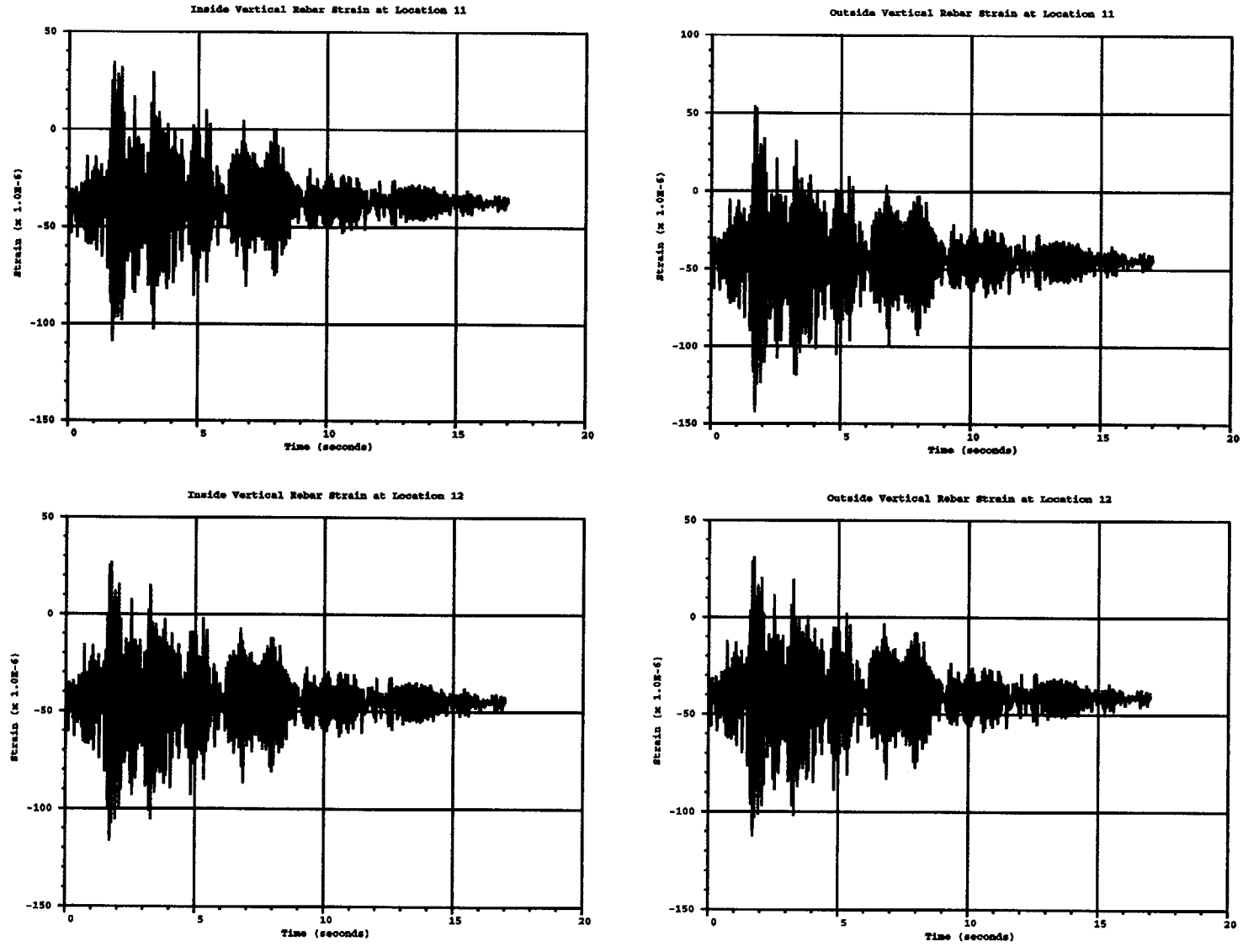

Figure A.9 Vertical rebar strains for RCCV under S1(H+V)

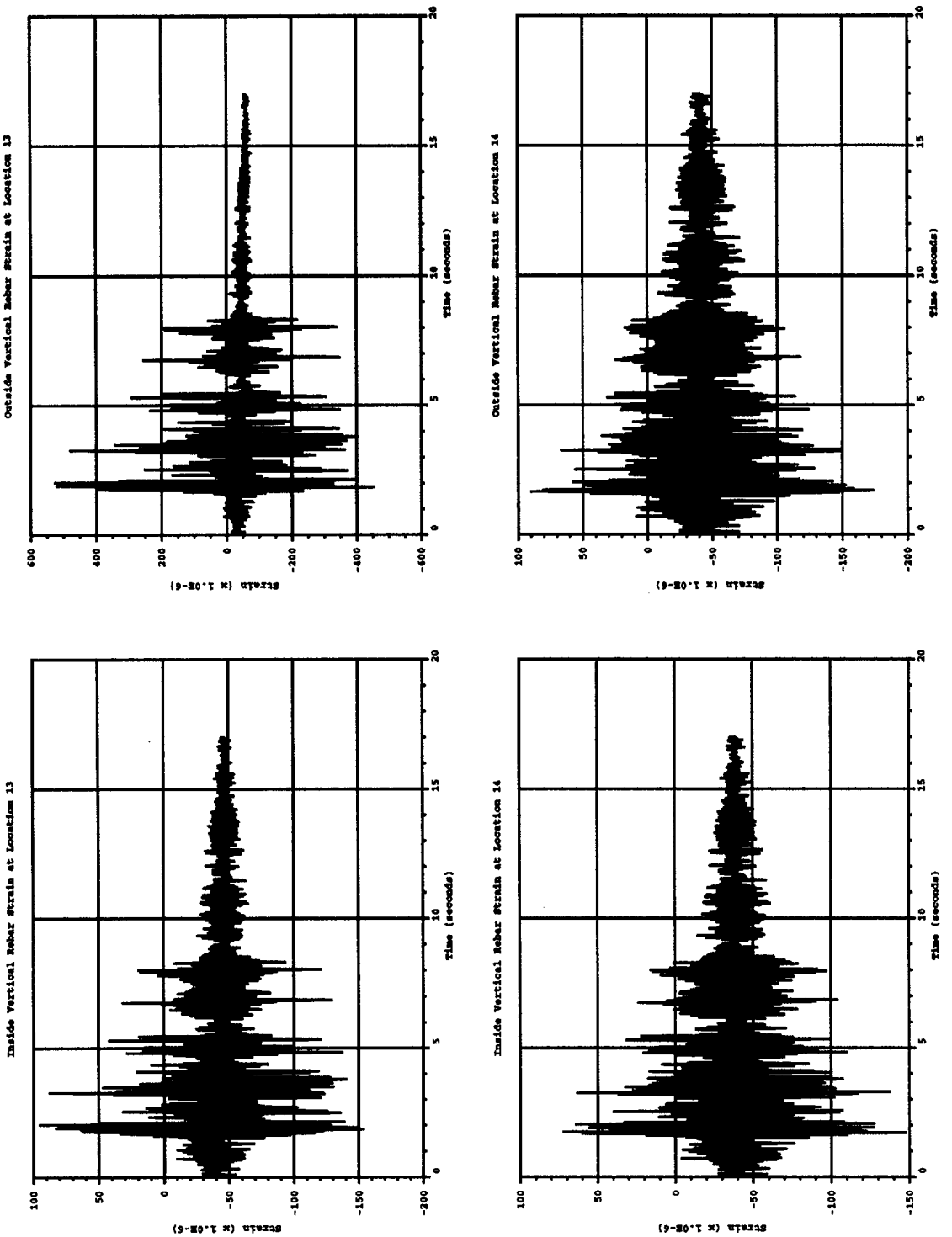

Figure A.10 Vertical rebar strains for RCCV under S1(H+V)

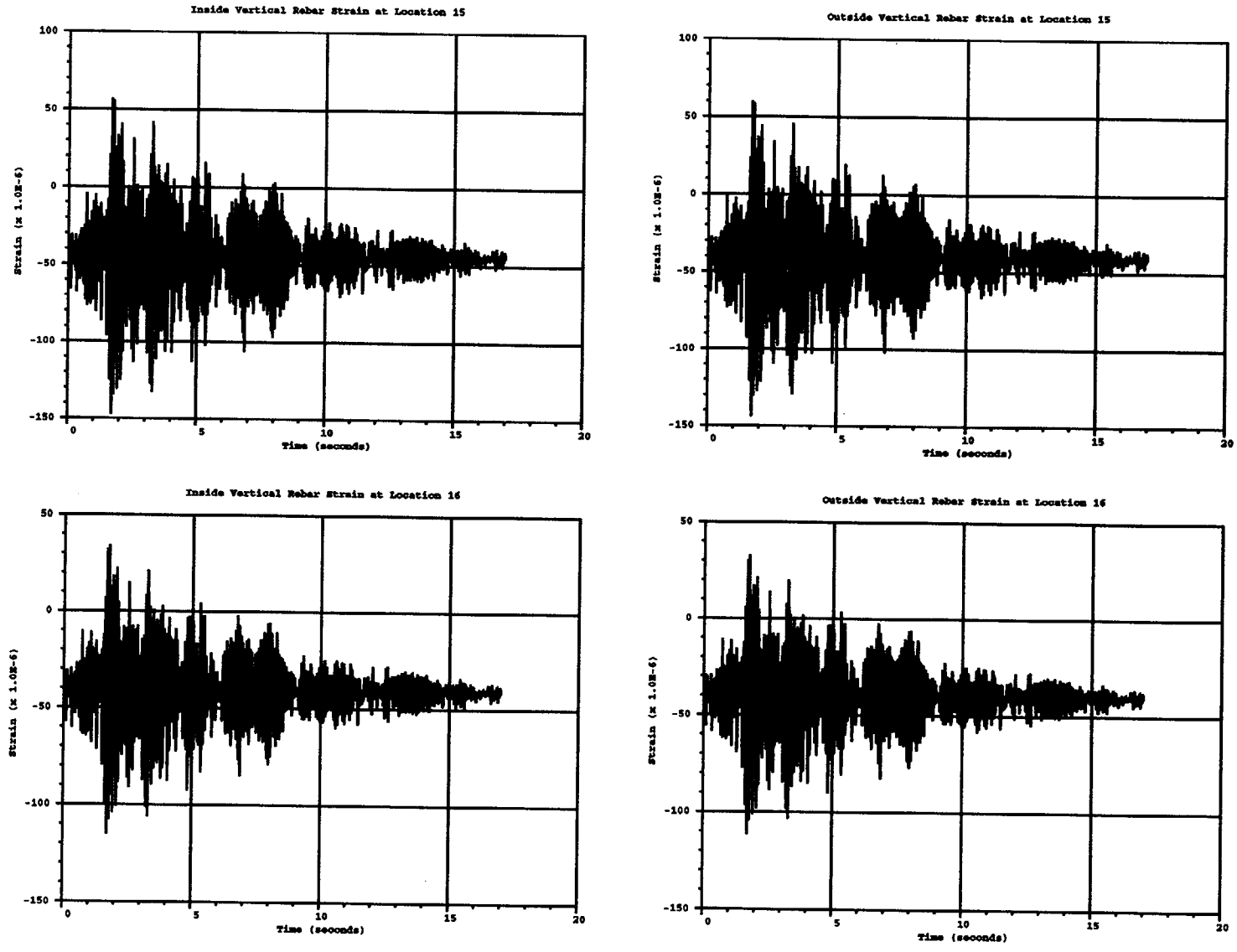

Figure A.11 Vertical rebar strains for RCCV under S1(H+V)

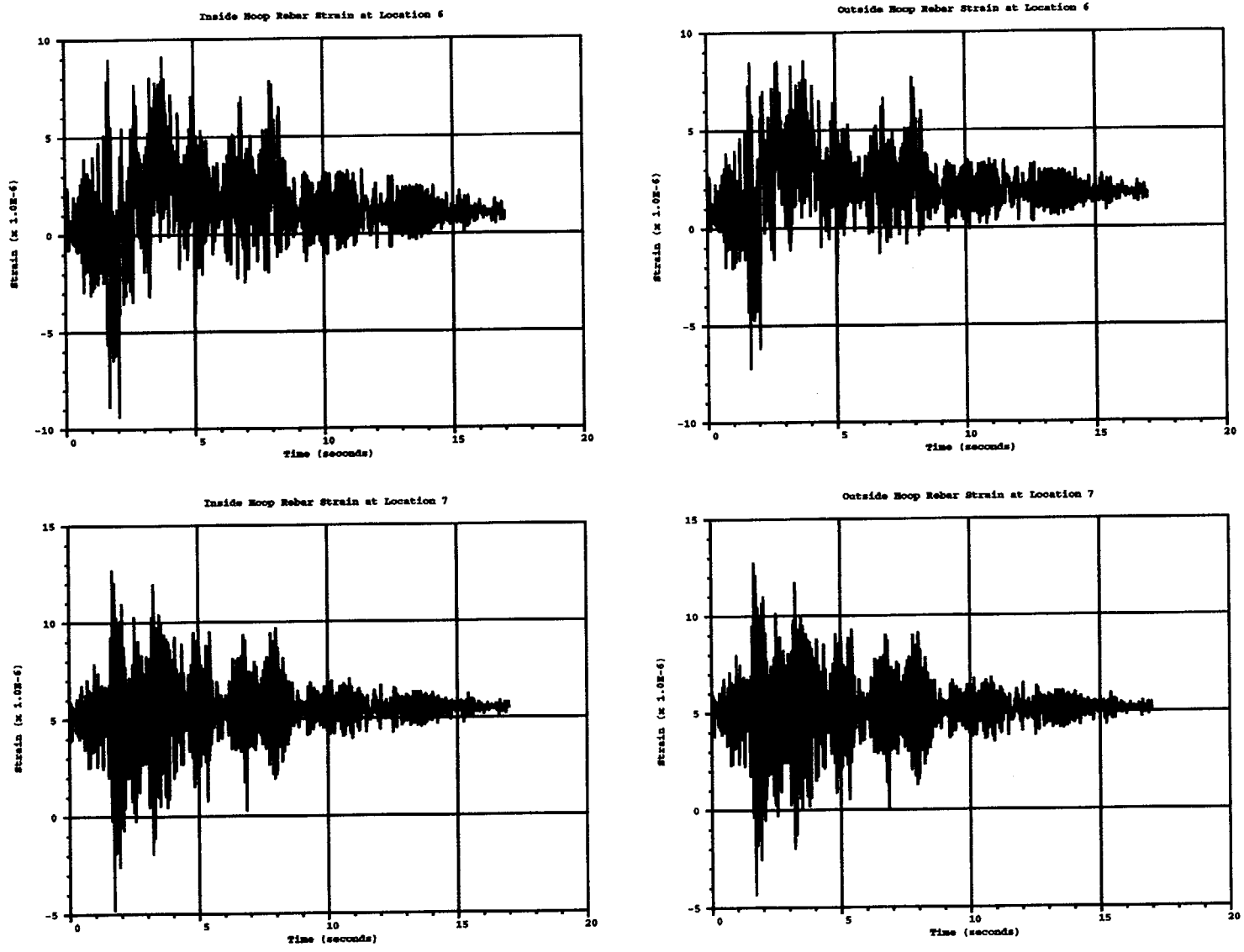

Figure A.12 Hoop rebar strains for RCCV under S1(H+V)

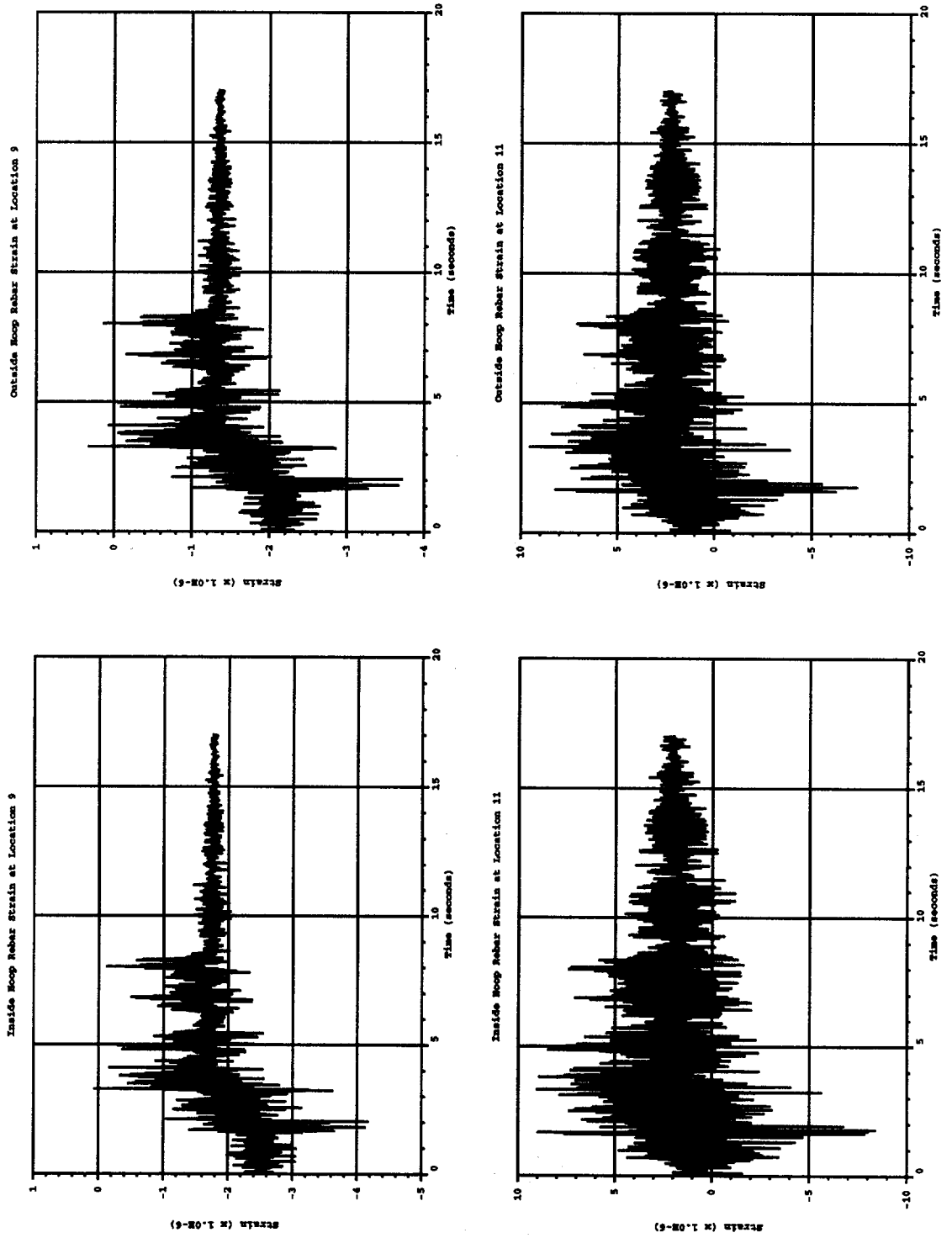

Figure A.13 Hoop rebar strains for RCCV under S1(H+V)

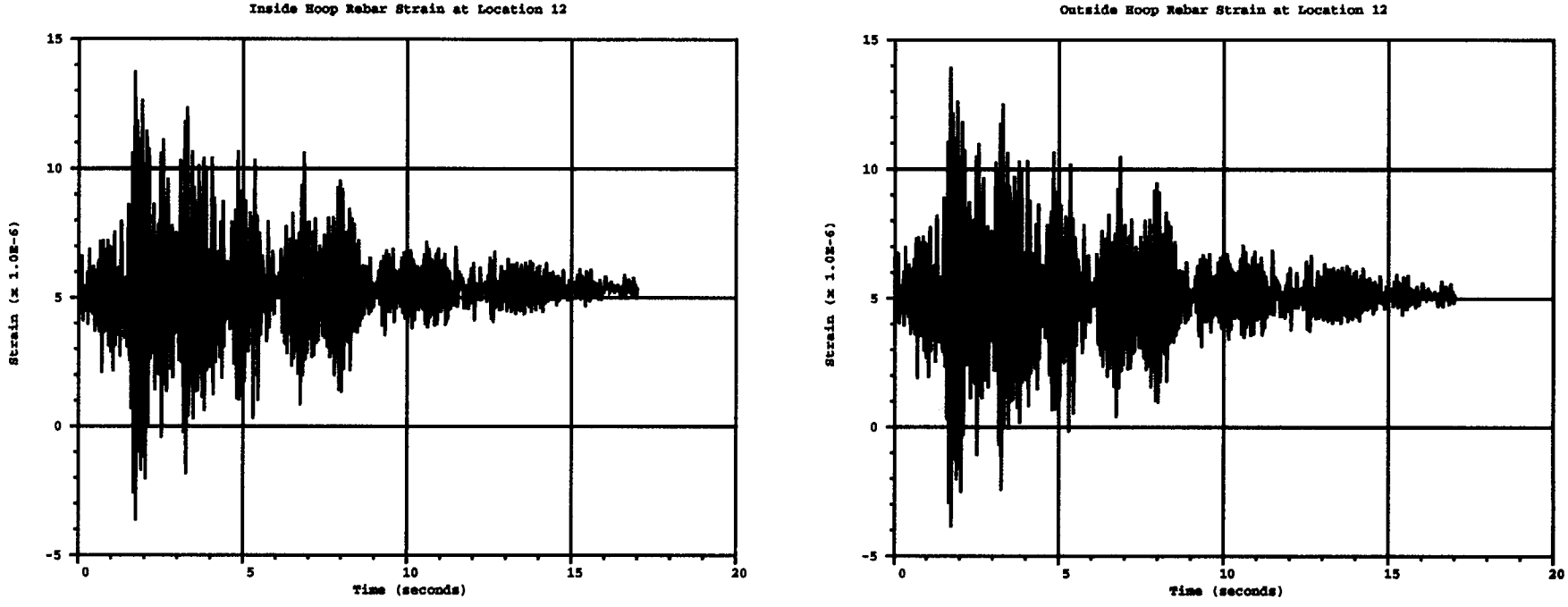

Figure A.14 Hoop rebar strains for RCCV under S1(H+V)

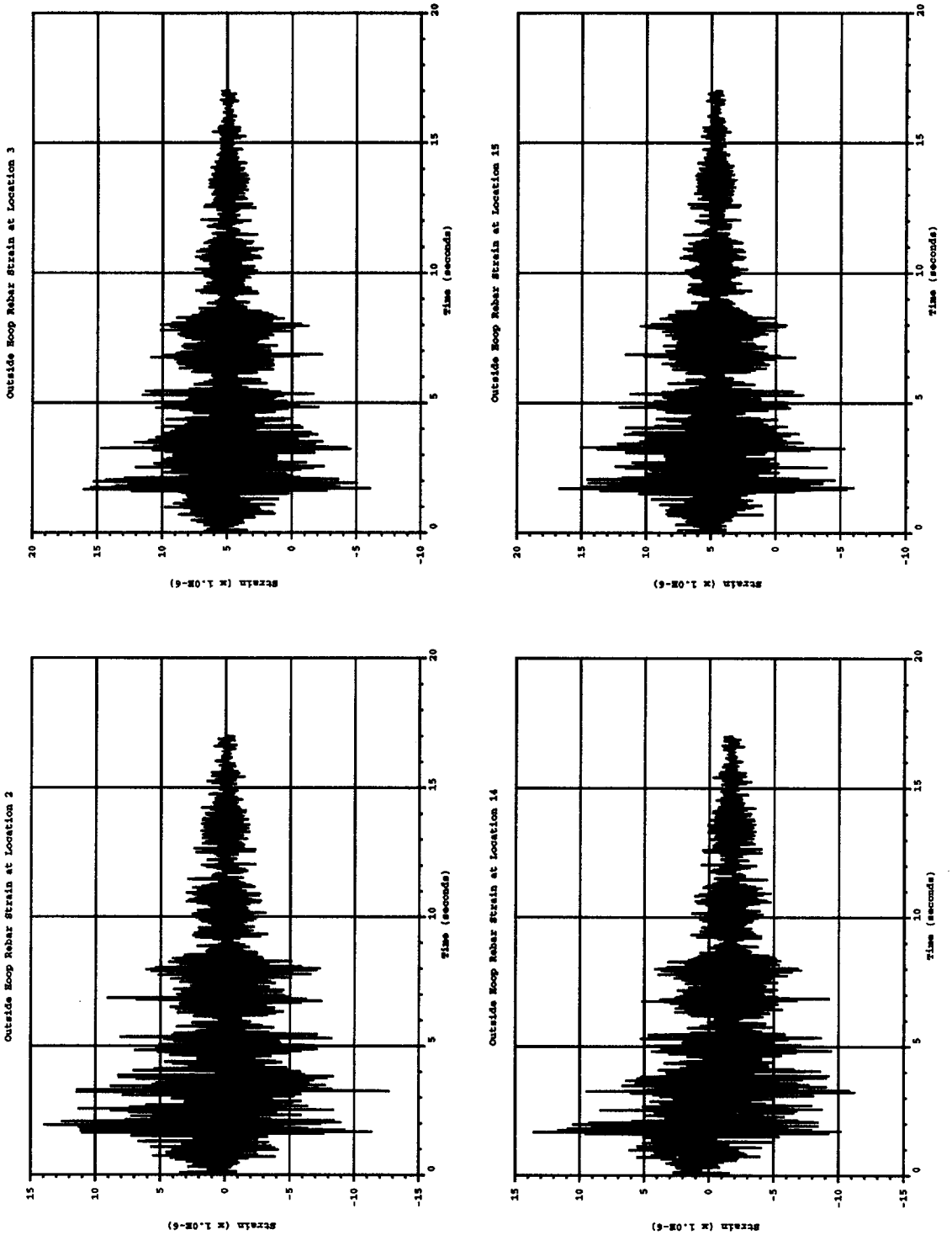

Figure A.15 Hoop rebar strains for RCCV under S1(H+V)

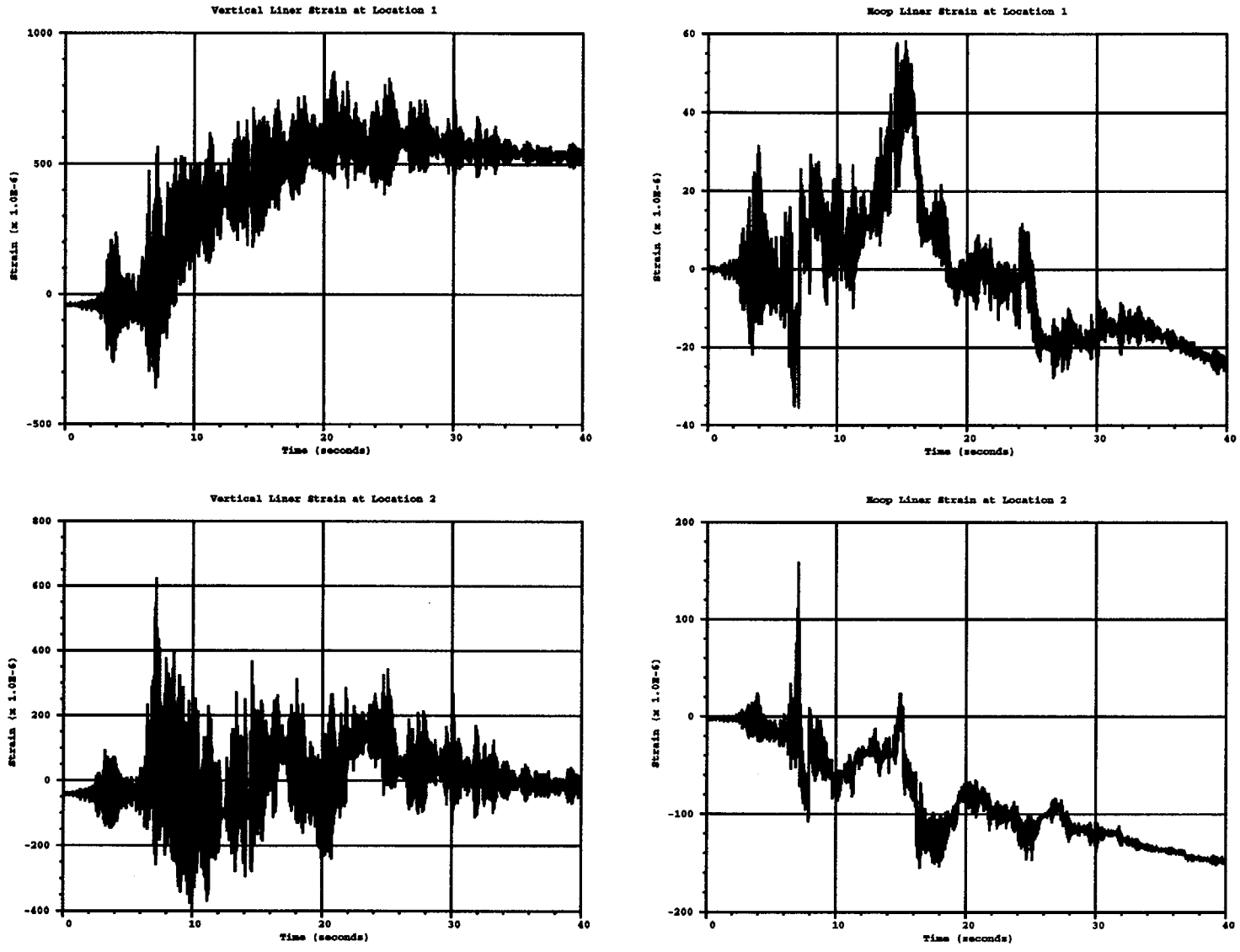

Figure A.16 Liner strains for RCCV under S2(H+V)

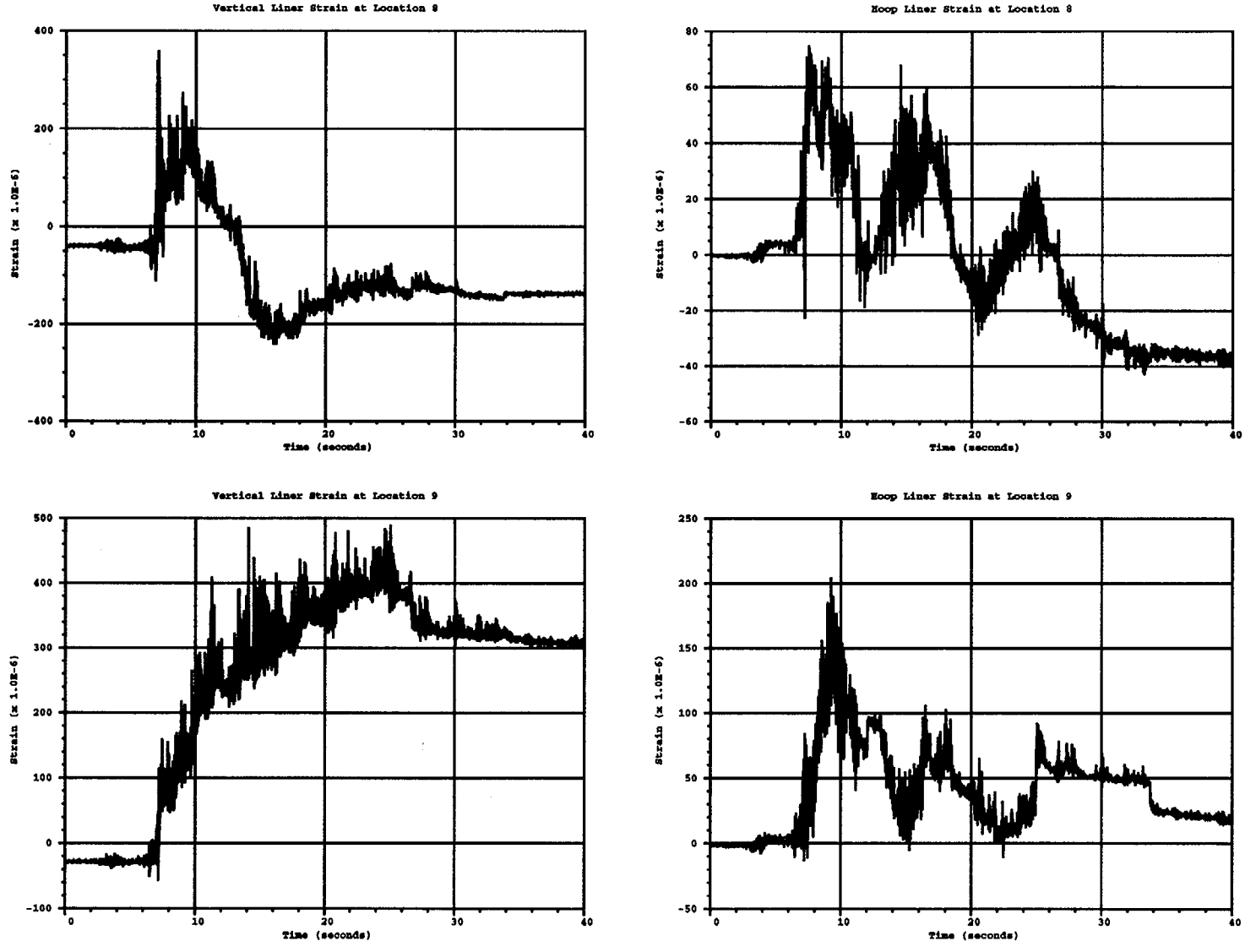

Figure A.17 Liner strains for RCCV under S2(H+V)

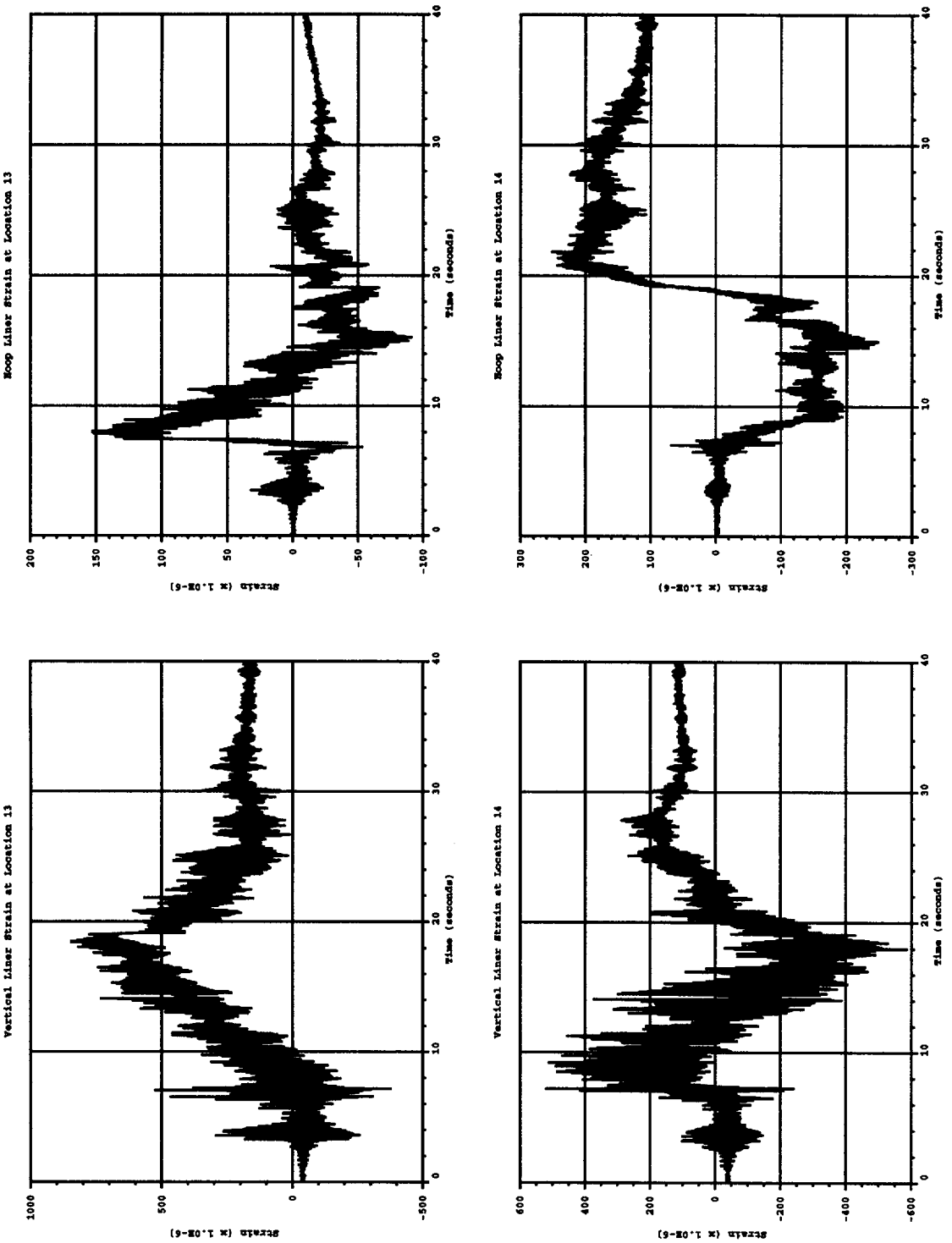

Figure A.18 Liner strains for RCCV under S2(H+V)

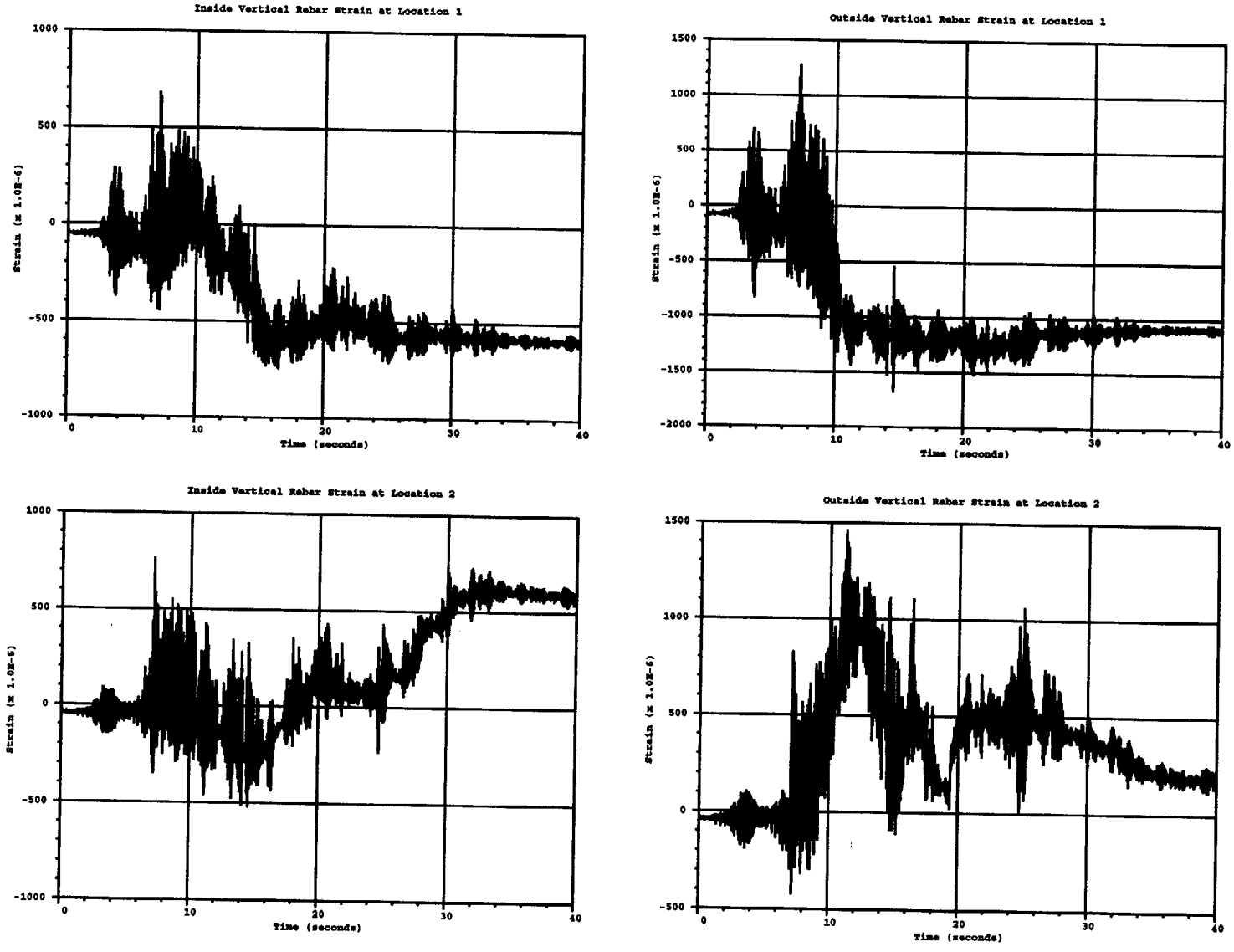

Figure A.19 Vertical rebar strains for RCCV under S2(H+V)

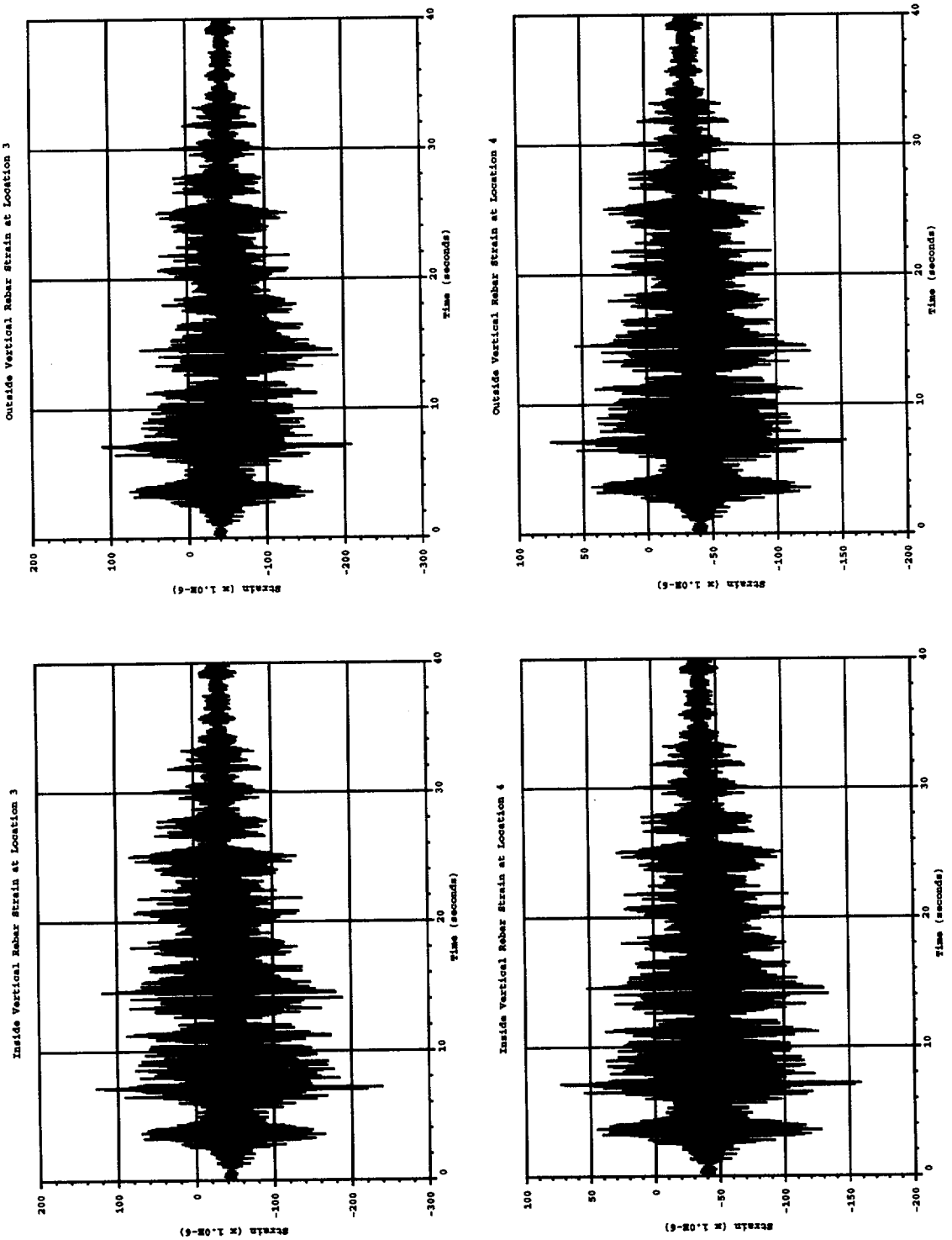

Figure A.20 Vertical rebar strains for RCCV under S2(H+V)

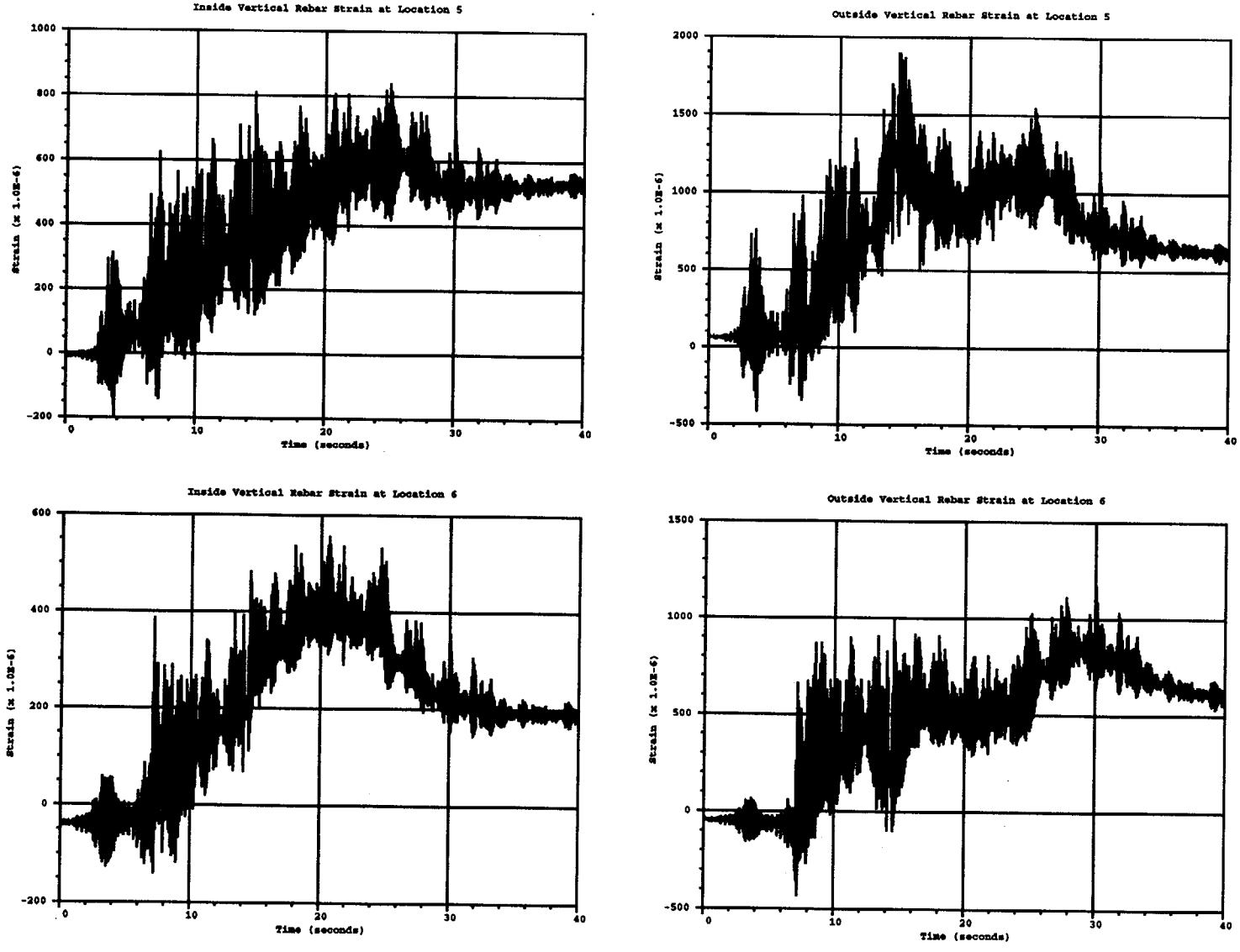

Figure A.21 Vertical rebar strains for RCCV under S2(H+V)

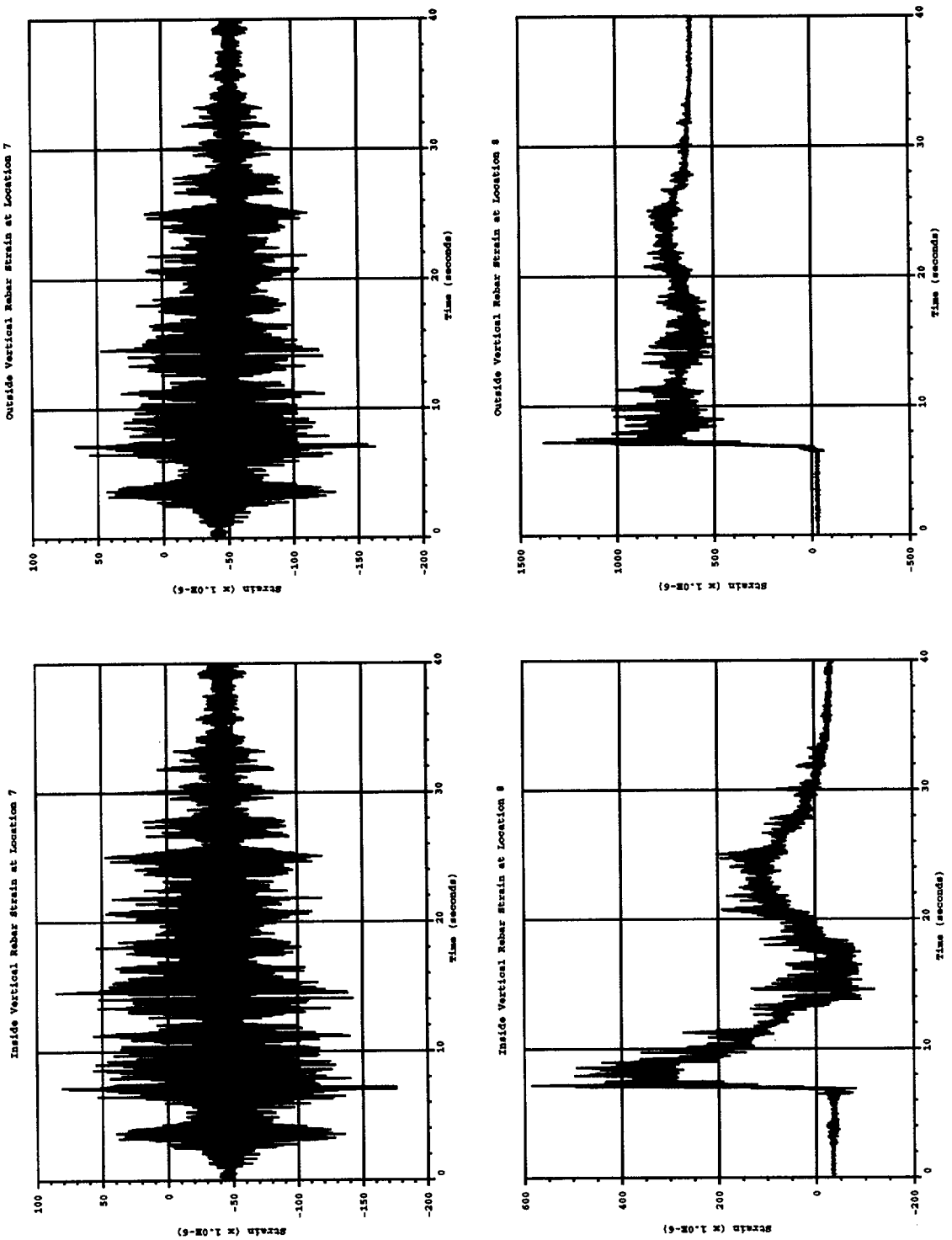

Figure A.22 Vertical rebar strains for RCCV under S2(H+V)

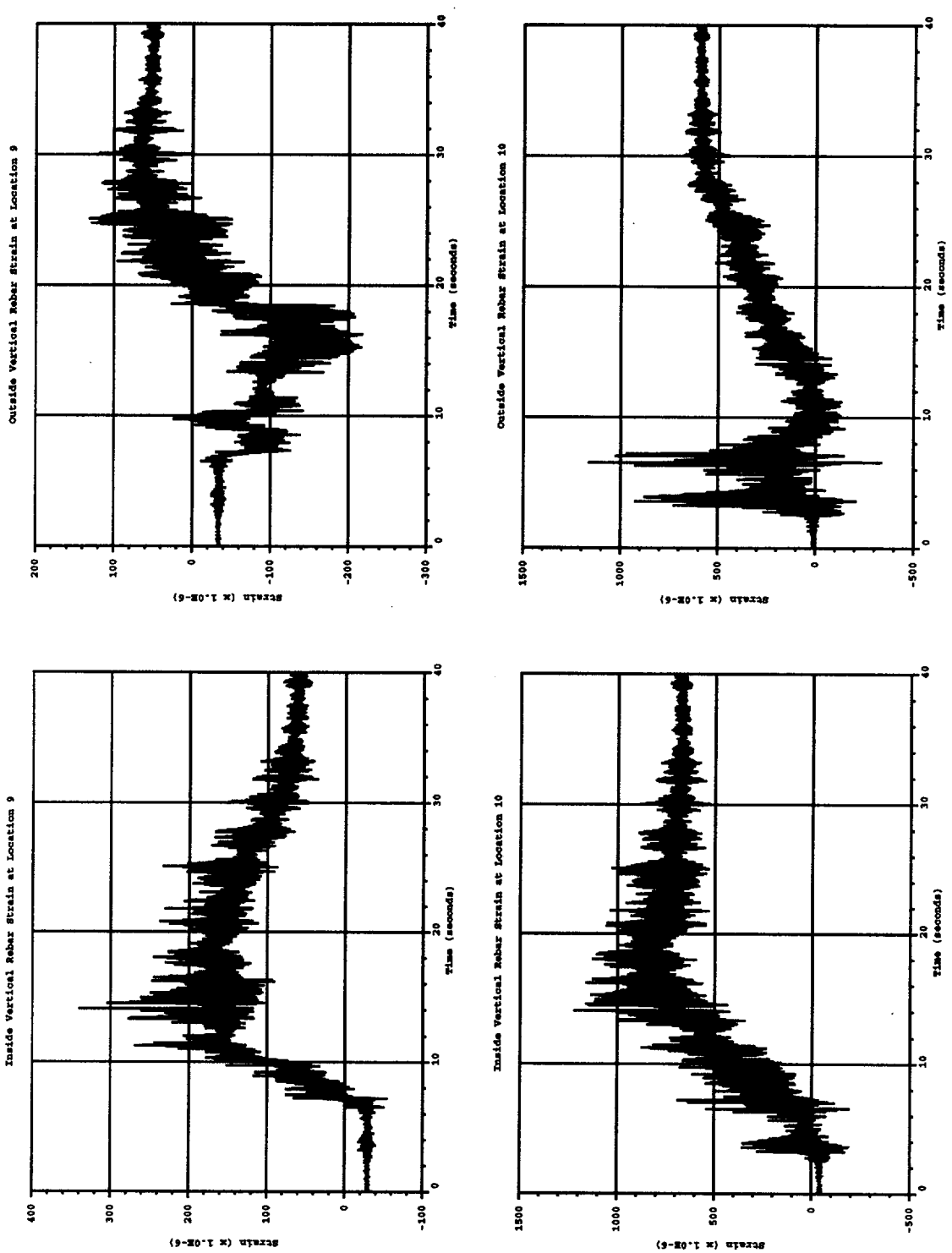

Figure A.23 Vertical rebar strains for RCCV under S2(H+V)

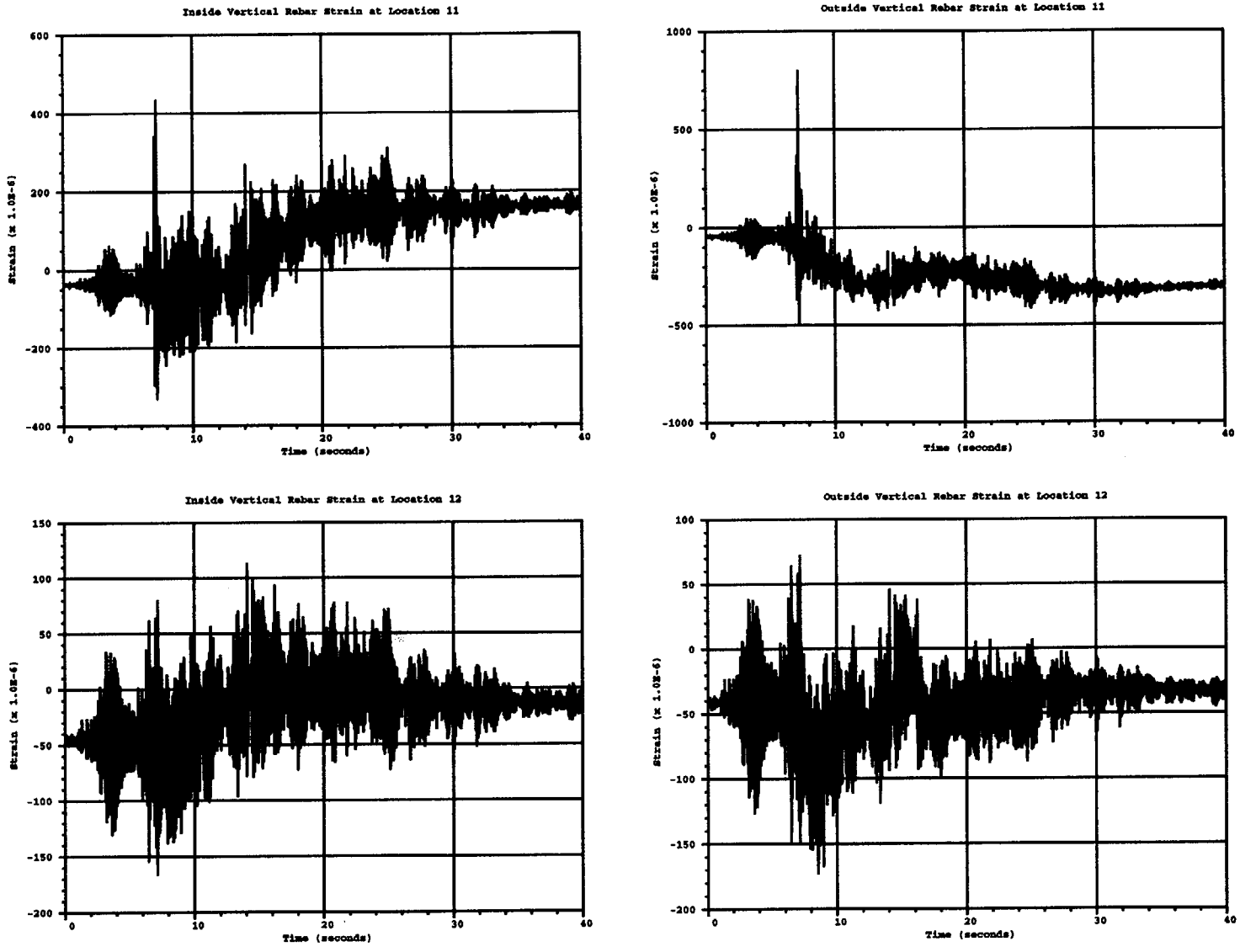

Figure A.24 Vertical rebar strains for RCCV under S2(H+V)

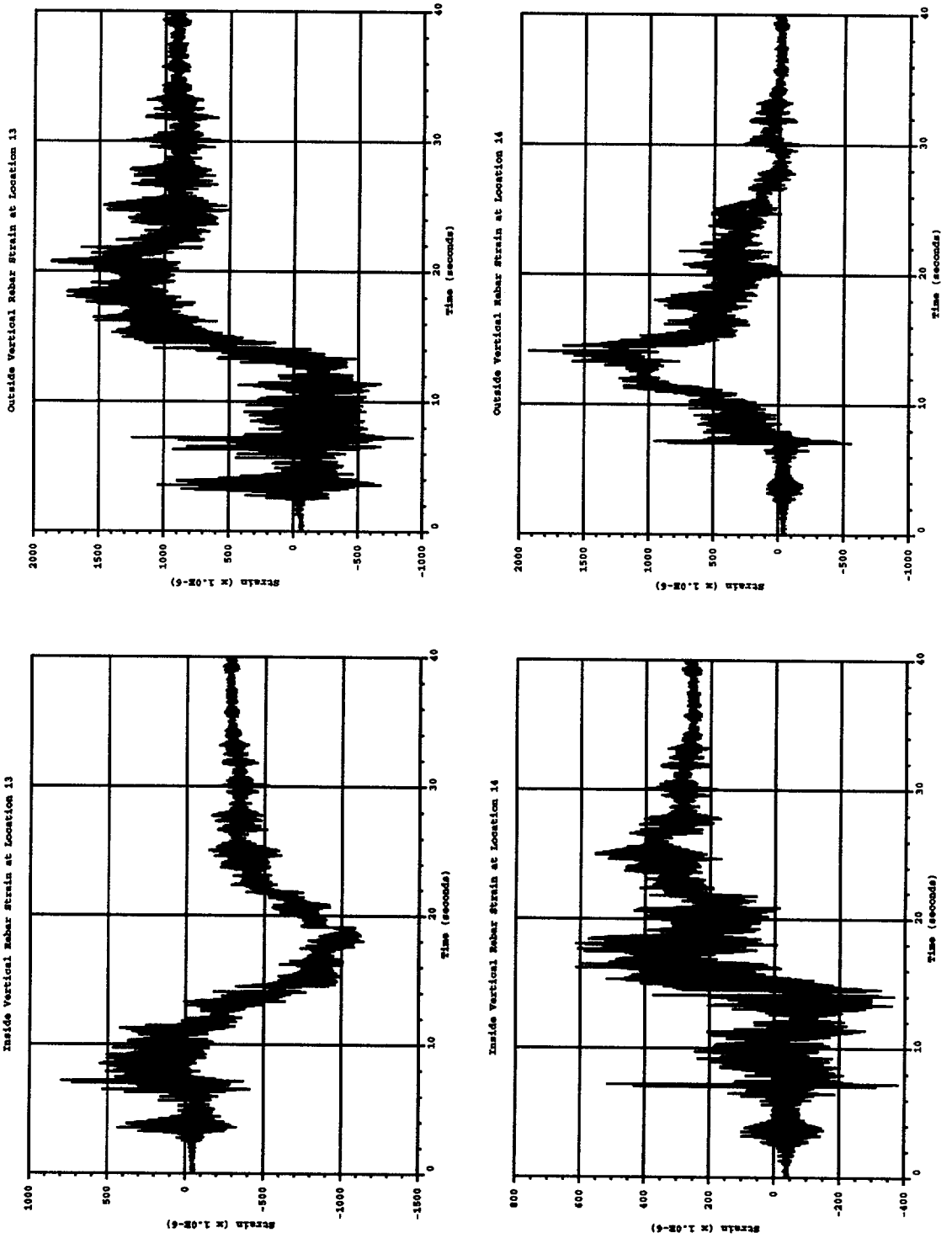

Figure A.25 Vertical rebar strains for RCCV under S2(H+V)

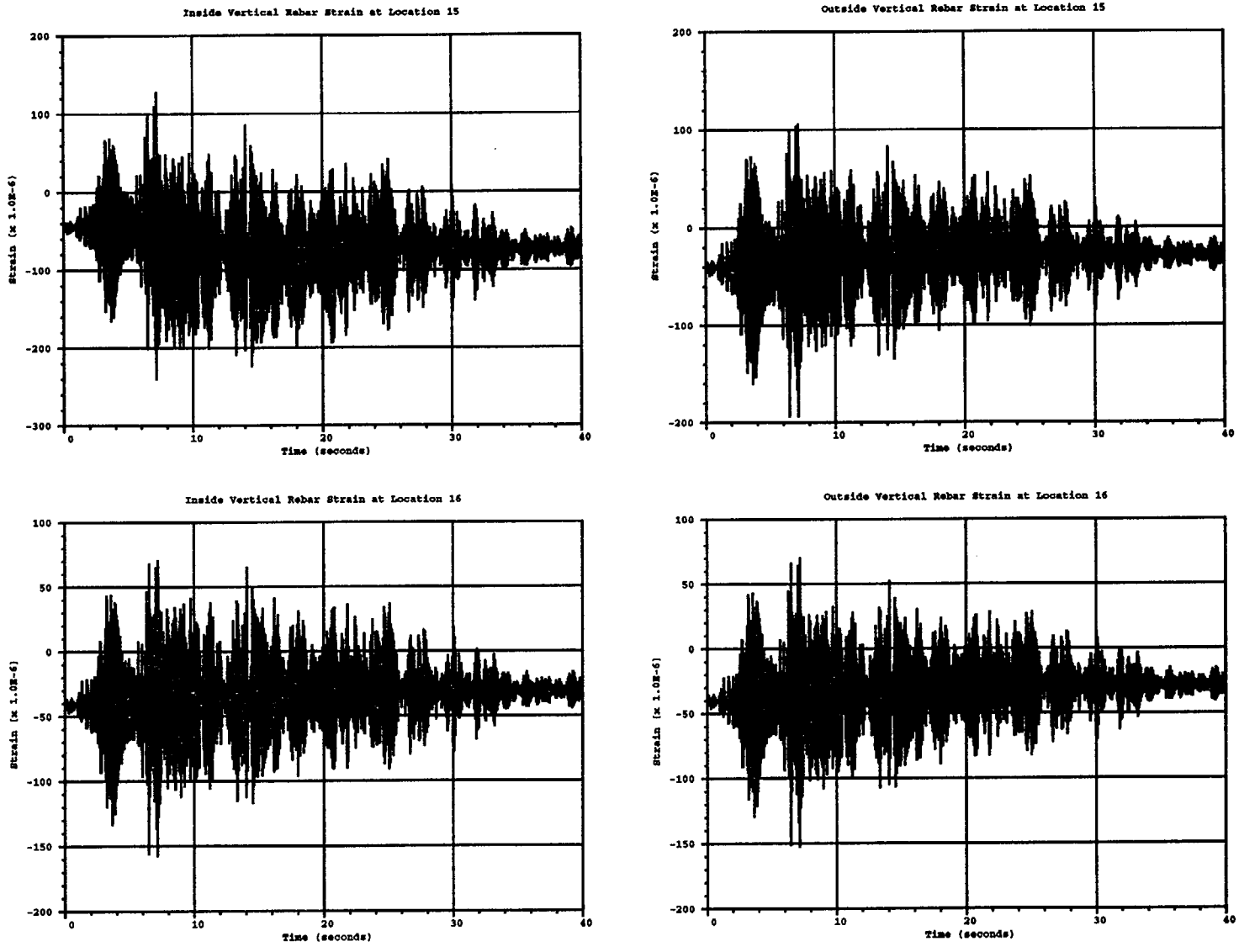

Figure A.26 Vertical rebar strains for RCCV under S2(H+V)

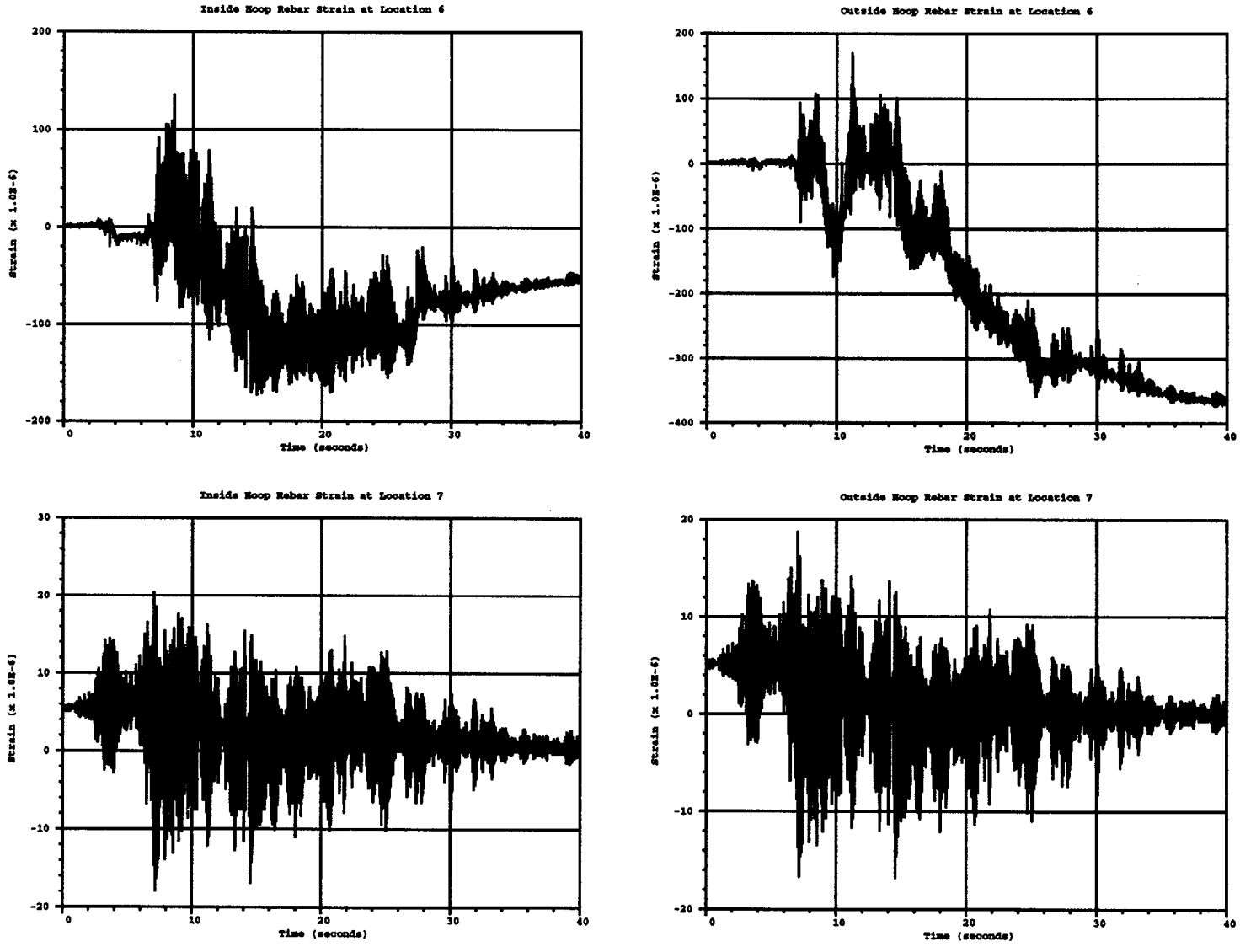

Figure A.27 Hoop rebar strains for RCCV under S2(H+V)

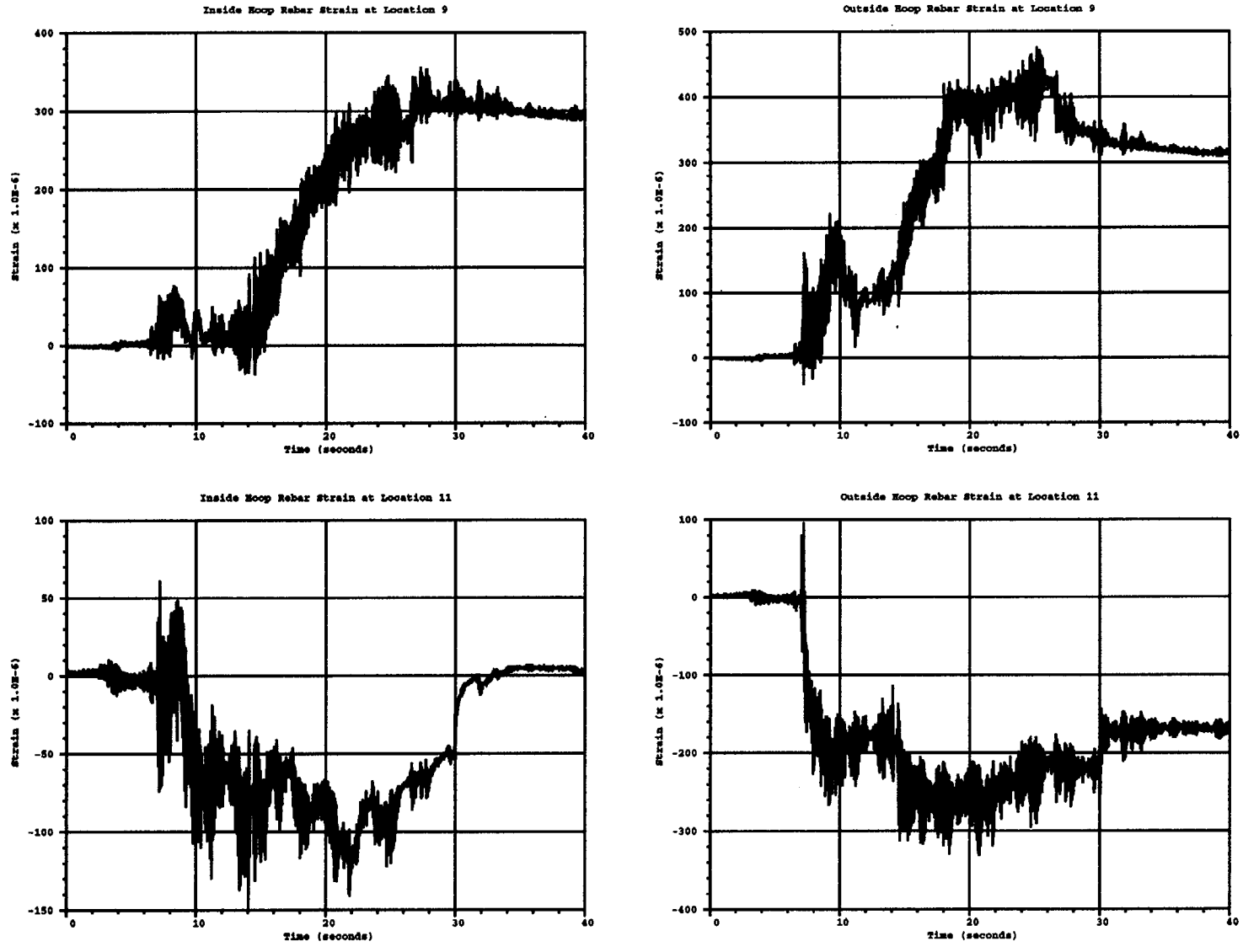

Figure A.28 Hoop rebar strains for RCCV under S2(H+V)

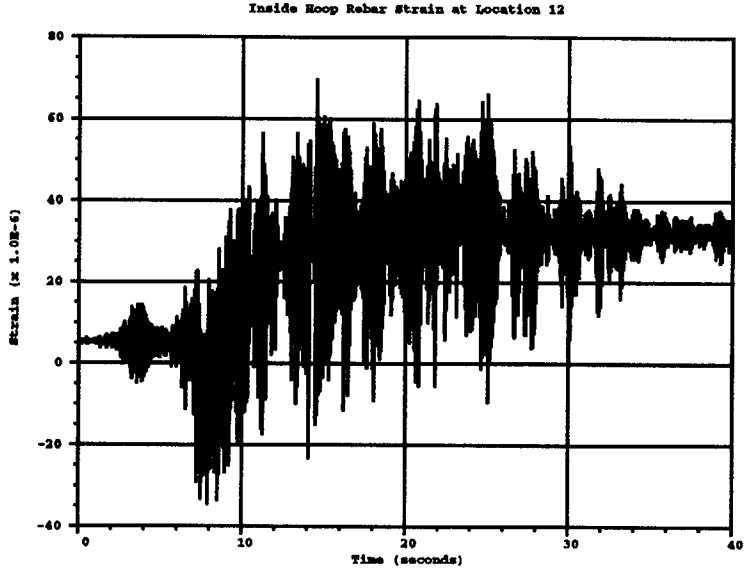

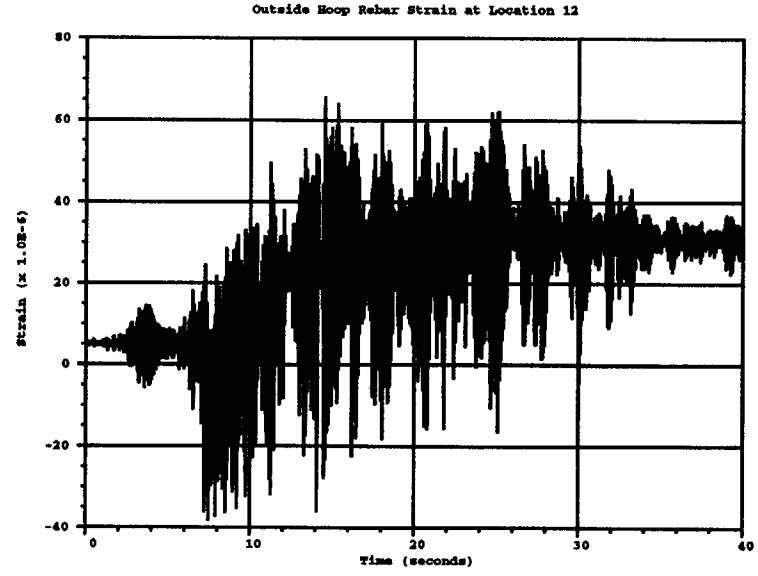

Figure A.29 Hoop rebar strains for RCCV under S2(H+V)

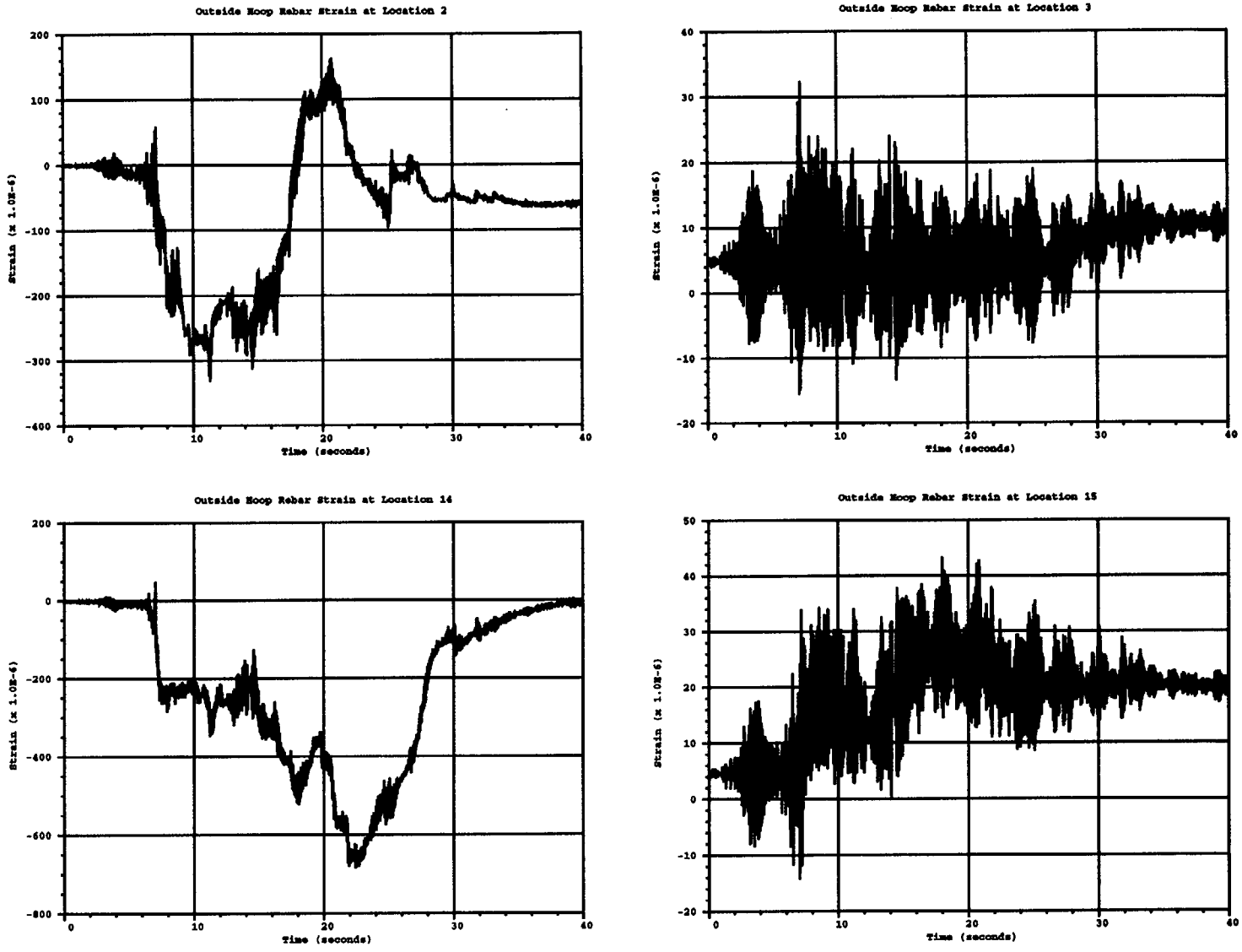

Figure A.30 Hoop rebar strains for RCCV under S2(H+V)

APPENDIX B

Posttest Analysis Results with Test Comparisons

APPENDIX B

Posttest Analysis Results with Test Comparisons

Figure B.1	Schematic for location of test gages.
Figure B.2 – B.20	S1(H+V)
Figure B.21 – B.39	S2(H+V)
Figure B.40 – B.58	2S2(H)
Figure B.59 – B.77	3S2(H)
Figure B.78 – B.96	5S2(H)

Notes

1. The test data in this appendix are provided by the Nuclear Power Engineering Corporation (NUPEC) and are based on reports to the Ministry of International Trade and Industry (MITI) of Japan. The tests were performed by NUPEC at Tadotsu Engineering Laboratory, located in Tadotsu, Japan. No modifications or changes were made to the recorded test results.

   Information about the tests was provided by NUPEC, under an agreement between the U.S. Nuclear Regulatory Commission (NRC) and MITI. The terms and conditions of the technical exchange and general cooperation agreement between the NRC and the Agency of National Resources and Energy of MITI in the field of nuclear regulatory matters and nuclear safety research are given in the agreement "Collaboration on Concrete Containment Vessels (CCV) Seismic Proving Test Program and Information Exchange between USNRC and NUPEC."

2. The data recorded by NUPEC start at zero for each test. However, residual values that existed at the end of each test have been tabulated by NUPEC, and these residual values can be used as starting values for subsequent test data.

3. Damage accumulates in the finite element analyses, so any residual force, strain, or displacement from the previous analysis is the starting point for the next analysis. However, to facilitate comparison with test data, all plots of the analytical results are shifted to start at zero.

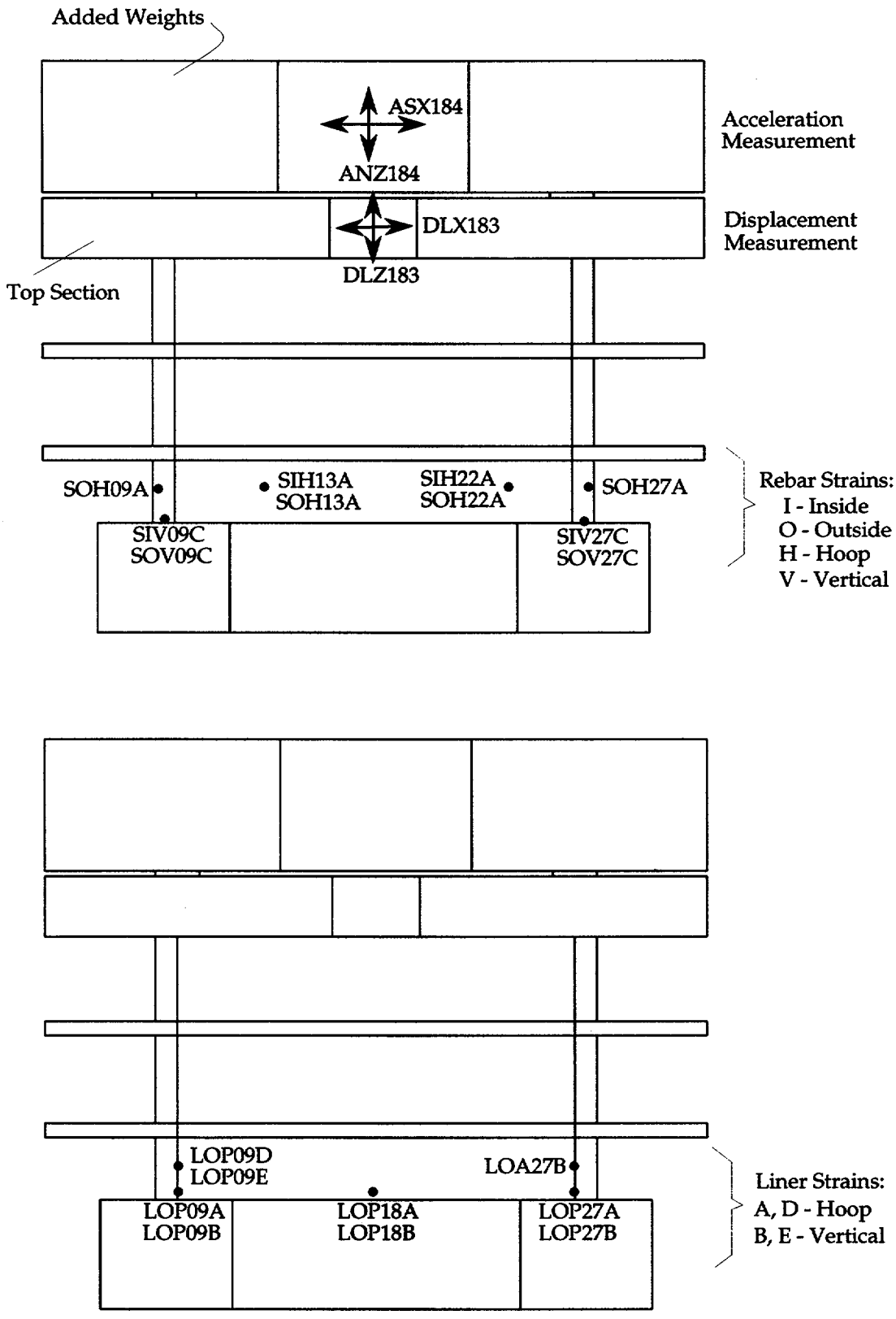

Figure B.1 Schematic for location of Test Gauges

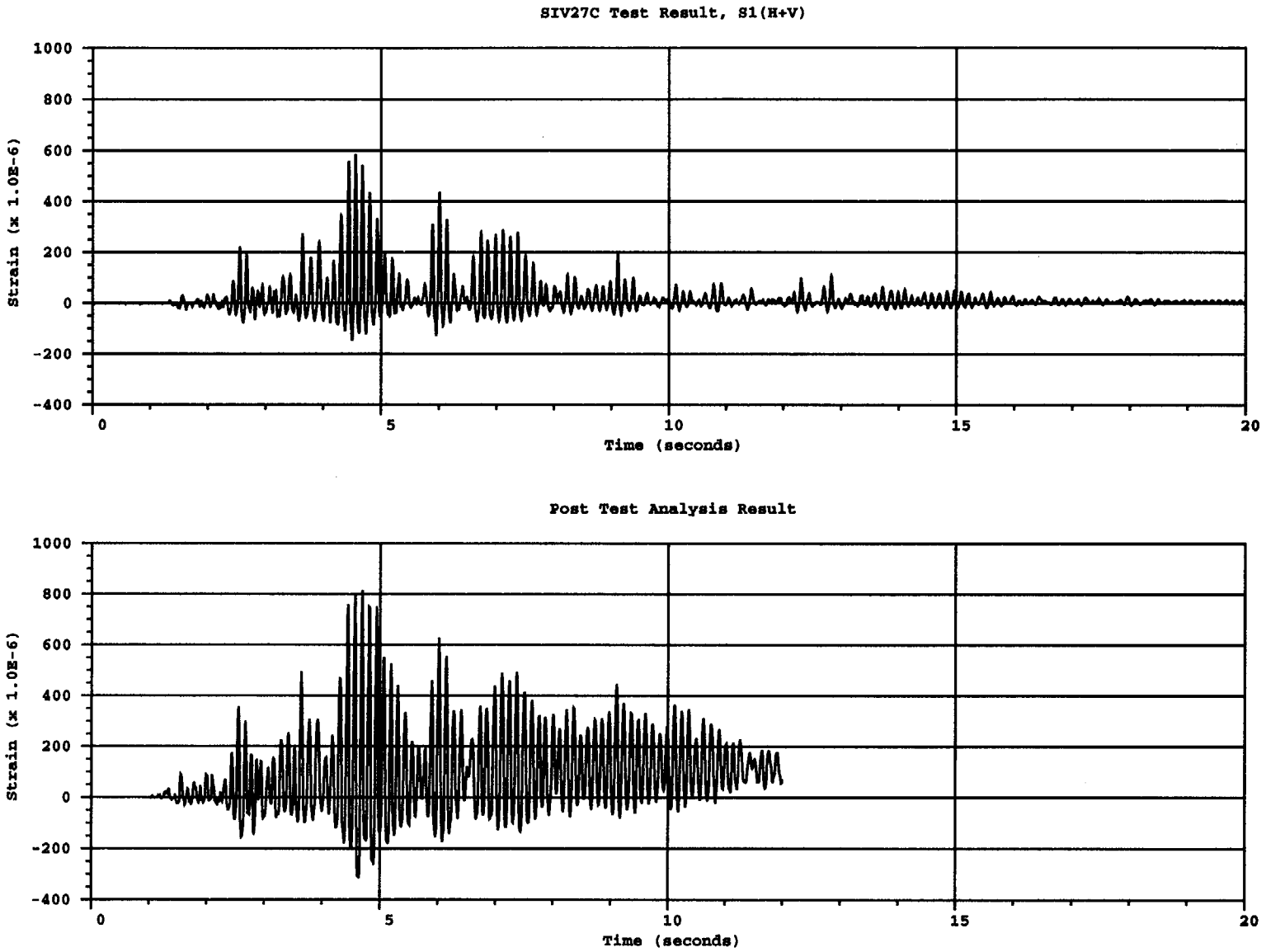

Figure B.2 Comparison of vertical rebar strain near gage SIV27C for S1(H+V) test

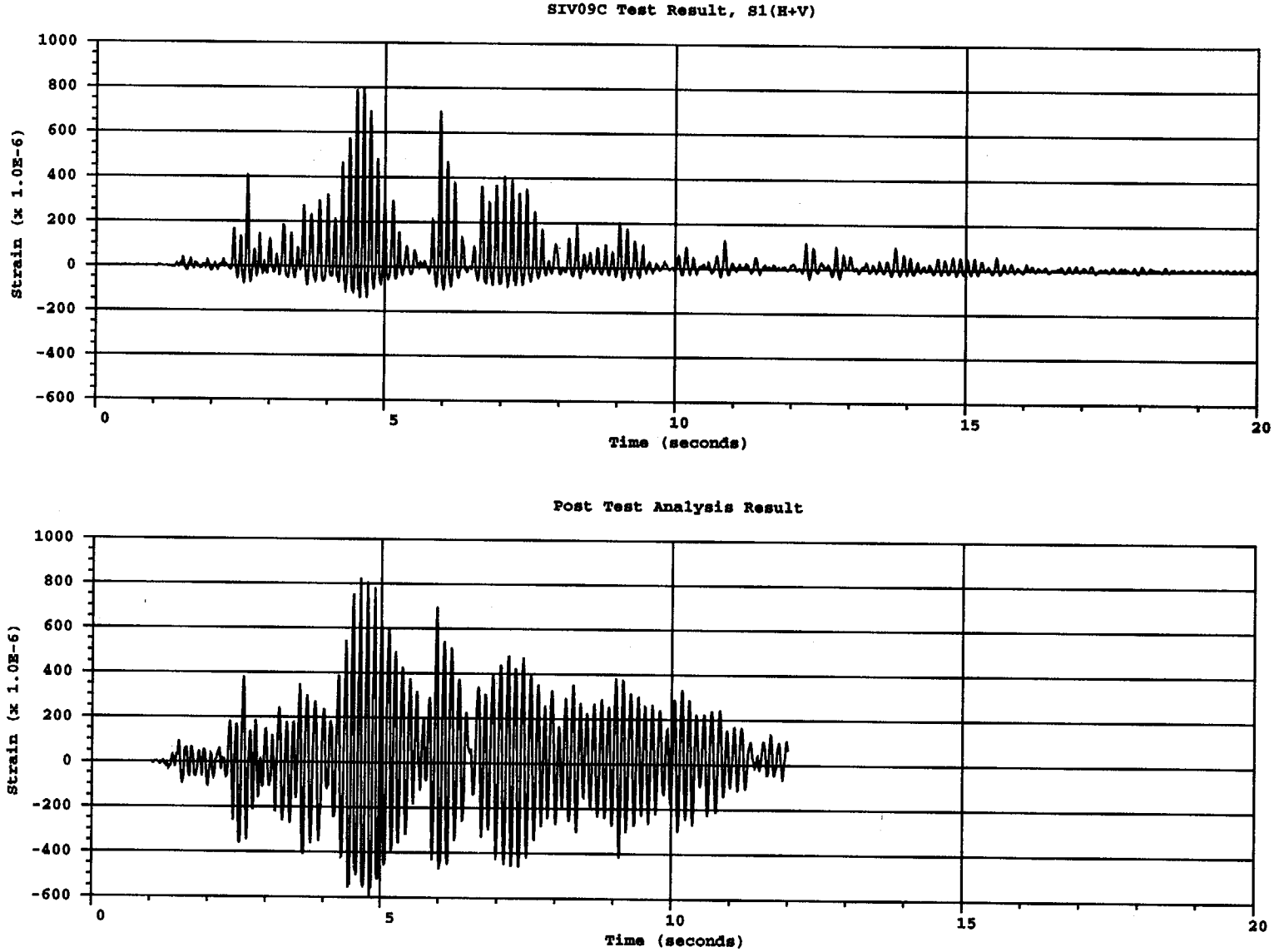

Figure B.3 Comparison of vertical rebar strain near gage SIV09C for S1(H+V) test

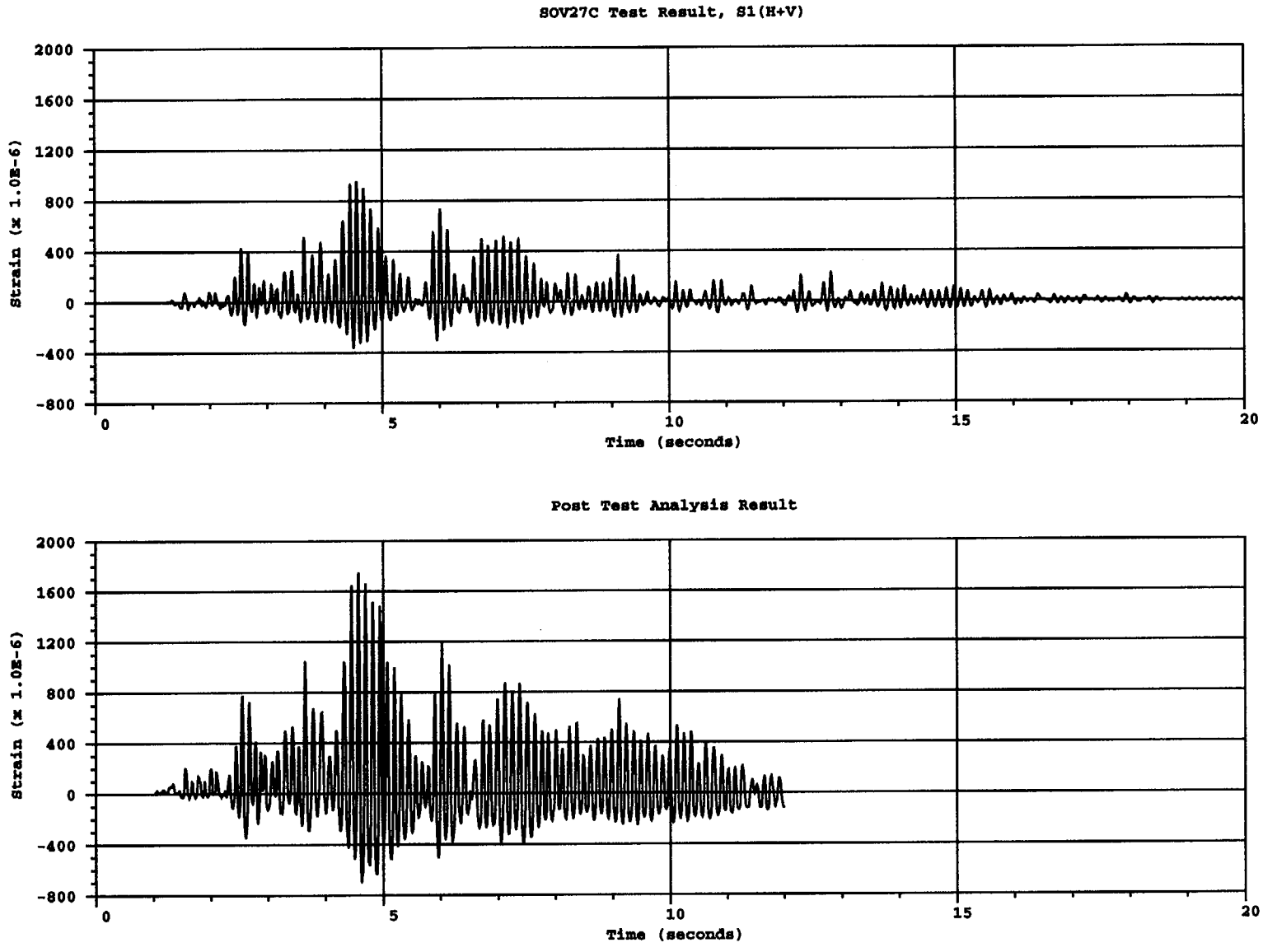

Figure B.4 Comparison of vertical rebar strain near gage SOV27C for S1(H+V) test

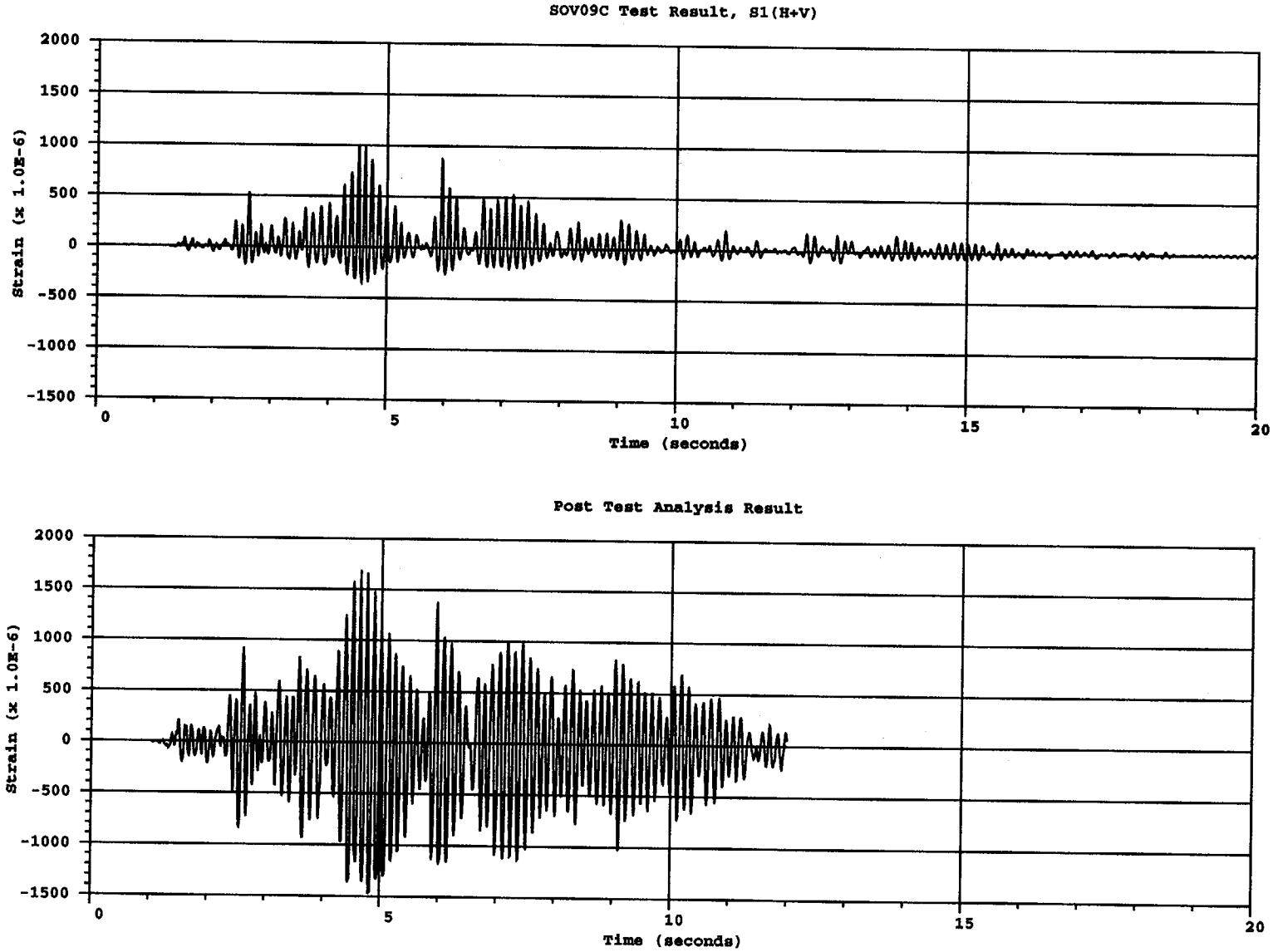

Figure B.5 Comparison of vertical rebar strain near gage SOV09C for S1(H+V) test

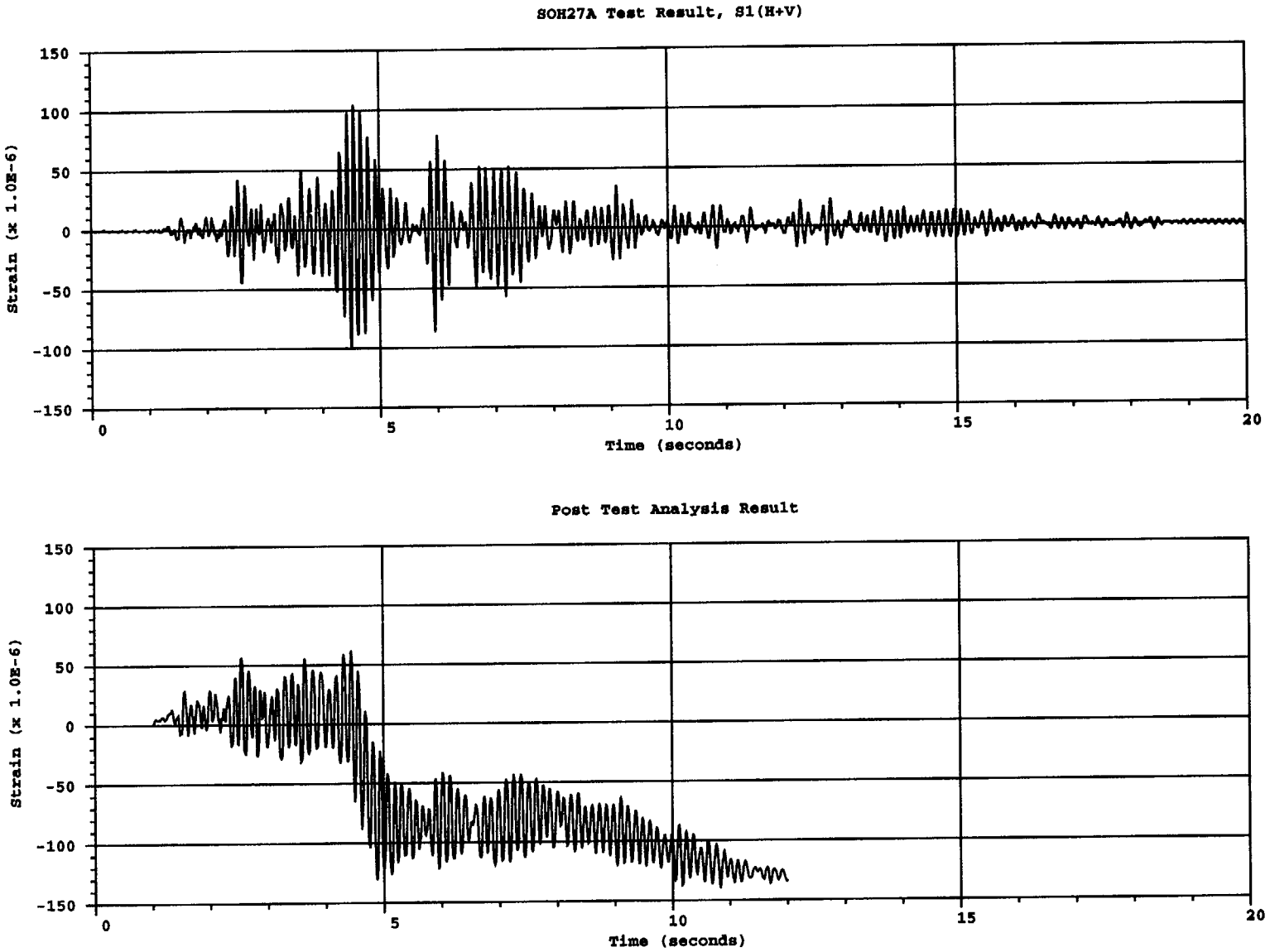

Figure B.6 Comparison of hoop rebar strain near gage SOH27A for S1(H+V) test

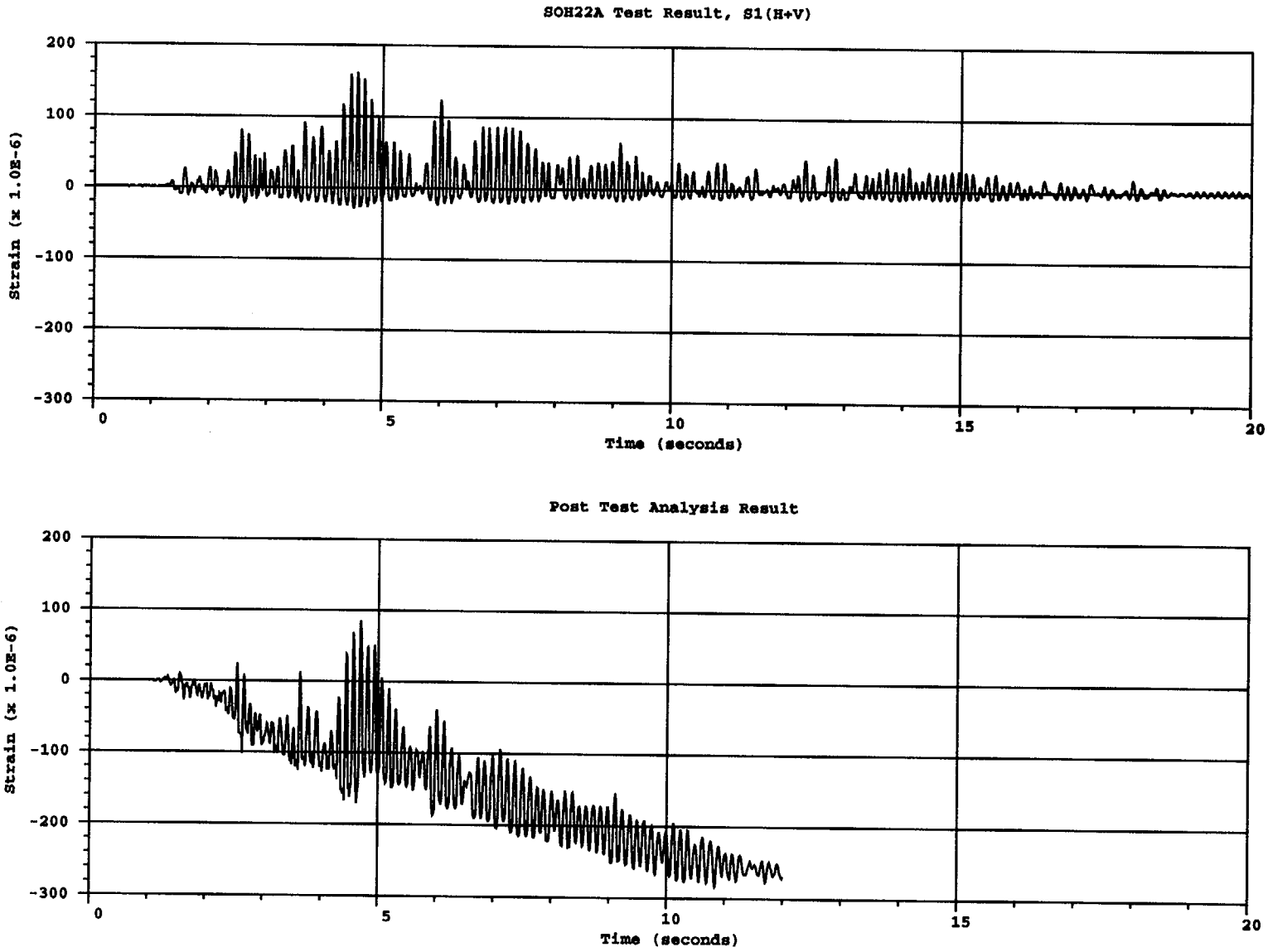

Figure B.7 Comparison of hoop rebar strain near gage SOH22A for S1(H+V) test

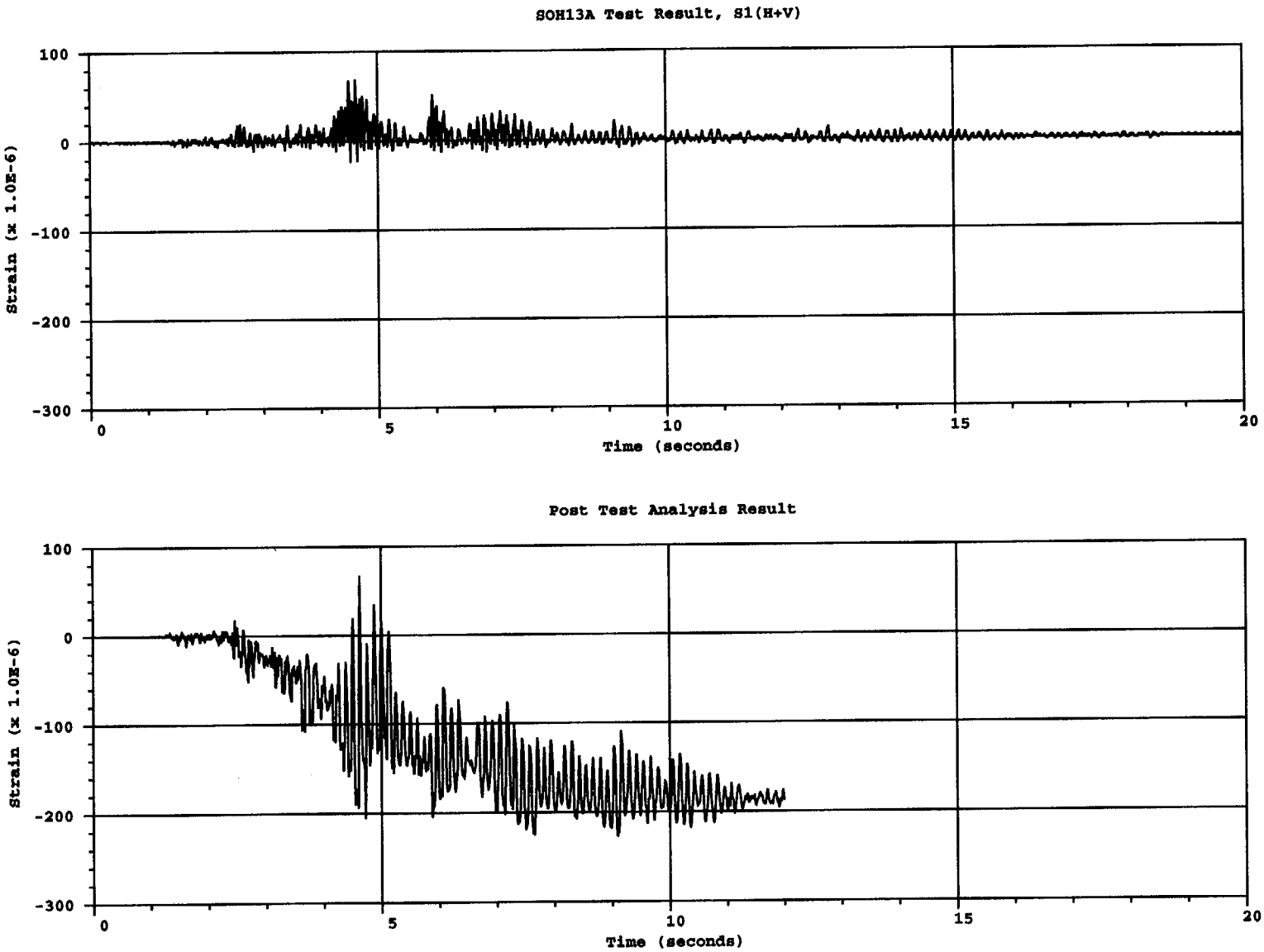

Figure B.8 Comparison of hoop rebar strain near gage SOH13A for S1(H+V) test

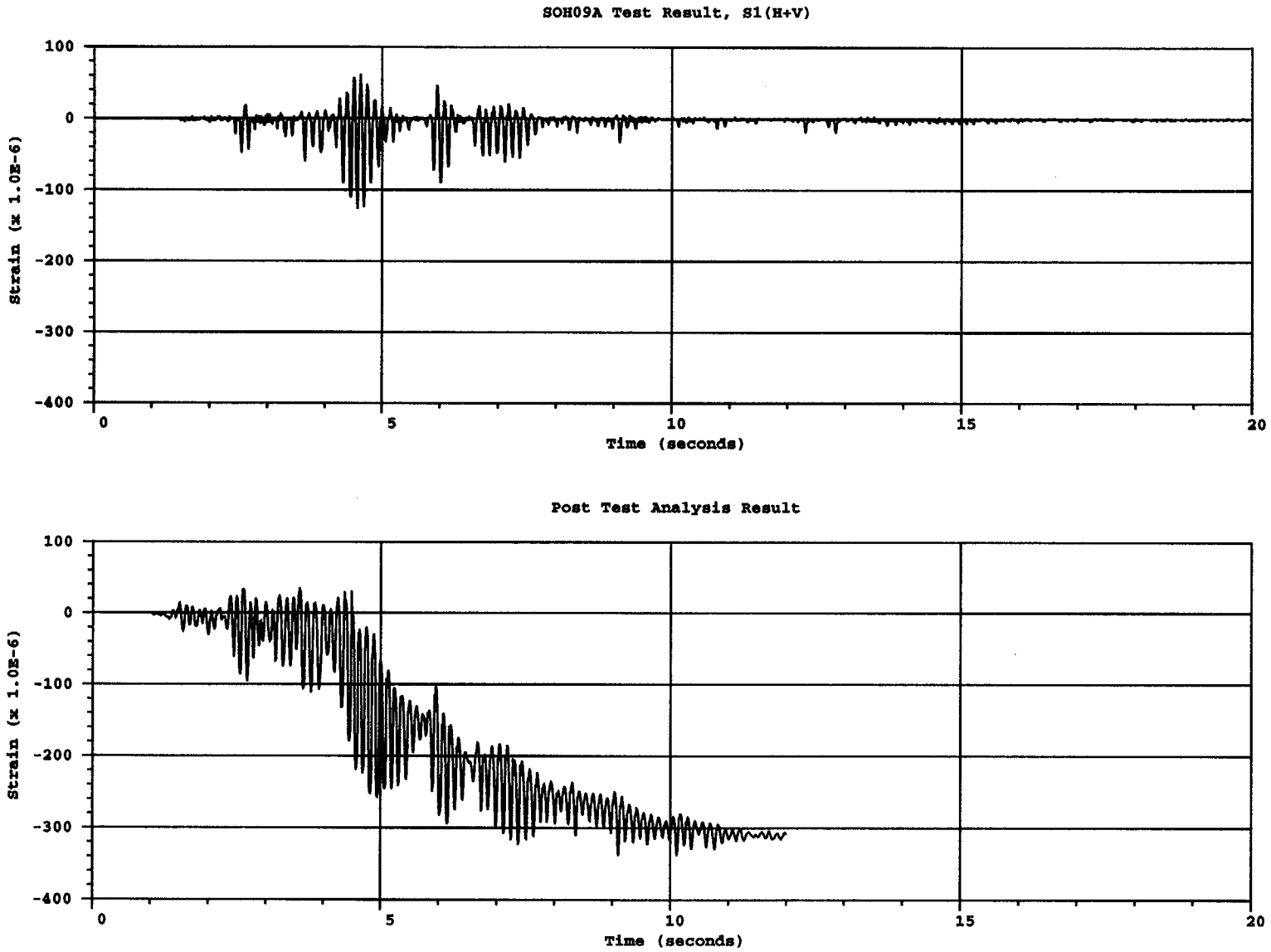

Figure B.9 Comparison of hoop rebar strain near gage SOH09A for S1(H+V) test

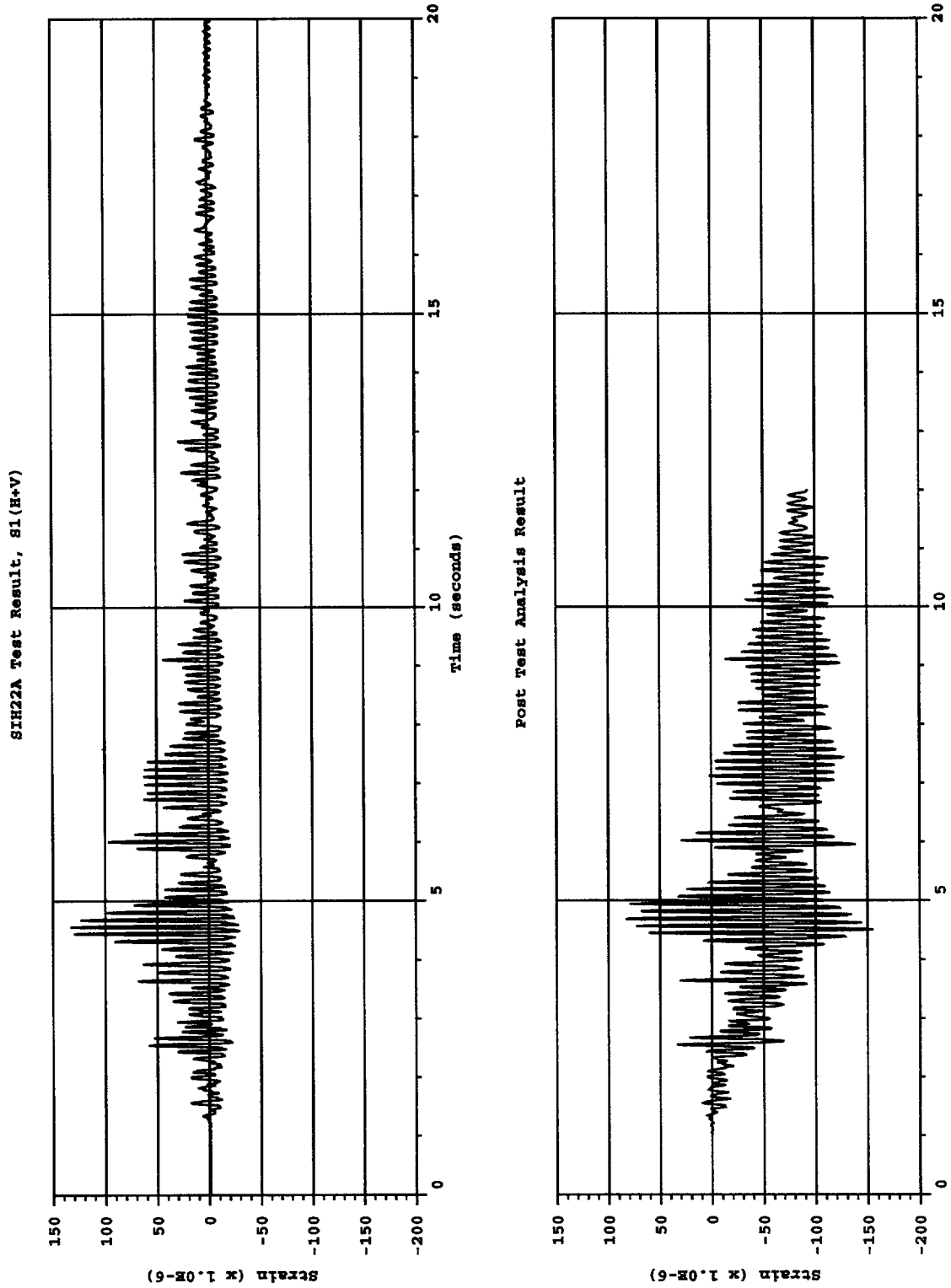

Figure B.10 Comparison of hoop rebar strain near gage S1H22A for S1(H+V) test

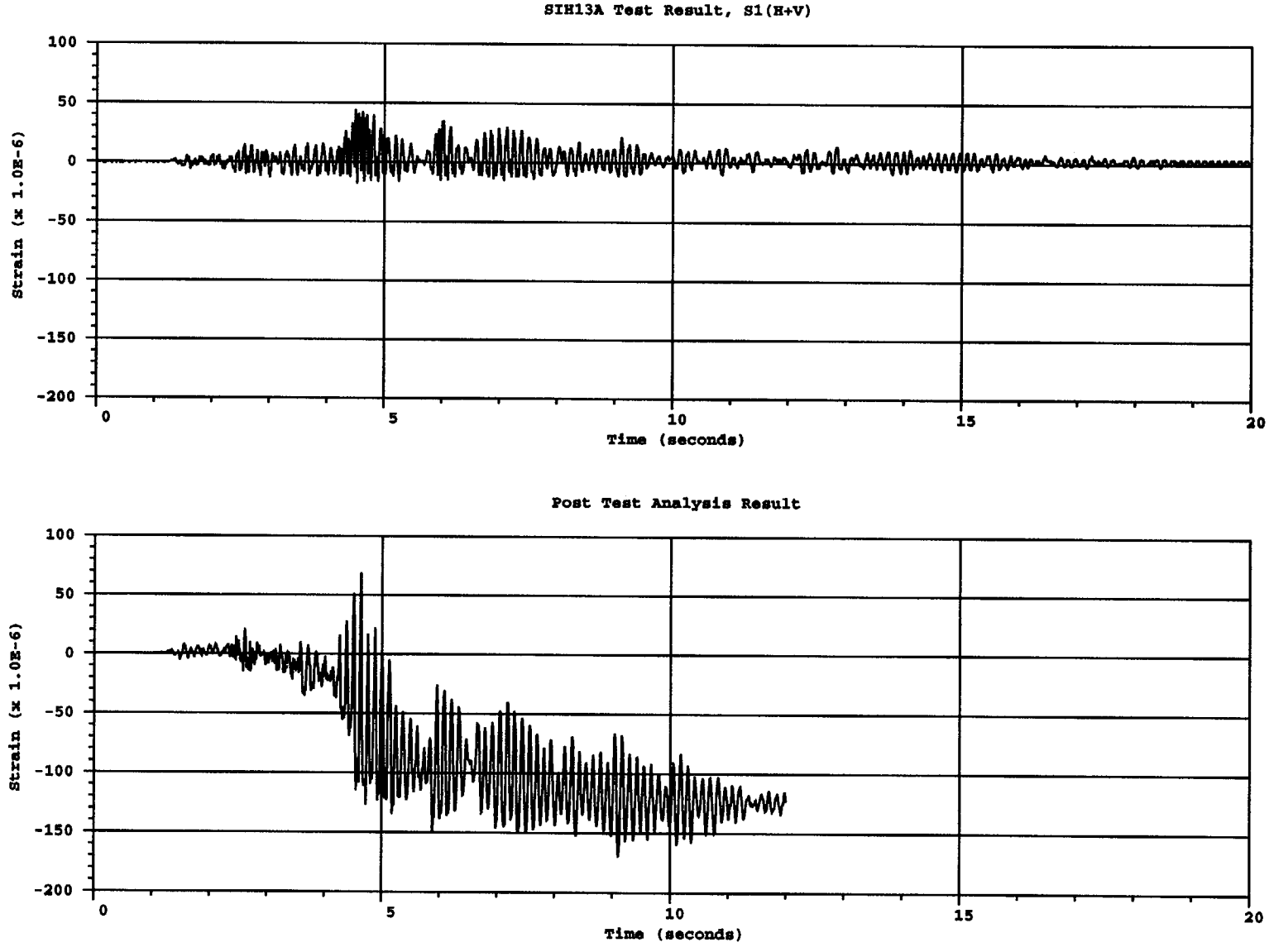

Figure B.11 Comparison of hoop rebar strain near gage S1H13A for S1(H+V) test

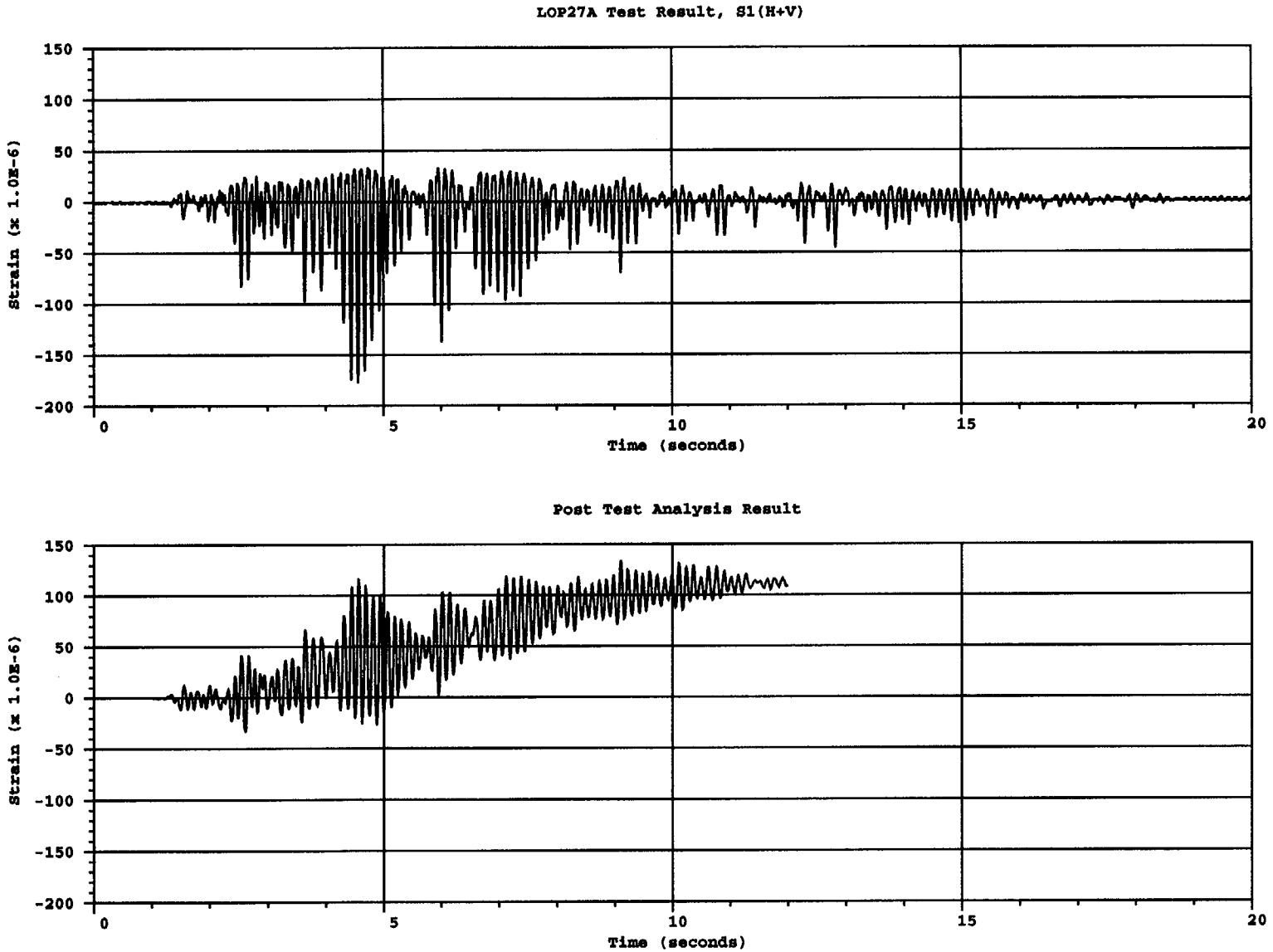

Figure B.12 Comparison of hoop liner strain near gage LOP27A for S1(H+V) test

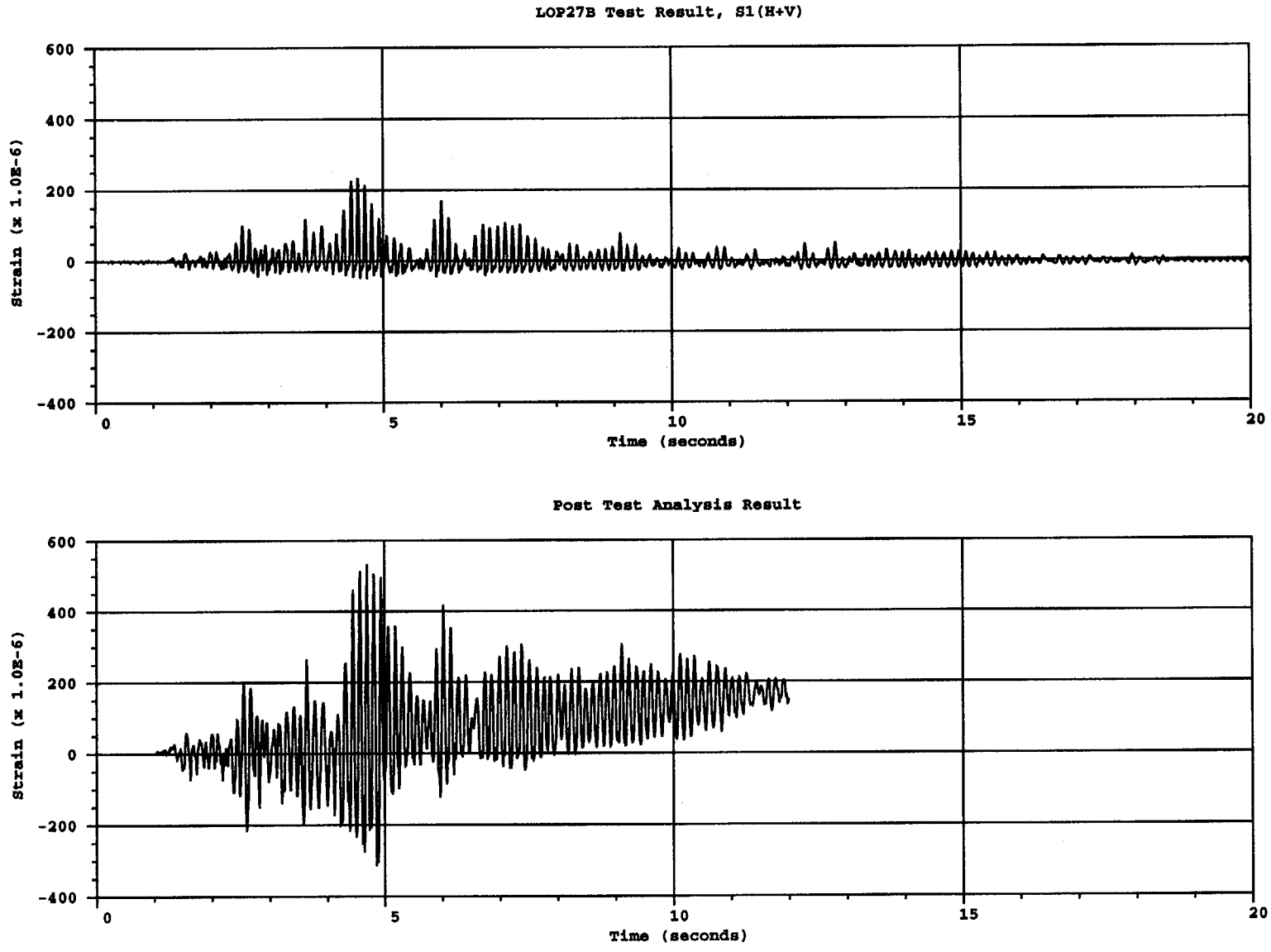

Figure B.13 Comparison of vertical liner strain near gage LOP27B for S1(H+V) test

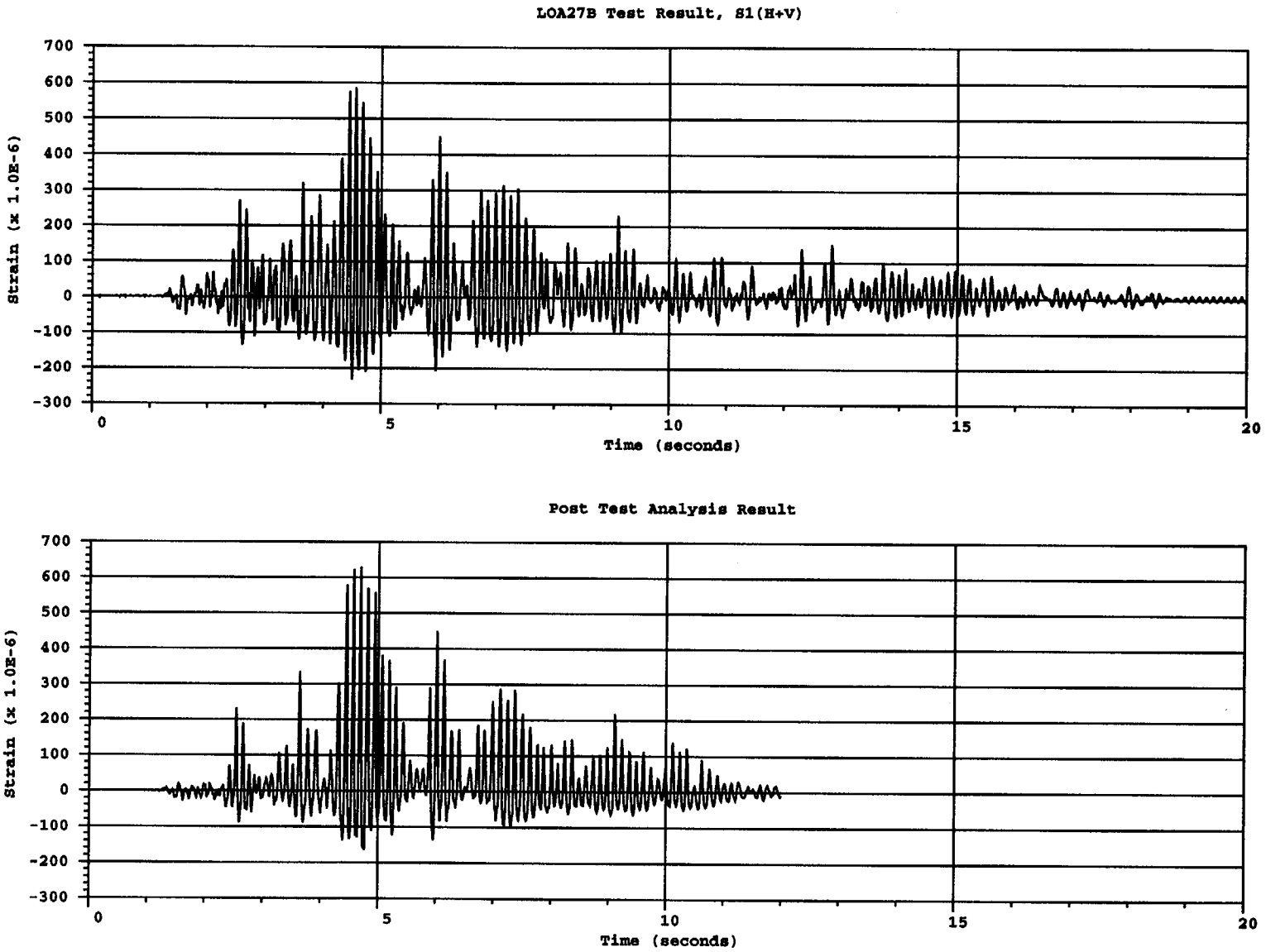

Figure B.14 Comparison of vertical liner strain near gage LOA27b for S1(H+V) test

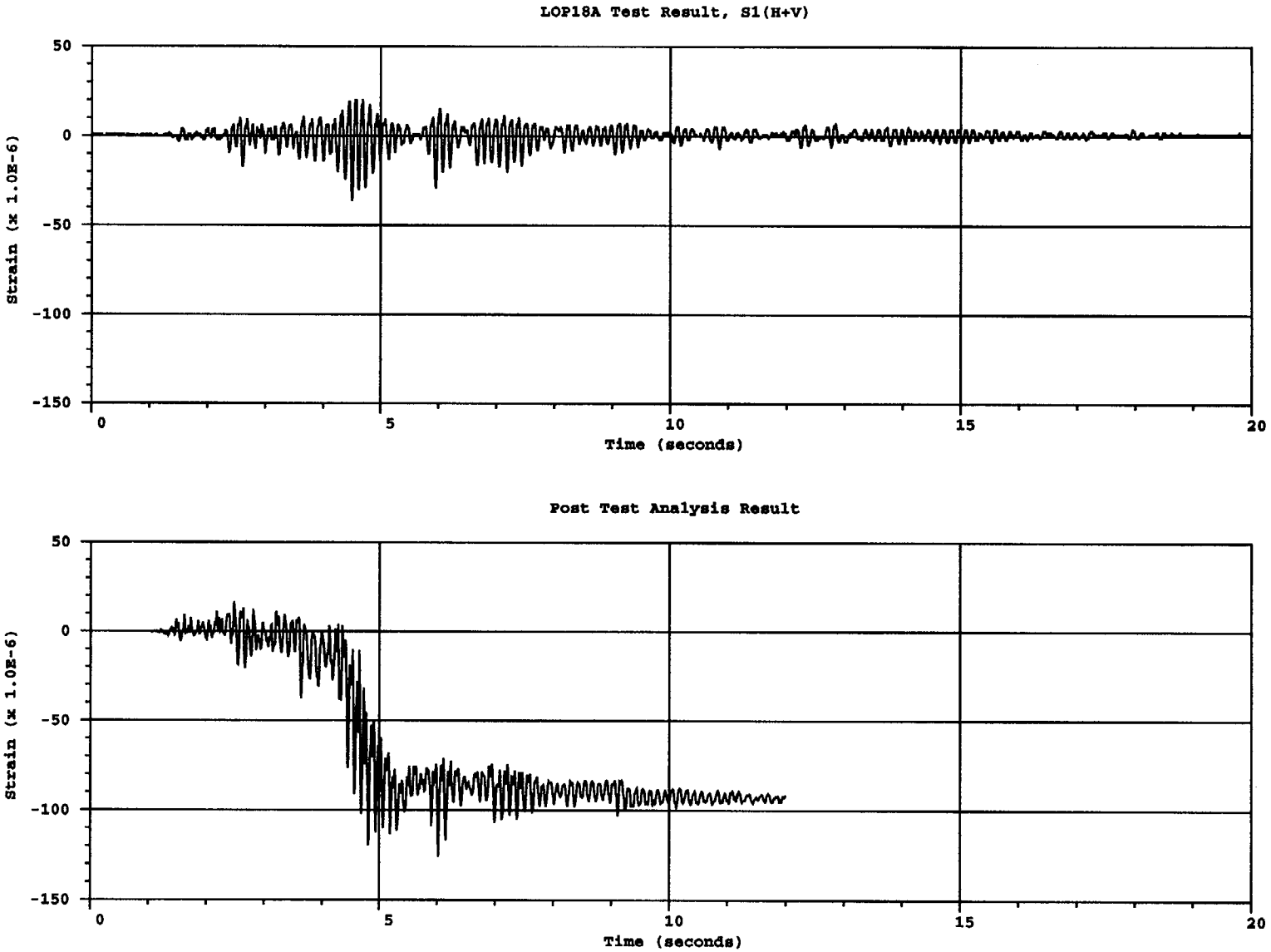

Figure B.15 Comparison of hoop liner strain near gage LOP18a for S1(H+V) test

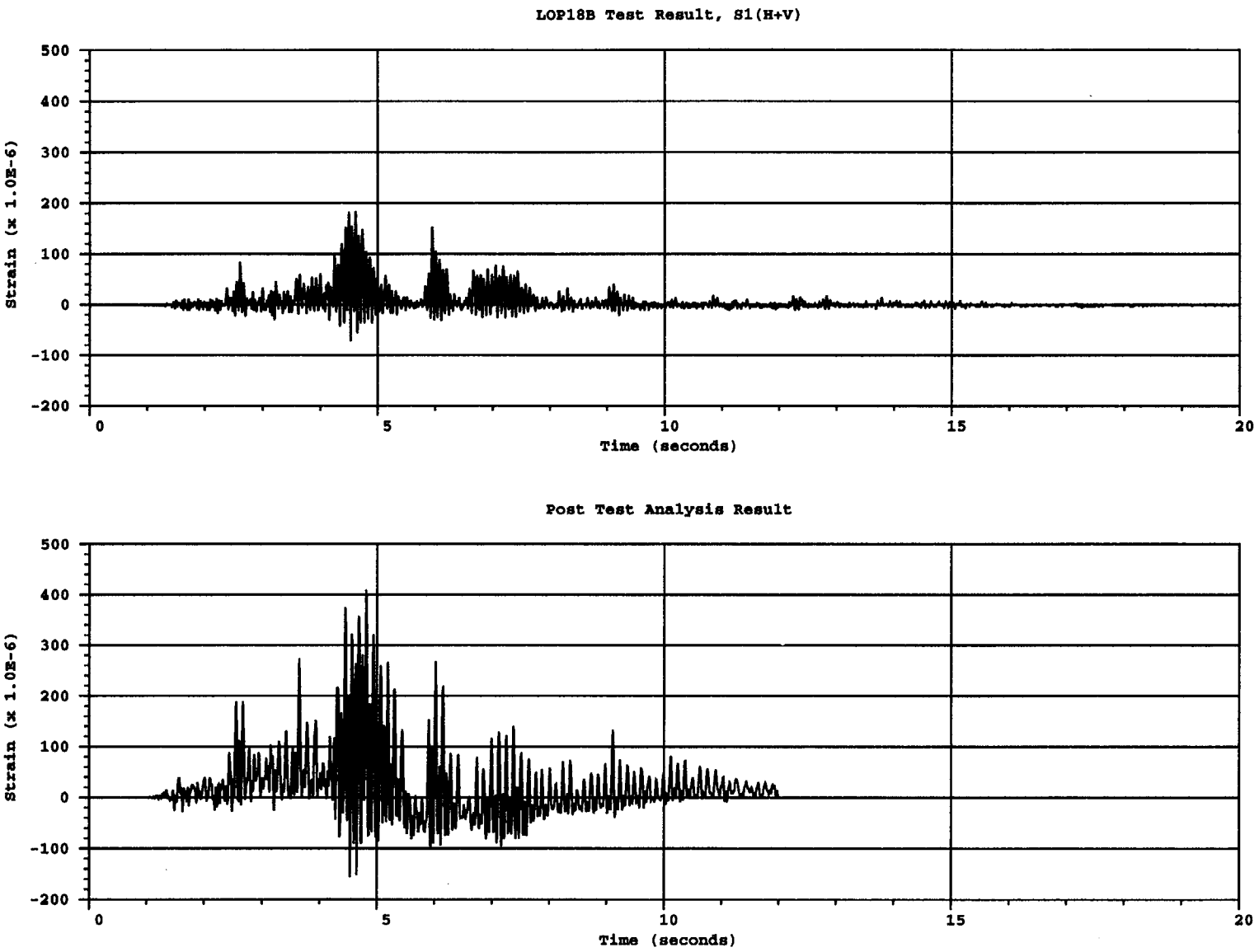

Figure B.16 Comparison of vertical liner strain near gage LOP18b for S1(H+V) test

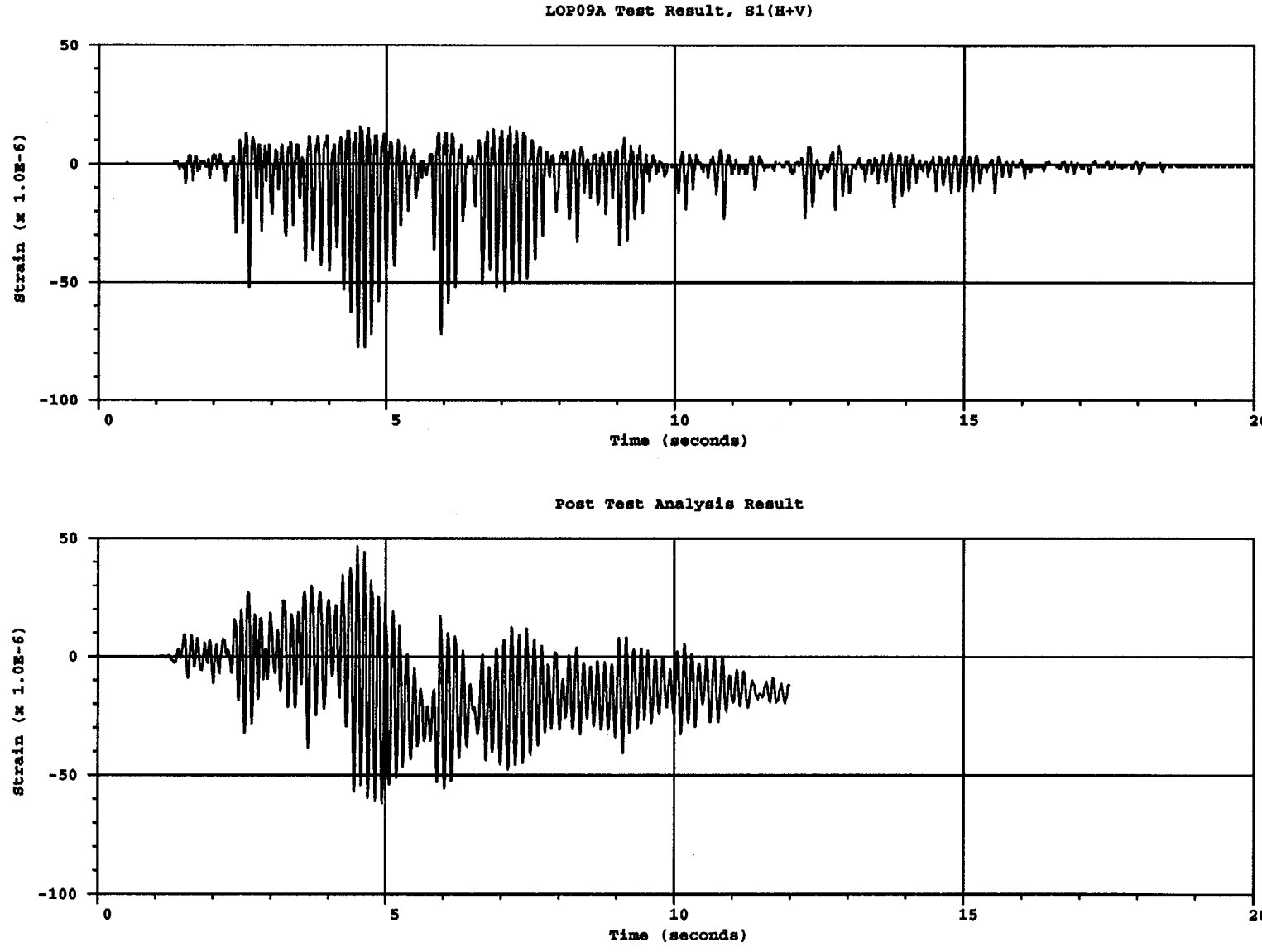

Figure B.17 Comparison of hoop liner strain near gage LOP09a for S1(H+V) test

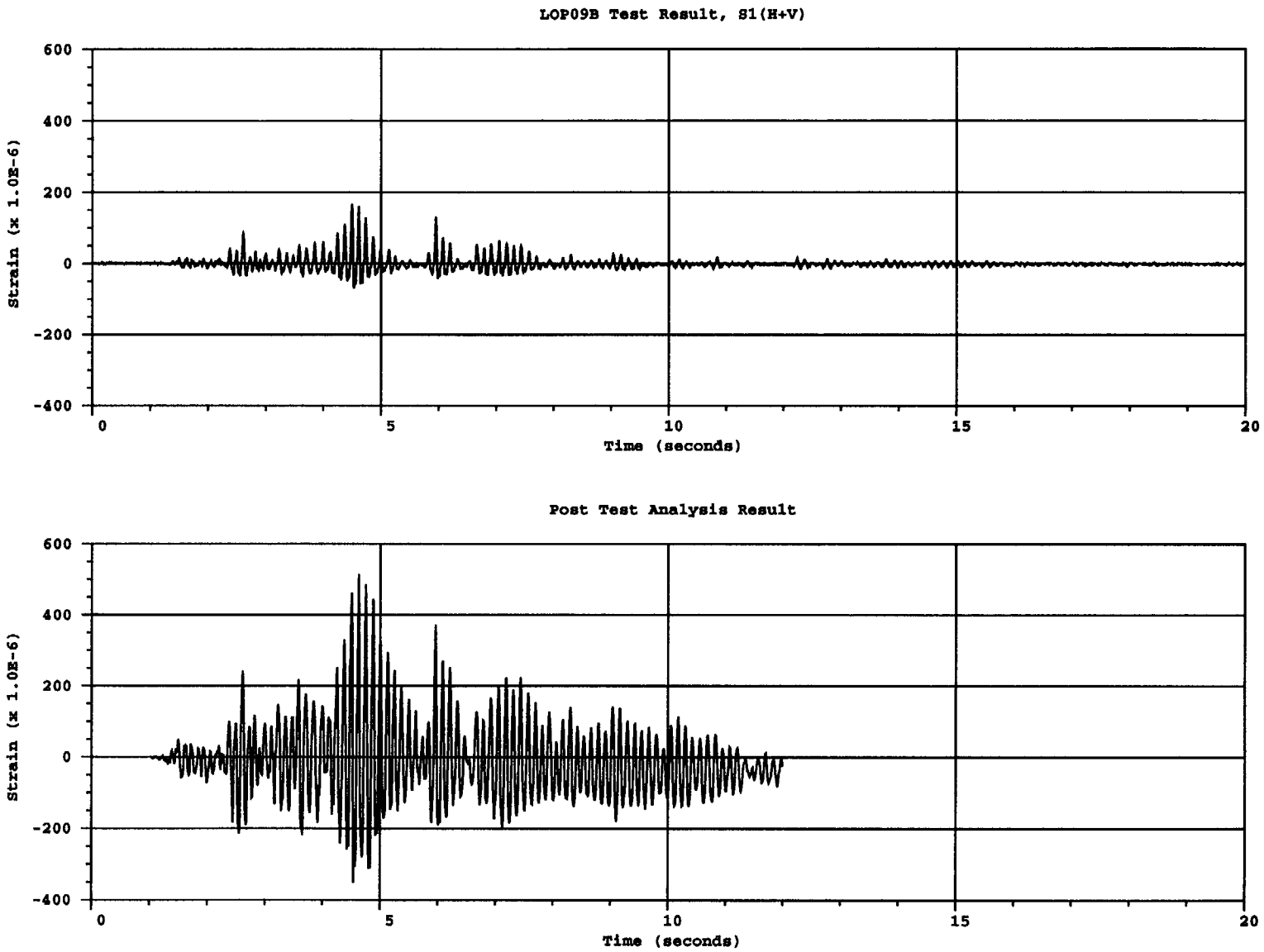

Figure B.18 Comparison of vertical liner strain near gage LOP09b for S1(H+V) test

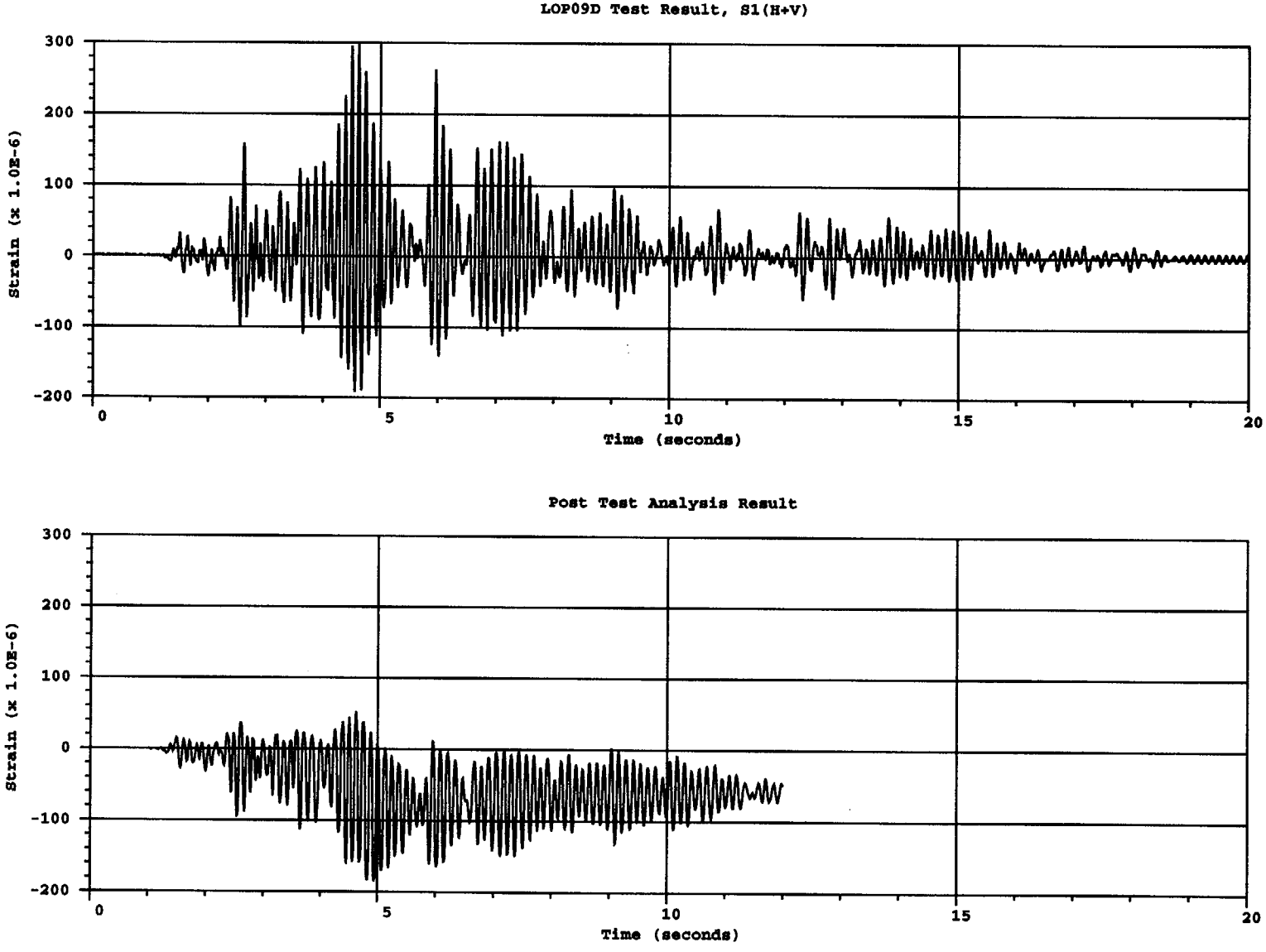

Figure B.19 Comparison of hoop liner strain near gage LOP09d for S1(H+V) test

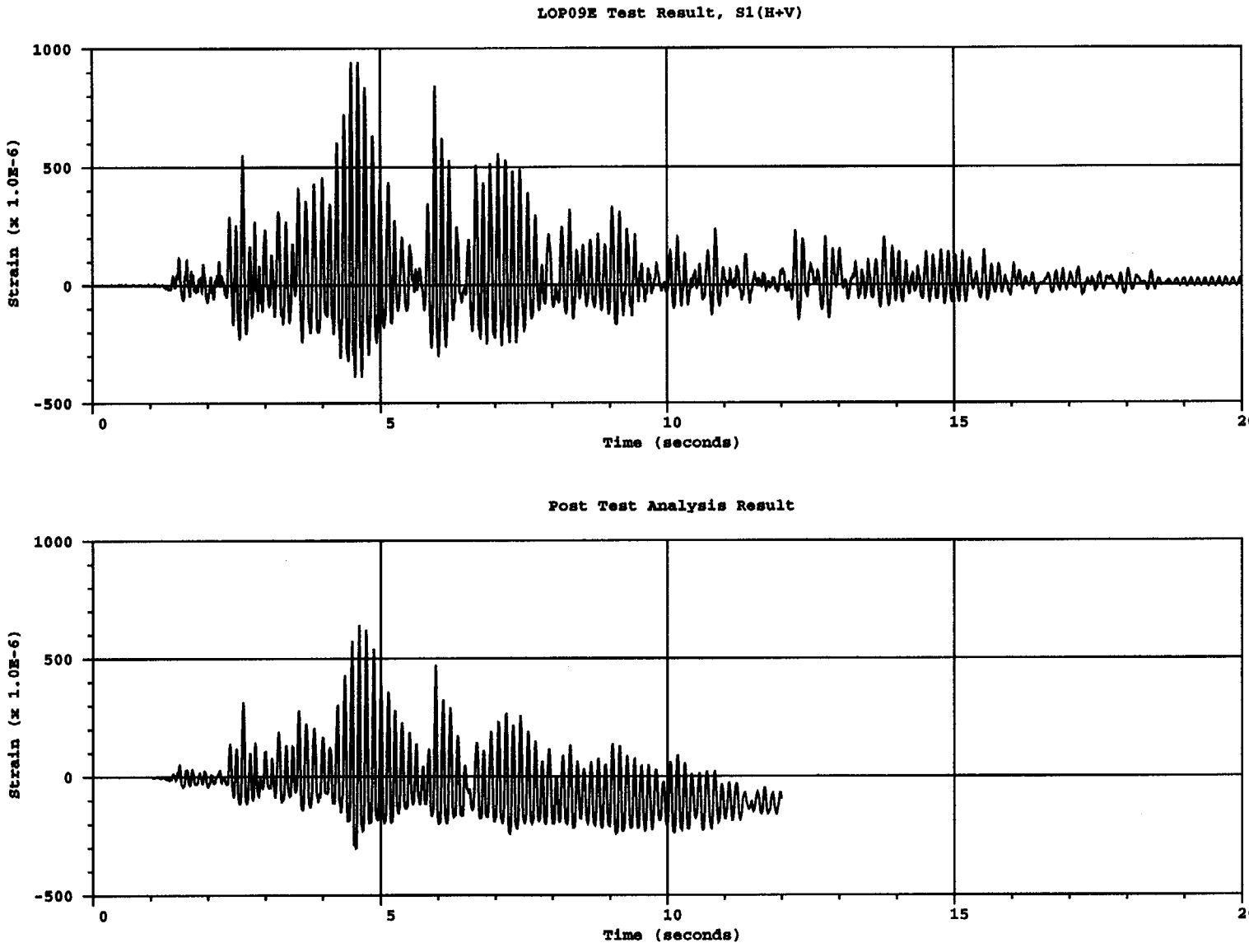

Figure B.20 Comparison of vertical liner strain near gage LOP09e for S1(H+V) test

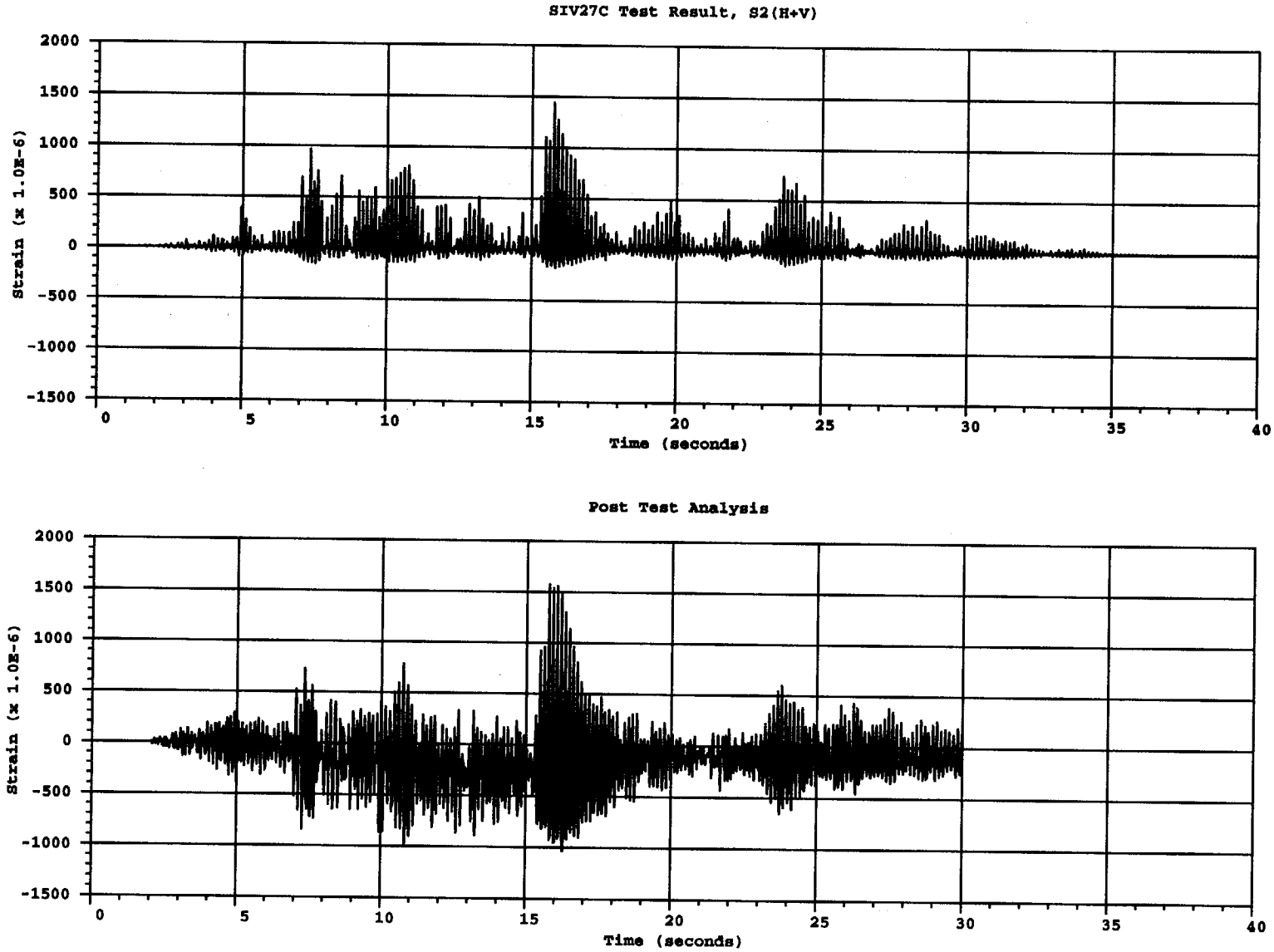

Figure B.21 Comparison of vertical inside rebar strain near gage SIV27c for S2(H+V) test

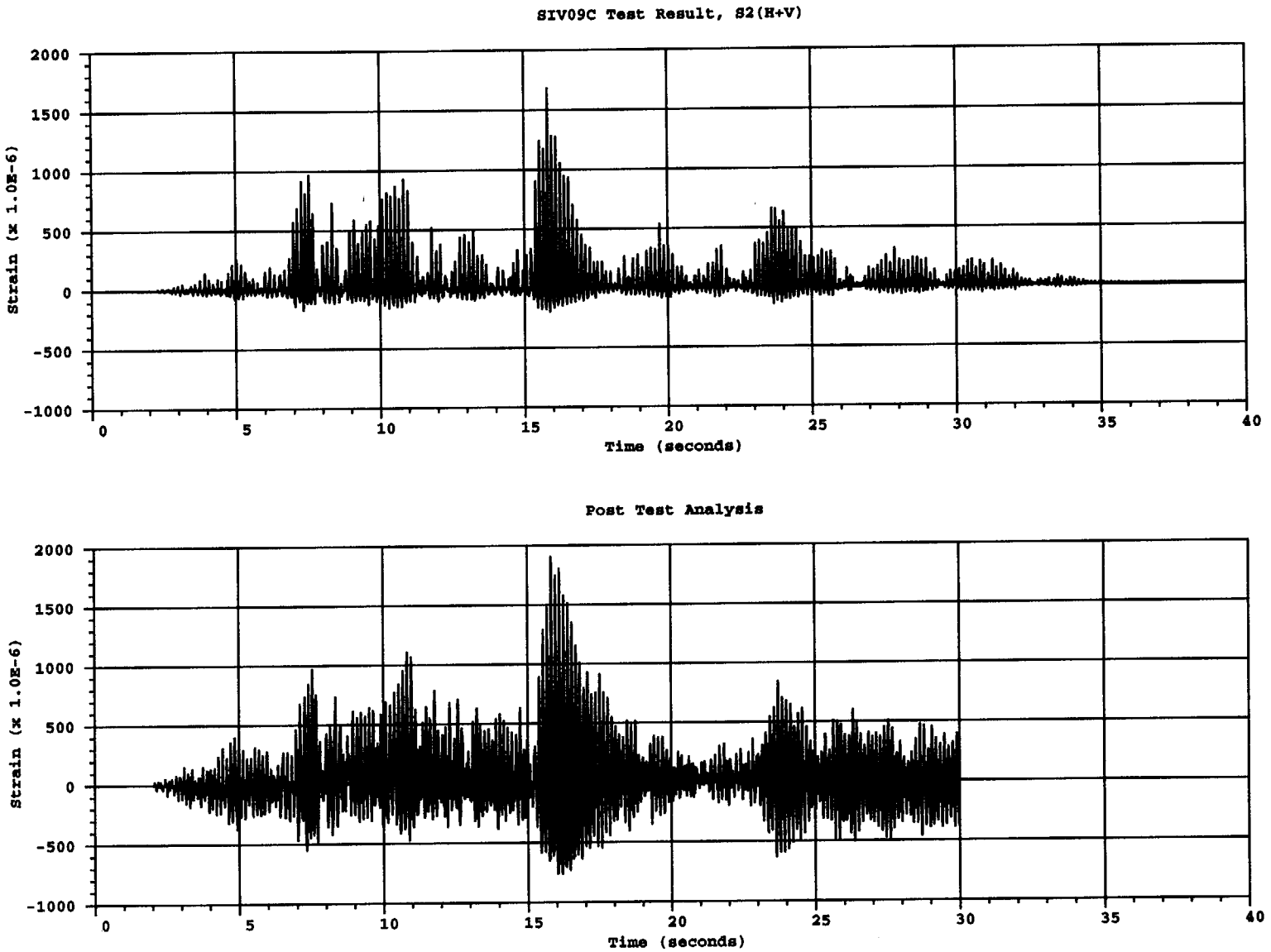

Figure B.22 Comparison of vertical outside rebar strain near gage SIV09c for S2(H+V) test

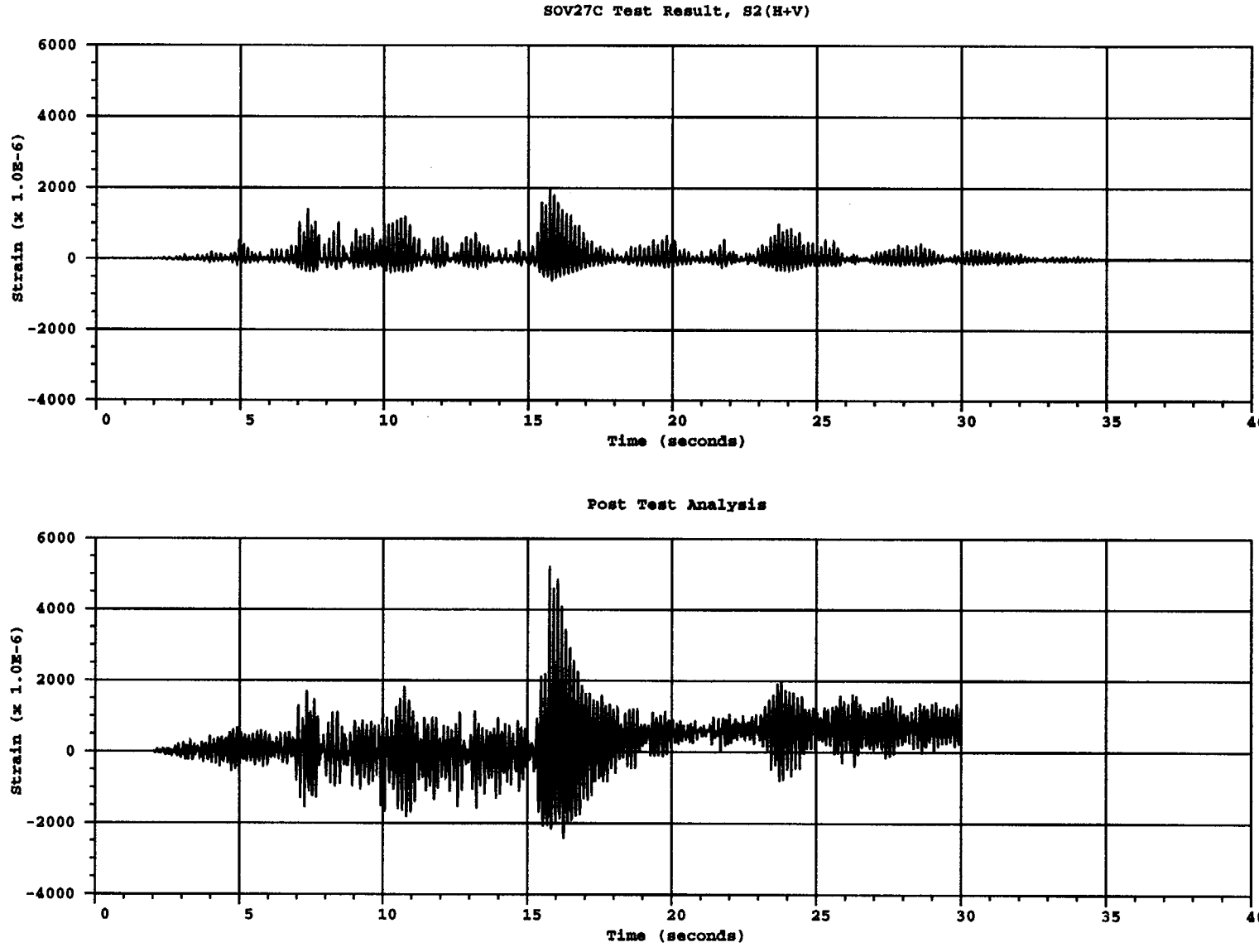

Figure B.23 Comparison of vertical outside rebar strain near gage SOV27c for S2(H+V) test

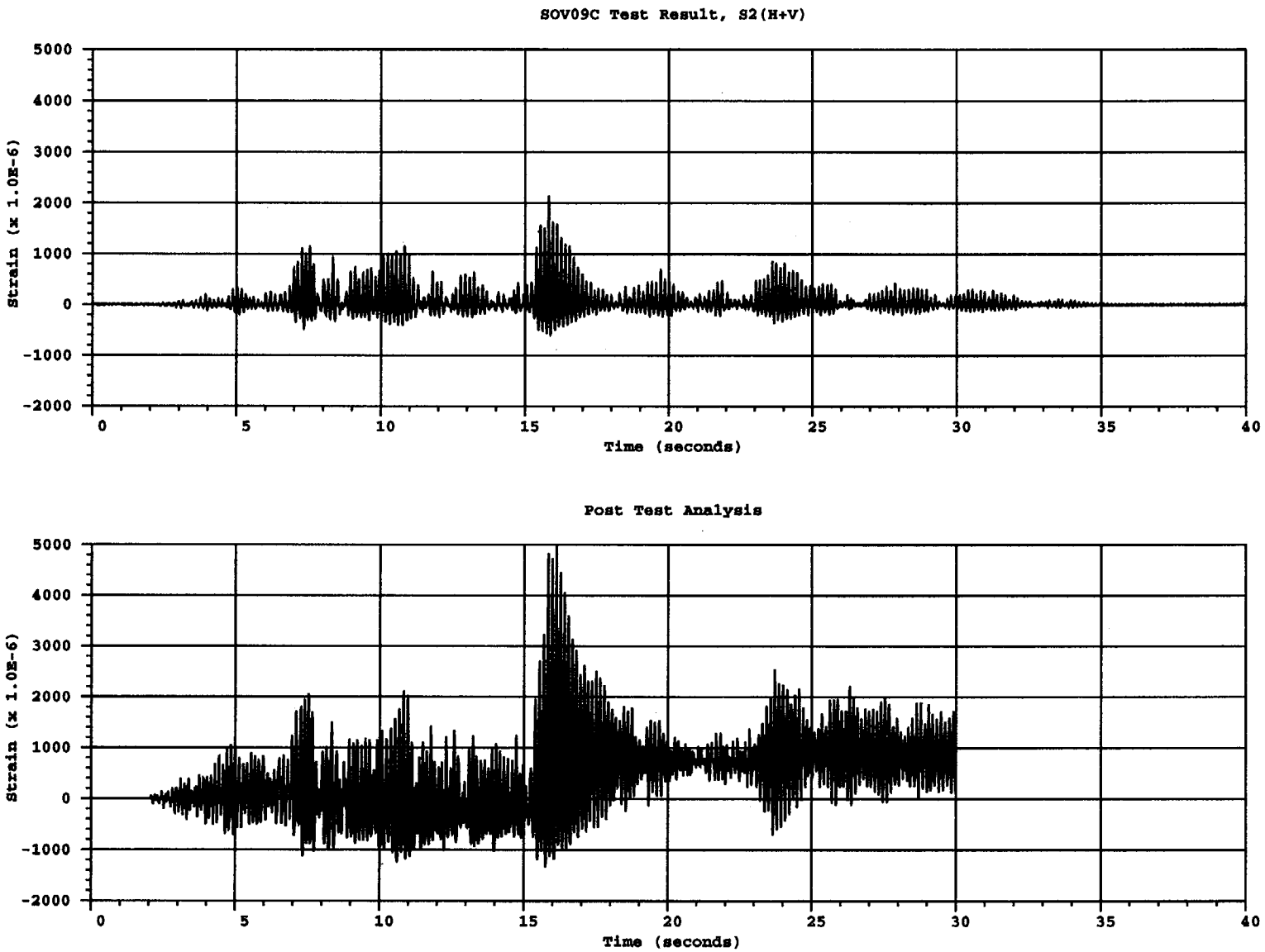

Figure B.24 Comparison of vertical outside rebar strain near gage SOV09c for S2(H+V) test

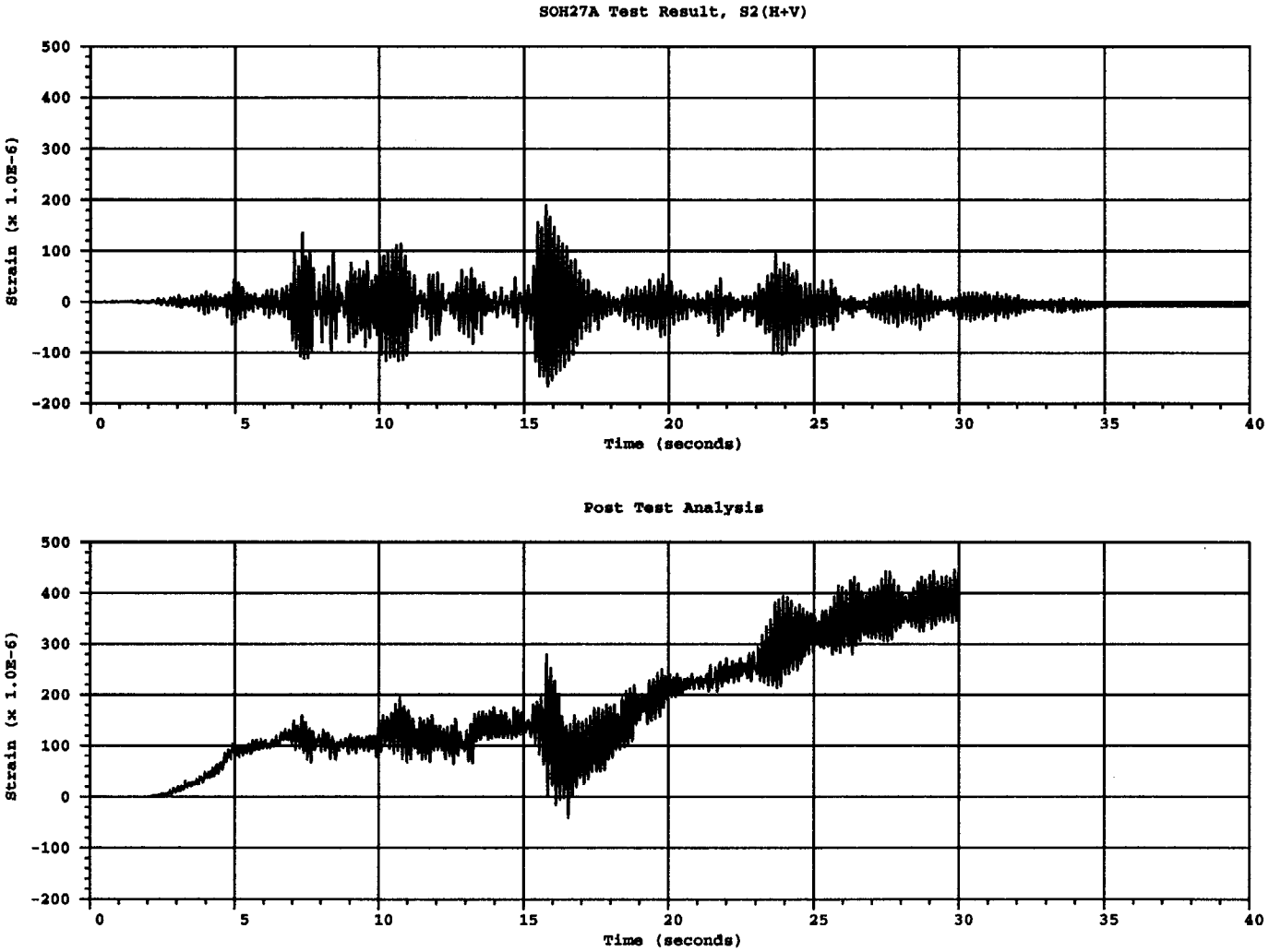

Figure B.25 Comparison of hoop outside rebar strain near gage SOH27a for S2(H+V) test

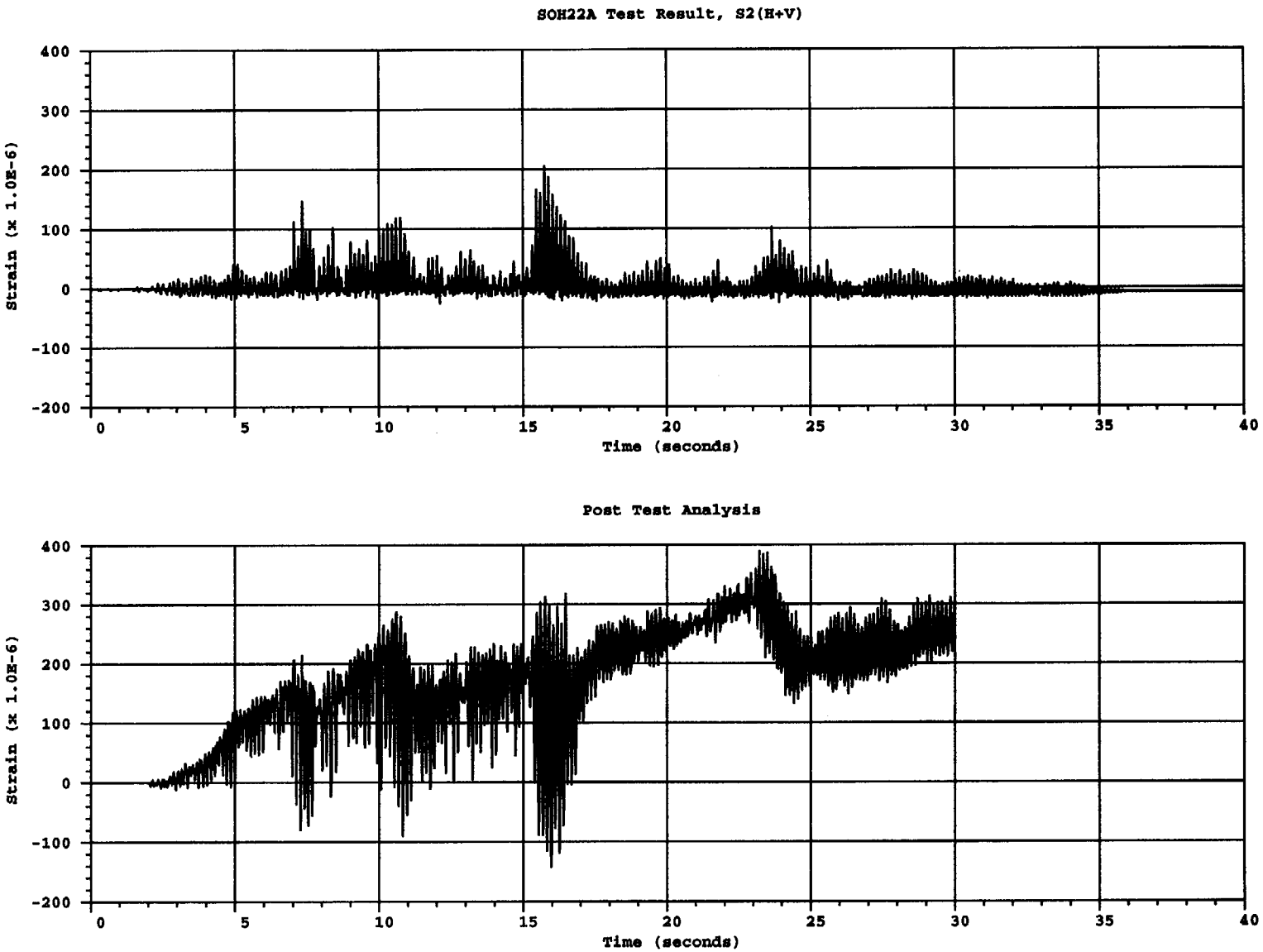

Figure B.26 Comparison of hoop outside rebar strain near gage SOH22a for S2(H+V) test

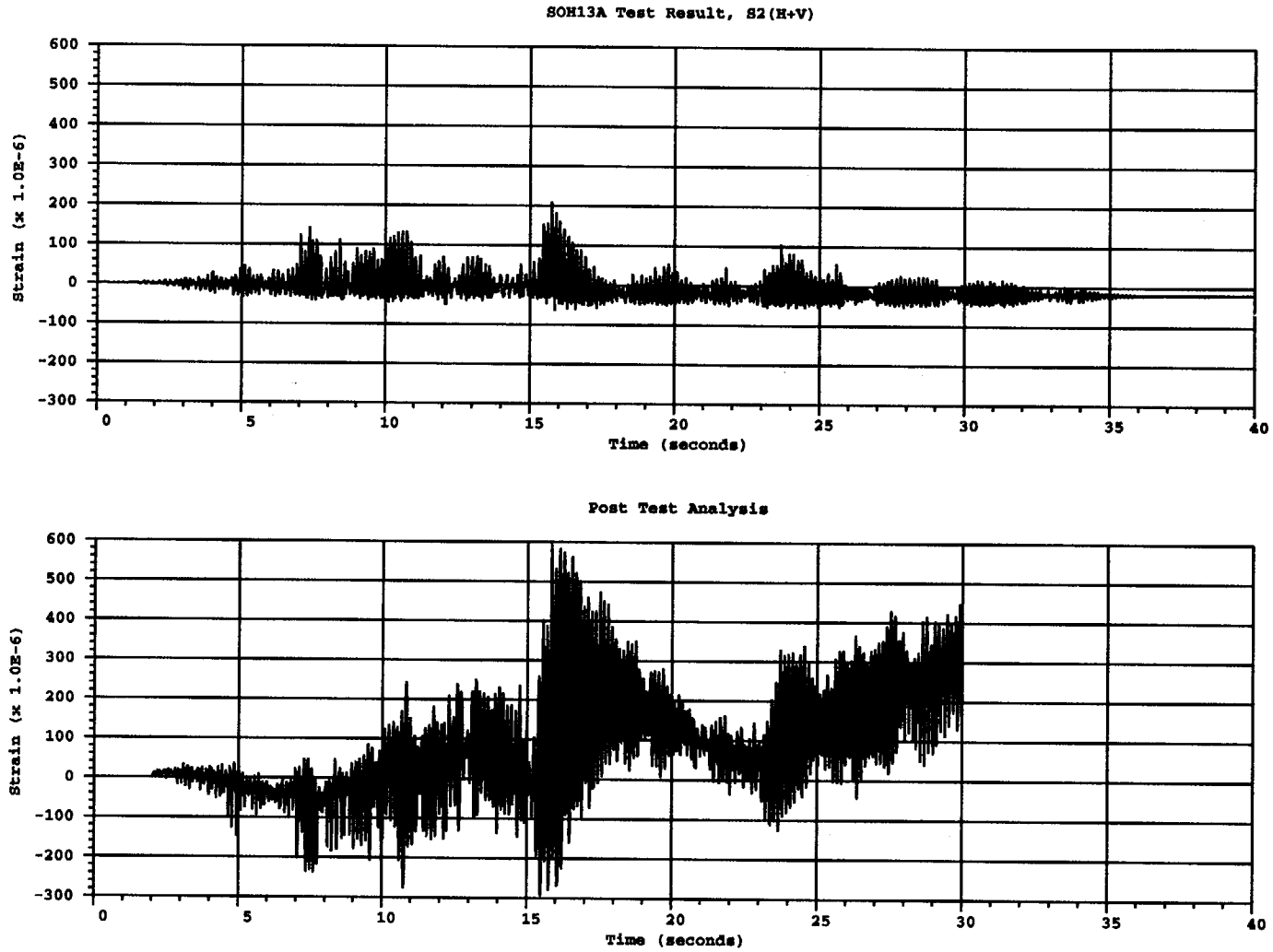

Figure B.27 Comparison of hoop outside rebar strain near gage SOH13a for S2(H+V) test

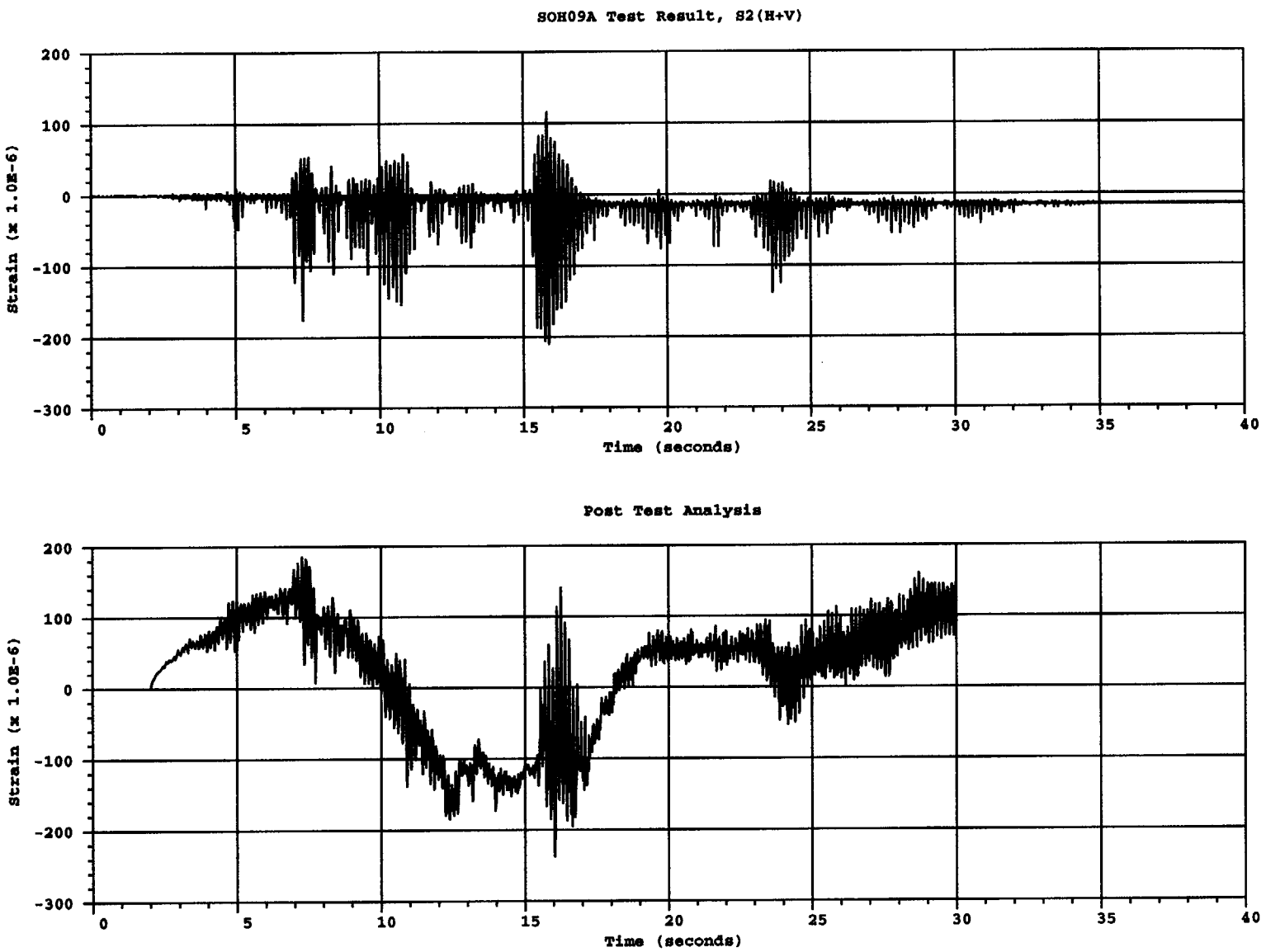

Figure B.28 Comparison of hoop outside rebar strain near gage SOH09a for S2(H+V) test

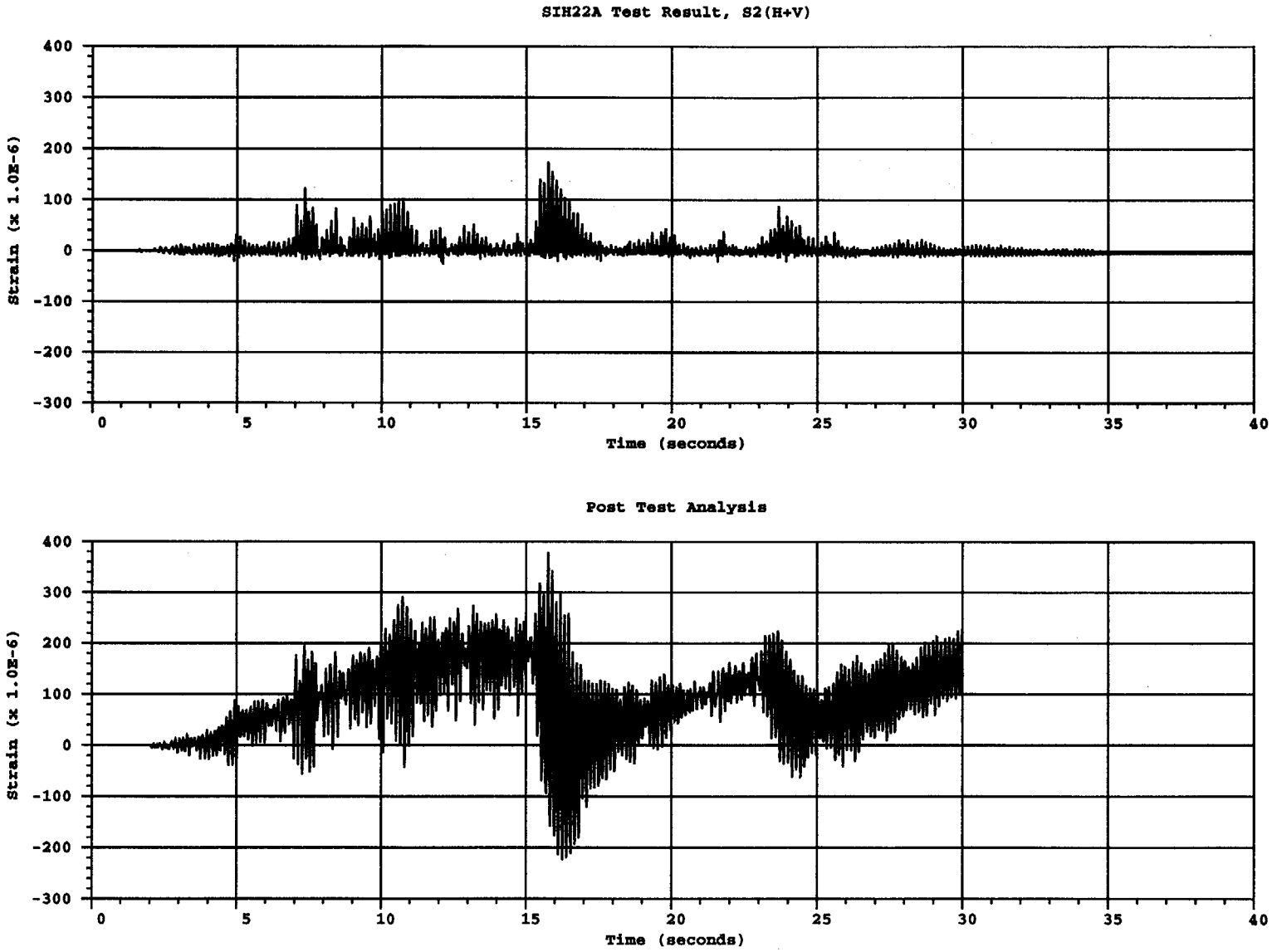

Figure B.29 Comparison of hoop inside rebar strain near gage SIH22a for S2(H+V) test

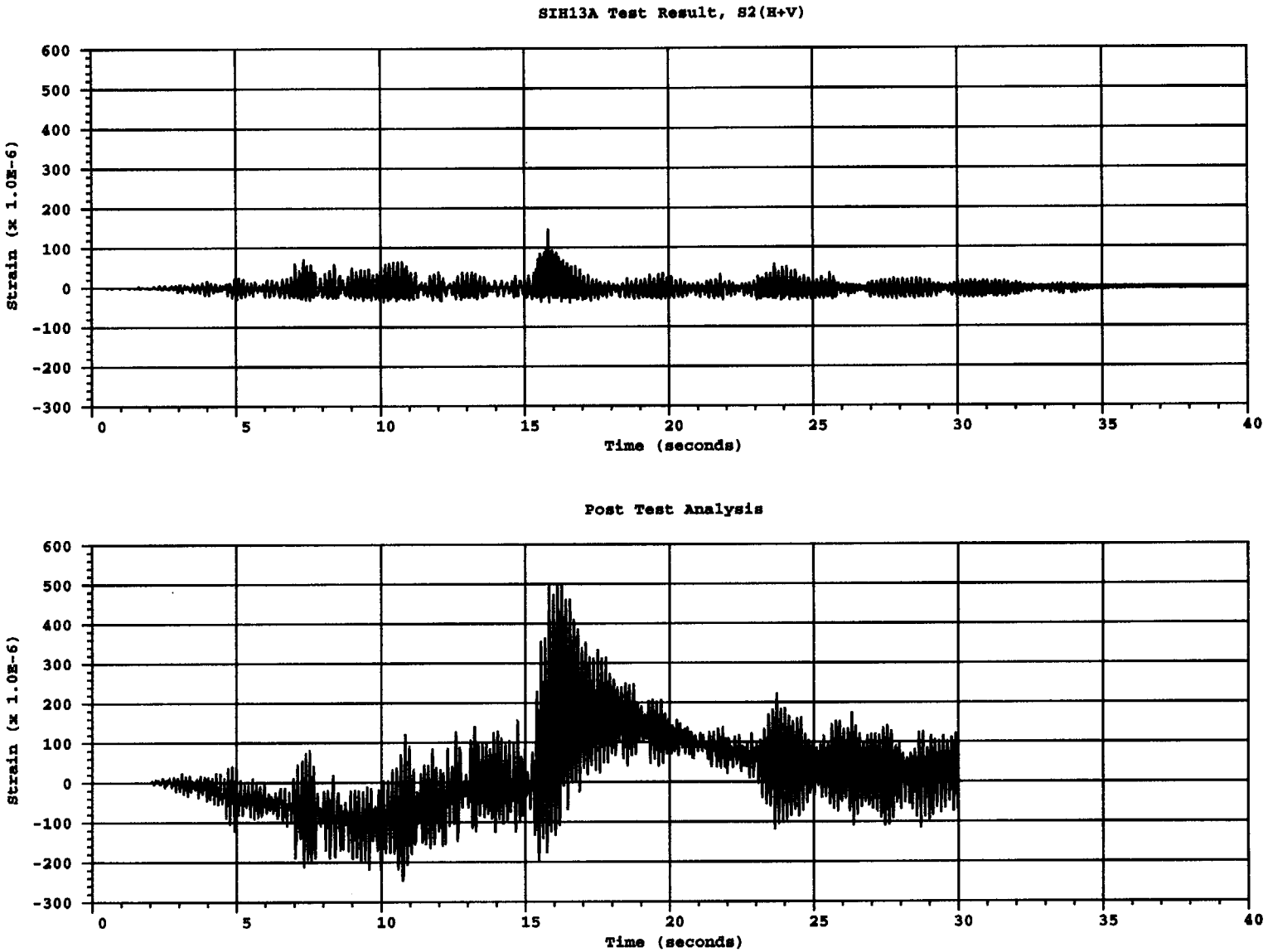

Figure B.30 Comparison of hoop inside rebar strain near gage SIH13a for S2(H+V) test

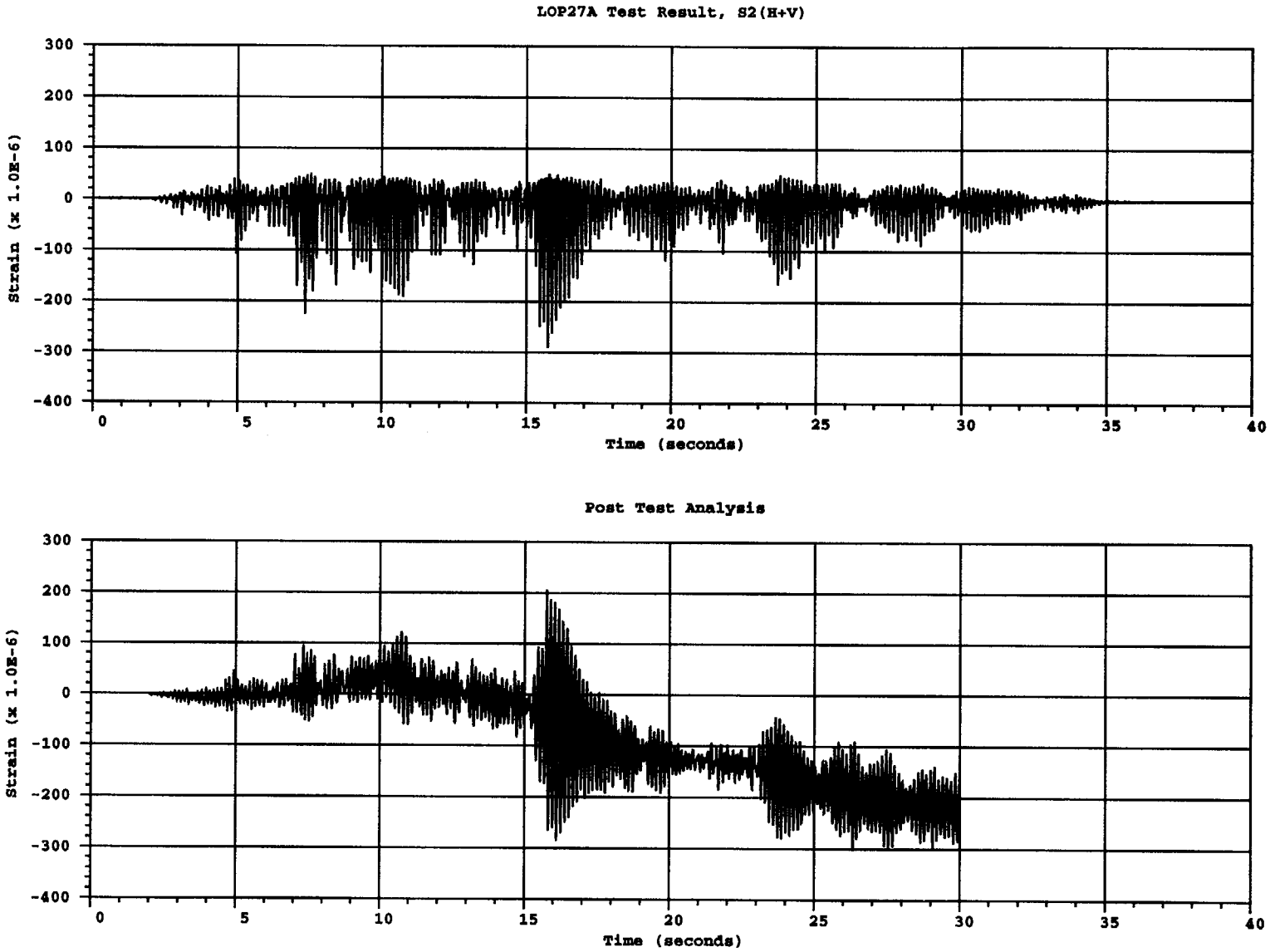

Figure B.31 Comparison of hoop liner rebar strain near gage LOP27a for S2(H+V) test

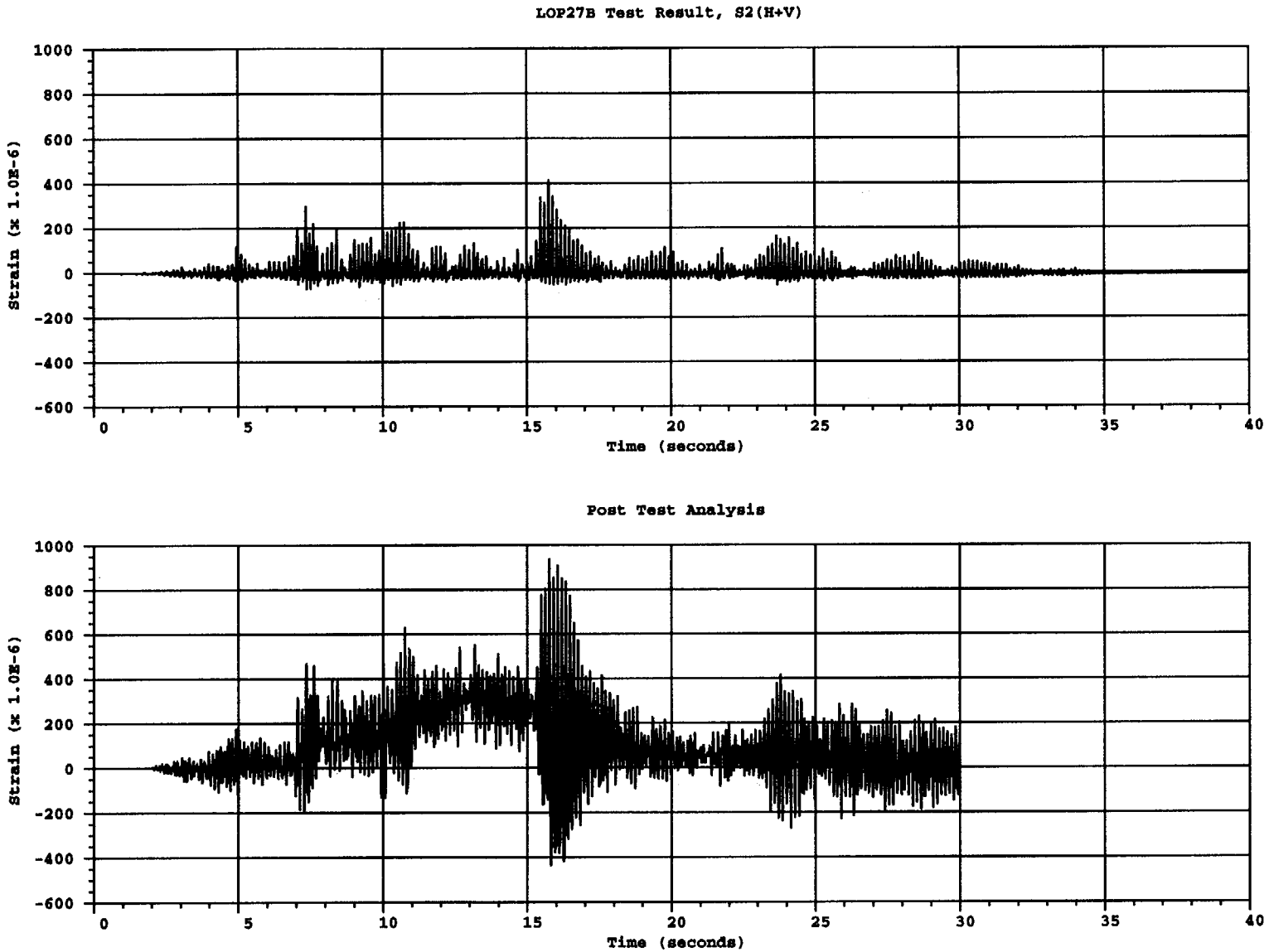

Figure B.32 Comparison of vertical liner rebar strain near gage LOP27b for S2(H+V) test

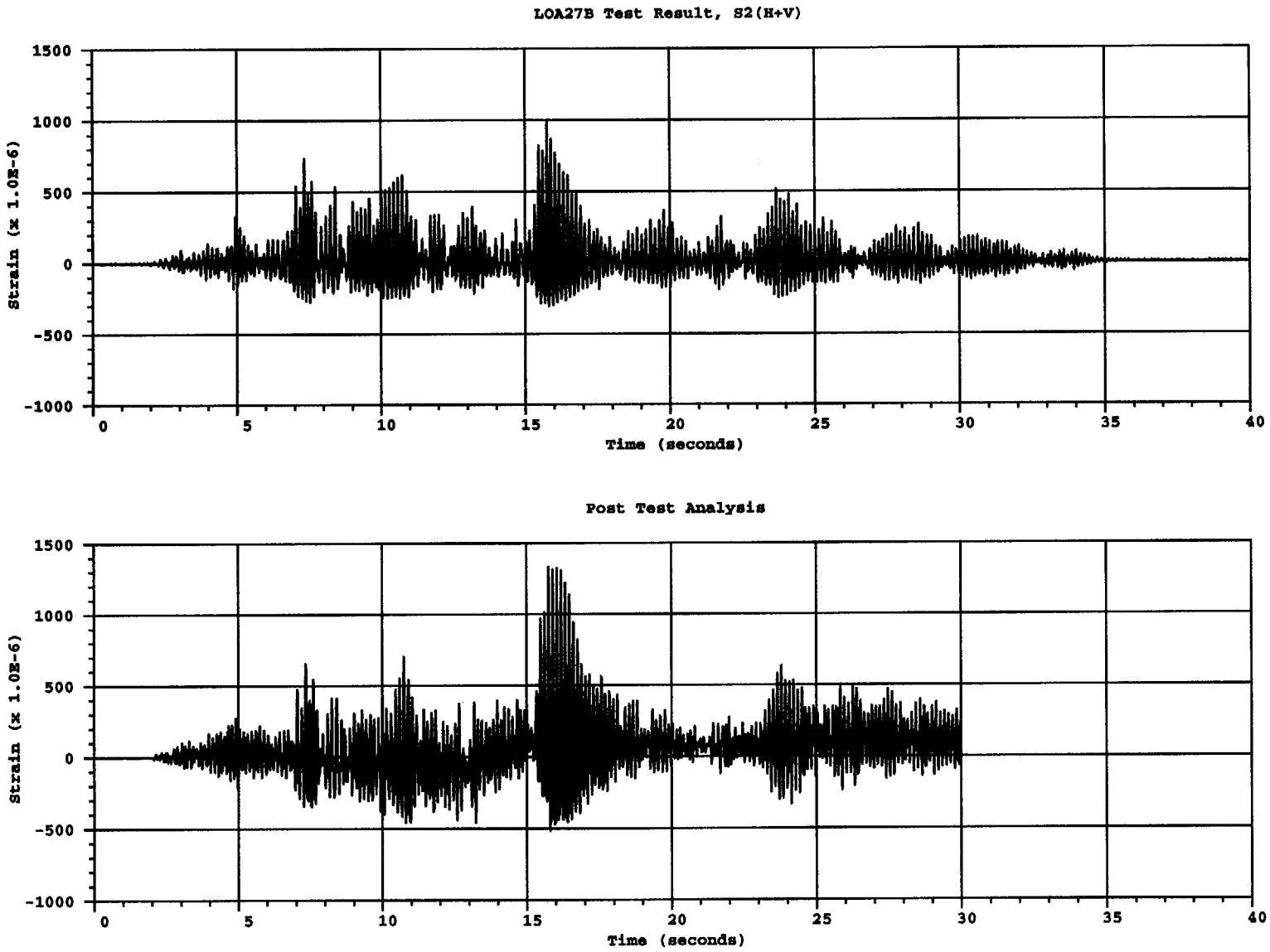

Figure B.33 Comparison of vertical liner rebar strain near gage LOA27b for S2(H+V) test

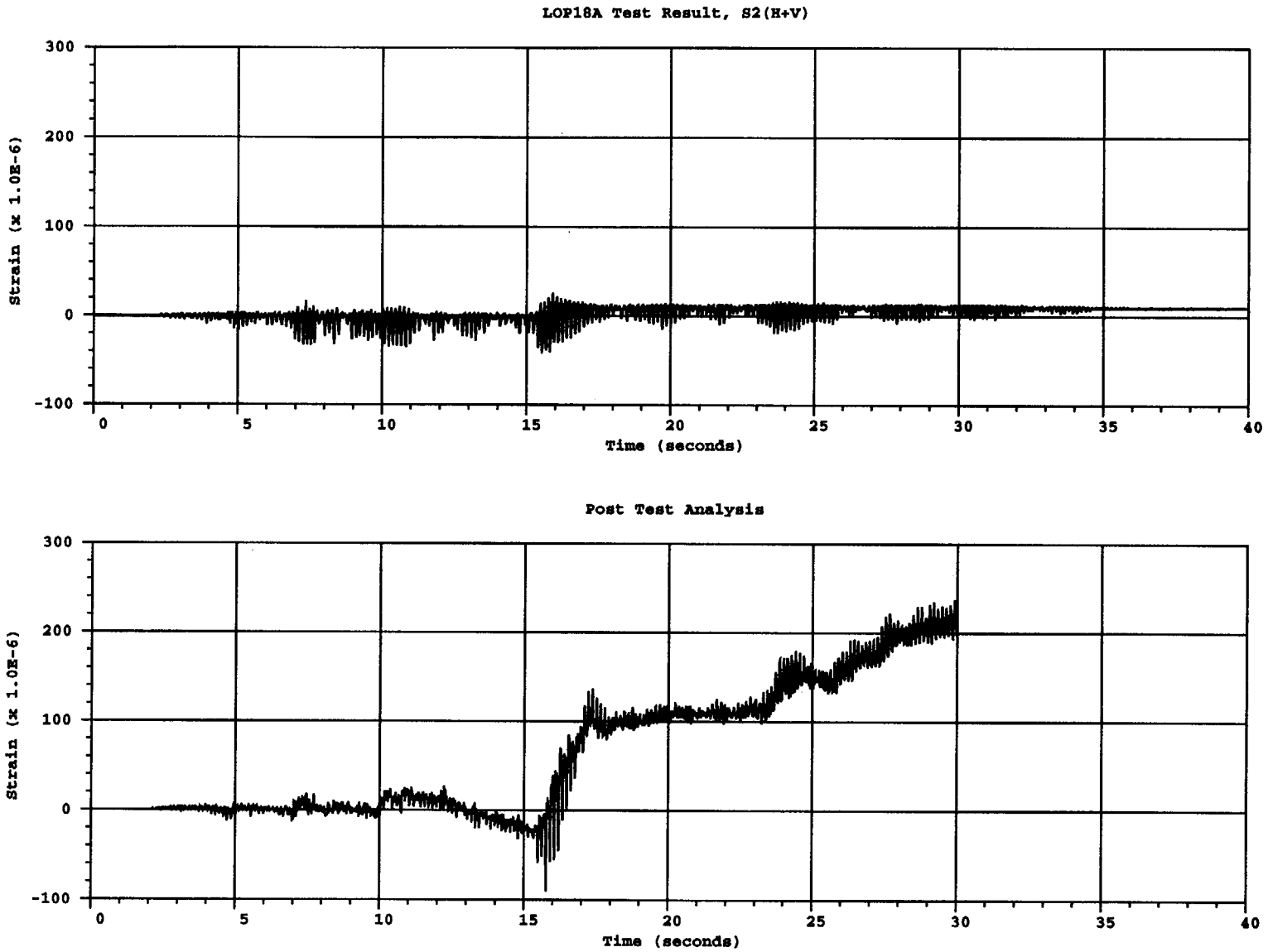

Figure B.34 Comparison of hoop liner rebar strain near gage LOP18a for S2(H+V) test

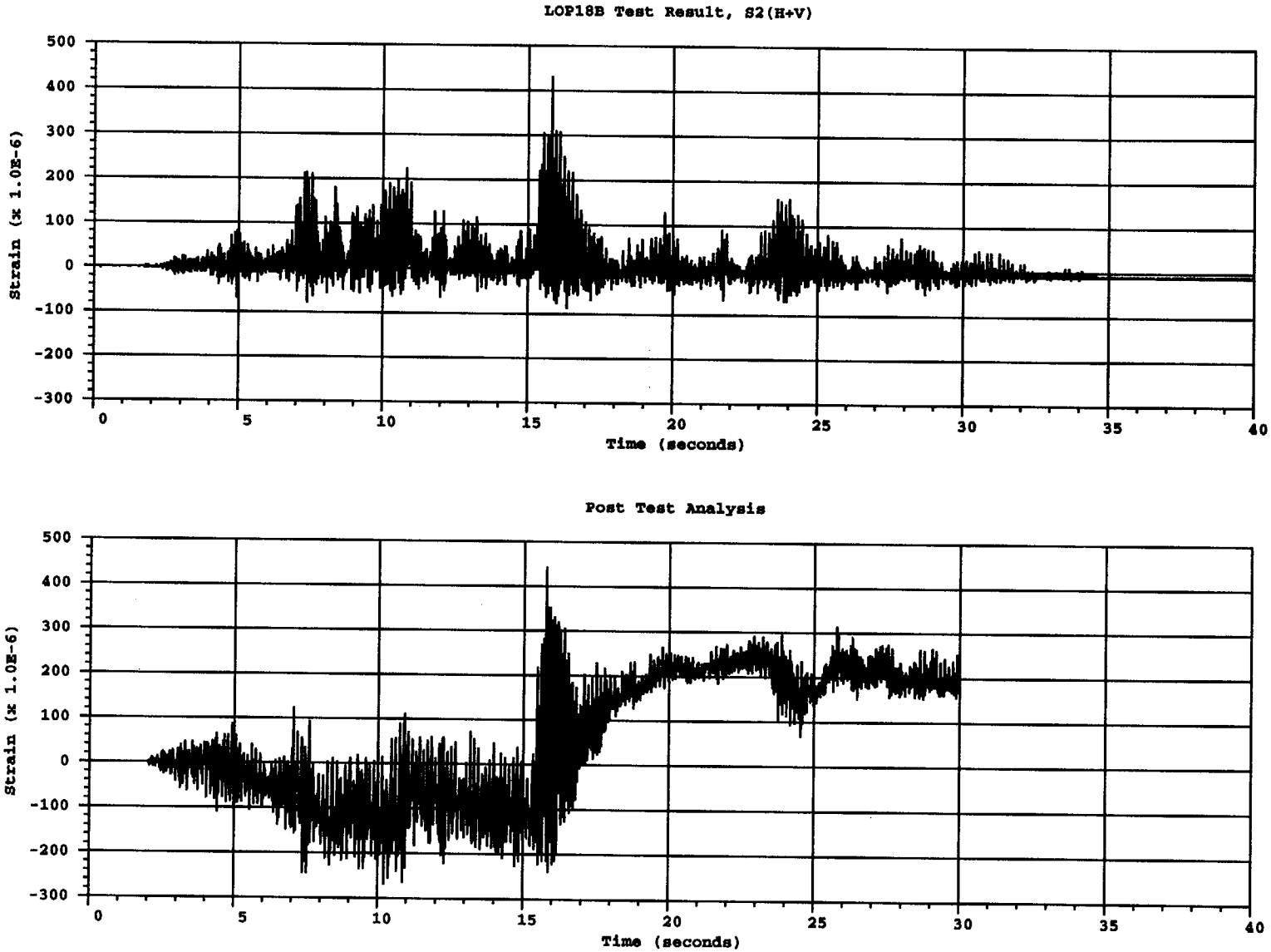

Figure B.35 Comparison of vertical liner strain near gage LOP18B for S2(H+V) test

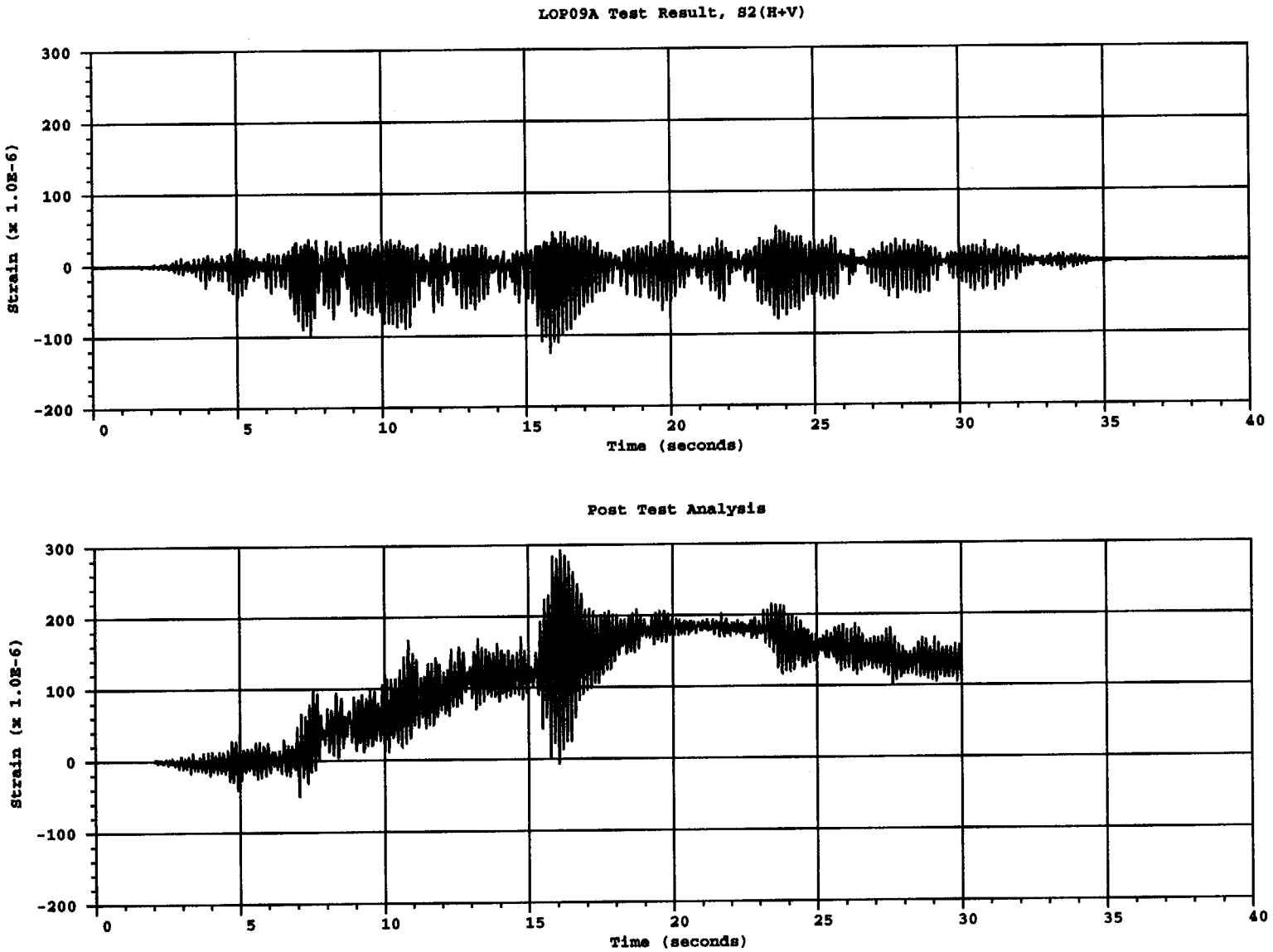

Figure B.36 Comparison of hoop liner strain near gage LOP09A for S2(H+V) test

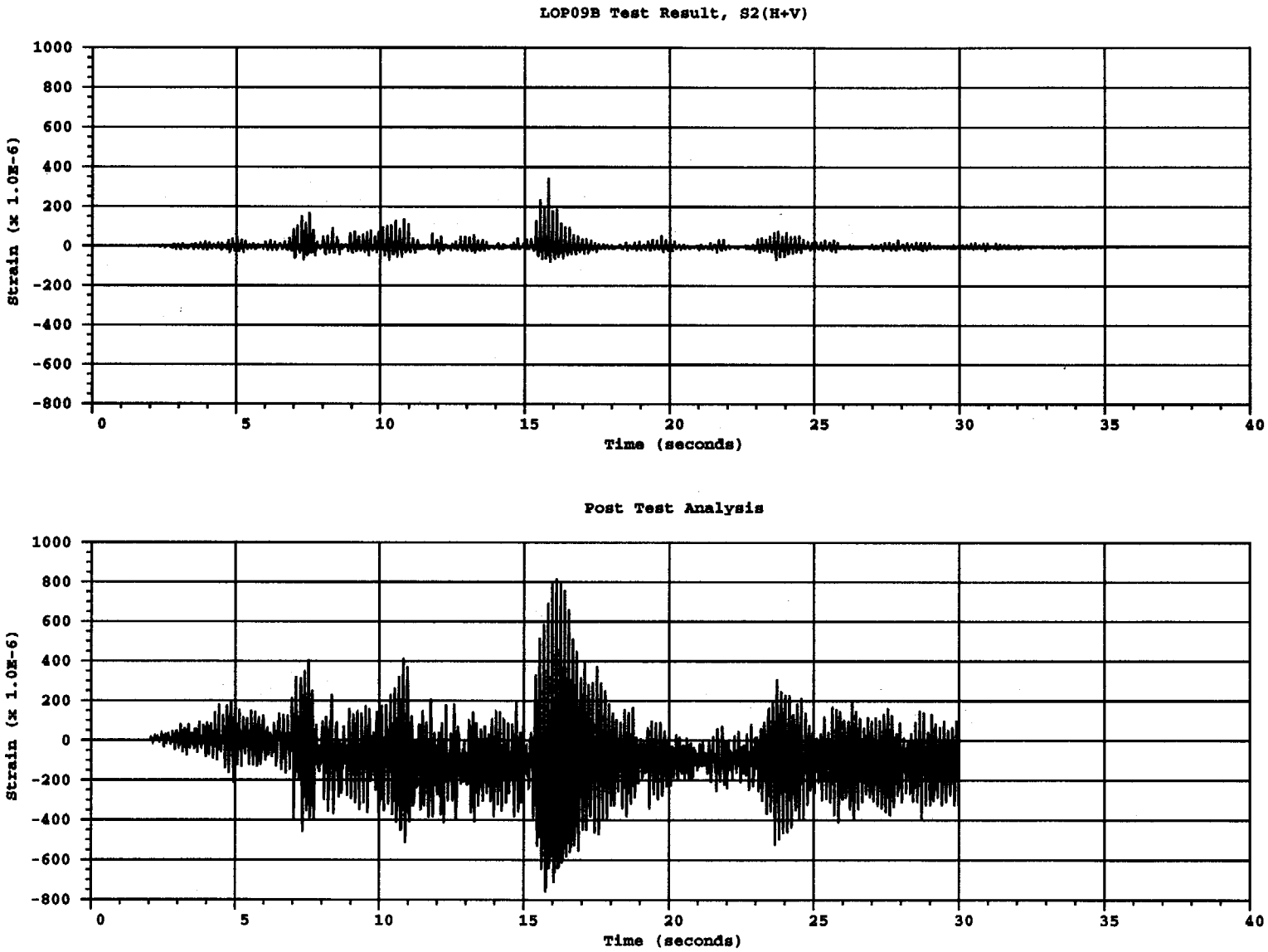

Figure B.37 Comparison of vertical liner strain near gage LOP09B for S2(H+V) test

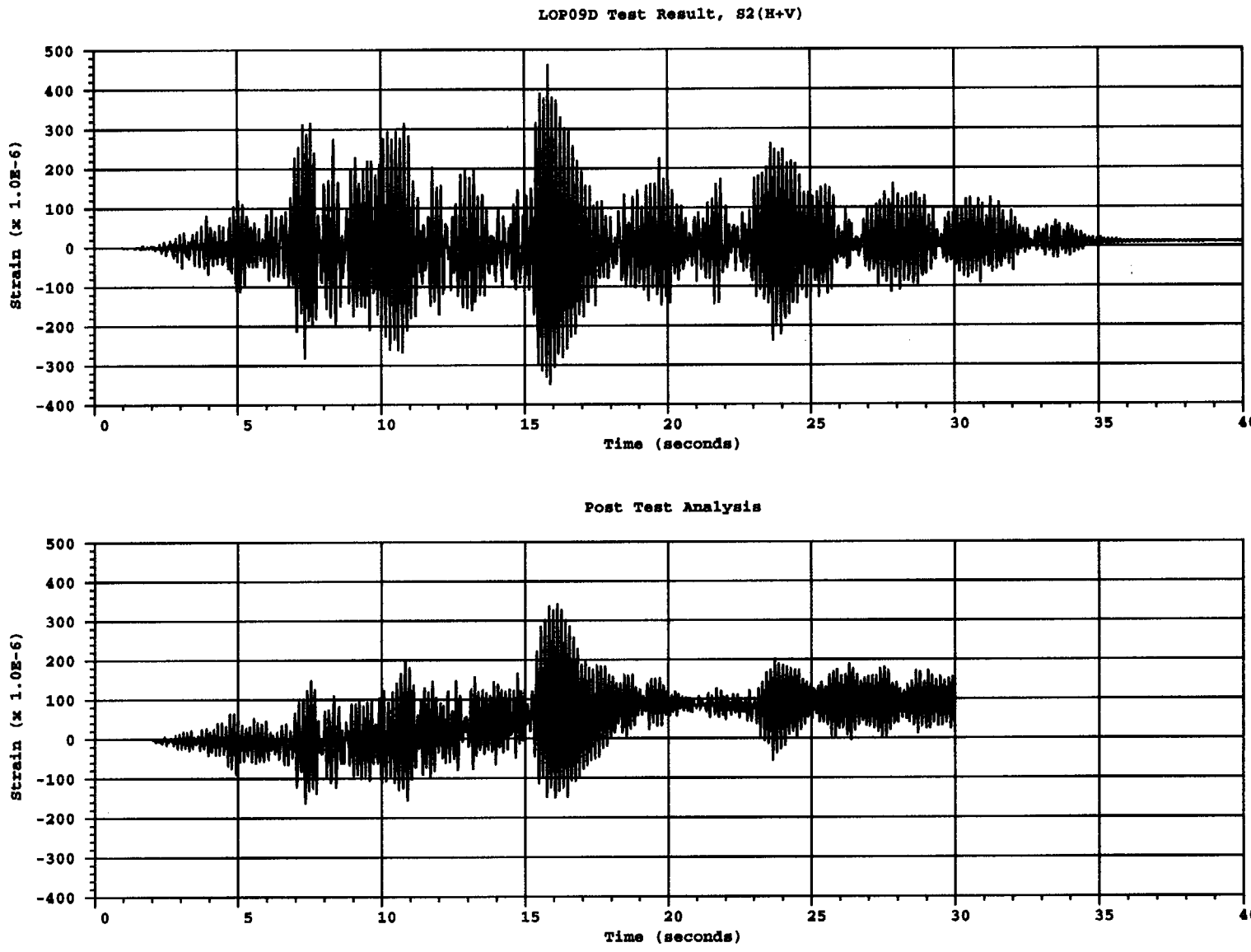

Figure B.38 Comparison of hoop liner strain near gage LOP09D for S2(H+V) test

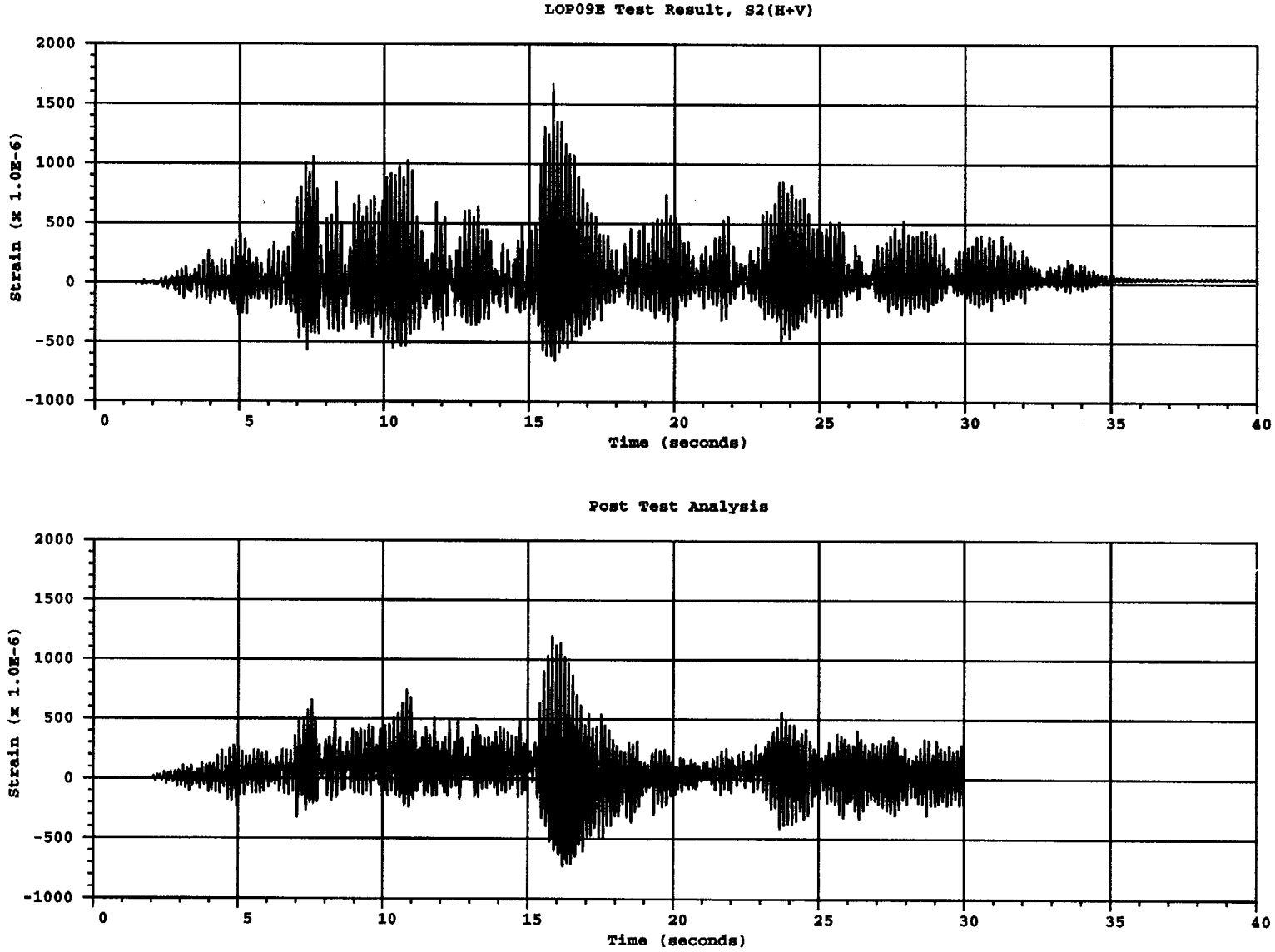

Figure B.39 Comparison of hoop liner strain near gage LOP09E for S2(H+V) test

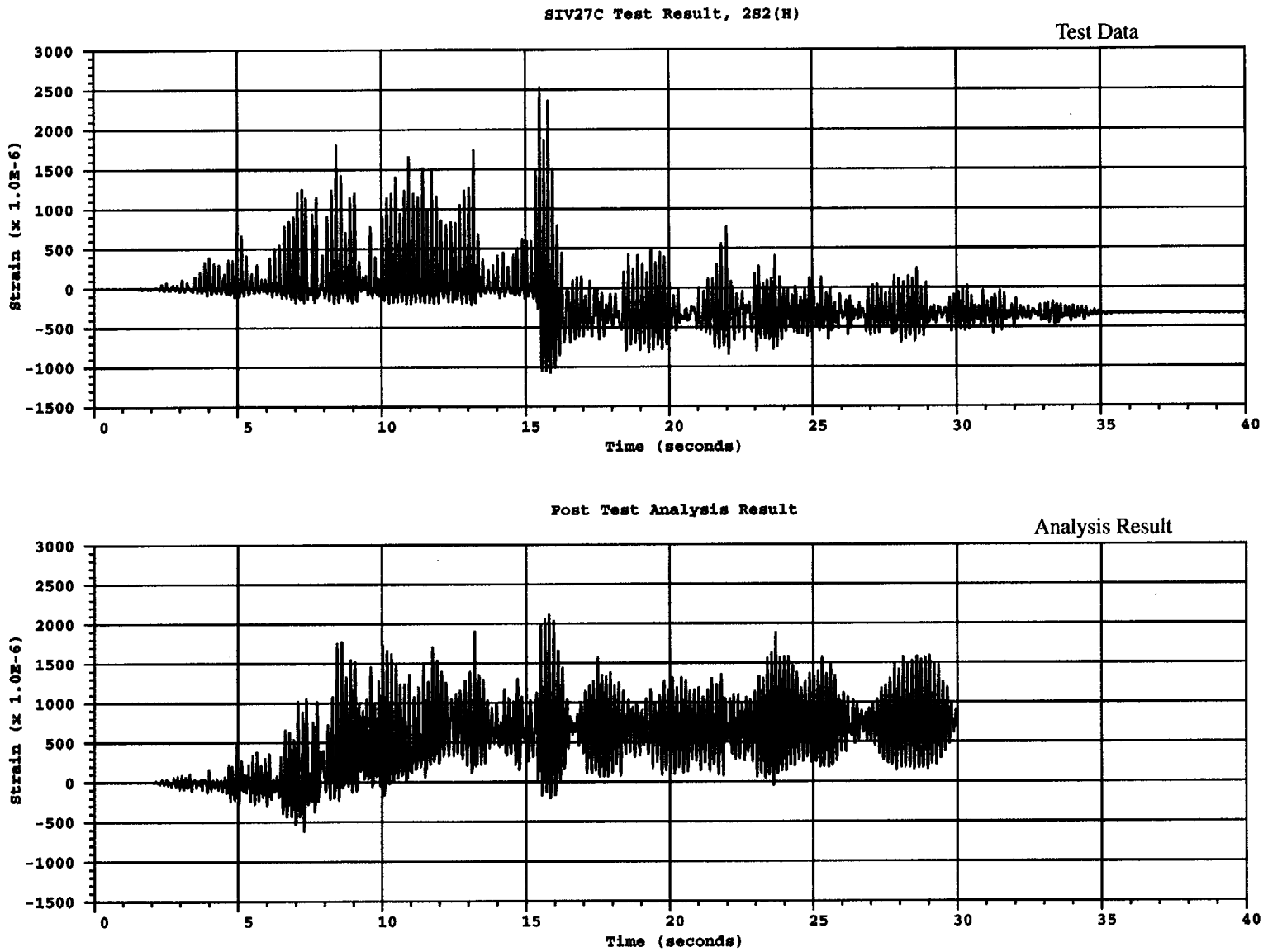

Figure B.40 Comparison of inside vertical rebar strain at SIV27C for 2S2(H) test

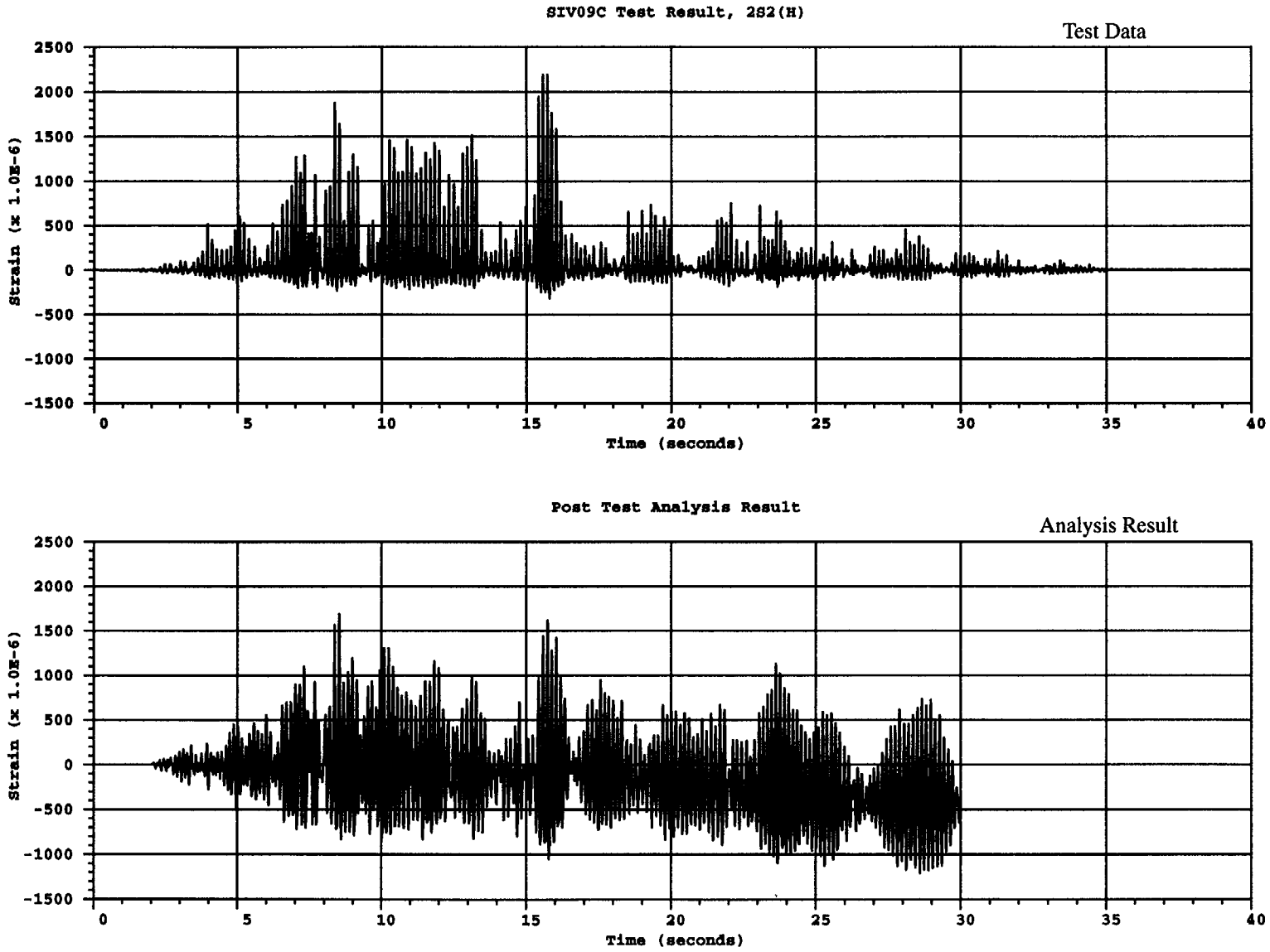

Figure B.41 Comparison of inside vertical rebar strain at SIV09C for 2S2(H) test

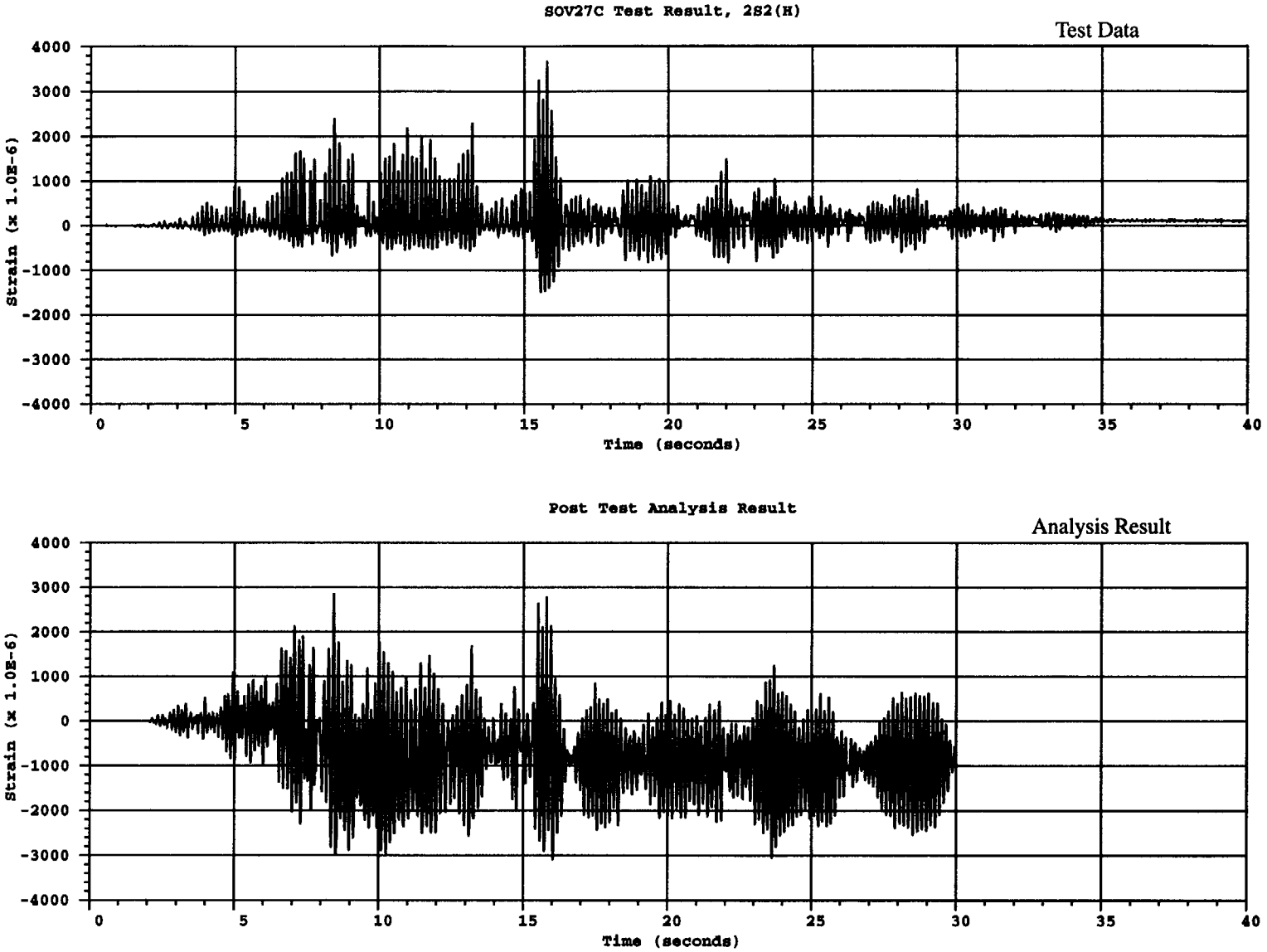

Figure B.42 Comparison of inside vertical rebar strain at SOV27C for 2S2(H) test

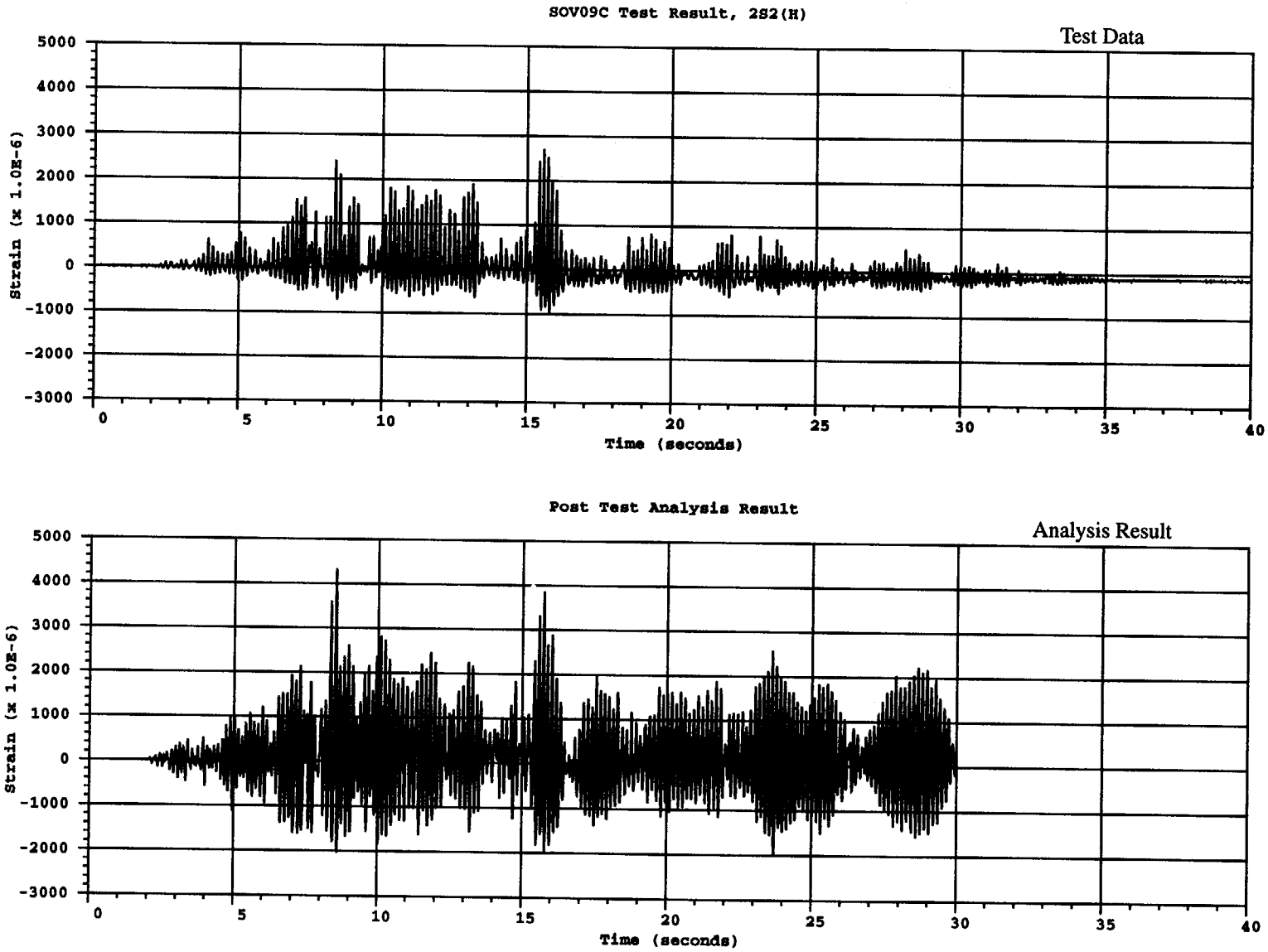

Figure B.43 Comparison of inside vertical rebar strain at SOV09C for 2S2(H) test

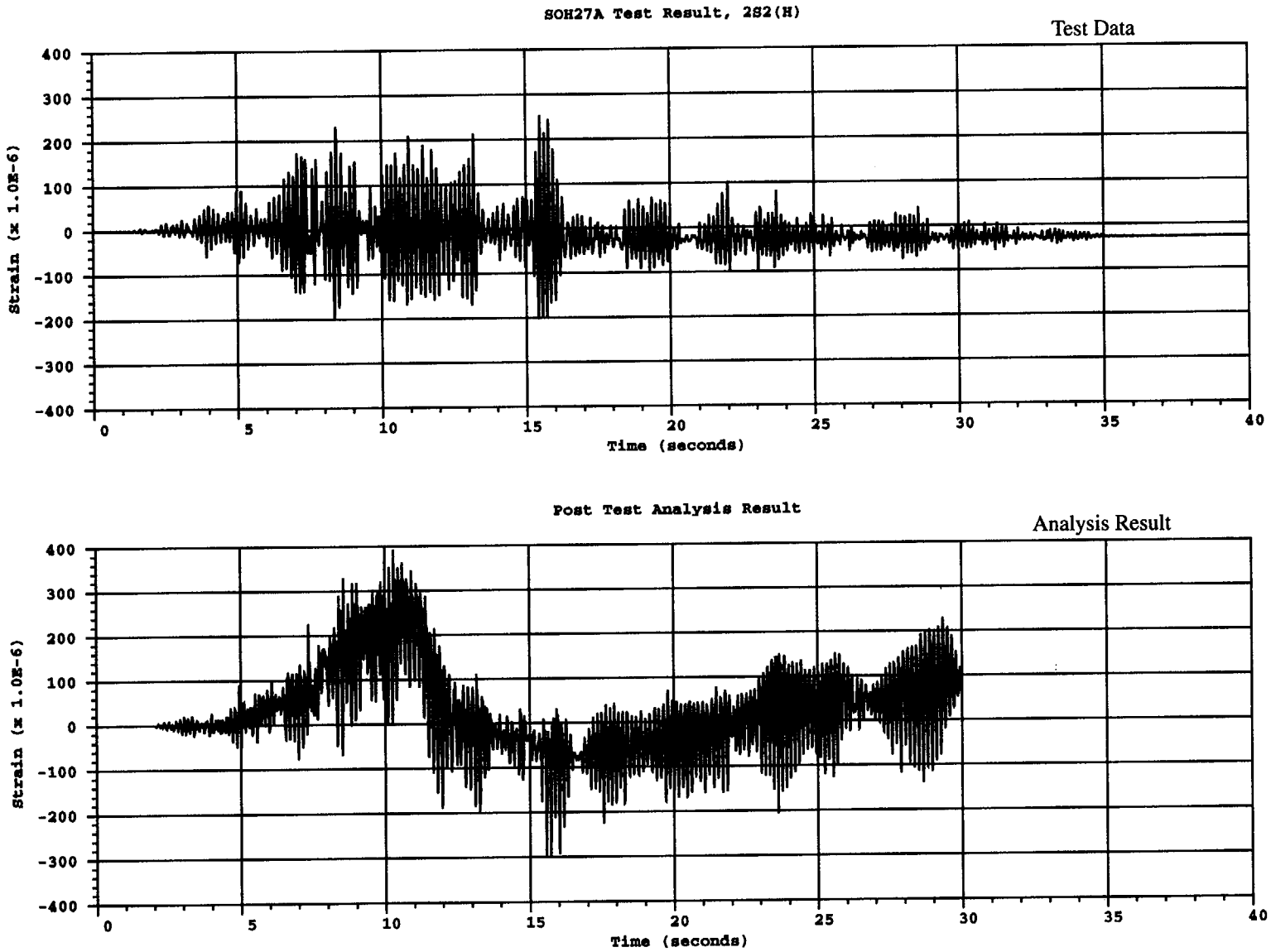

Figure B.44 Comparison of inside hoop rebar strain at SOH27A for 2S2(H) test

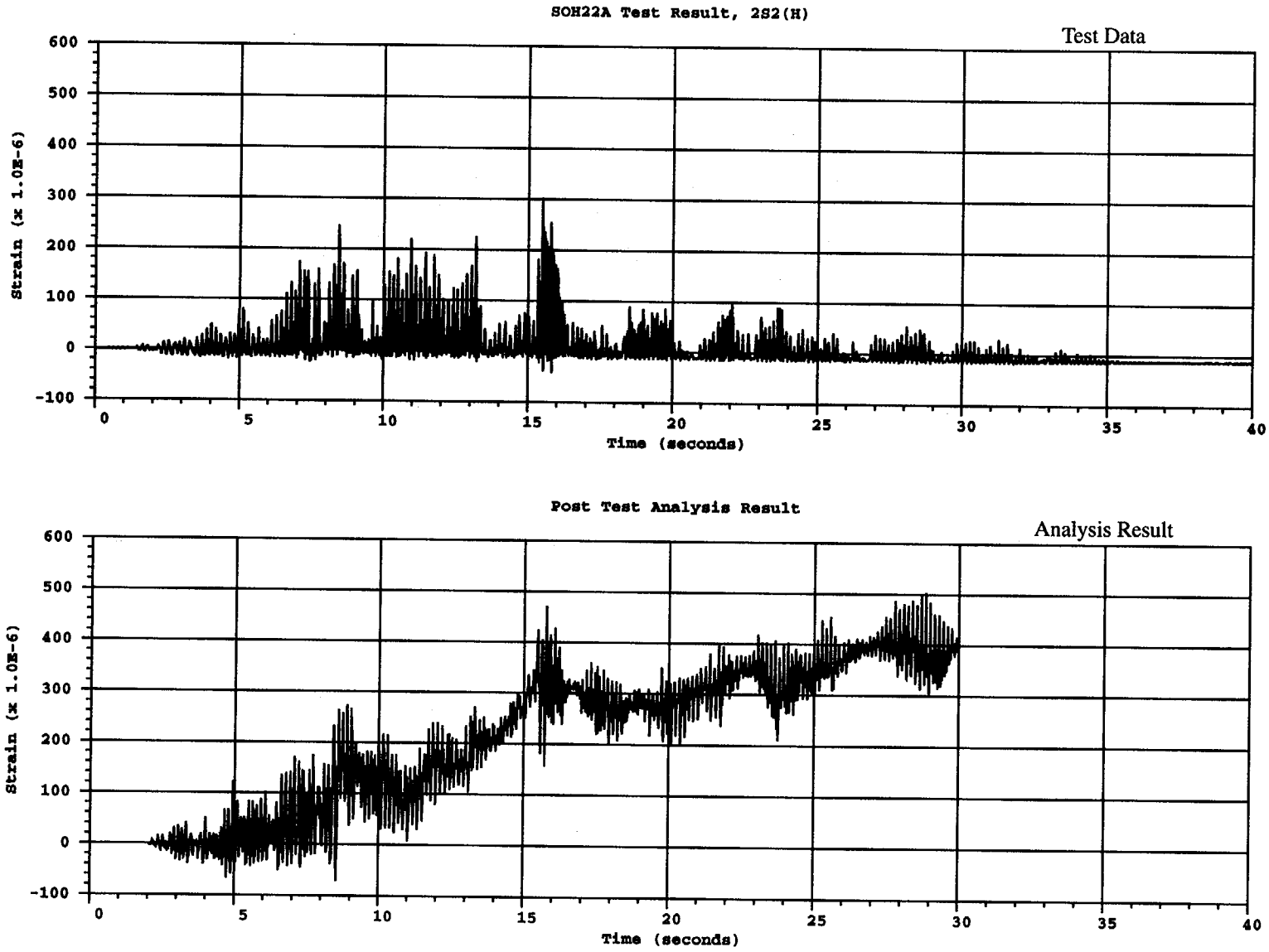

Figure B.45 Comparison of inside hoop rebar strain at SOH22A for 2S2(H) test

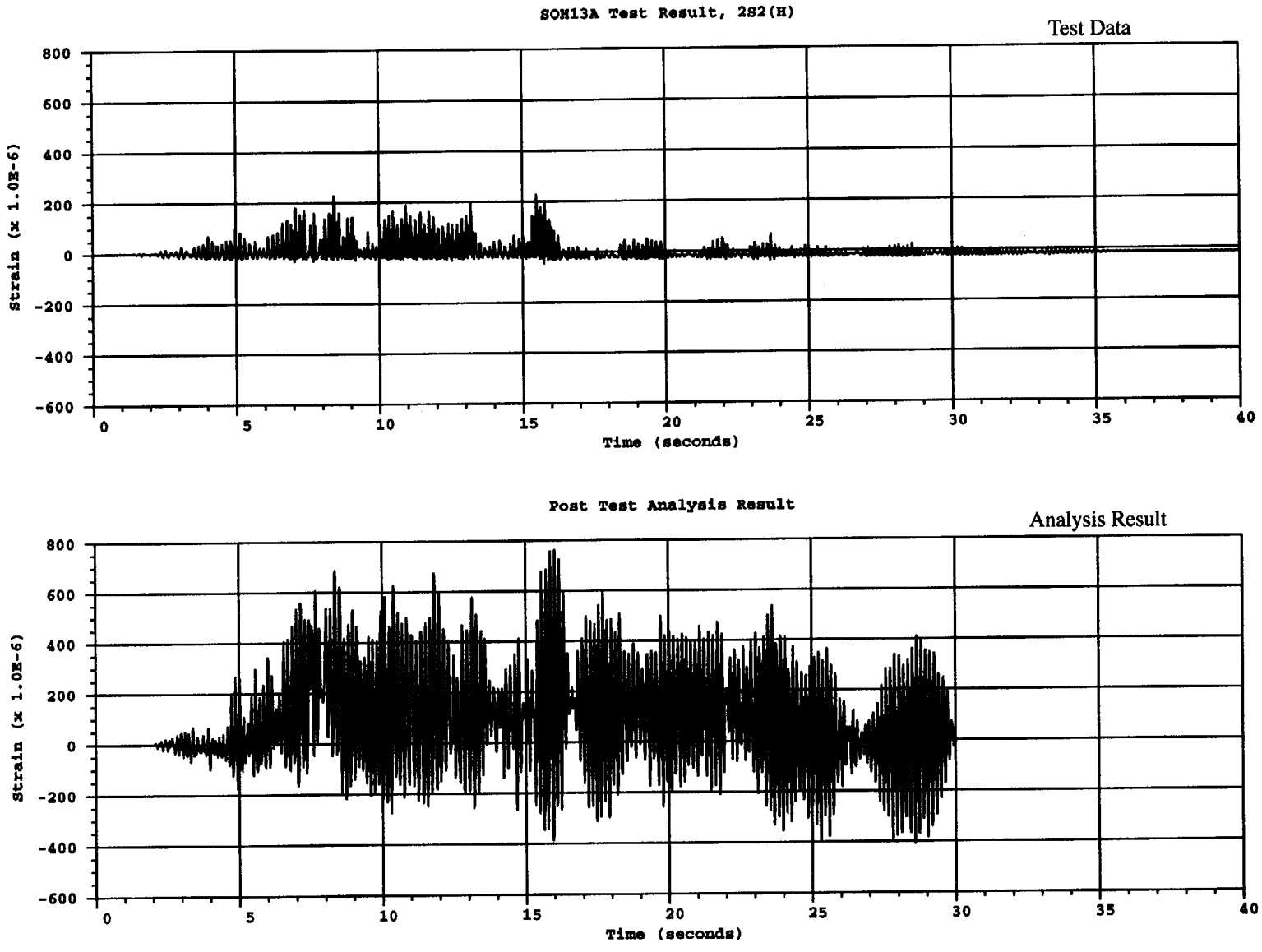

Figure B.46 Comparison of inside hoop rebar strain at SOH13A for 2S2(H) test

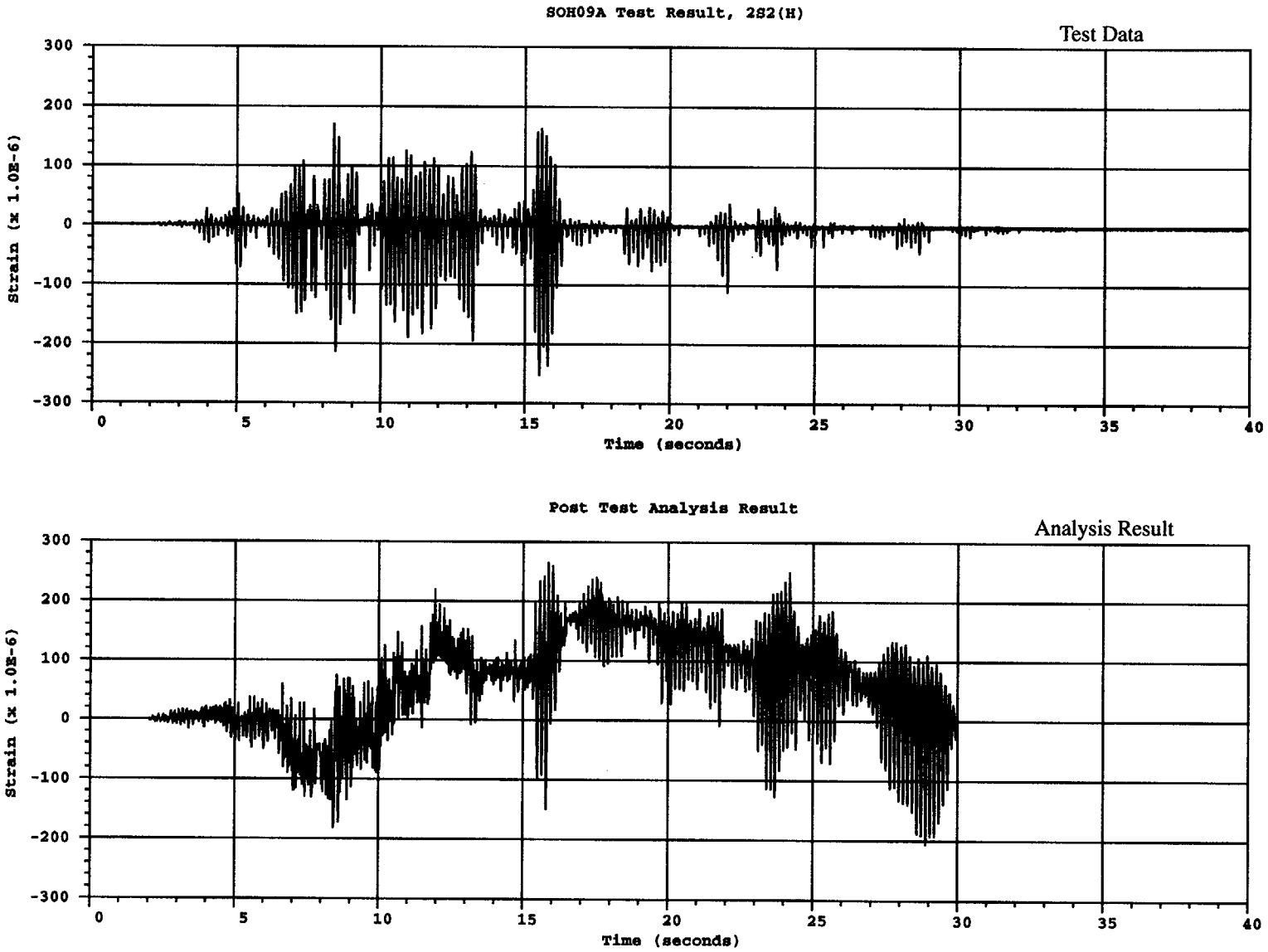

Figure B.47 Comparison of inside hoop rebar strain at SOH09A for 2S2(H) test

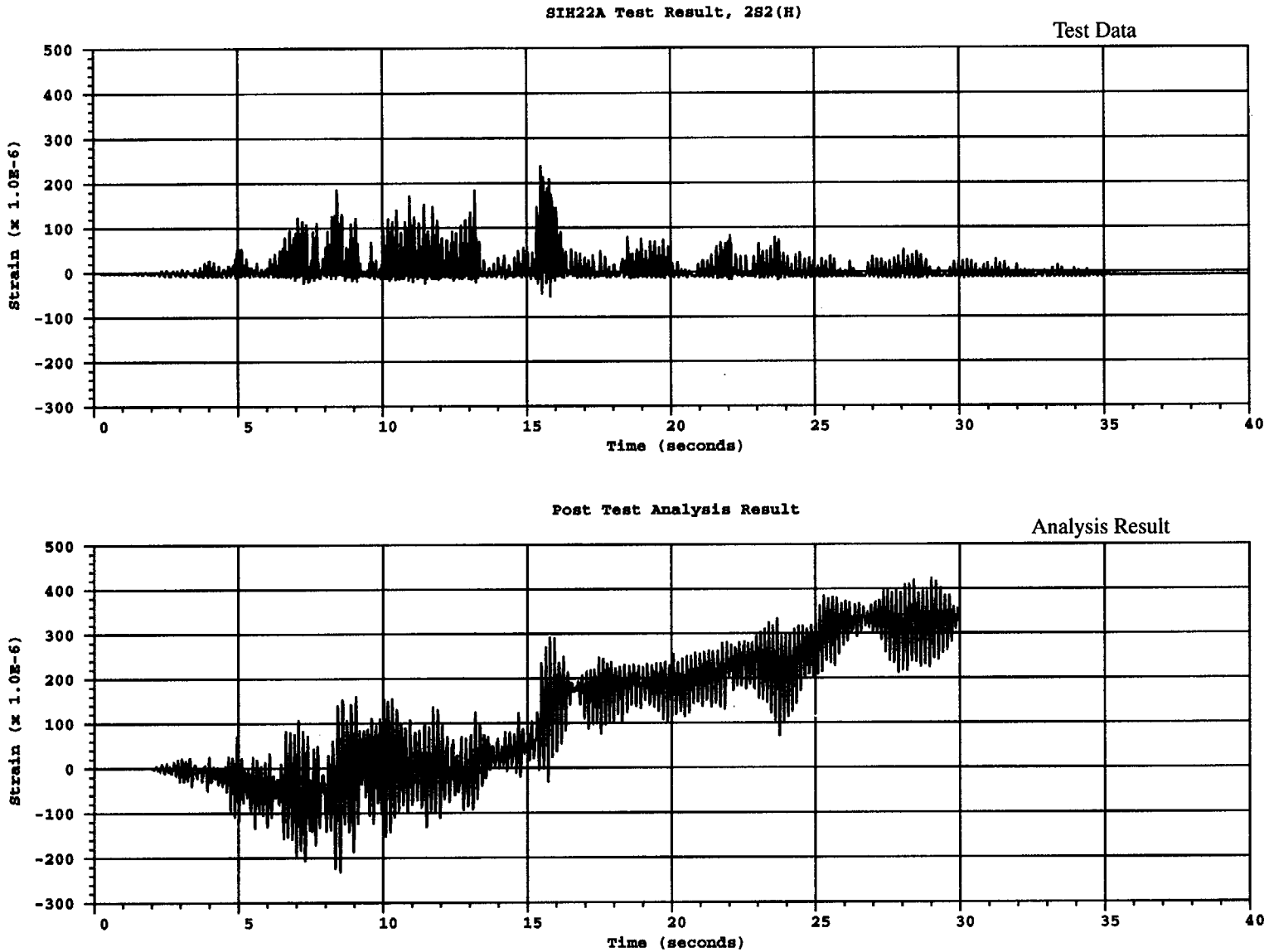

Figure B.48 Comparison of inside hoop rebar strain at SIH22A for 2S2(H) test

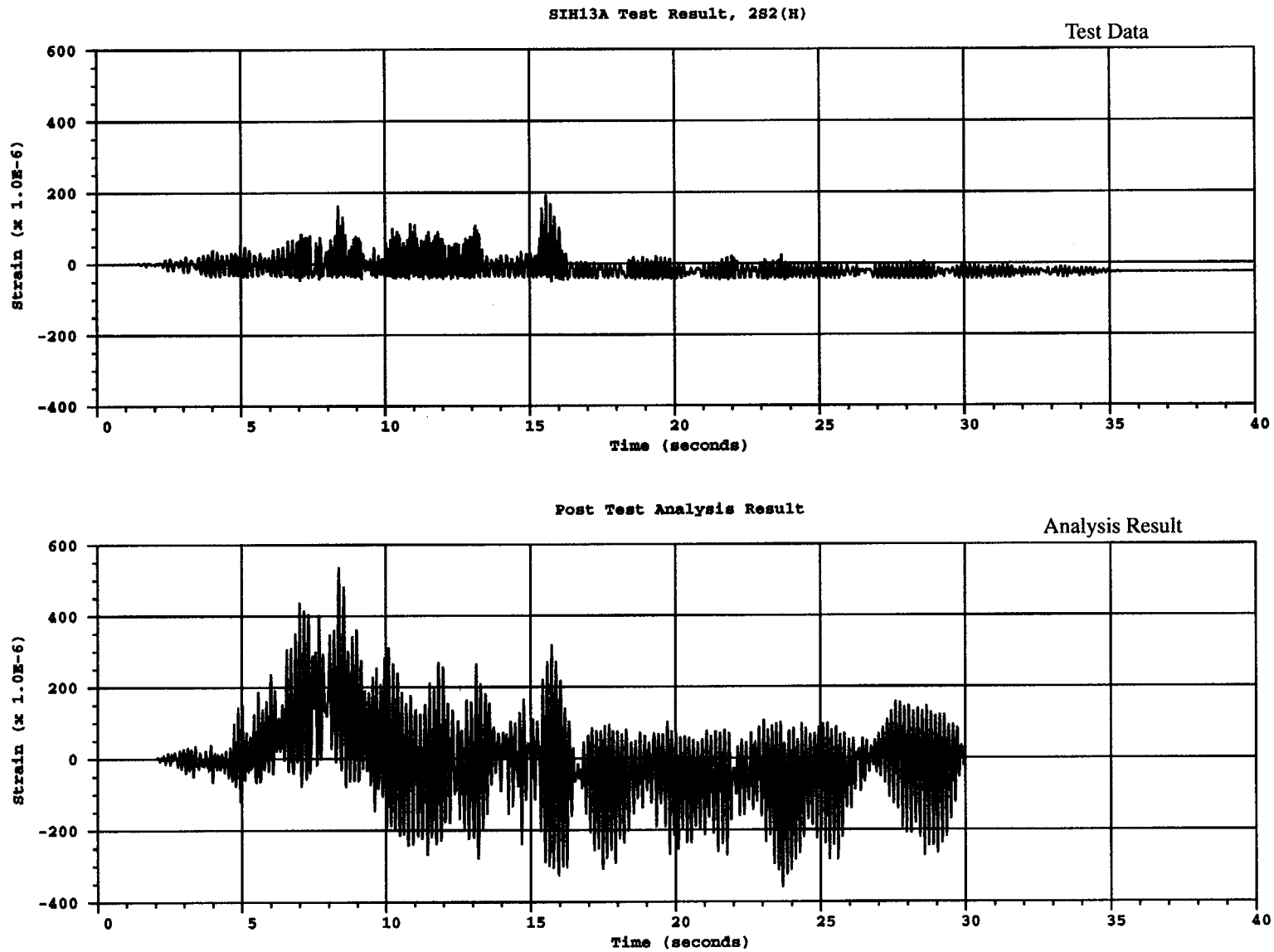

Figure B.49 Comparison of inside hoop rebar strain at SIH13A for 2S2(H) test

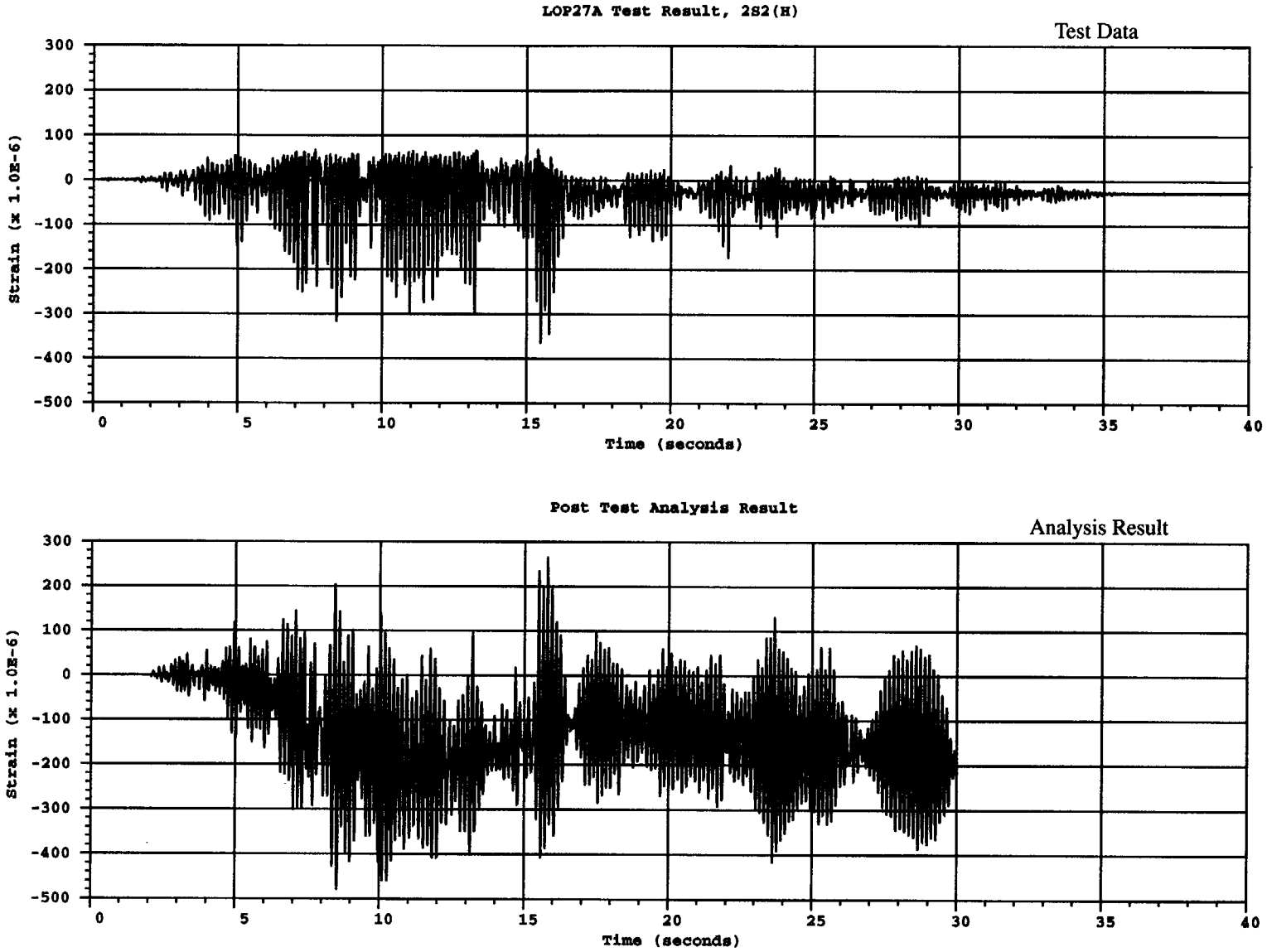

Figure B.50 Comparison of inside hoop liner strain at LOP27A for 2S2(H) test

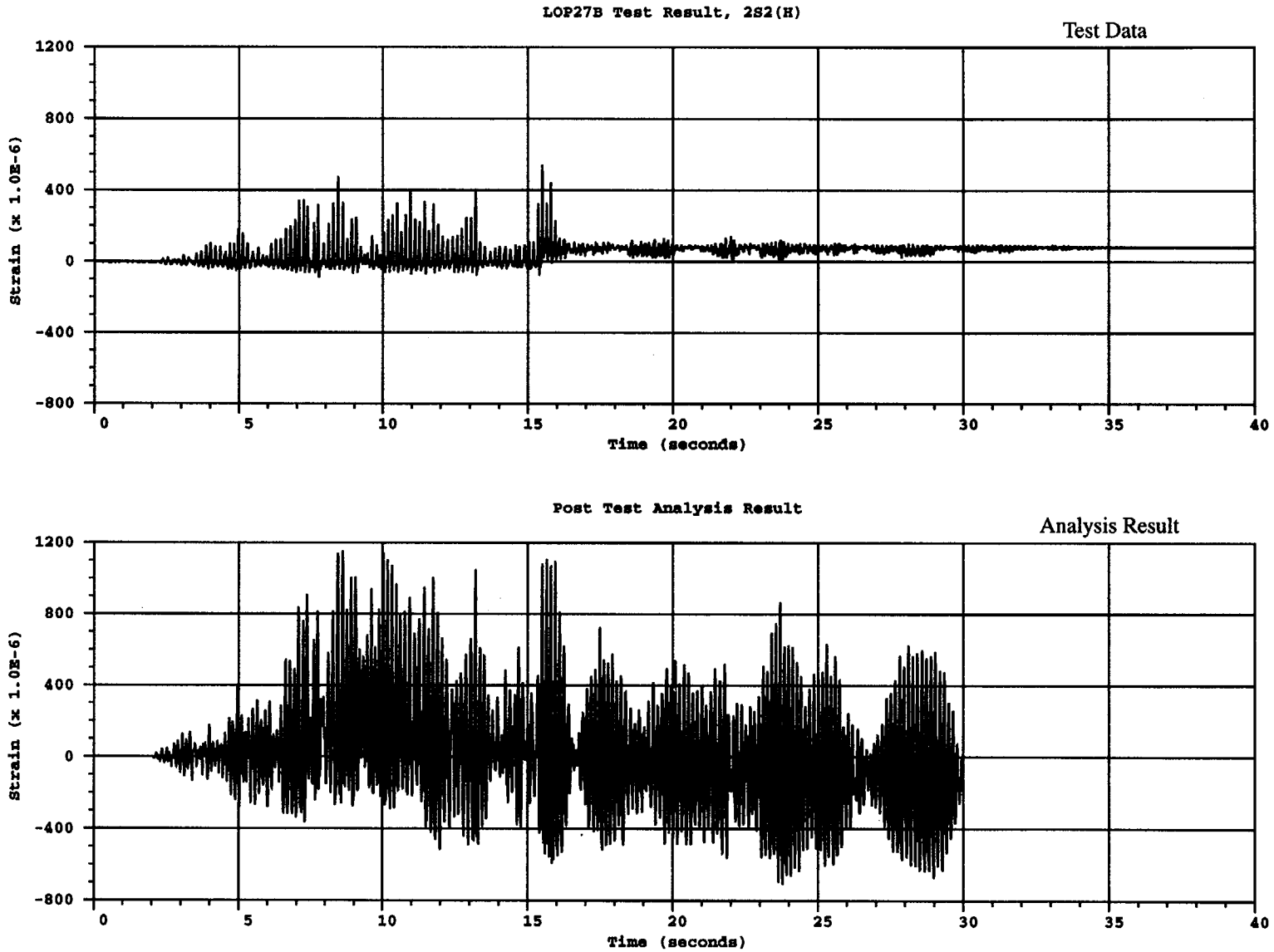

Figure B.51 Comparison of inside vertical liner strain at LOP27B for 2S2(H) test

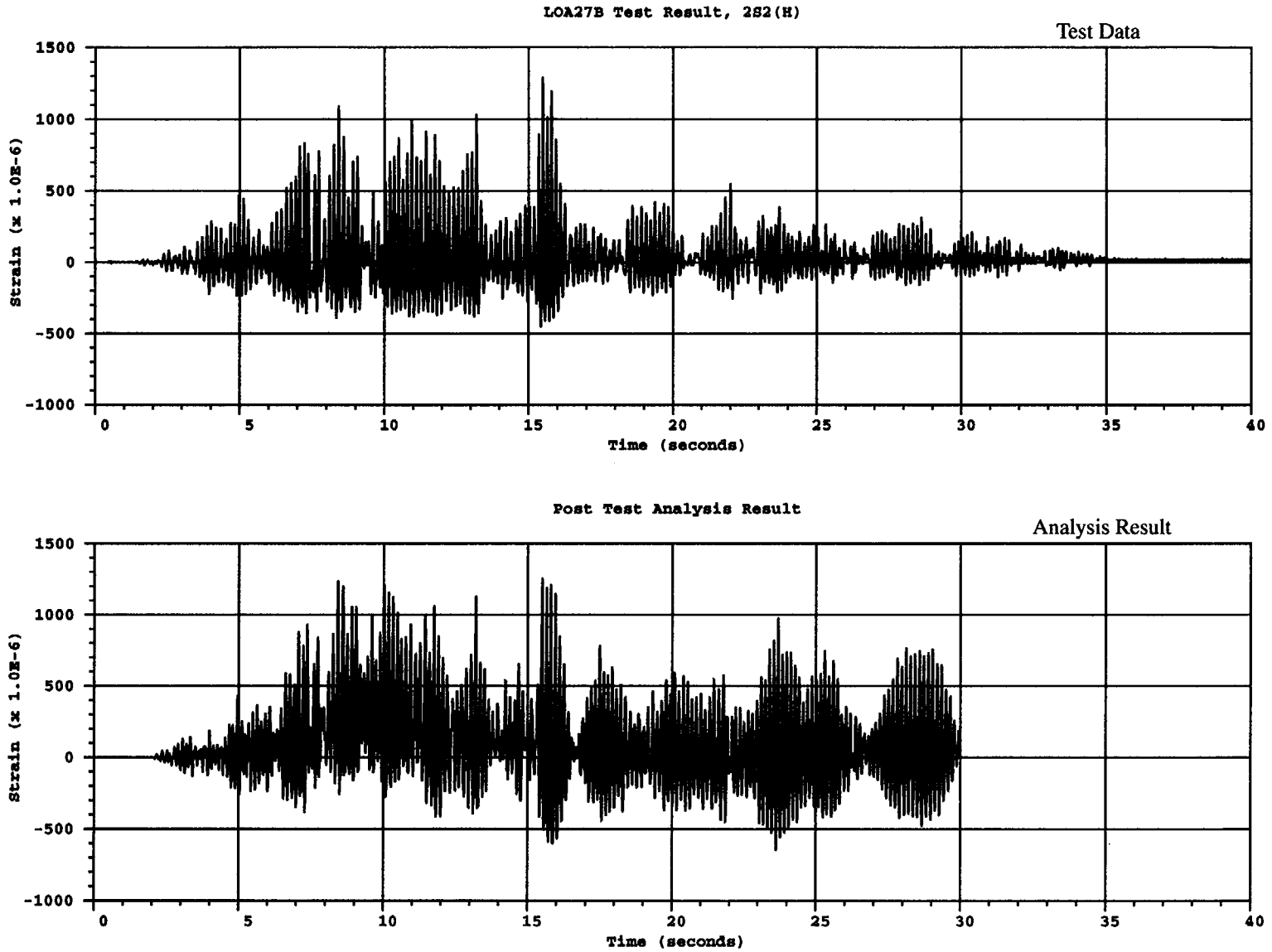

Figure B.52 Comparison of inside vertical liner strain at LOA27B for 2S2(H) test

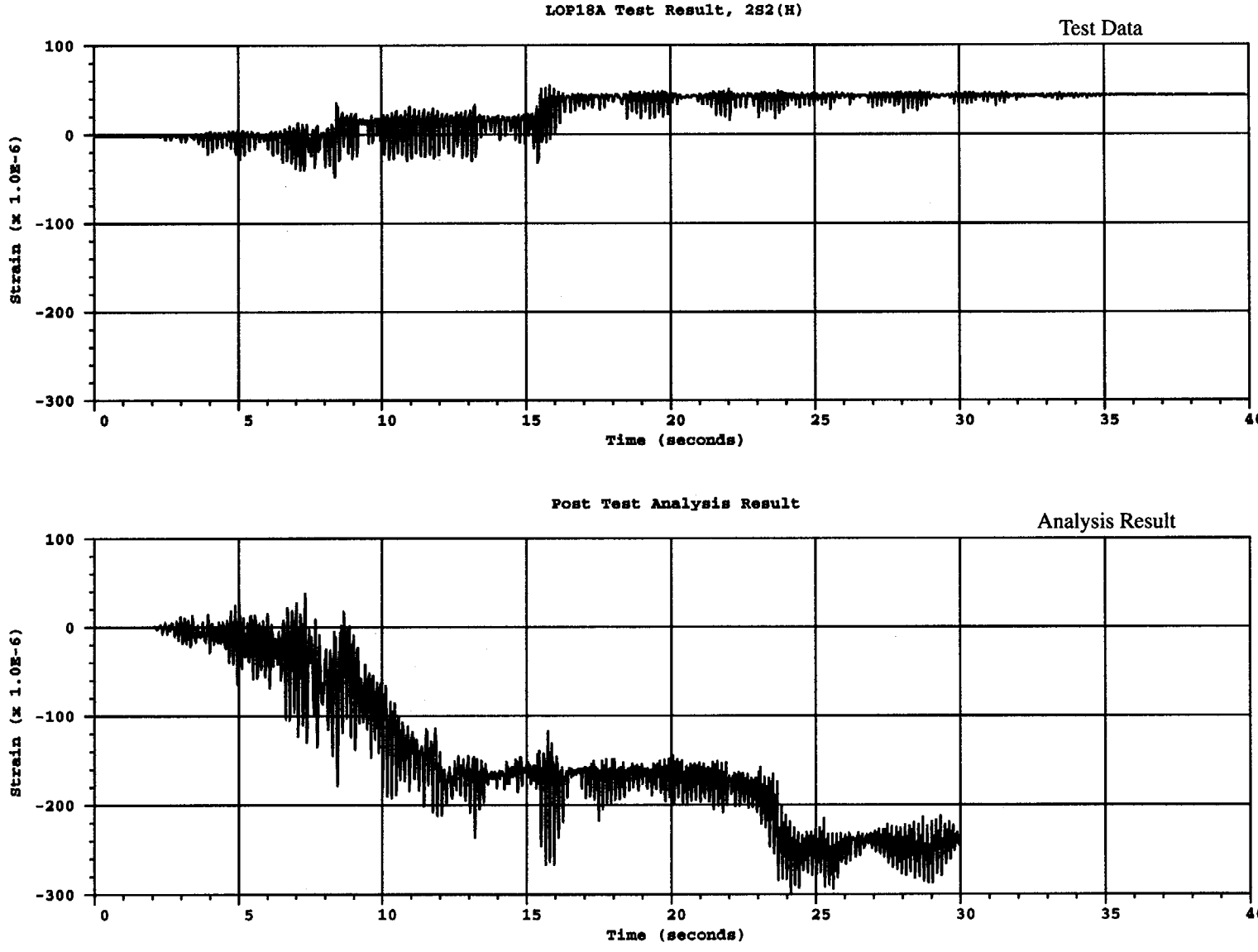

Figure B.53 Comparison of inside hoop liner strain at LOP18A for 2S2(H) test

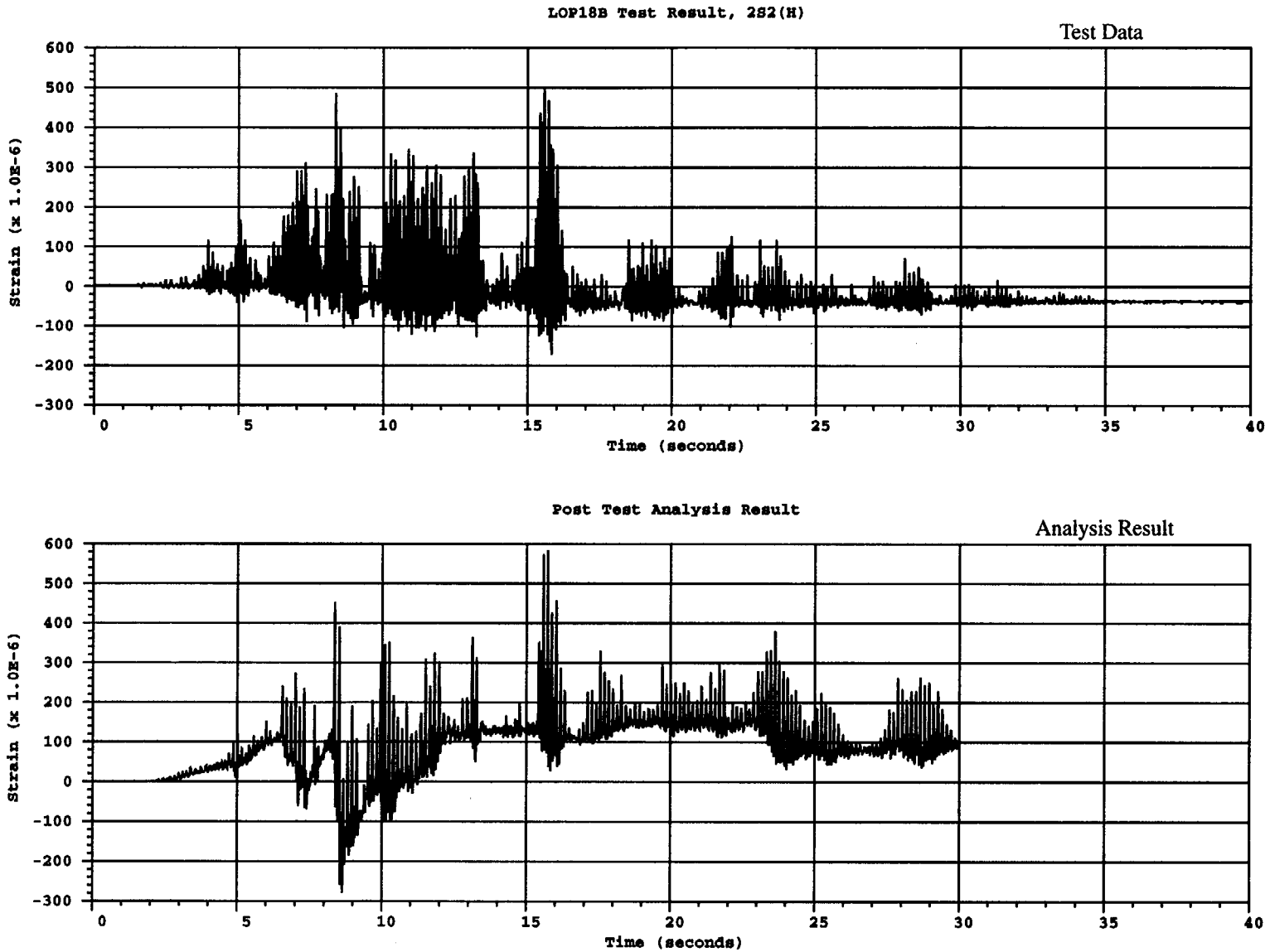

Figure B.54 Comparison of inside vertical liner strain at LOP18B for 2S2(H) test

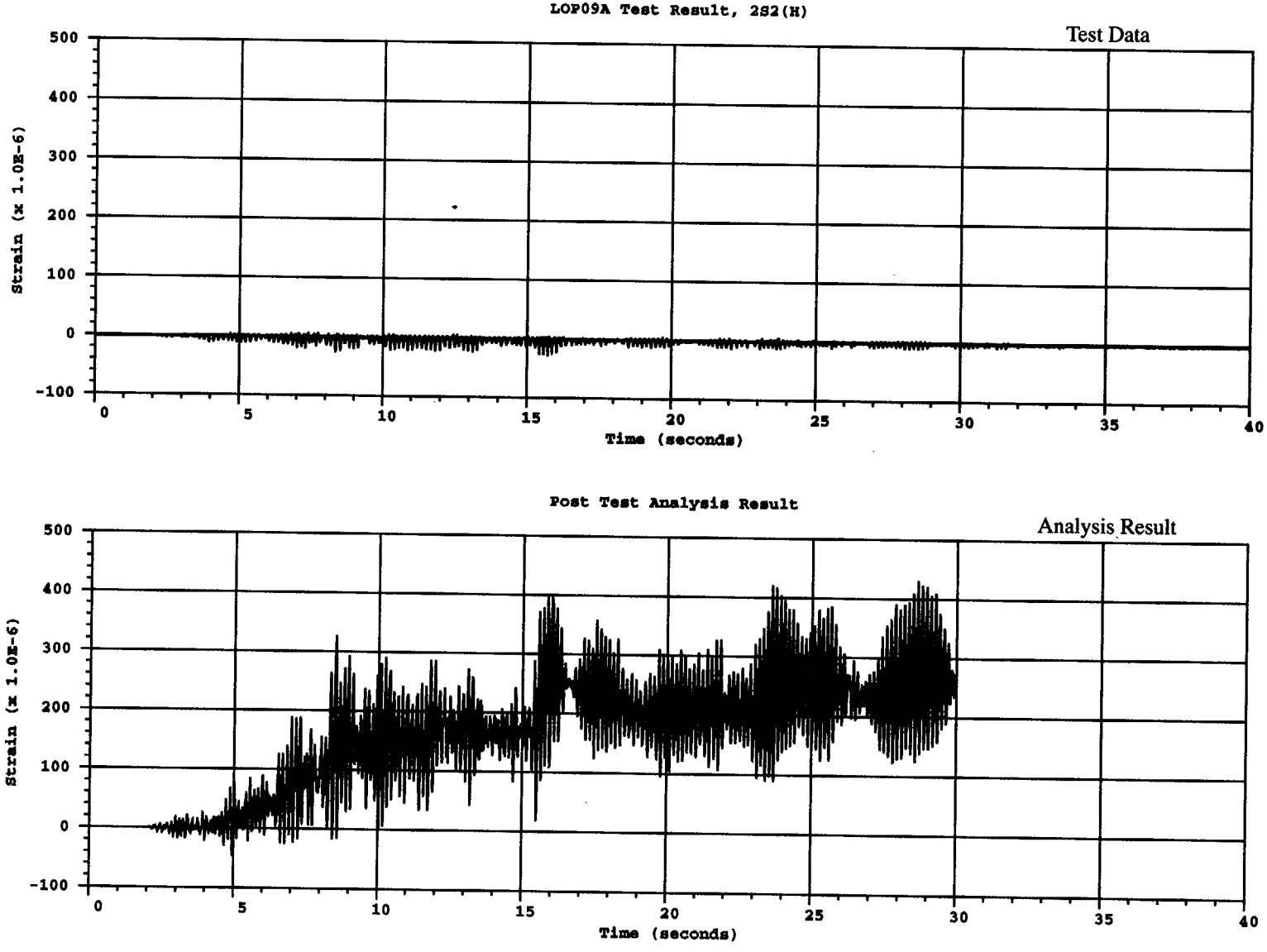

Figure B.55 Comparison of inside hoop liner strain at LOP09A for 2S2(H) test

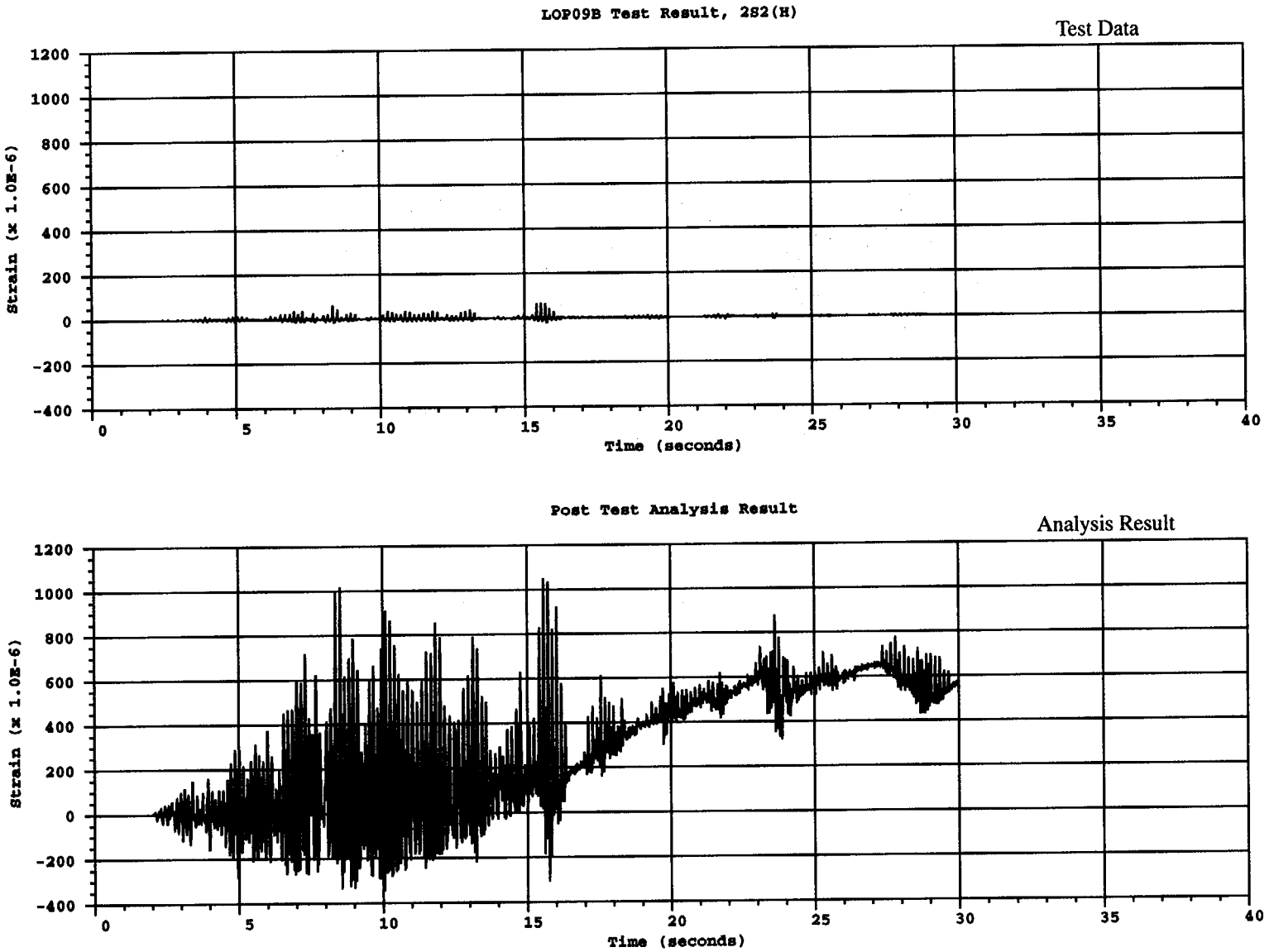

Figure B.56 Comparison of inside vertical liner strain at LOP09B for 2S2(H) test

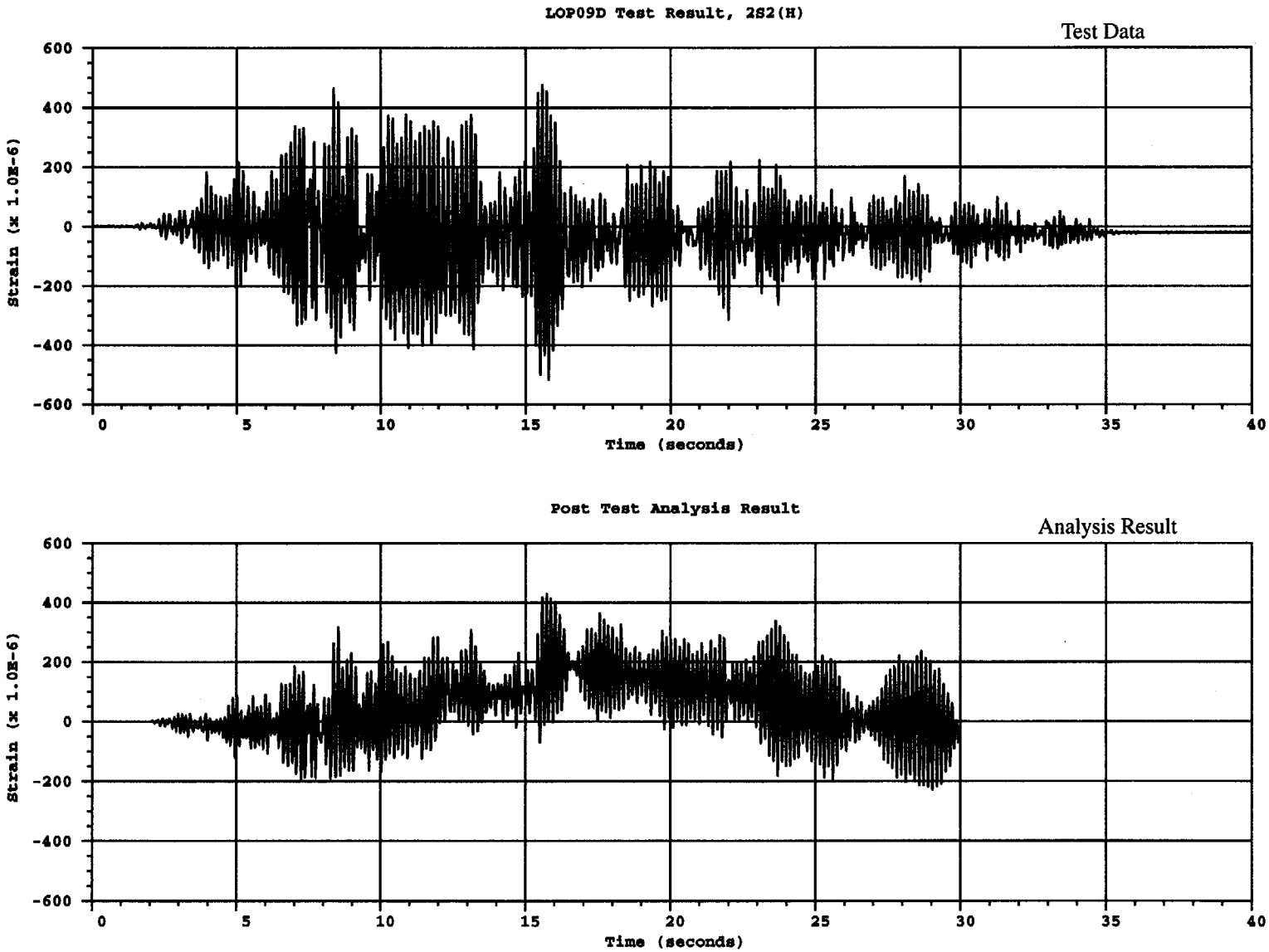

Figure B.57 Comparison of inside hoop liner strain at LOP09D for 2S2(H) test

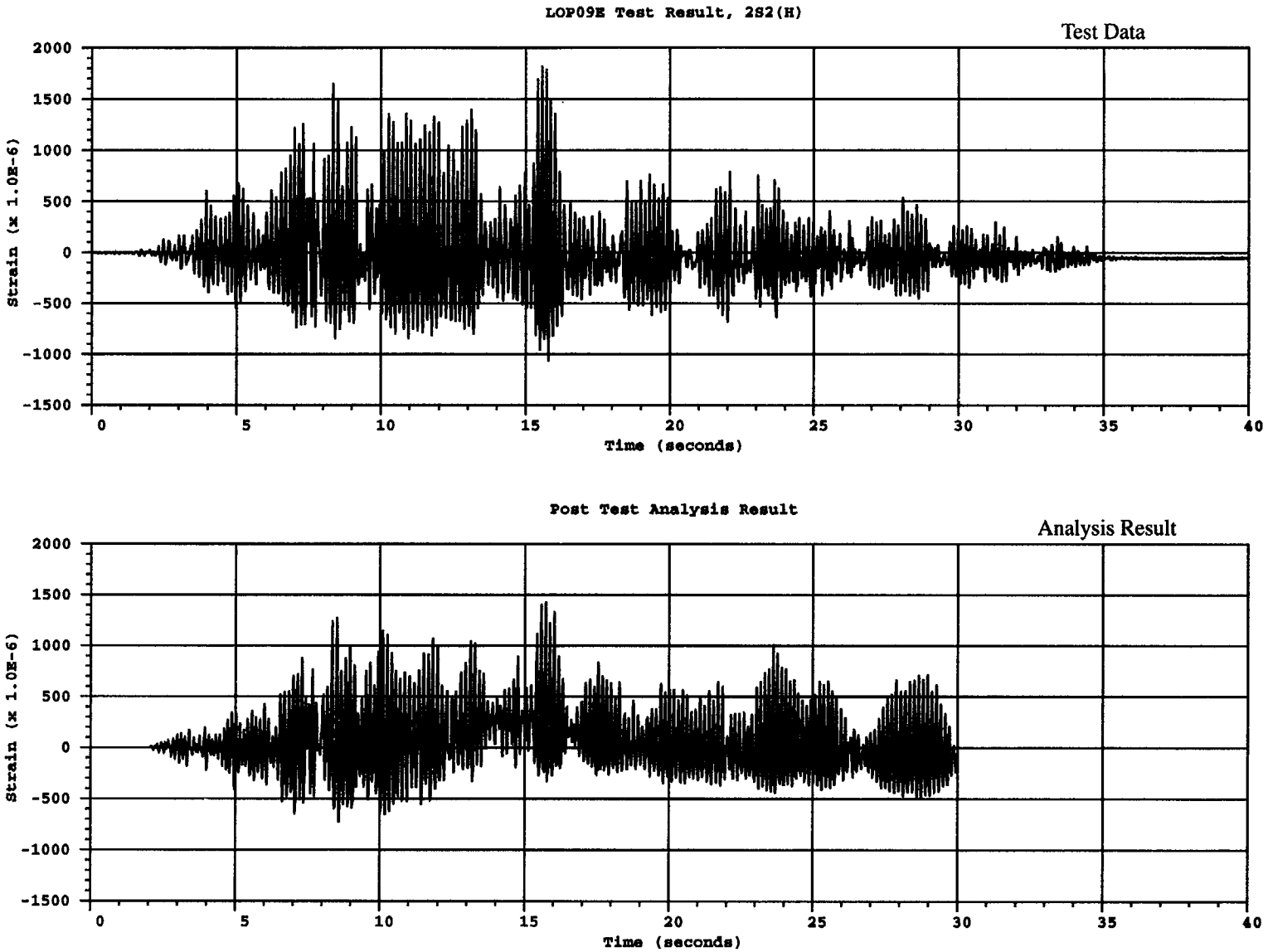

Figure B.58 Comparison of inside hoop liner strain at LOP09E for 2S2(H) test

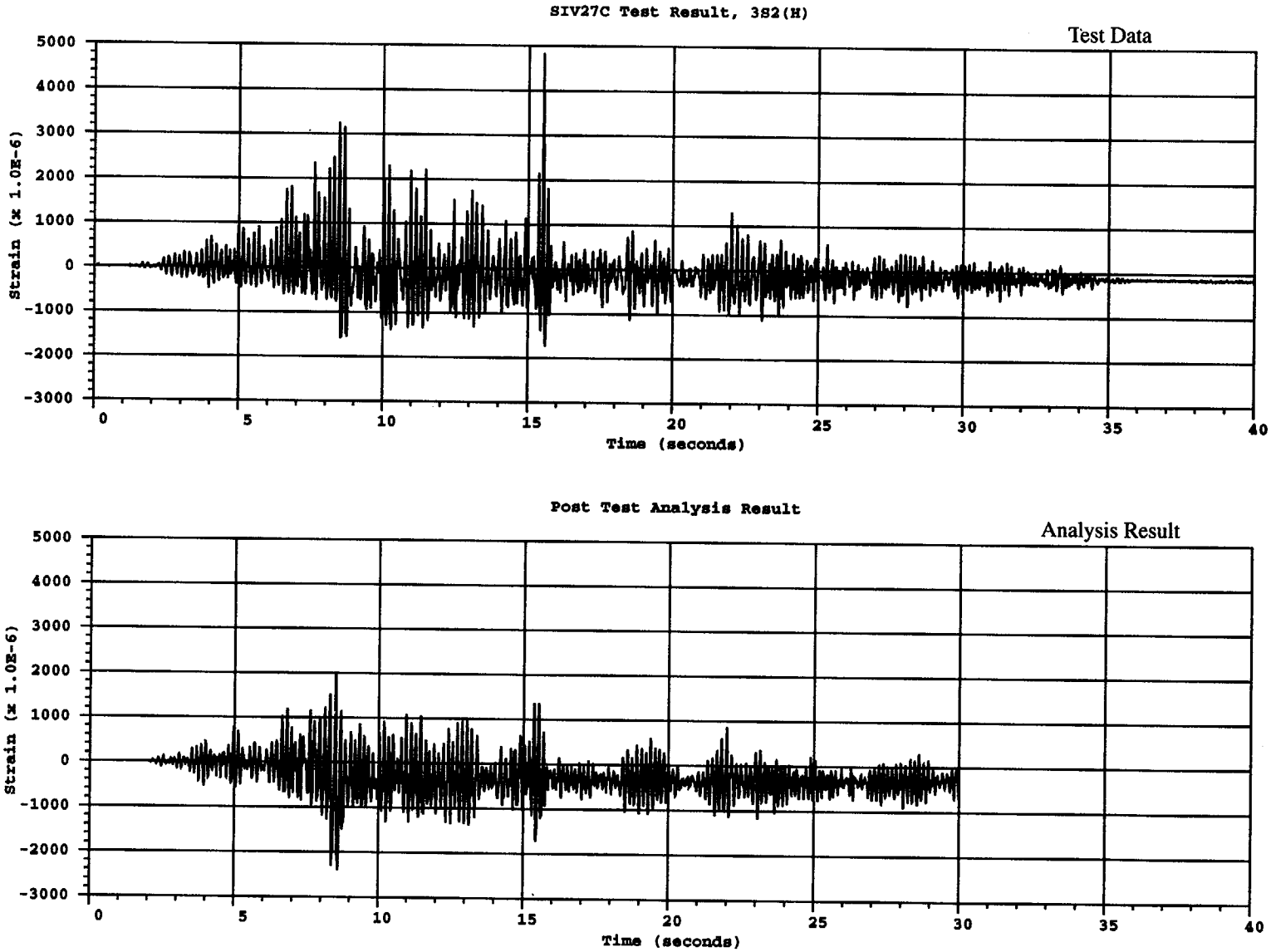

Figure B.59 Comparison of inside vertical rebar strain at SIV27C for 3S2(H) test

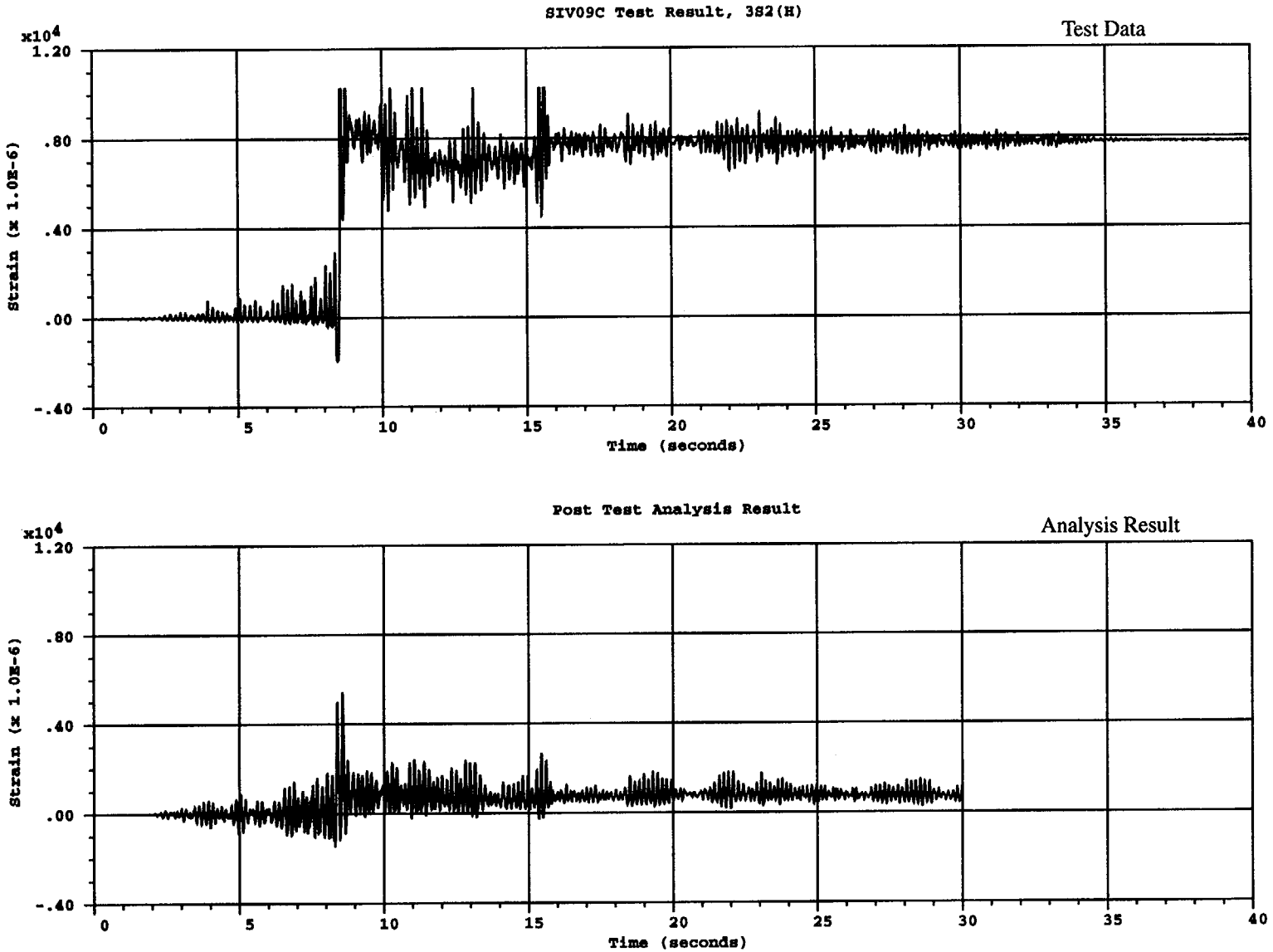

Figure B.60 Comparison of inside vertical rebar strain at SIV09C for 3S2(H) test

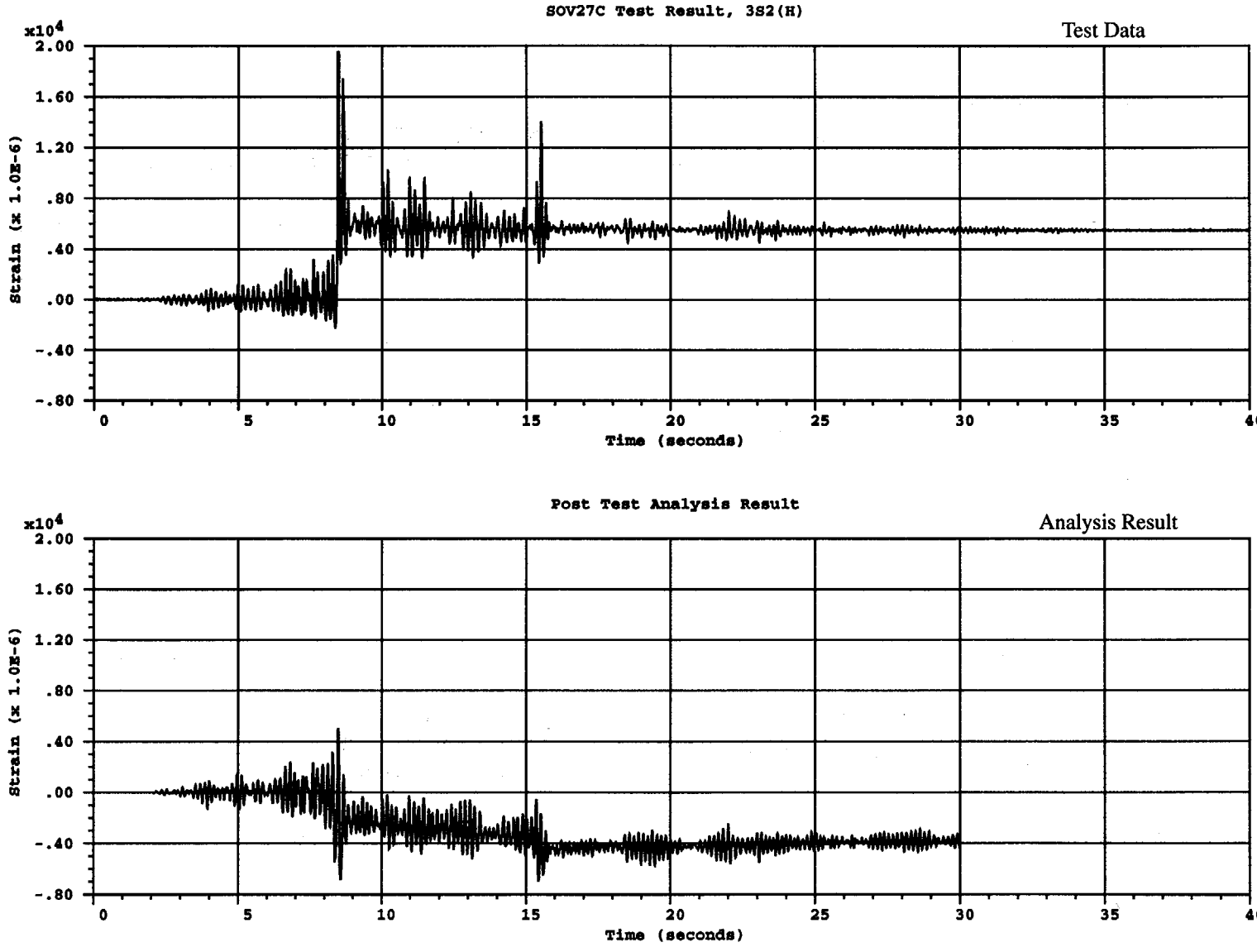

Figure B.61 Comparison of inside vertical rebar strain at SOV27C for 3S2(H) test

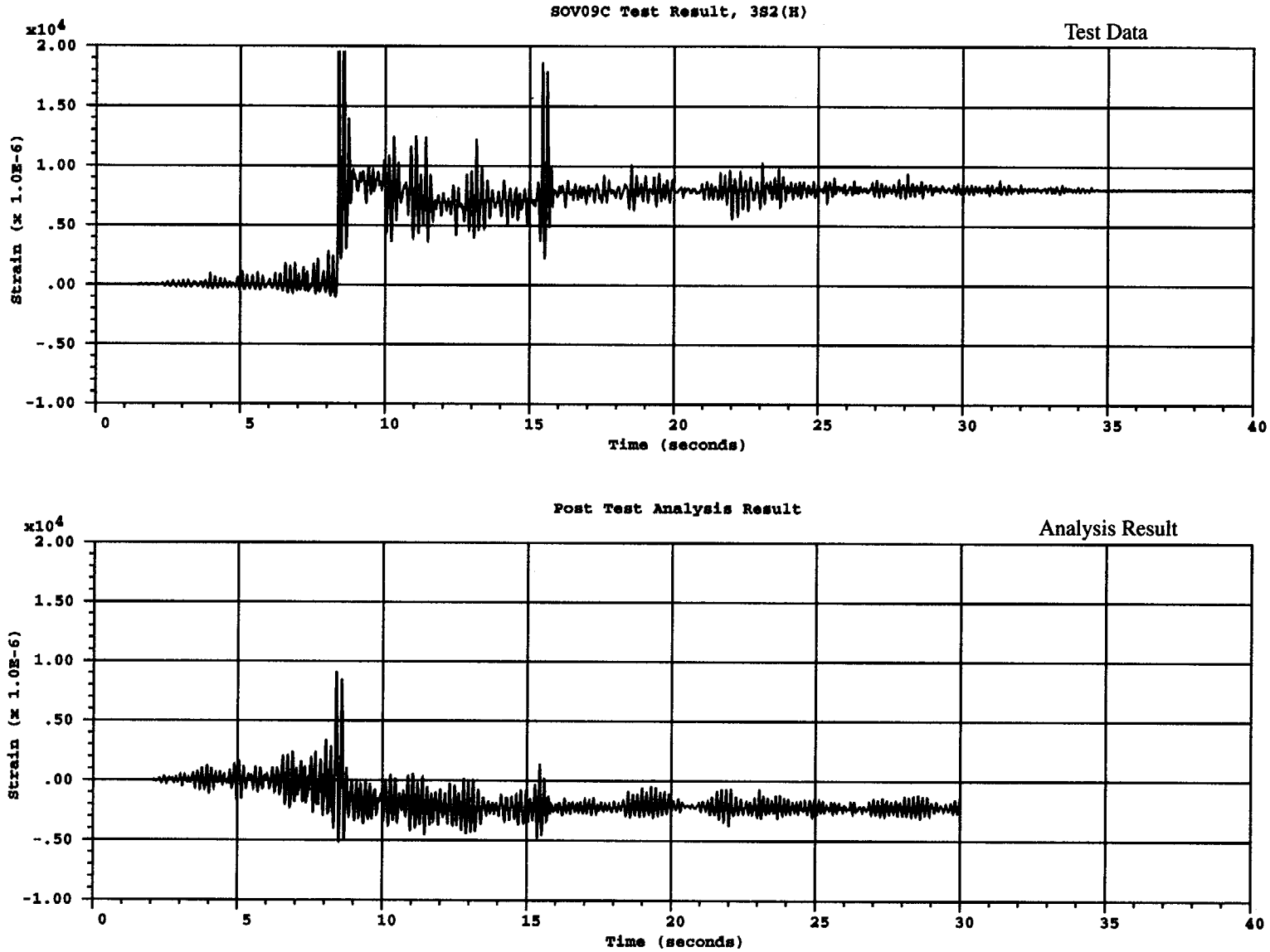

Figure B.62 Comparison of inside vertical rebar strain at SOV09C for 3S2(H) test

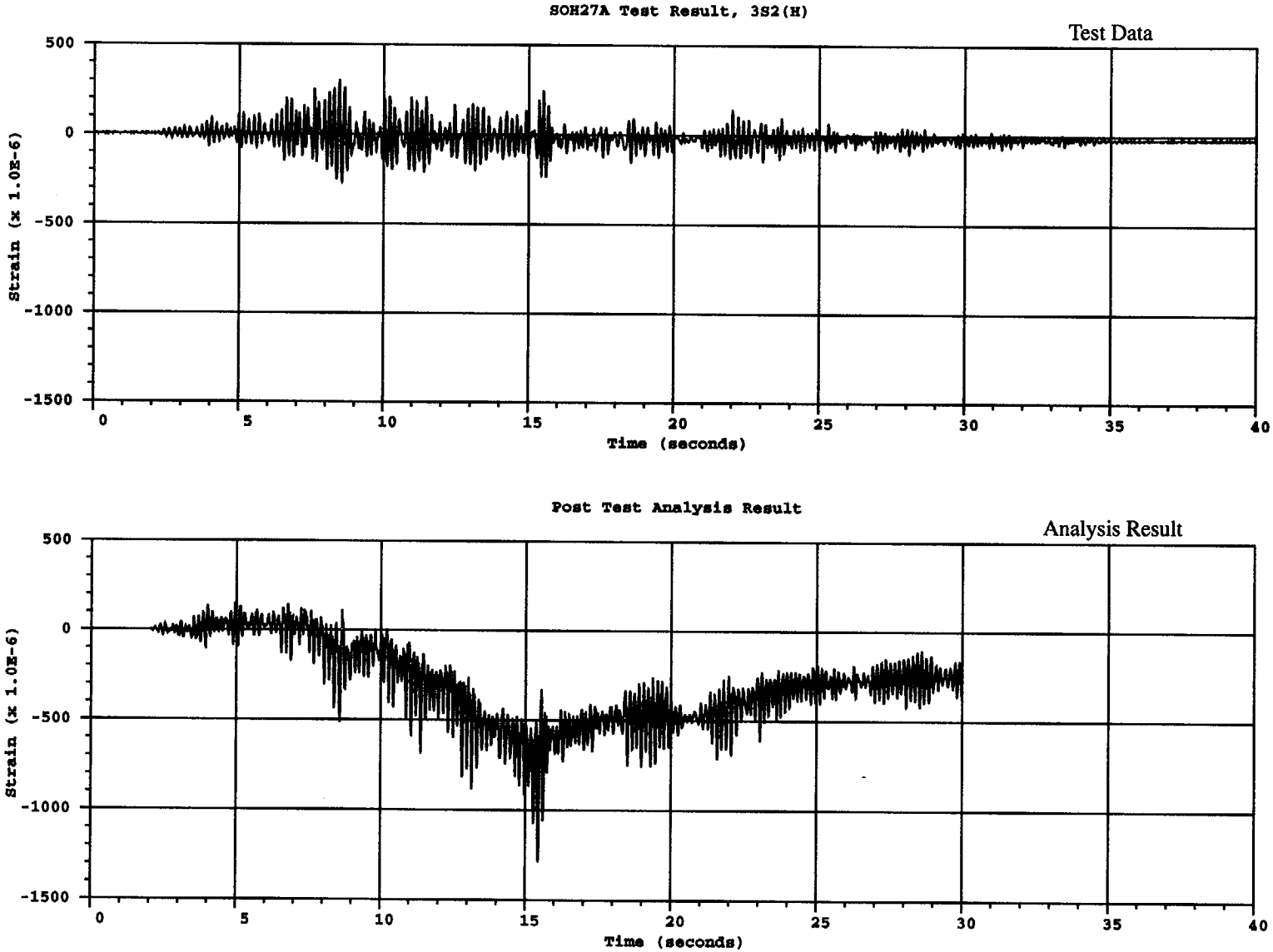

Figure B.63 Comparison of inside hoop rebar strain at SOH27A for 3S2(H) test

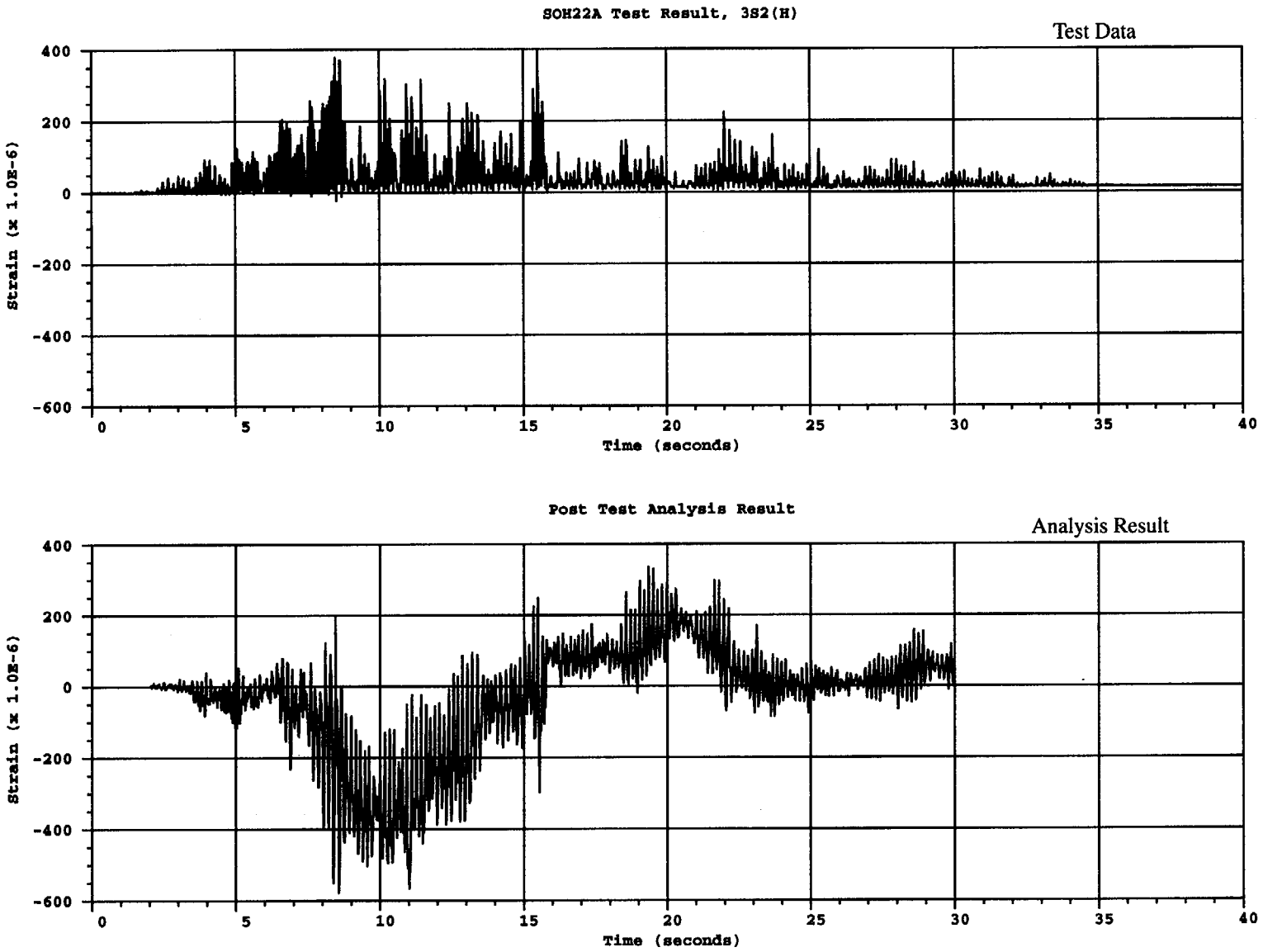

Figure B.64 Comparison of inside hoop rebar strain at SOH22A for 3S2(H) test

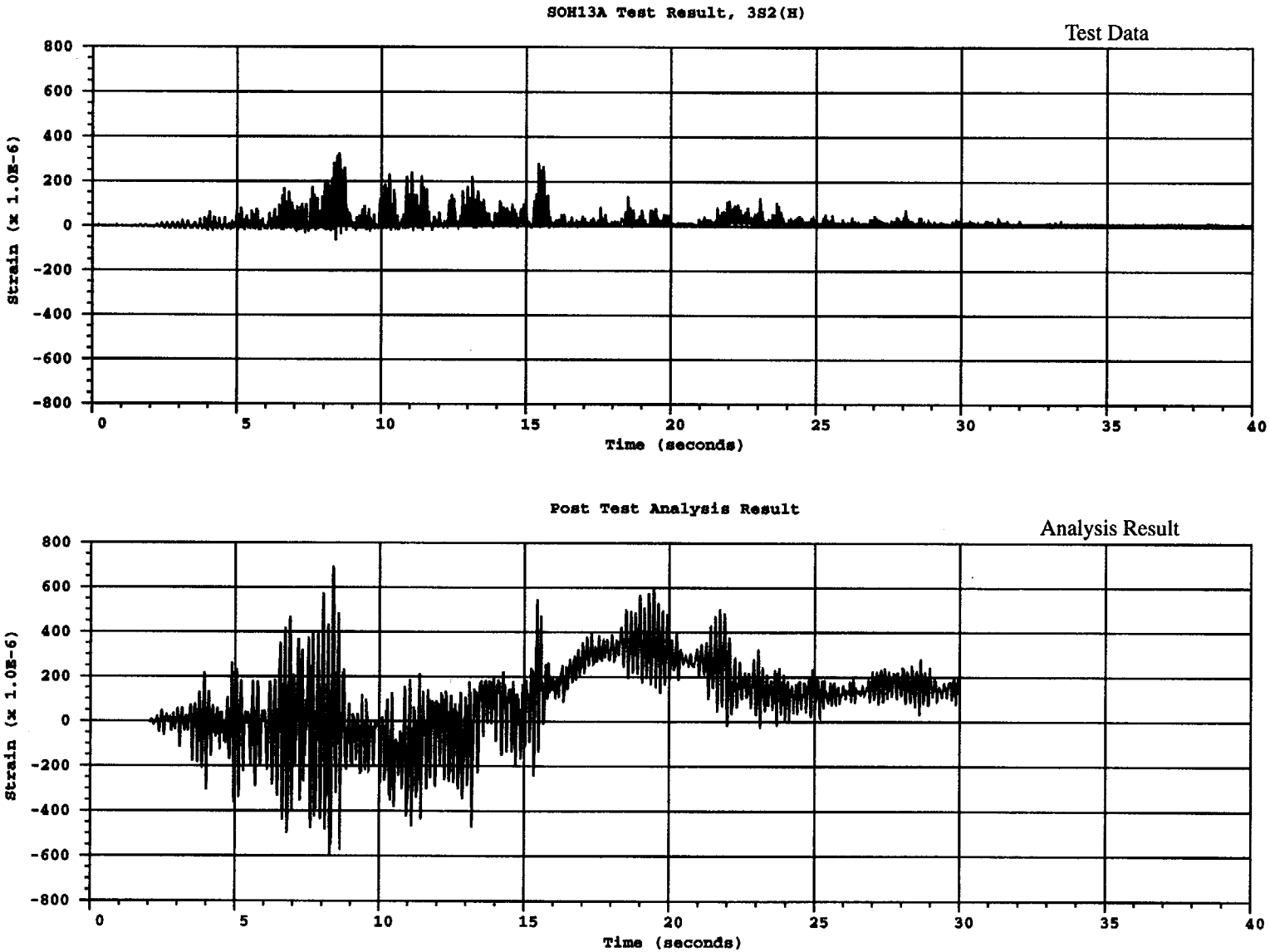

Figure B.65 Comparison of inside hoop rebar strain at SOH13A for 3S2(H) test

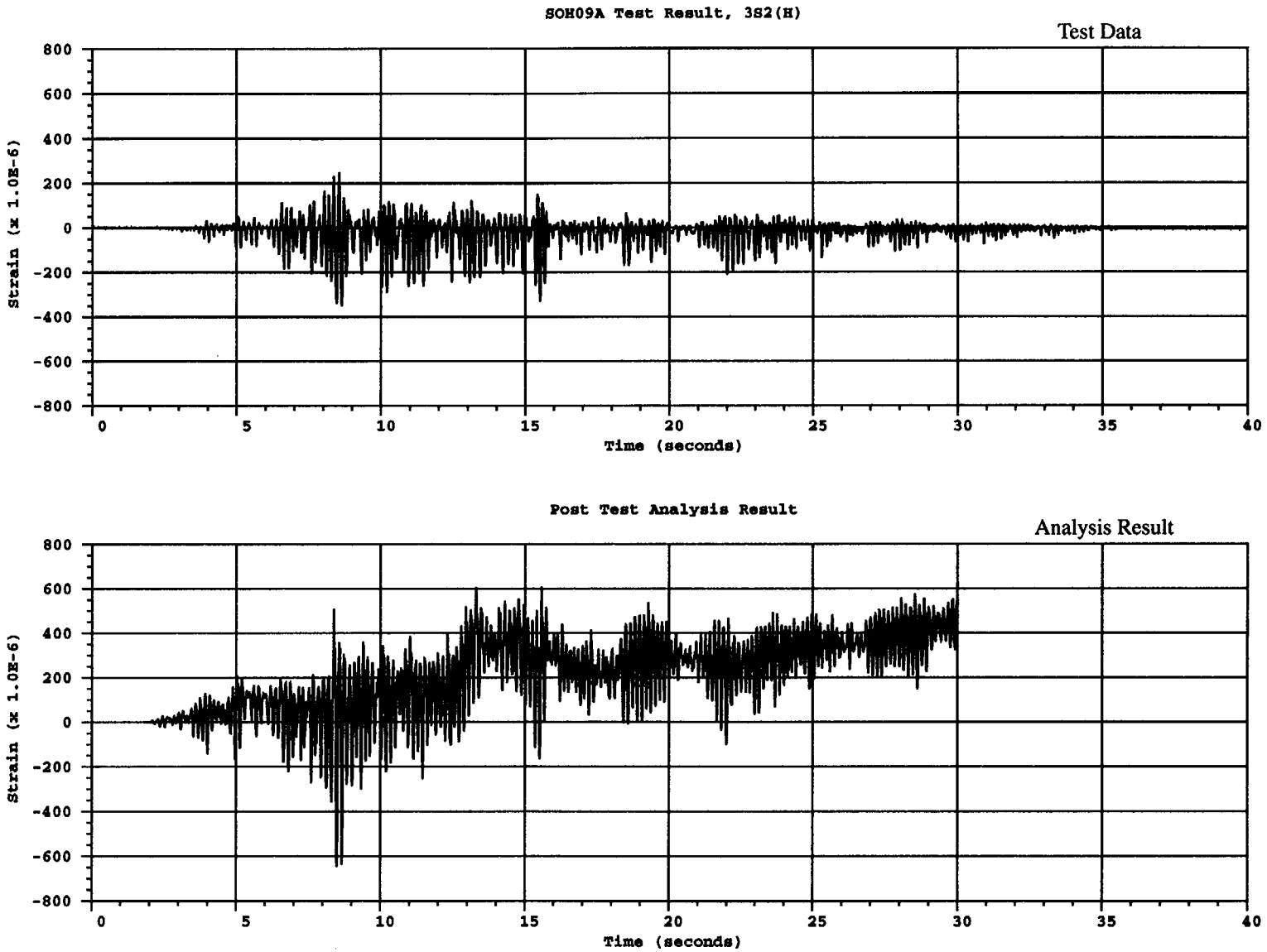

Figure B.66 Comparison of inside hoop rebar strain at SOH09A for 3S2(H) test

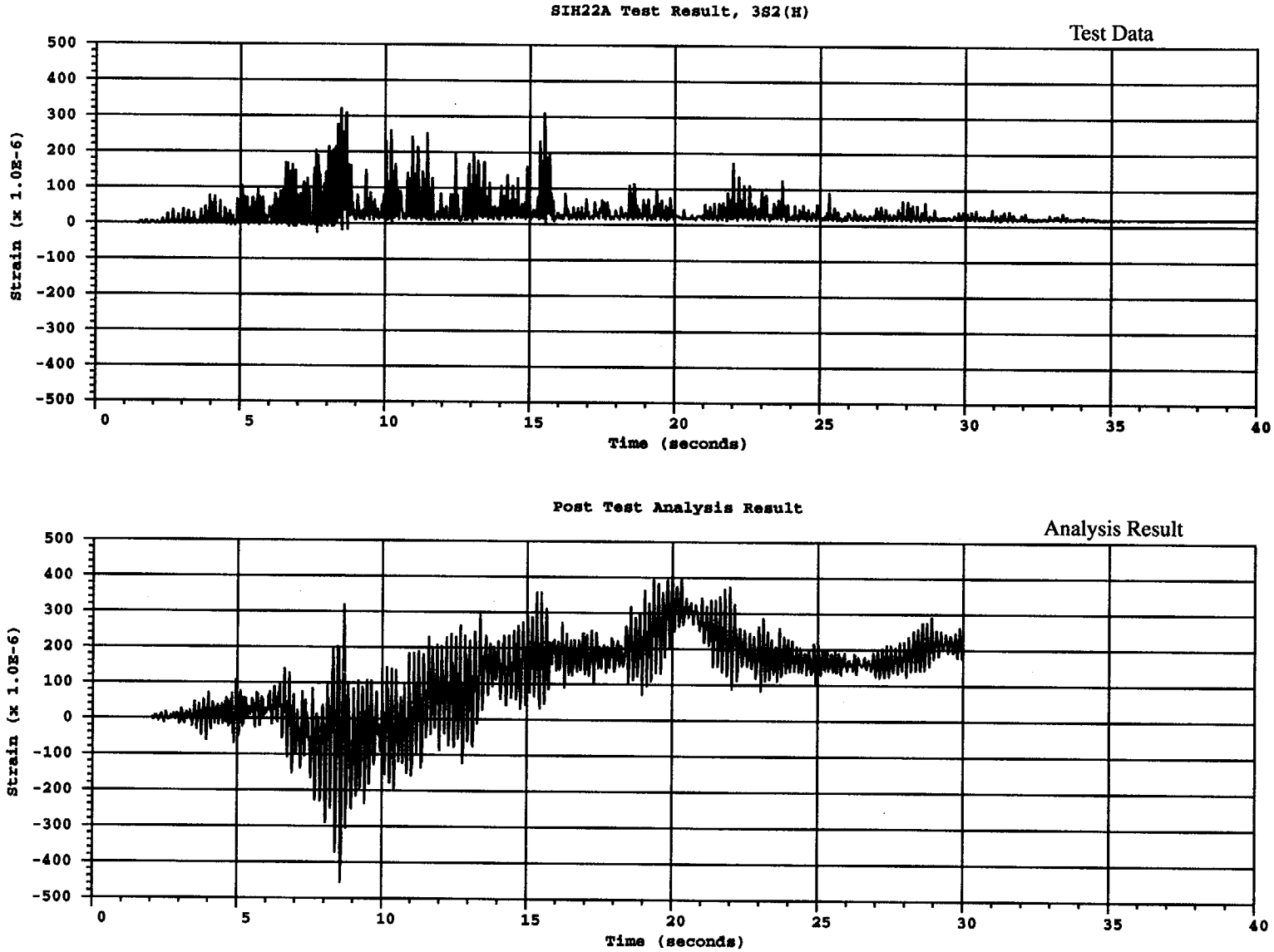

Figure B.67 Comparison of inside hoop rebar strain at SIH22A for 3S2(H) test

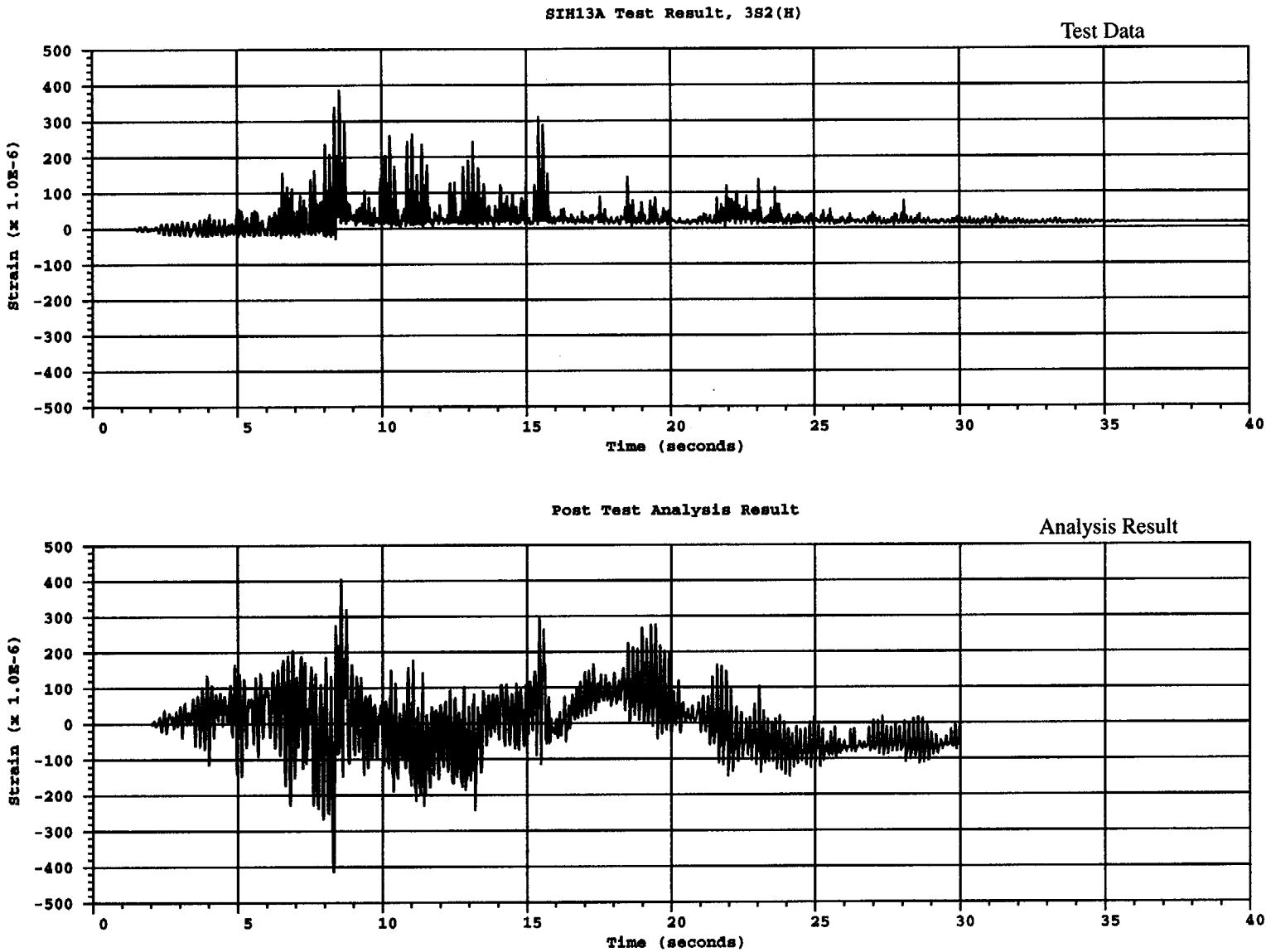

Figure B.68 Comparison of inside hoop rebar strain at SIH13A for 3S2(H) test

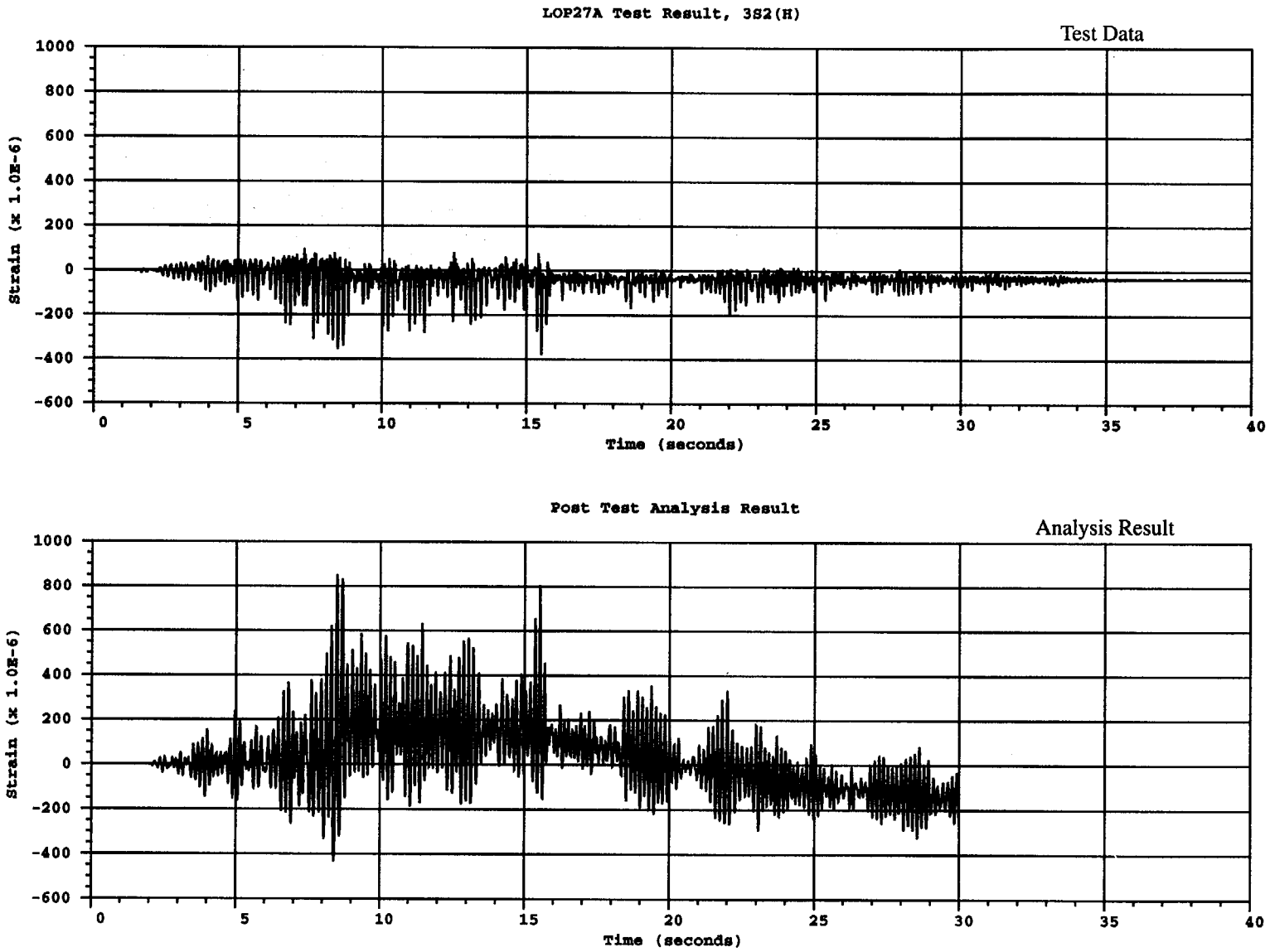

Figure B.69 Comparison of inside hoop liner strain at LOP27A for 3S2(H) test

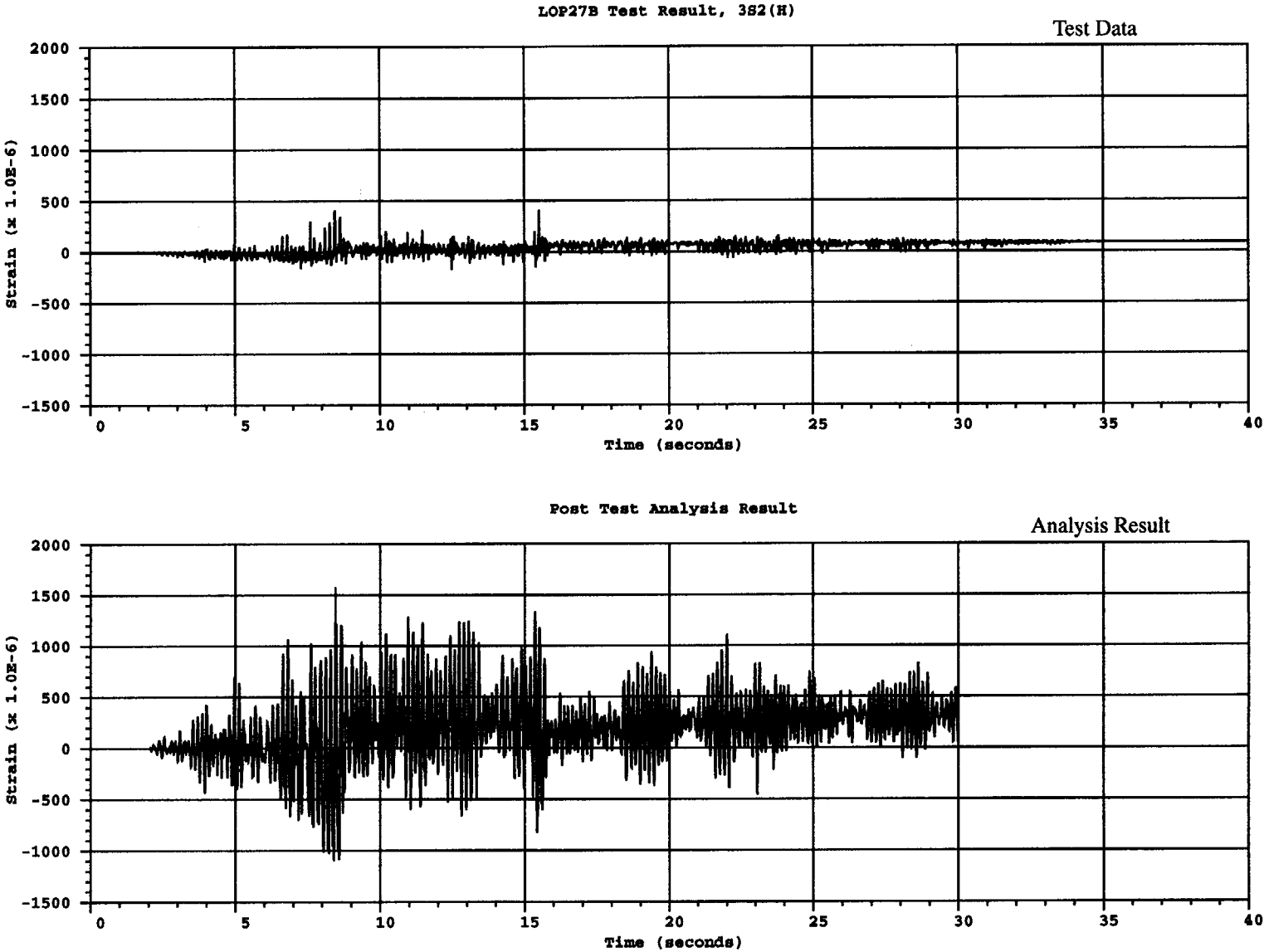

Figure B.70 Comparison of inside vertical liner strain at LOP27B for 3S2(H) test

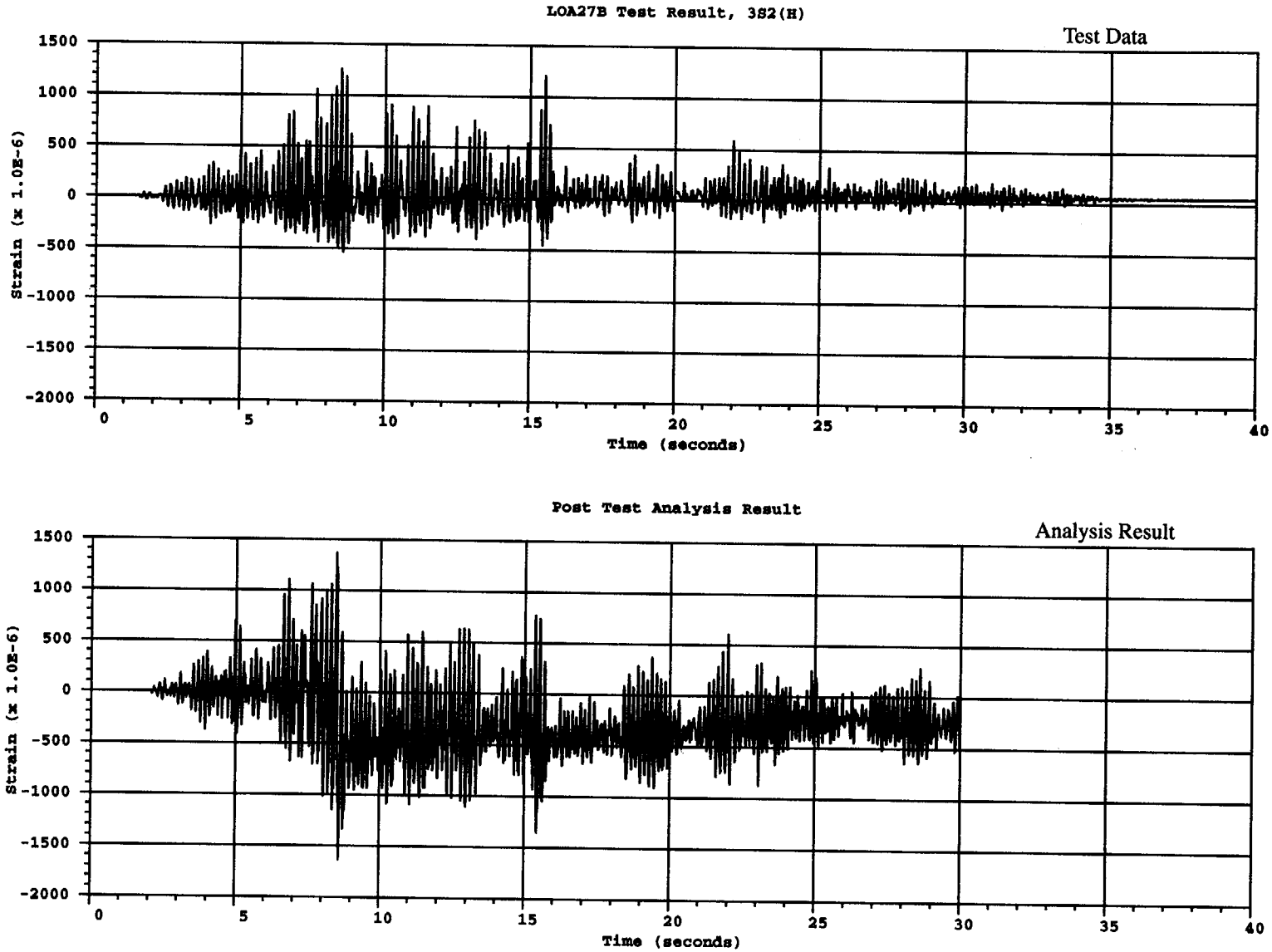

Figure B.71 Comparison of inside vertical liner strain at LOA27B for 3S2(H) test

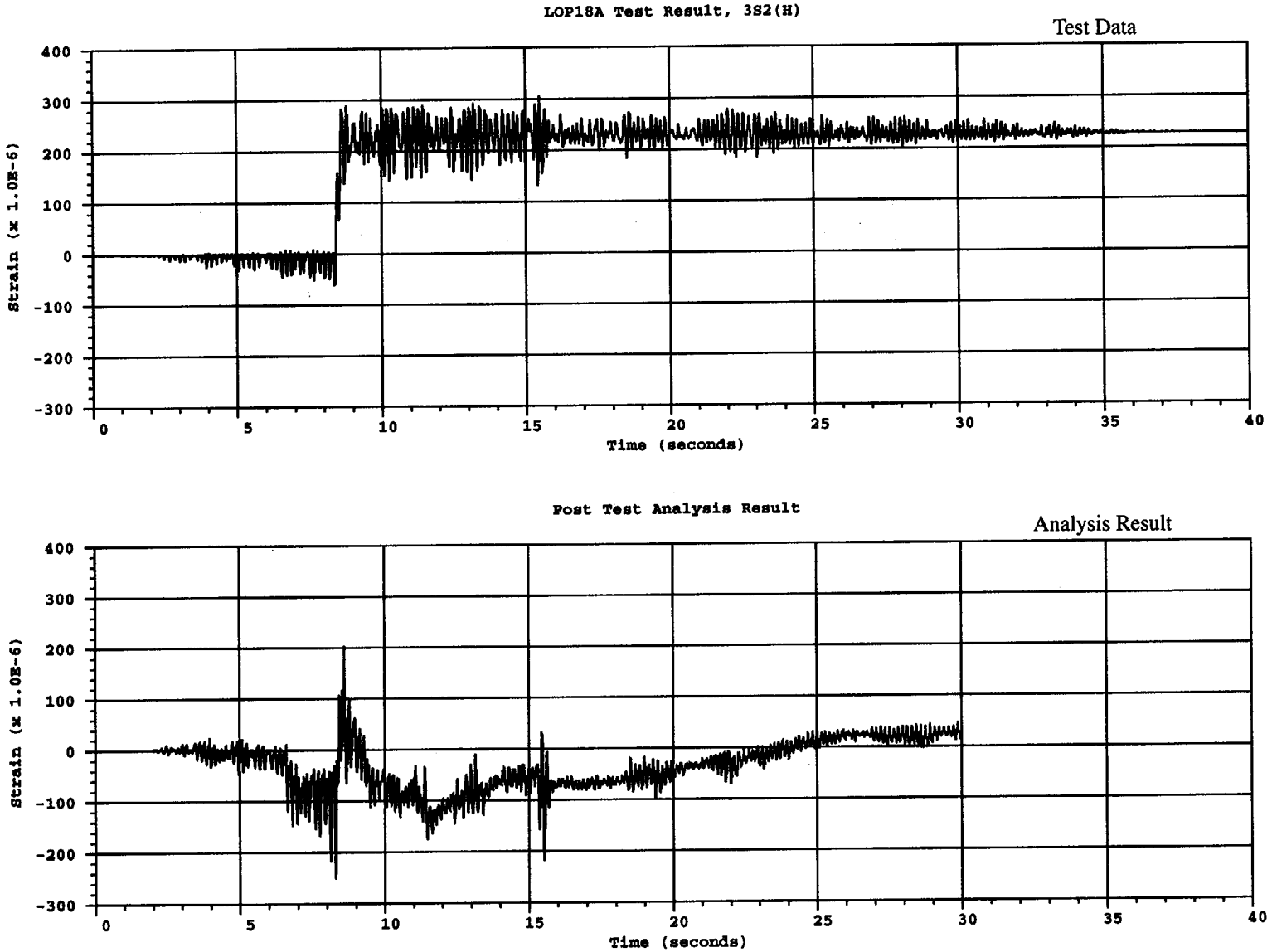

Figure B.72 Comparison of inside hoop liner strain at LOP18A for 3S2(H) test

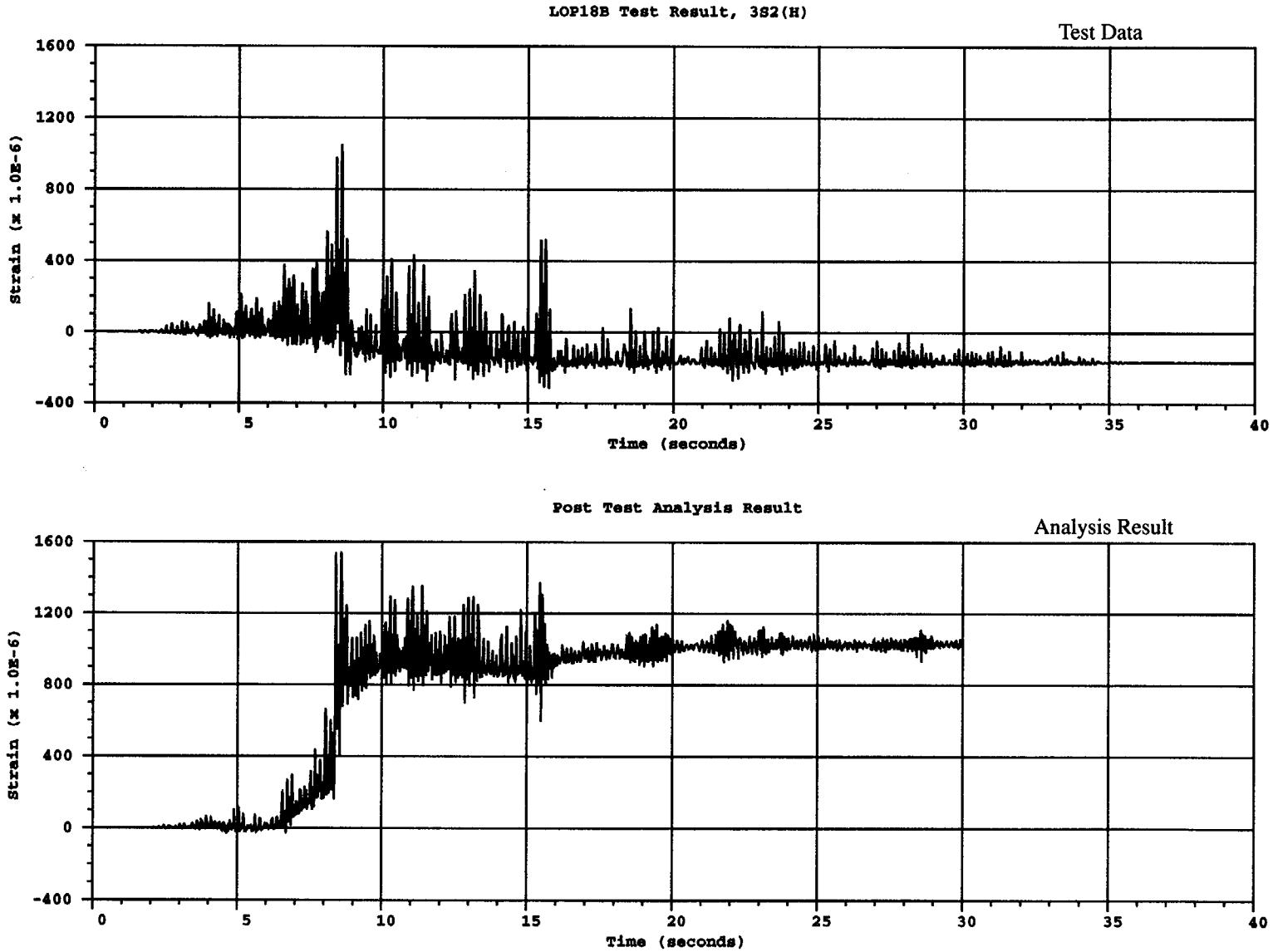

Figure B.73 Comparison of inside vertical liner strain at LOP18B for 3S2(H) test

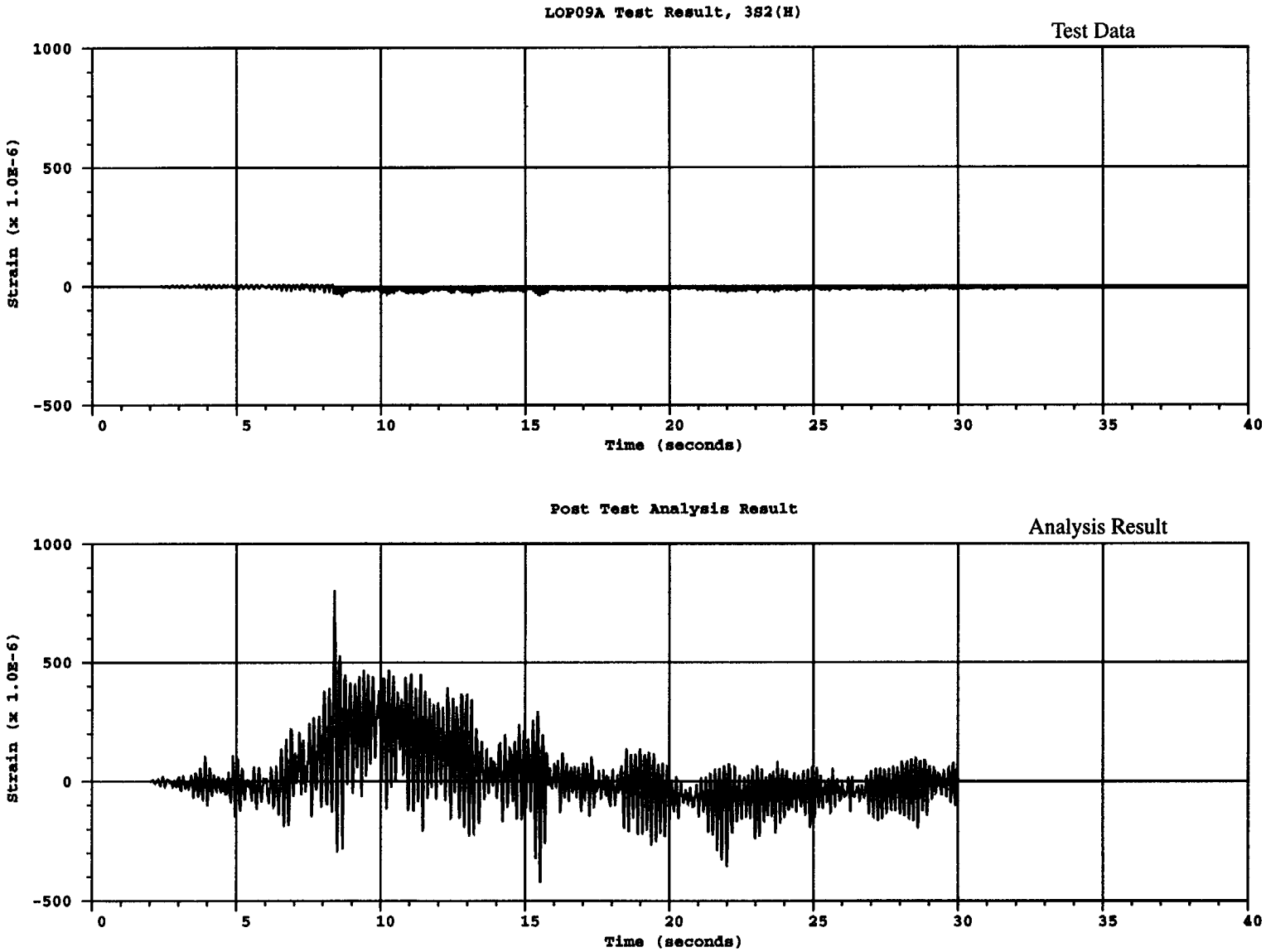

Figure B.74 Comparison of inside hoop liner strain at LOP09A for 3S2(H) test

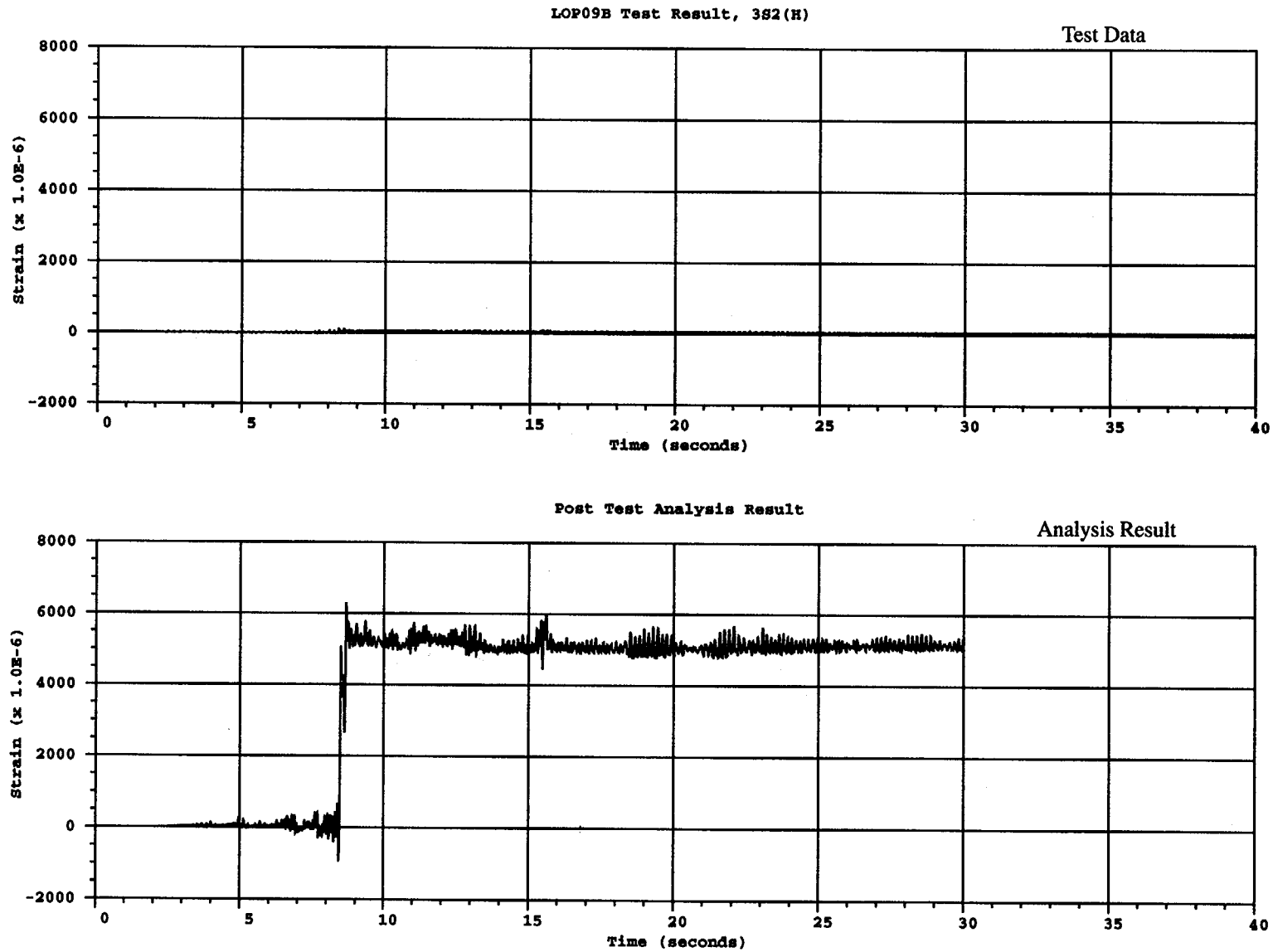

Figure B.75 Comparison of inside vertical liner strain at LOP09B for 3S2(H) test

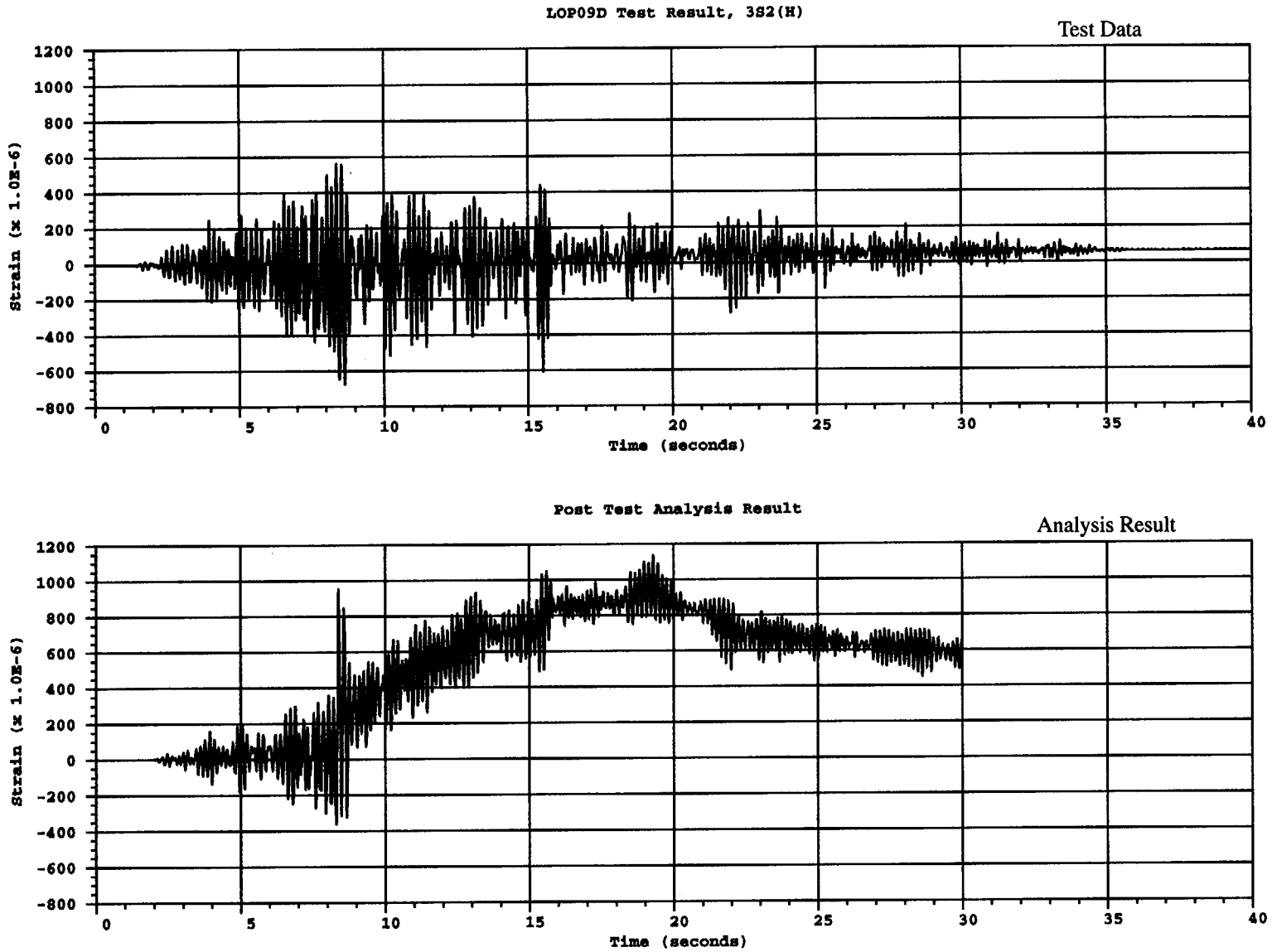

Figure B.76 Comparison of inside hoop liner strain at LOP09D for 3S2(H) test

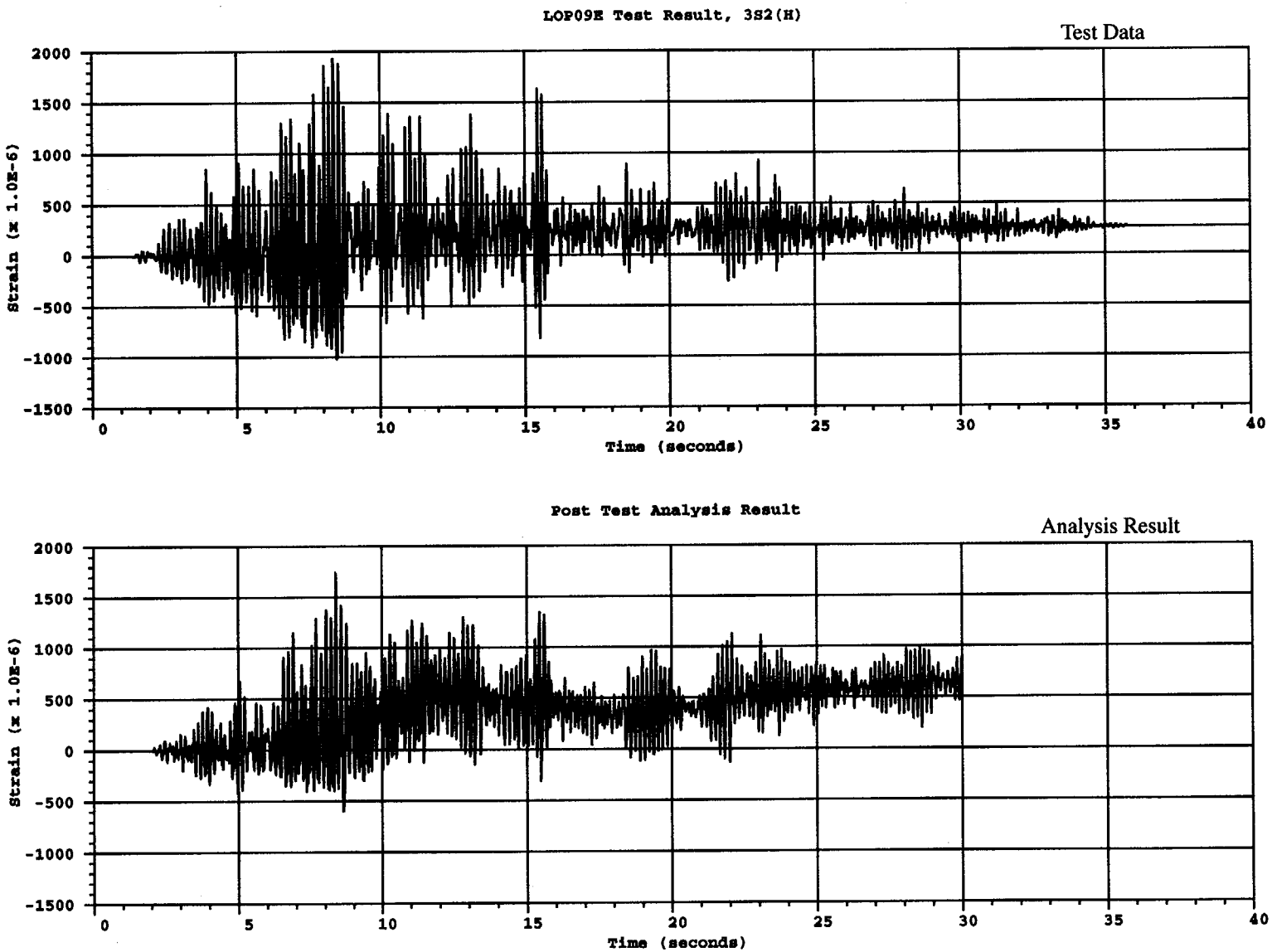

Figure B.77 Comparison of inside vertical liner strain at LOP09E for 3S2(H) test

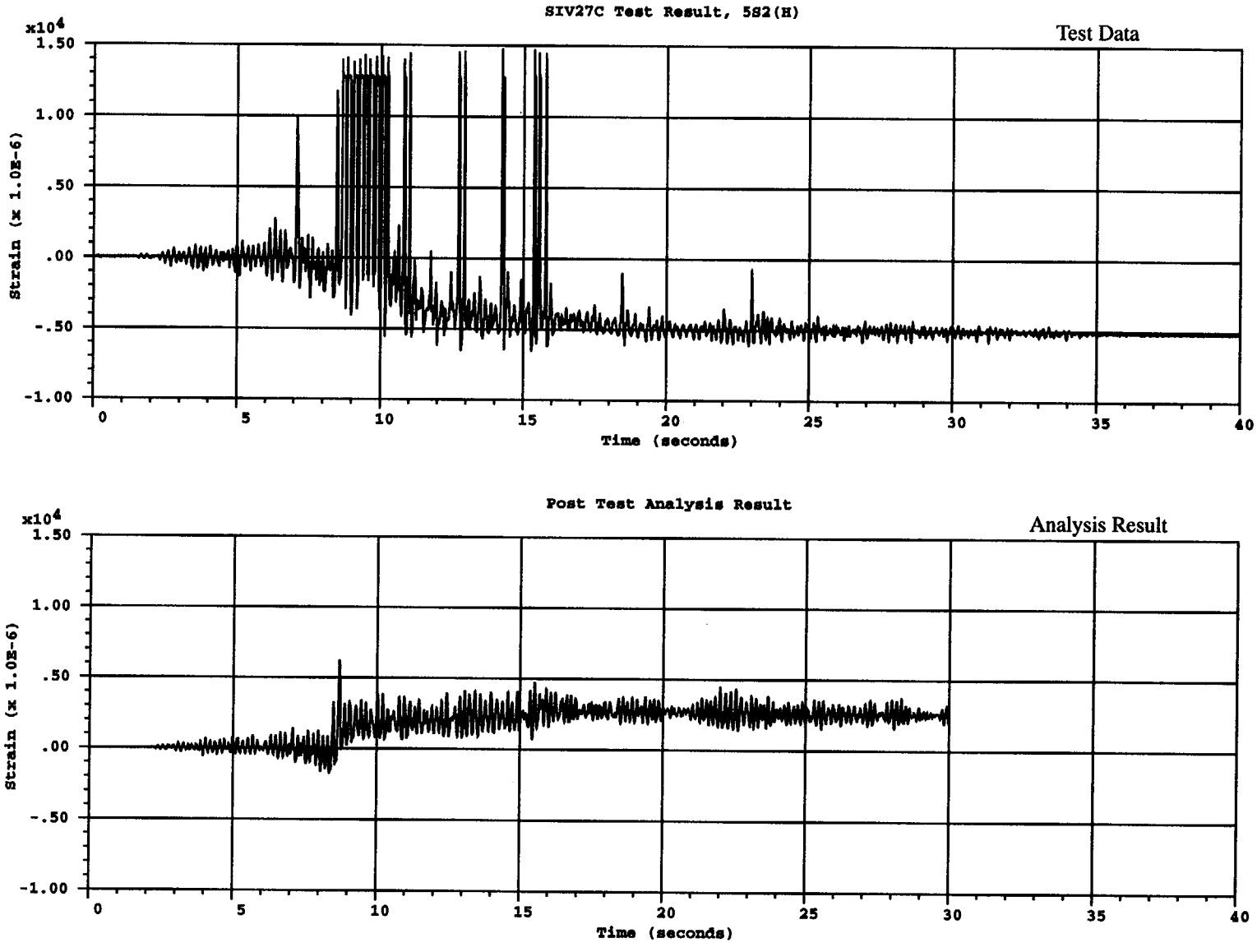

Figure B.78 Comparison of inside vertical liner strain at SIV27C for 5S2(H) test

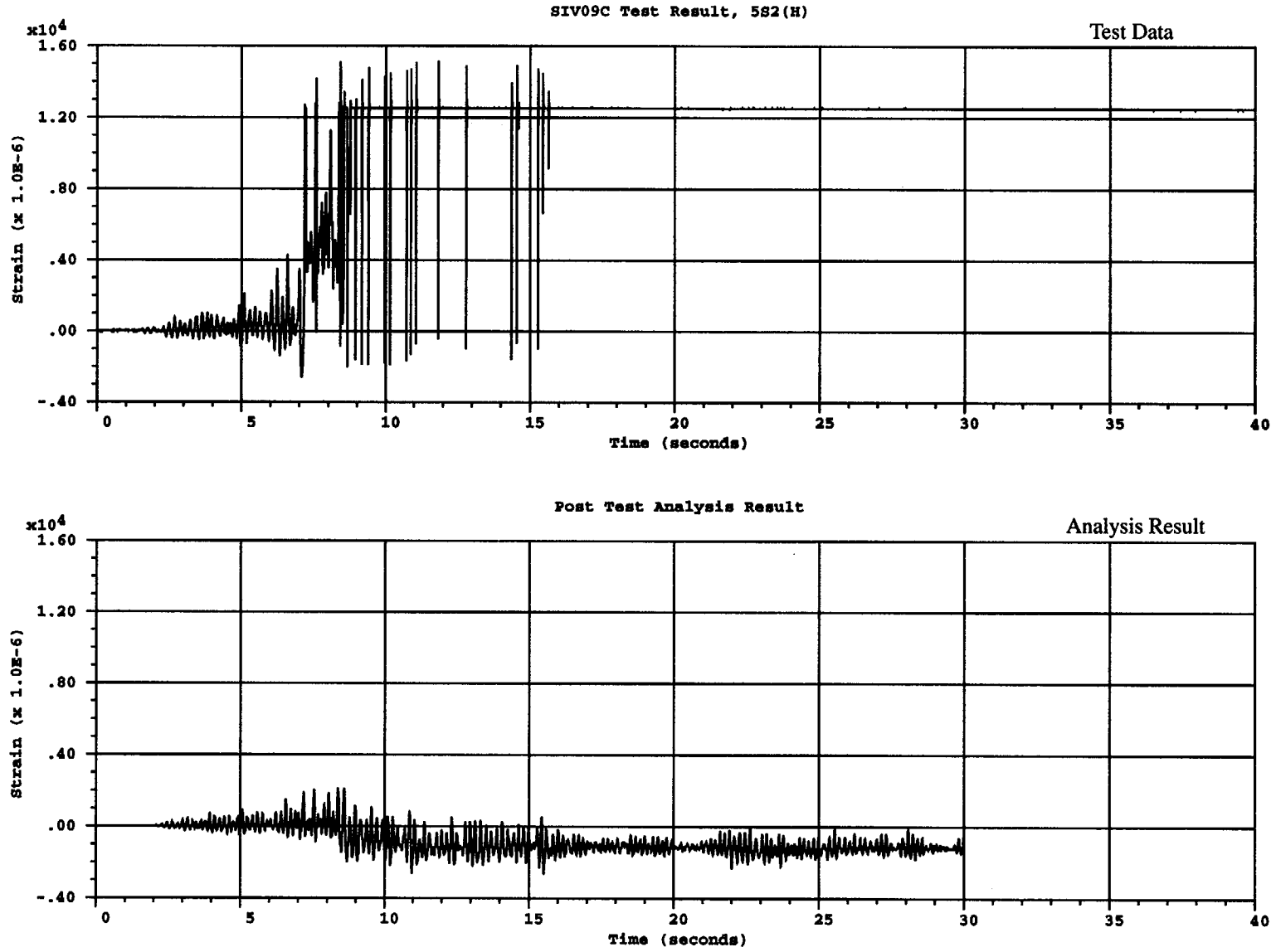

Figure B.79 Comparison of inside vertical liner strain at SIV09C for 5S2(H) test

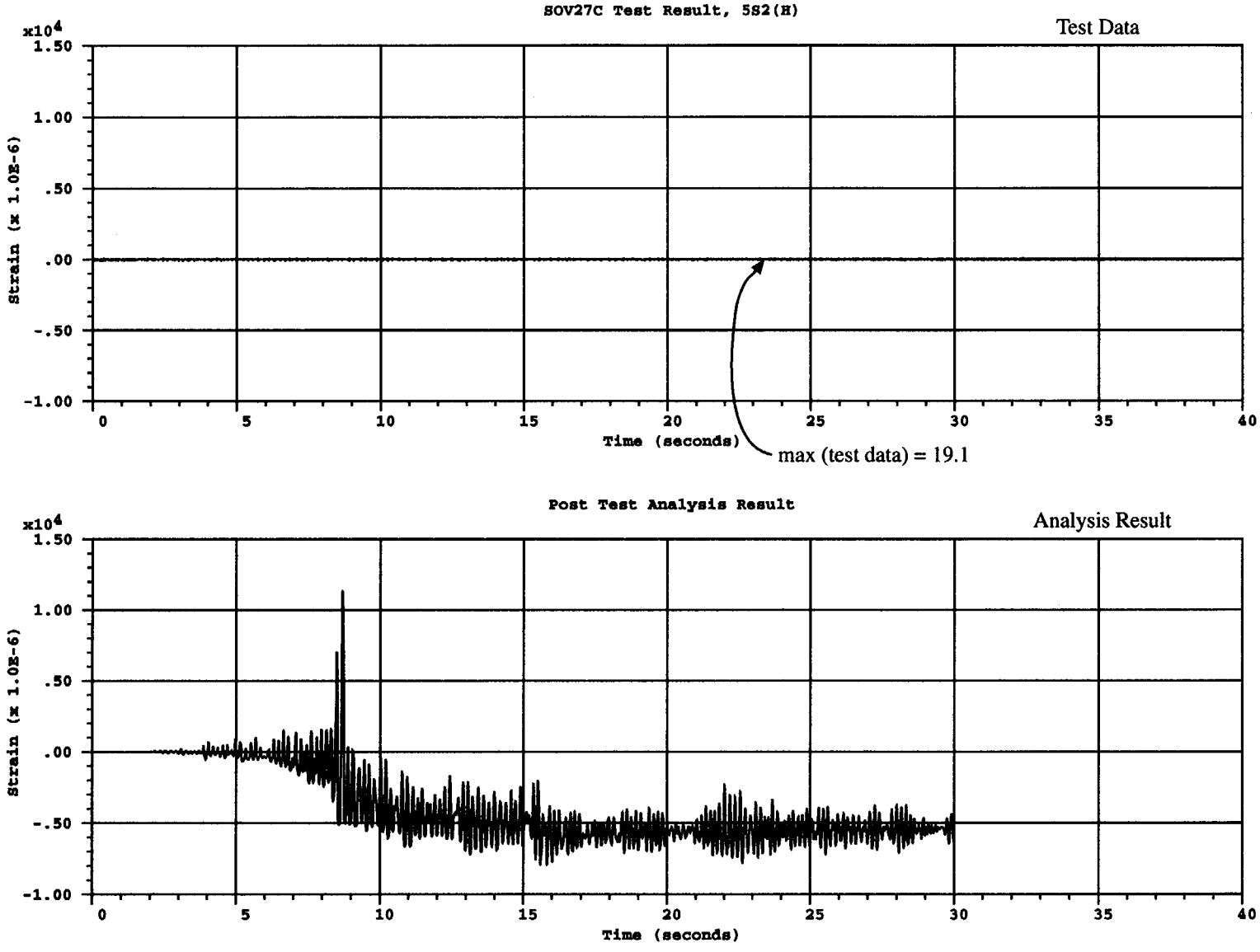

Figure B.80 Comparison of outside vertical rebar strain at SOV27C for 5S2(H) test

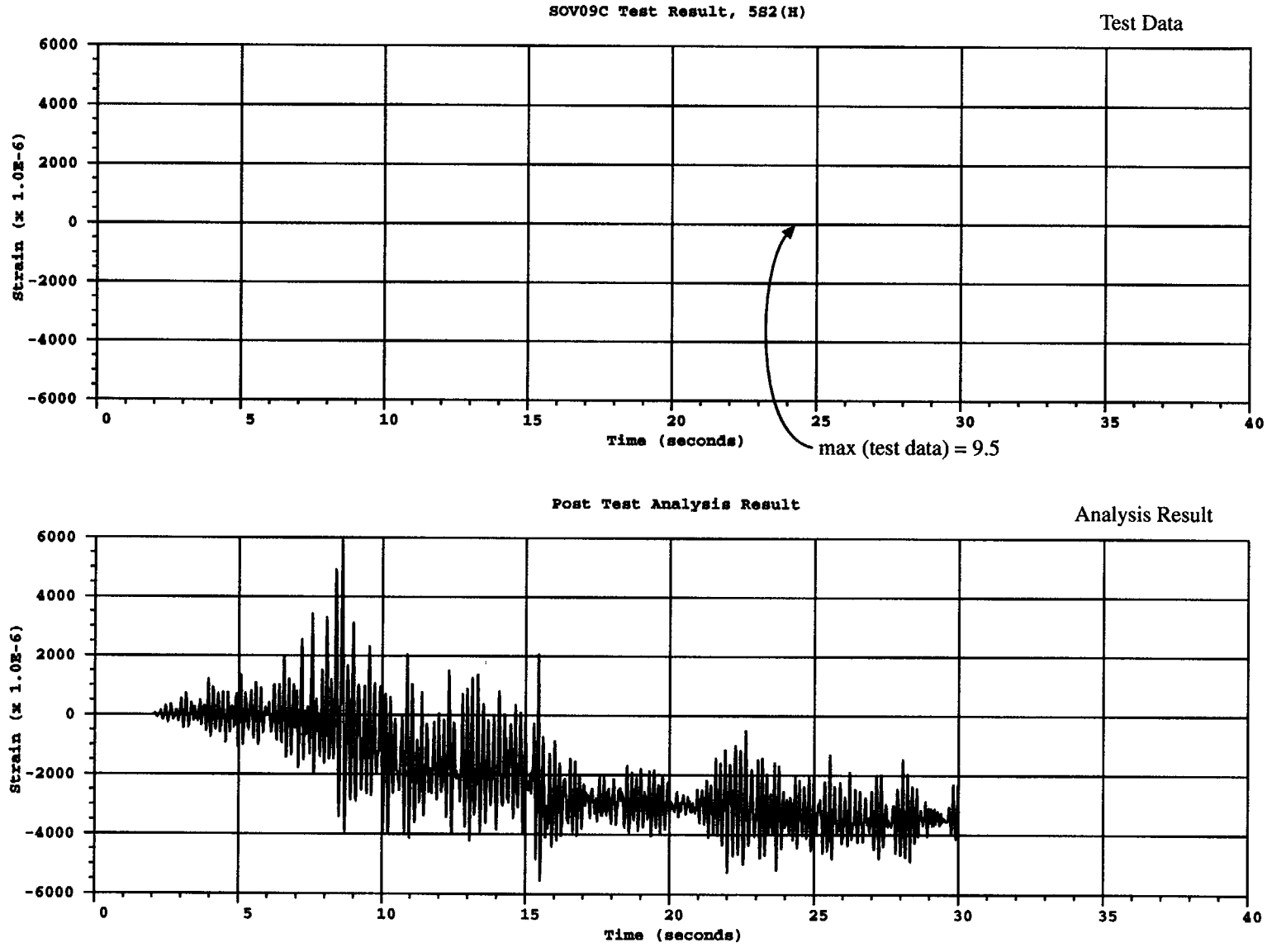

Figure B.81 Comparison of outside vertical rebar strain at SOV09C for 5S2(H) test

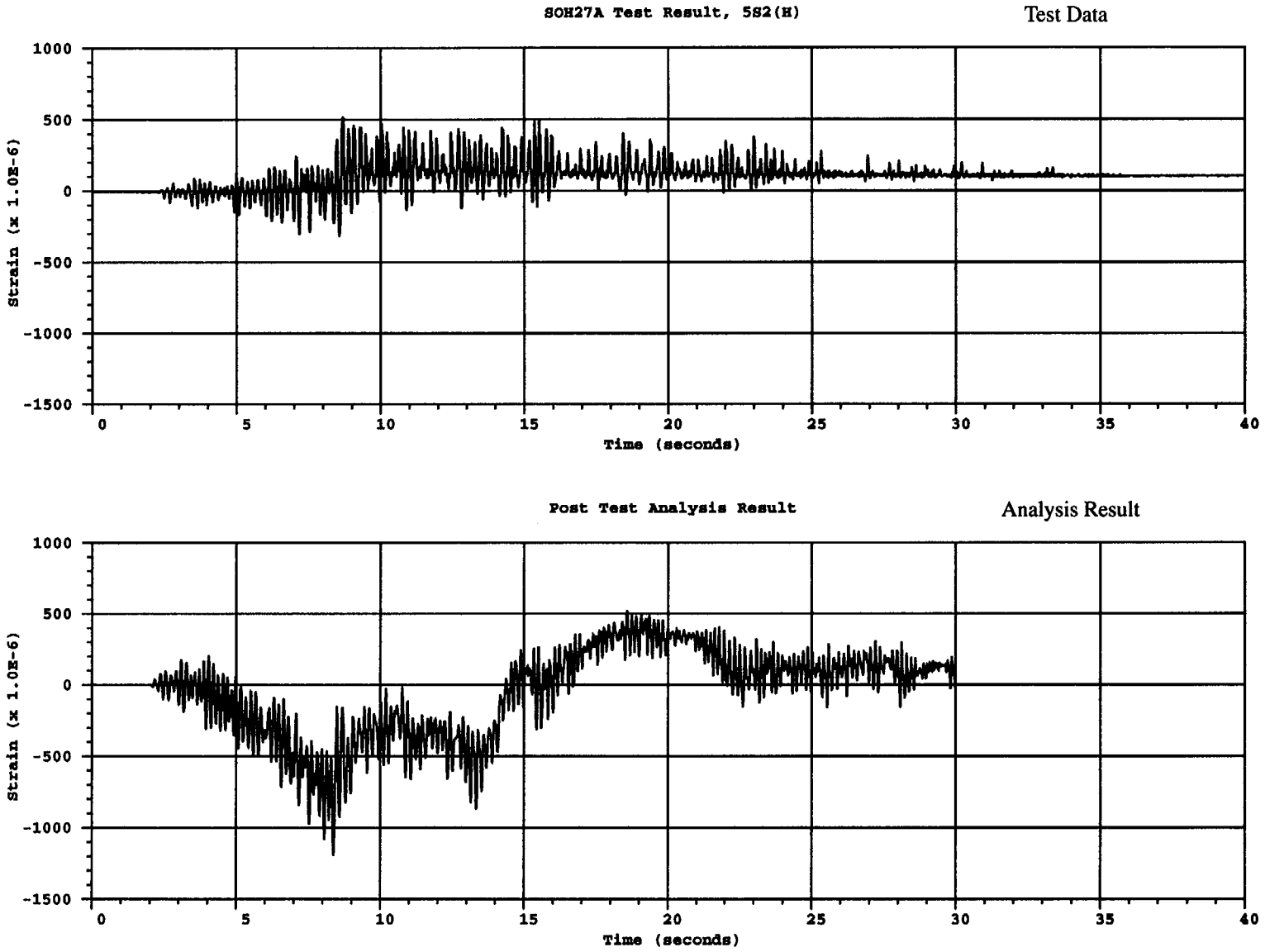

Figure B.82 Comparison of outside hoop rebar strain at SOH27A for 5S2(H) test

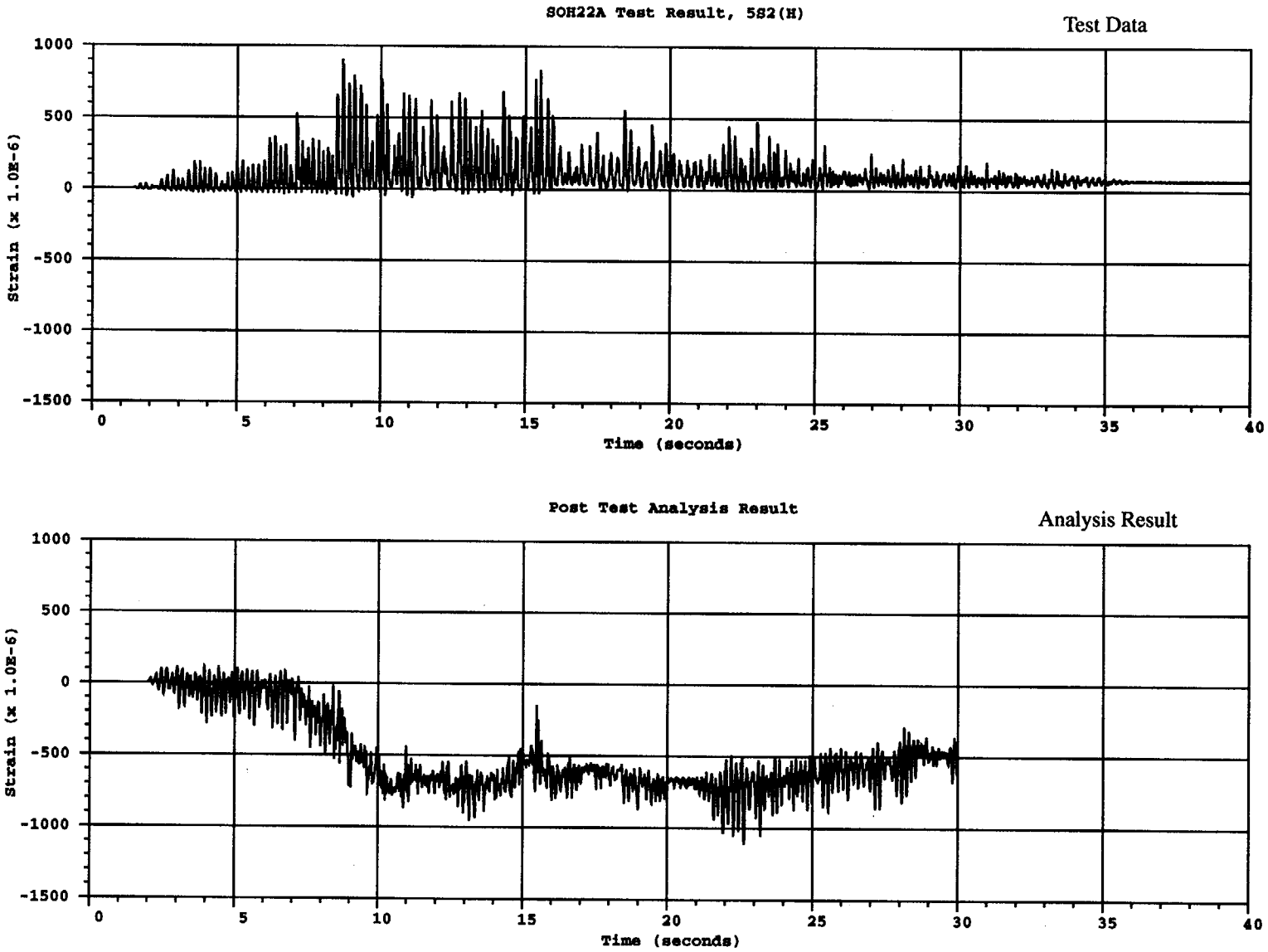

Figure B.83 Comparison of outside hoop rebar strain at SOH22A for 5S2(H) test

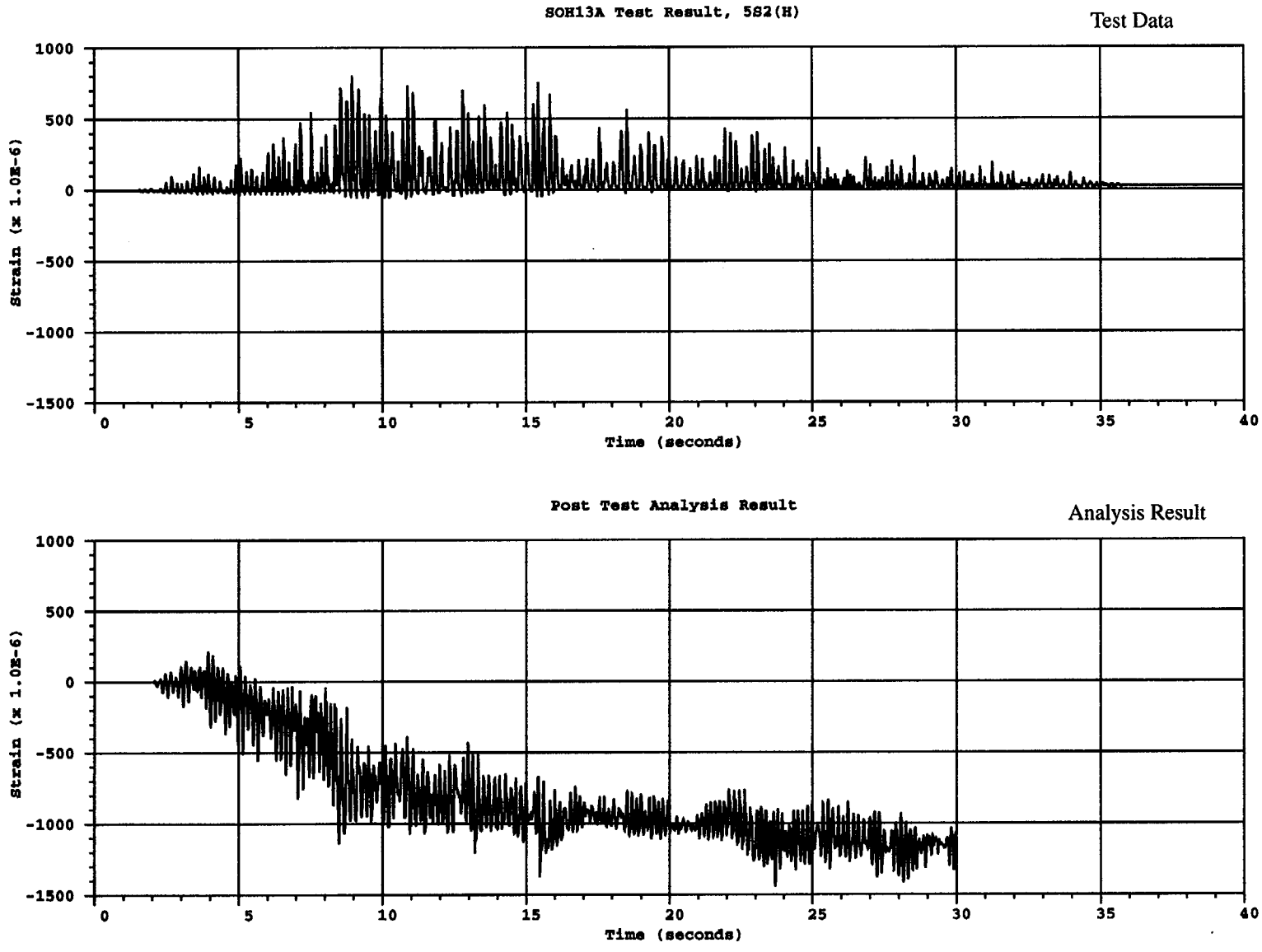

Figure B.84 Comparison of outside hoop rebar strain at SOH13A for 5S2(H) test

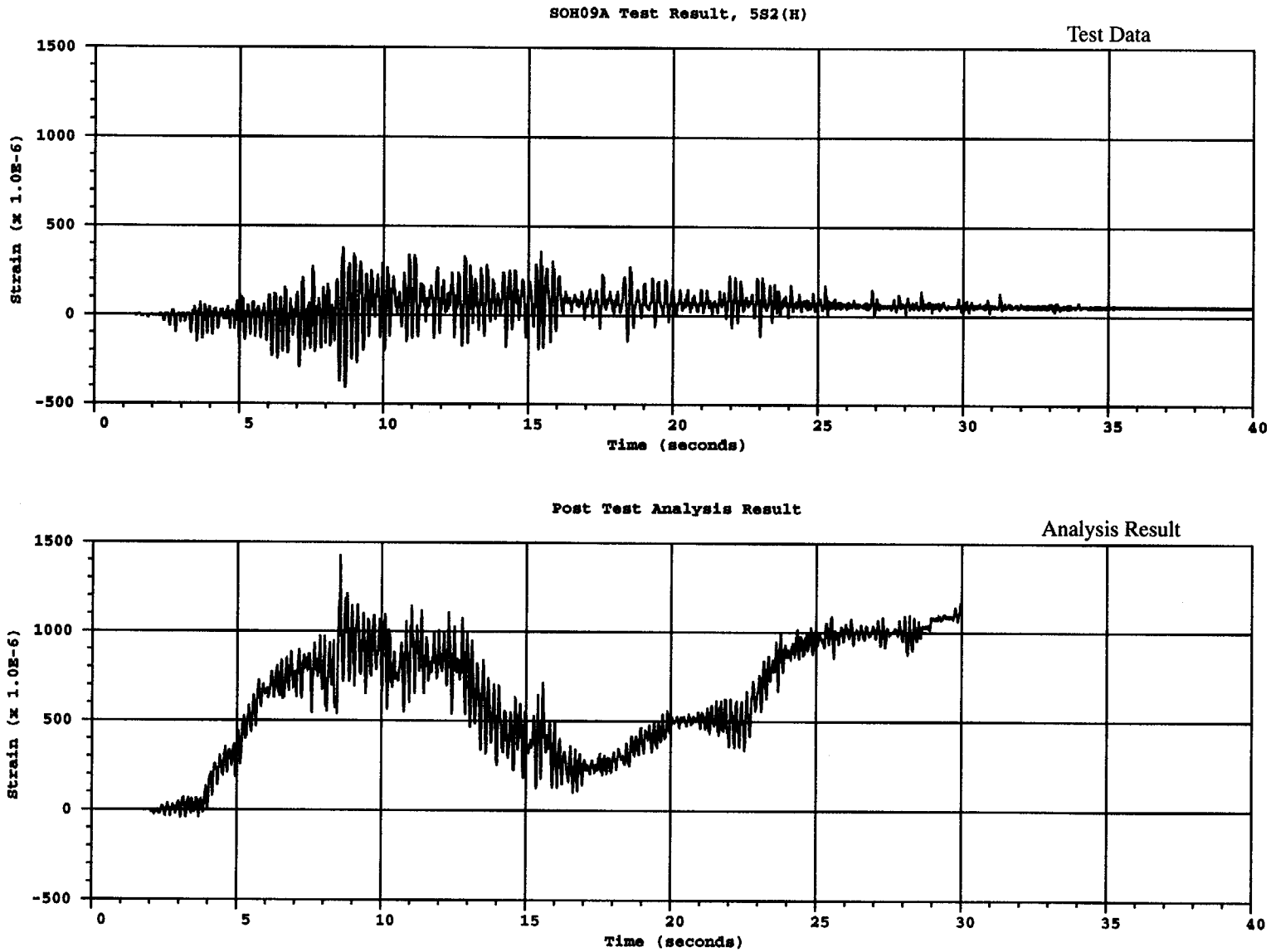

Figure B.85 Comparison of outside hoop rebar strain at SOH09A for 5S2(H) test

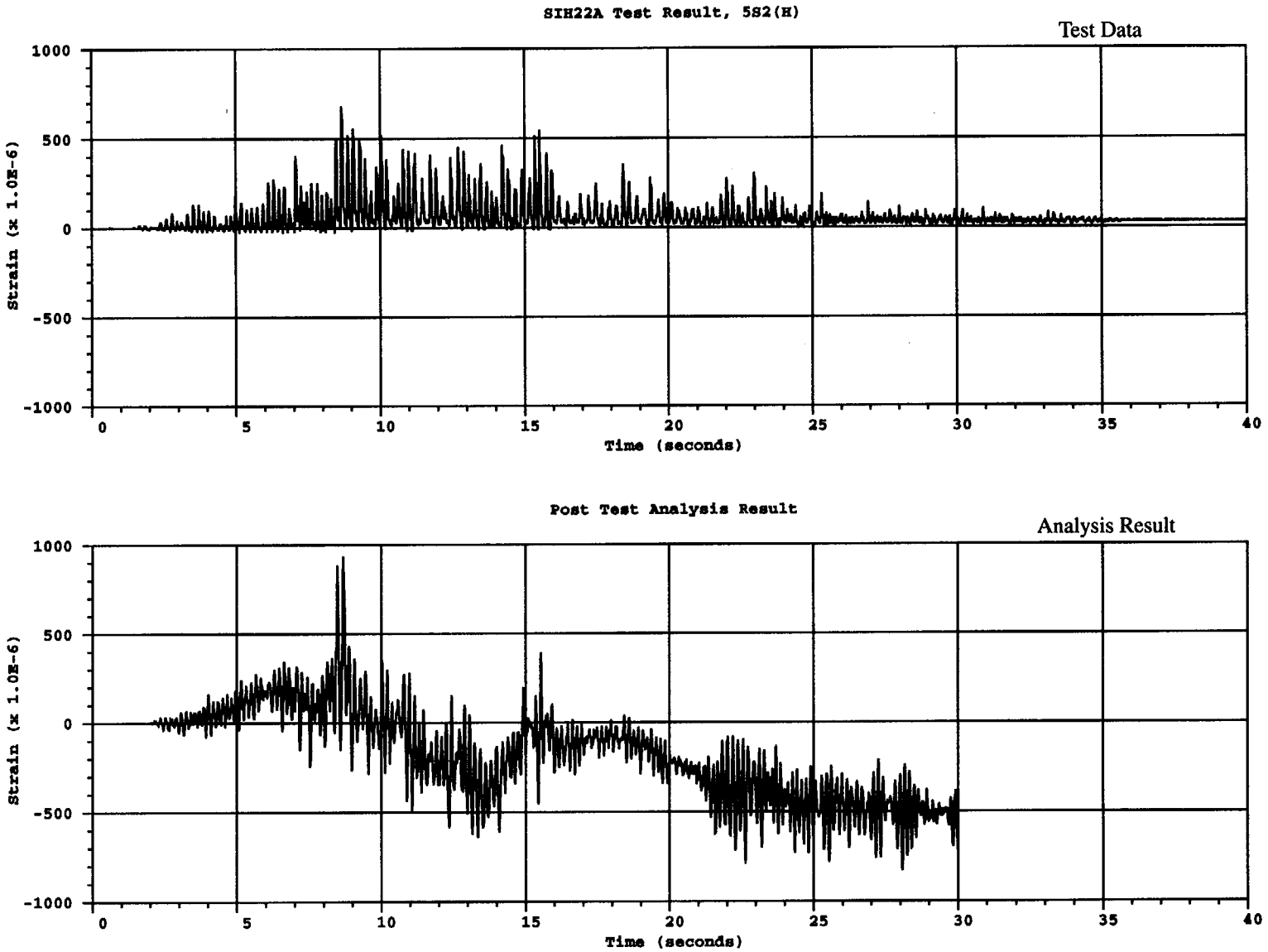

Figure B.86 Comparison of inside hoop rebar strain at SIH22A for 5S2(H) test

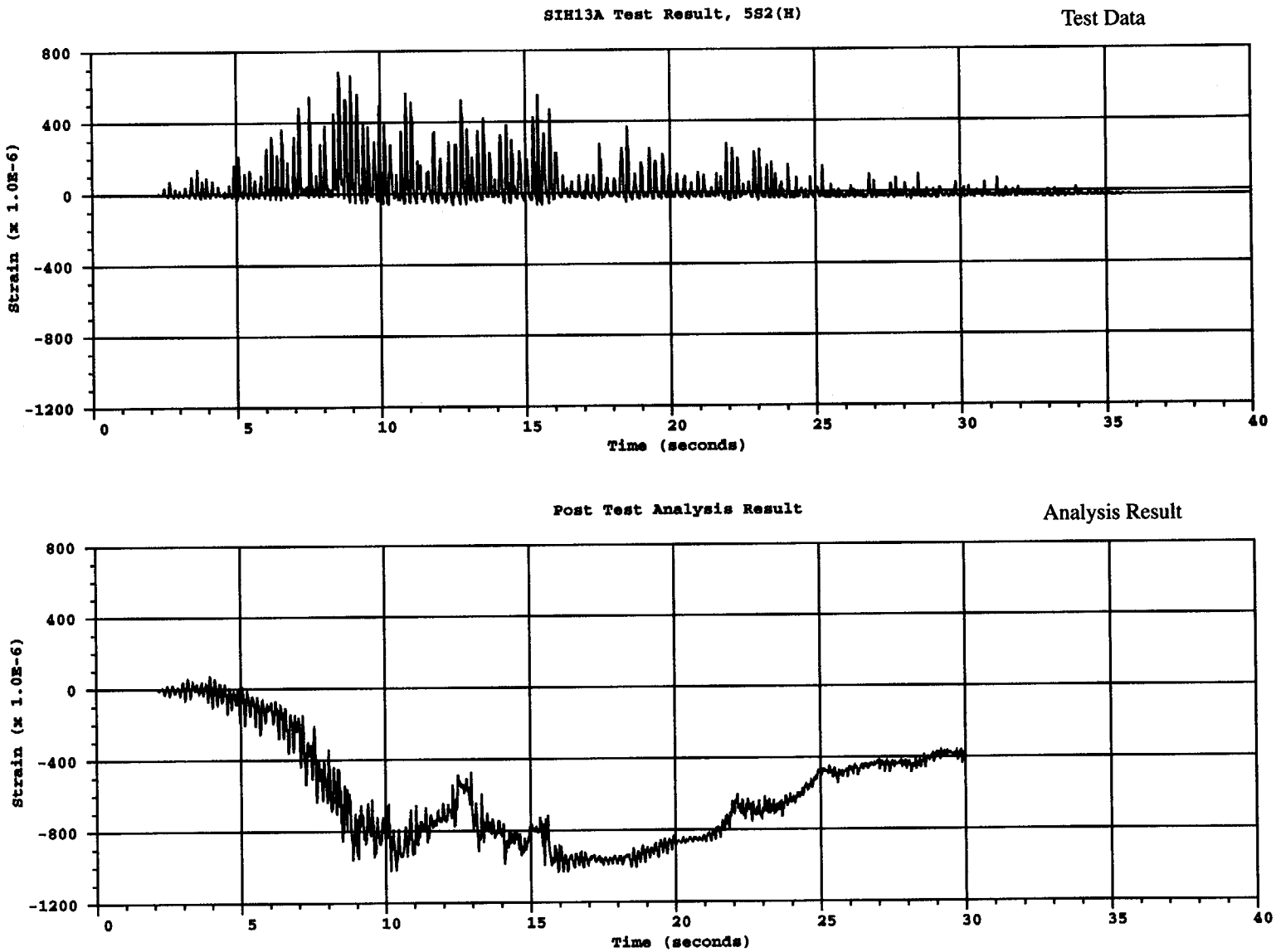

Figure B.87 Comparison of inside hoop rebar strain at SIH13A for 5S2(H) test

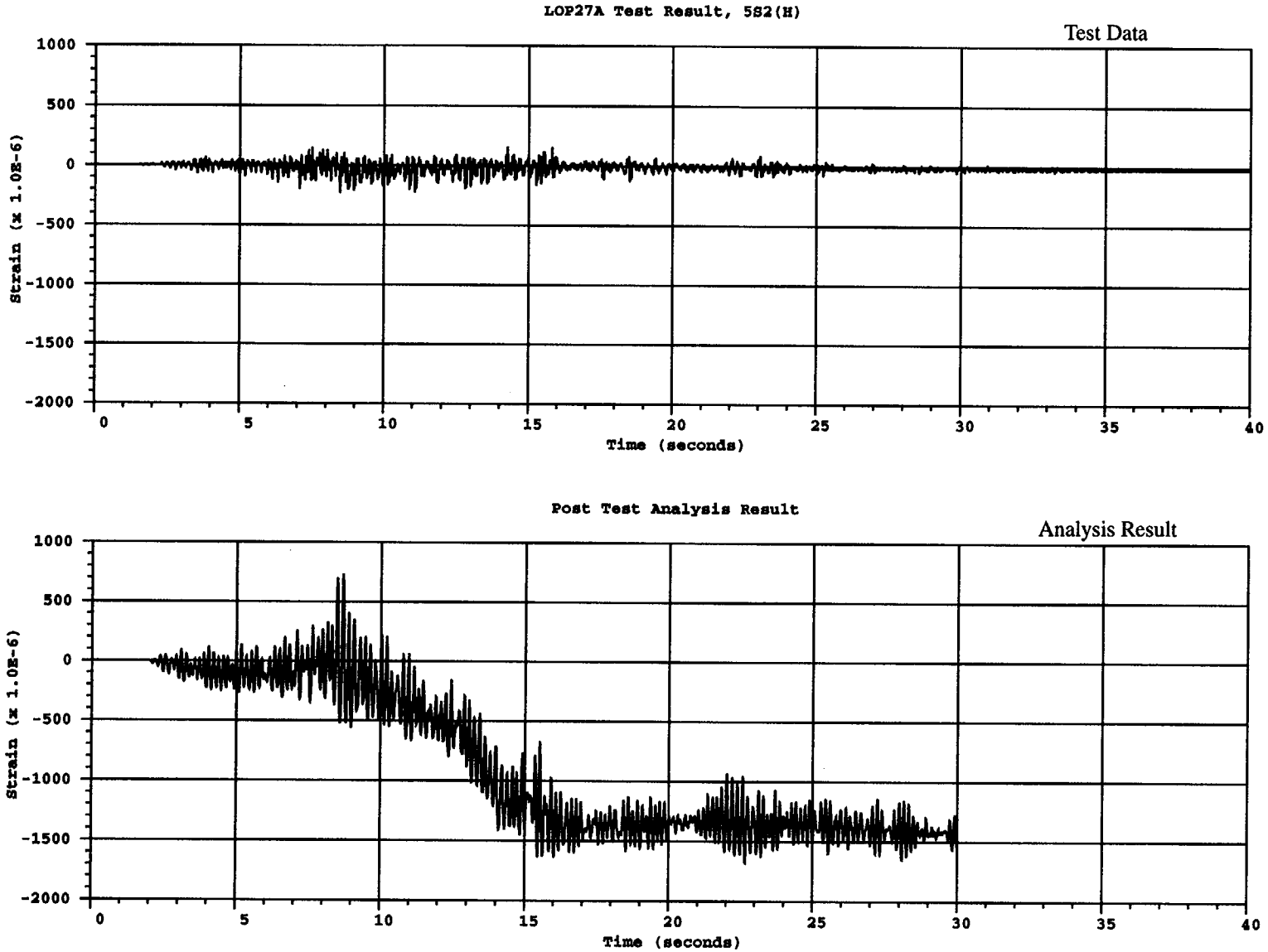

Figure B.88 Comparison of hoop liner strain at LOP27A for 5S2(H) test

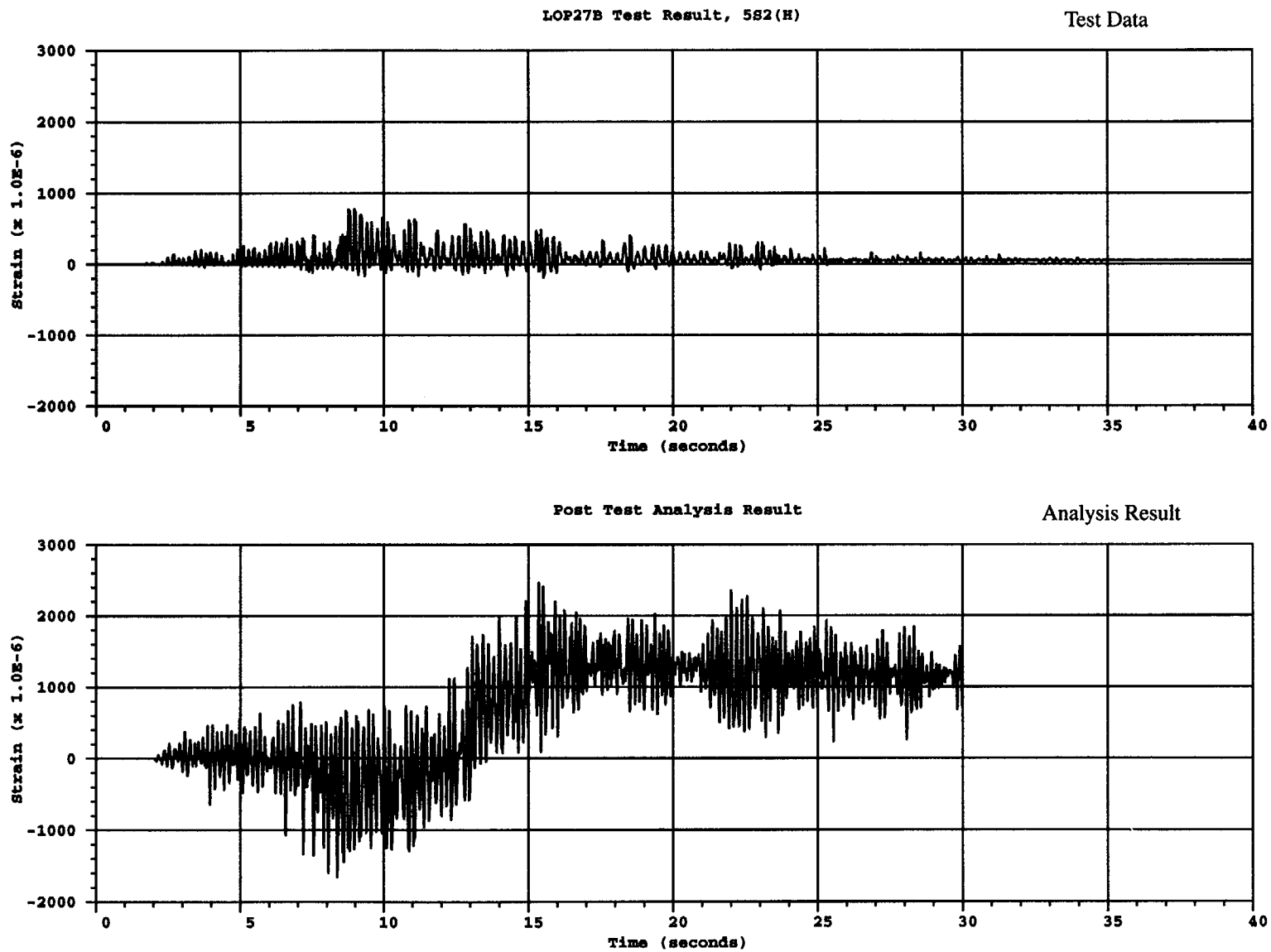

Figure B.89 Comparison of vertical liner strain at LOP27B for 5S2(H) test

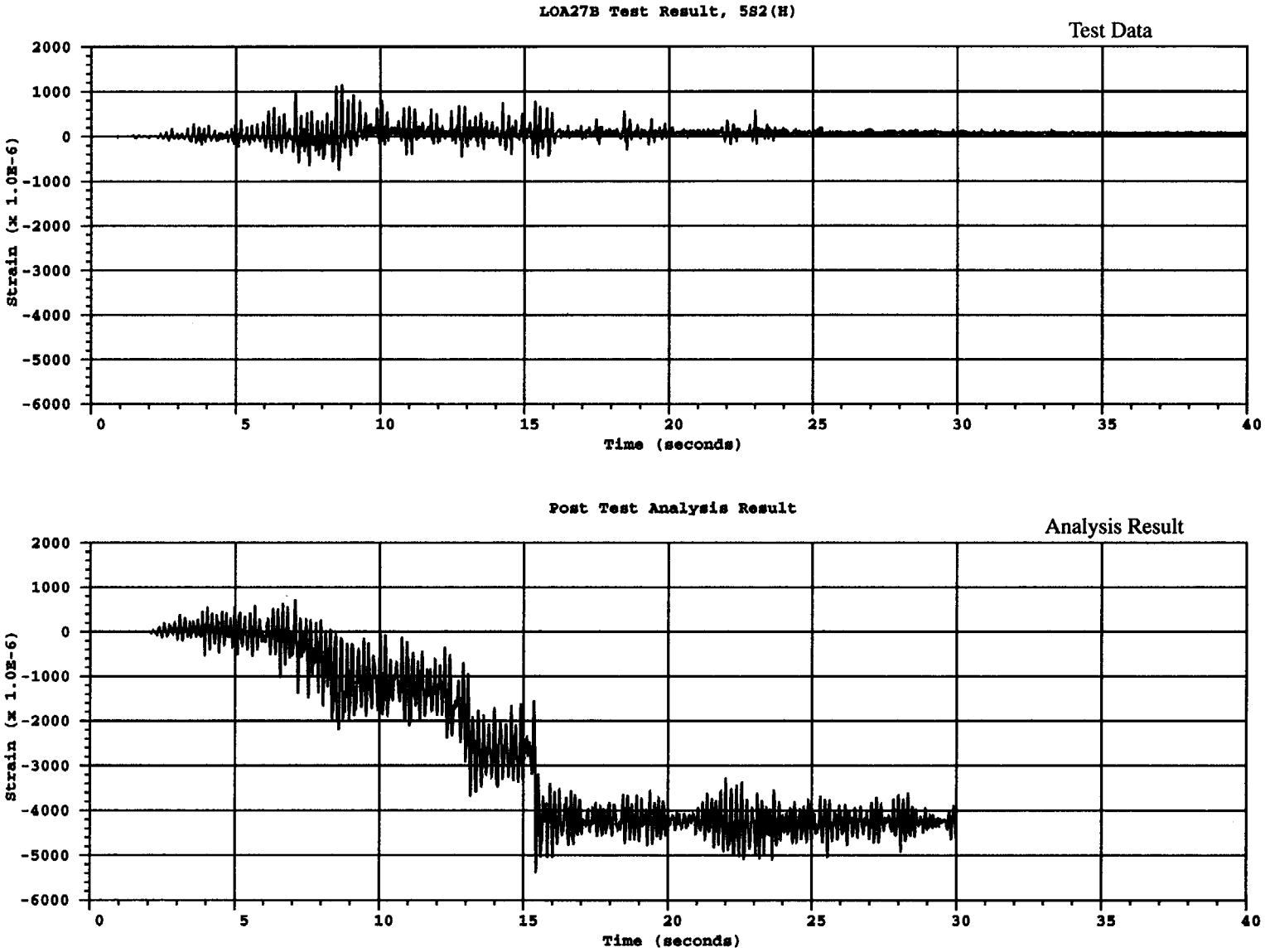

Figure B.90 Comparison of vertical liner strain at LOA27B for 5S2(H) test

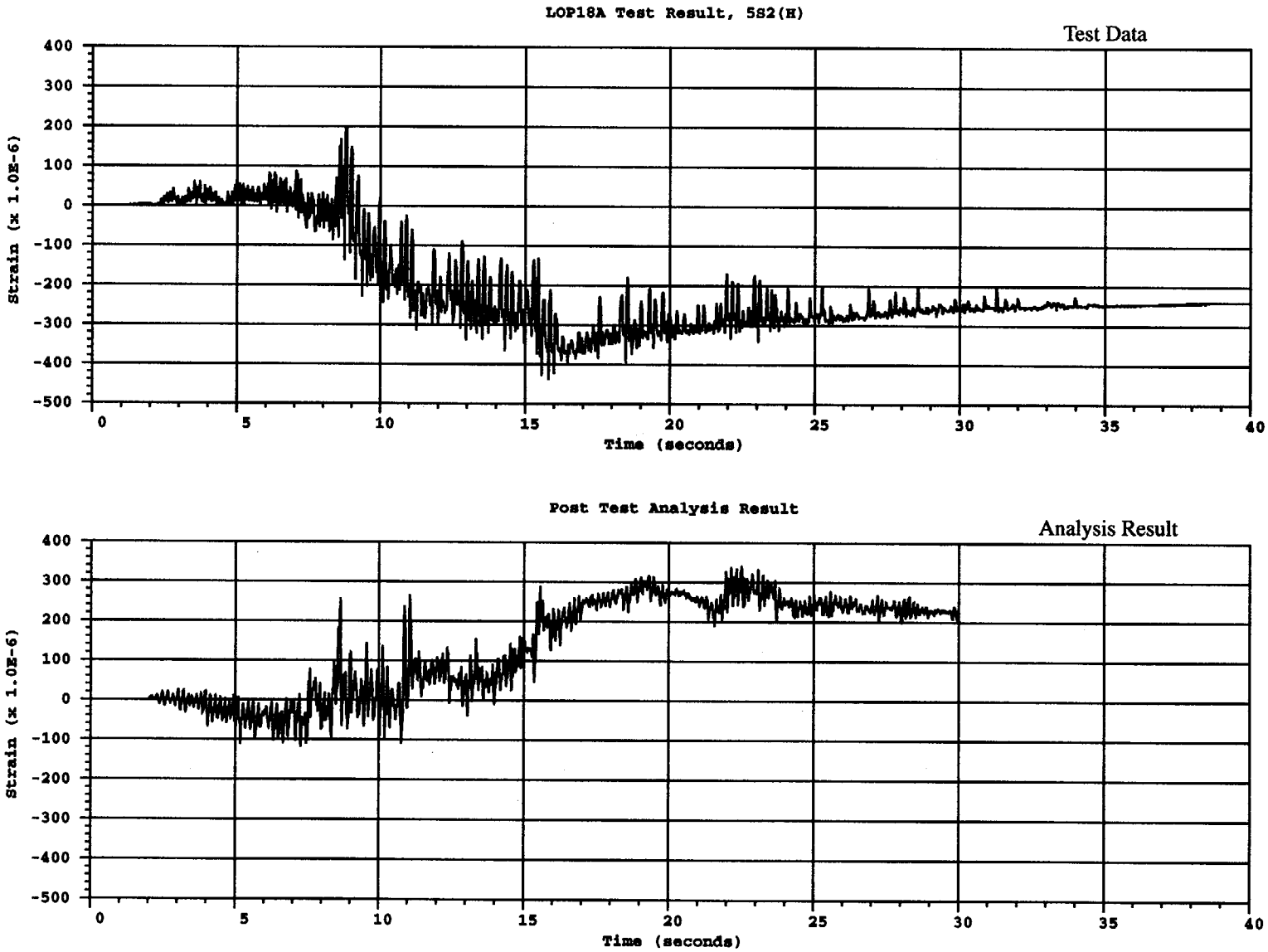

Figure B.91 Comparison of hoop liner strain at LOP18A for 5S2(H) test

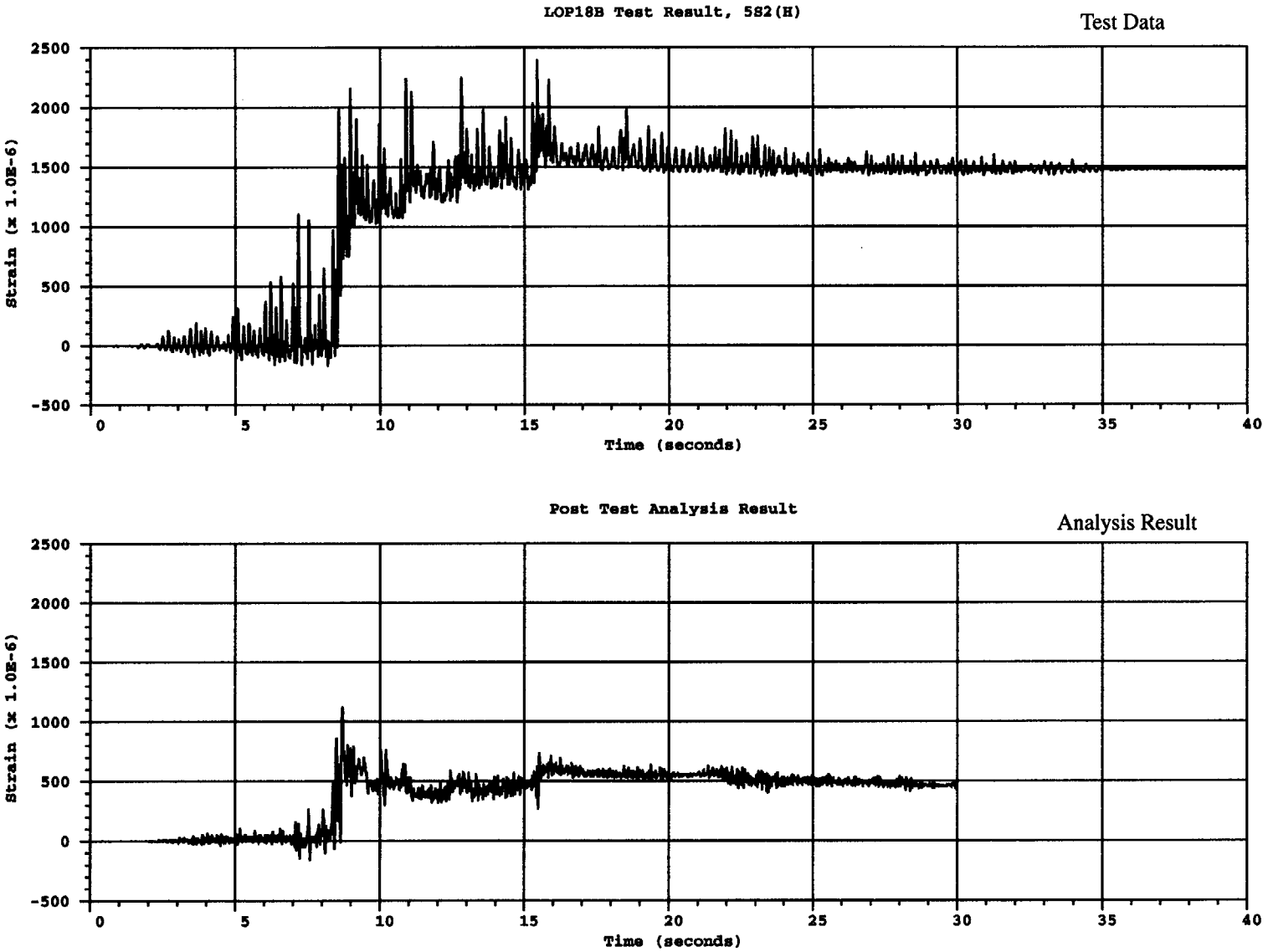

Figure B.92 Comparison of vertical liner strain at LOP18B for 5S2(H) test

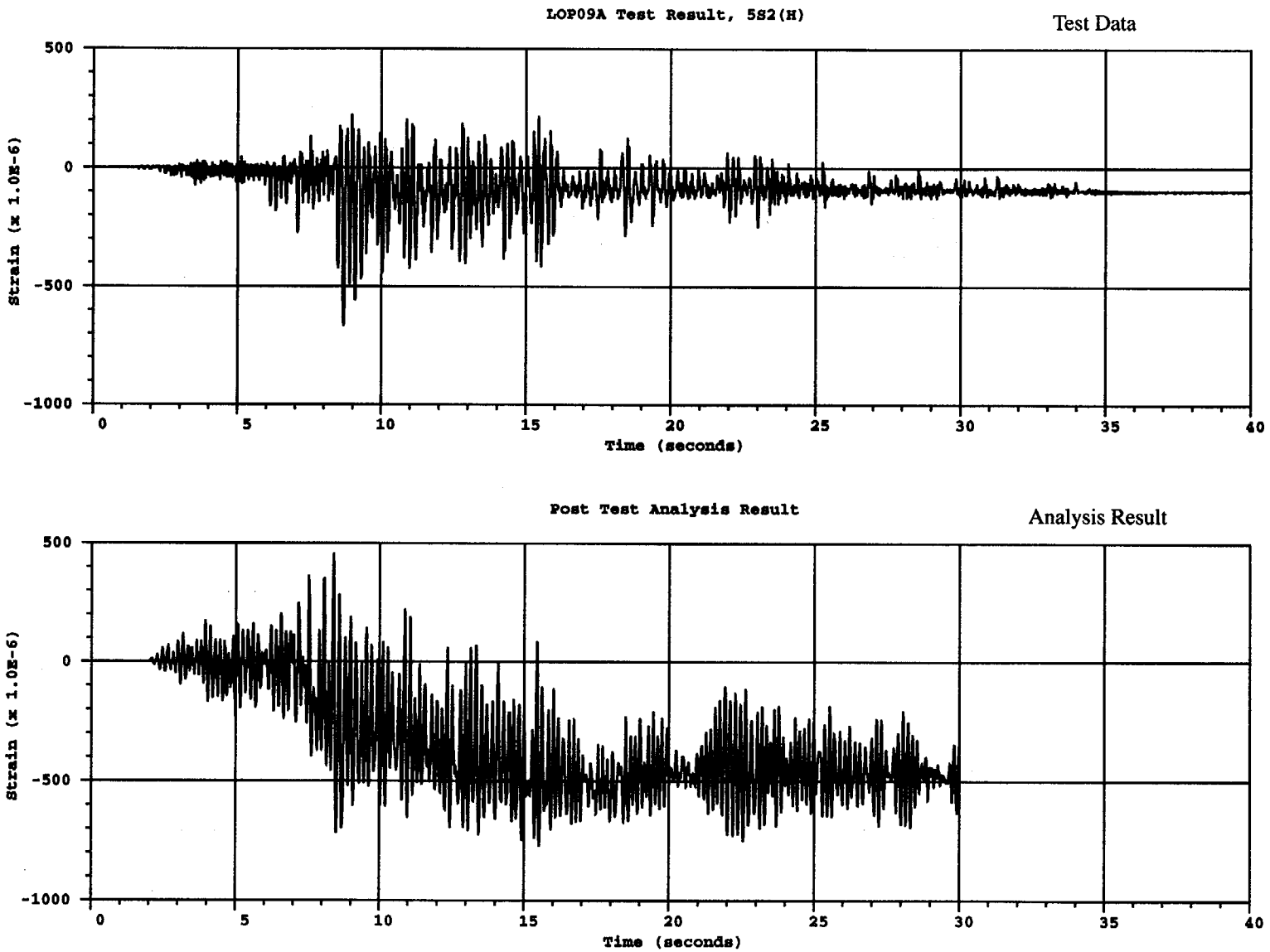

Figure B.93 Comparison of hoop liner strain at LOP09A for 5S2(H) test

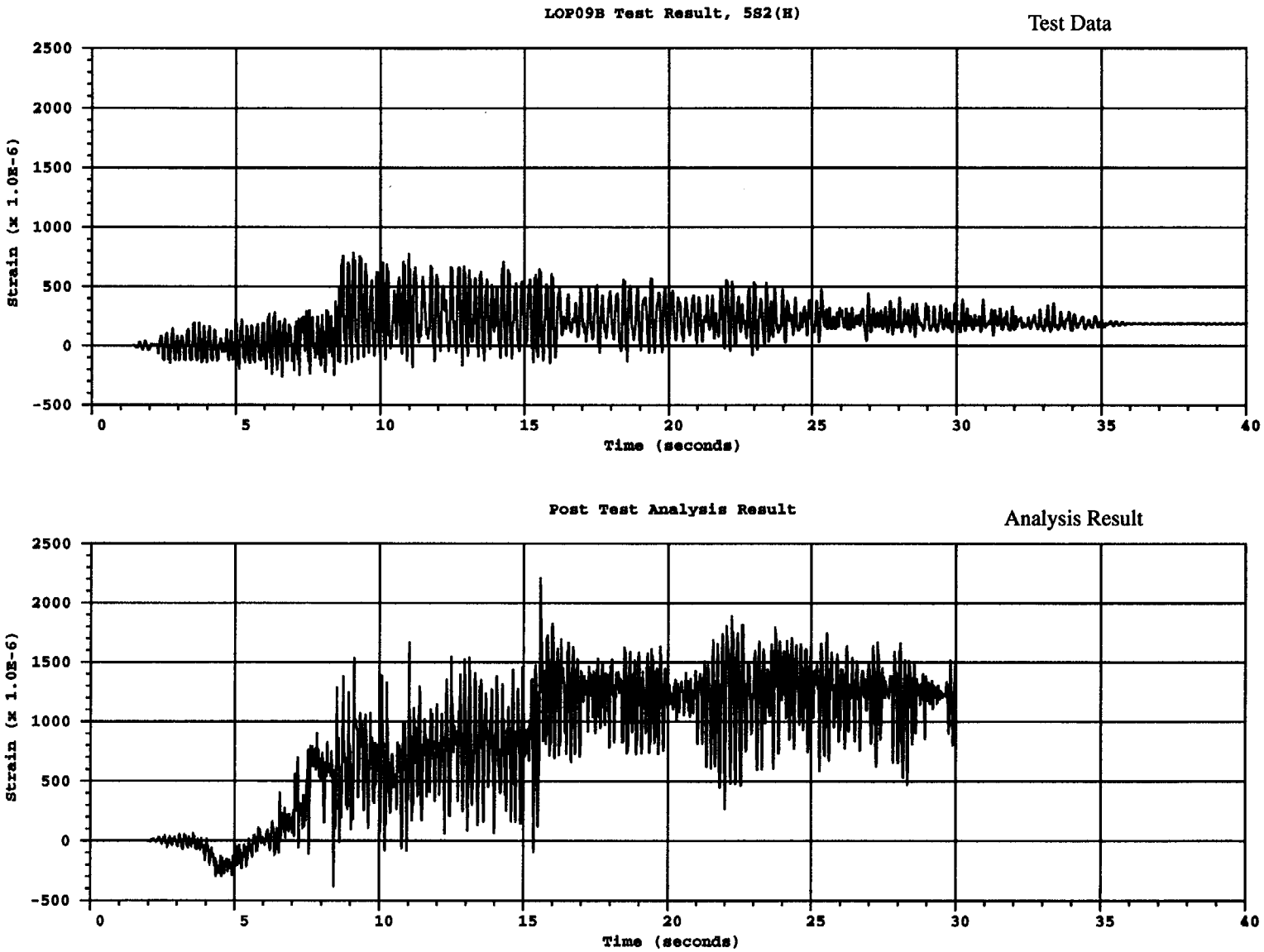

Figure B.94 Comparison of vertical liner strain at LOP09B for 5S2(H) test

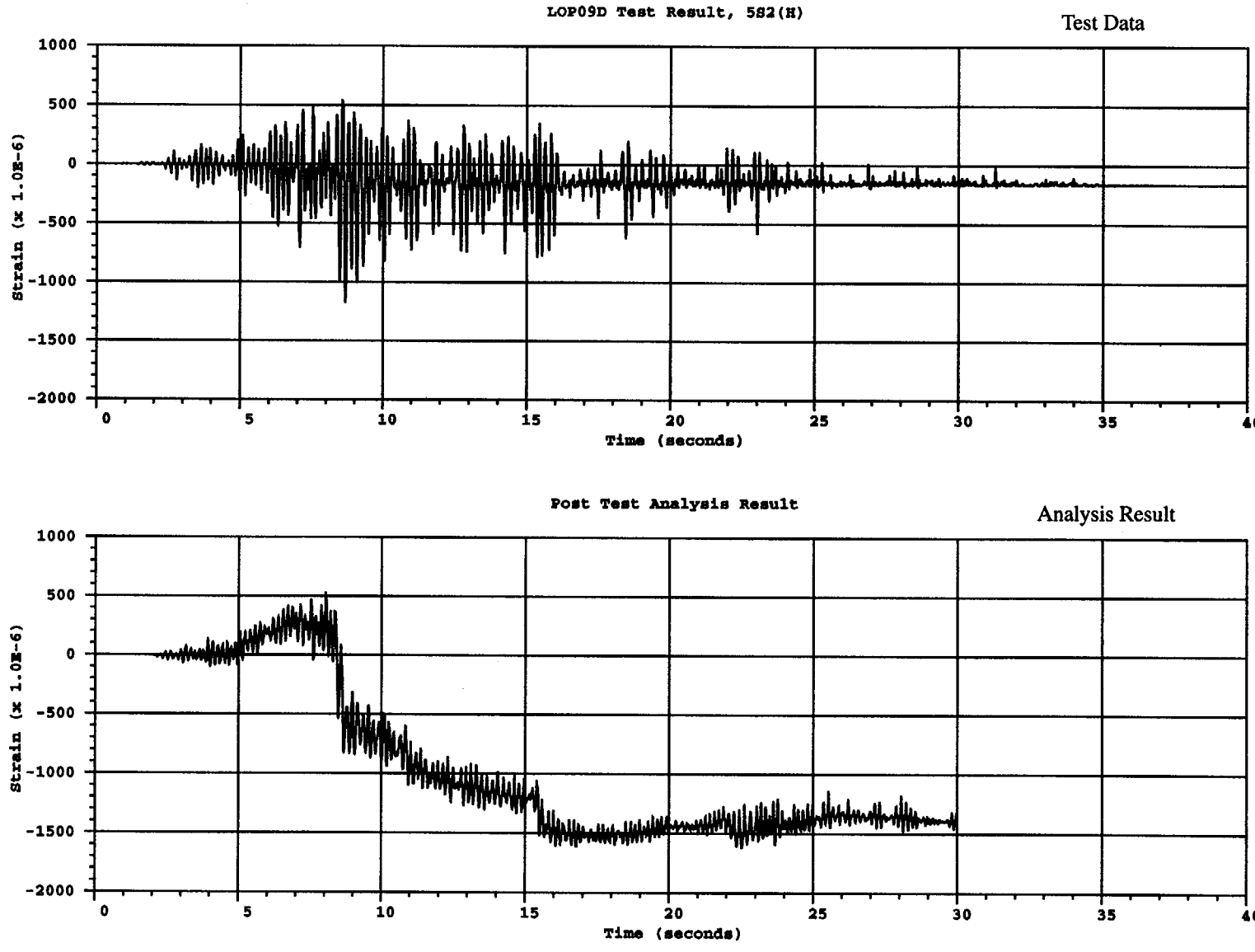

Figure B.95 Comparison of hoop liner strain at LOP09D for 5S2(H) test

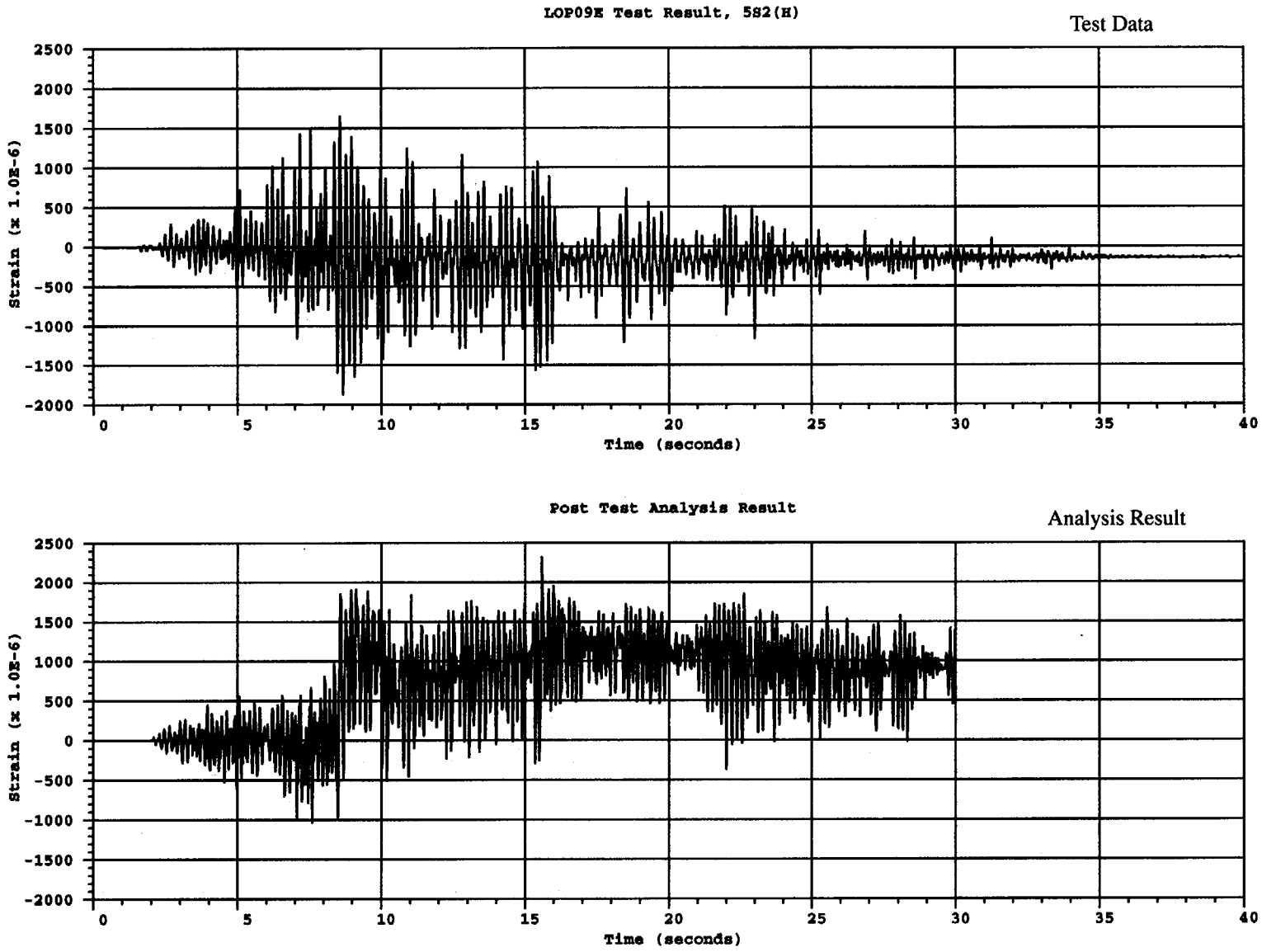

Figure B.96 Comparison of verical liner strain at LOP09E for 5S2(H) test

APPENDIX C

Derivation of the Cycle Dependence of the Reinforced Concrete Constitutive Model

APPENDIX C

Derivation of the Cycle Dependence of the Reinforced Concrete Constitutive Model

The RCCV model testing program brought out an important behavior regime that heretofore has been assumed to be present in reinforced concrete structures but had not been possible to quantify; that is, the dependence of structural response degradation on low-amplitude load cycles typical of design-level earthquake loading. Although abundant cyclic static test data has been generated to describe ductility capacities of flexural members, such data is of little or no value in describing the cyclic degradation of complex concrete structures under low-amplitude vibrations. The RCCV seismic simulation tests illustrated this degradation behavior quite dramatically, as can be observed in Figure C.1. As this figure shows, the first fundamental frequency, which is almost a direct measure of the structure's shear stiffness, decreased with each test, with the largest drop, 2.75 Hz., seen in the first dynamic test designated as 1.3S1(H). Even the preceding pressure test, which normally produces different crack patterns than a horizontal-shaking test, caused a frequency drop of about 1.5 Hz. The 1.3 factor means that the applied motion, which was intended to be the horizontal component of the S1 target input, exceeded the intended target by 30%. Moreover, as discussed in Section 4 of the report, the interaction between the shake table and the RCCV structure produced vertical and rocking acceleration components that are of nearly equal magnitude to the controlled horizontal component. Following the first dynamic test, the stiffness degradation depicted in Figure B.1 exhibits a dependence on the number of dynamic tests regardless of the type of motion applied. After the eighth dynamic test, the frequency degradation rate slows down, although the amplitude of the motion rises above the design level. For example, the frequency drops by 3 Hz., from 9.5 Hz. to 6.5 Hz., between the 1.3S1(H) test and the 2S2(H) test, but only by 1.5 Hz for all subsequent beyond-design-basis tests including the 5S2(H) test. This behavior indicates a strong nonlinear dependence on the number of cycles, as can be discerned from the repeated similar-amplitude tests. The dramatic drop in frequency after the failure test 9S2(H) is clearly due to the complete failure of the model.

In order to translate this global response to a material constitutive behavior at the local material point level, cycle dependent degradation was introduced in the following properties, namely, the shear moduli at a crack surface and the compression modulus of a closed crack. The same degradation expression was used for these two properties as shown below.

The cycle-dependent degradation factor at an element integration point with a pre-determined crack is given by,

$$F(N) = 1 + .9(N/400)^2(N/200 - 3), \qquad (1)$$

where N stands for the cumulative number of crack open-close cycles and $0 \le N \le 400$. As can be deduced from the above expression, the degradation factor is normalized to unity for zero cycles, and gives a value of 0.1 at 400 cycles. For N greater than 400 cycles, the factor remains constant at 0.1.

The change of state of an existing crack from open to close, or visa versa, is counted as a cycle when the following two conditions are satisfied simultaneously:

(a) The strain normal to the crack surface changes sign during the cycle, and
(b) The magnitude of the change in the strain during the cycle exceeds the initial cracking strain for intact material.

This degradation factor is computed at the element integration point and applied to the three constitutive properties discussed above.

The shear response is expressed as follows,

$$G = G_C(\varepsilon, \varepsilon_f) * F(N) \qquad (2)$$

In the above expression, G stands for the instantaneous value of the shear modulus along the crack plane, Gc is the crack history-dependent shear modulus, which is a function of the crack-opening strain ε and fracture strain ε_f.

Similarly, the cyclic degradation of the concrete's compression modulus is expressed as

$$E = E_C(\sigma, \varepsilon) * F(N), \qquad (3)$$

where E_C stands for the instantaneous compression modulus normal to the surface of a closed crack, and

is dependent on the current stress state and the material's prior stress-strain history at the element integration point.

The local damping ratio is treated in similar way, but with a cycle-dependent enhancement factor rather than a degradation factor, as follows,

$$\lambda = \lambda_C(s, n_C) + 0.02 * (N/200)^2 \qquad (4)$$

In the above expression, λ stands for the instantaneous damping ratio, $\lambda_C(s, n_C)$ is the cracking-dependent damping ratio, with s and n_C standing for, respectively, the crack status (open or closed) and the number (1, 2 or 3) of pre-determined cracks at the integration point. As seen in eq.(4), the second term in the equation adds a maximum value of 2% after 200 cycles to the user-input cracking-consistent damping value. As a protection against excessive damping, ANACAP-U software limits the cycle-dependent added damping to a maximum of 3%. It should be noted also that local damping at the integration point is assigned different values depending upon how the crack changes status from open to closed and visa versa. Eq.(4) is first calculated without regard to the crack status and then applied in full if a previously closed crack remains closed. However, if the crack changes status between the previous and the current step, eq.(4) value is averaged with the user-input minimum damping value. This minimum damping value is also applied to a previously open crack that remains open in the current step, as well as to an intact material point with no prior cracking history.

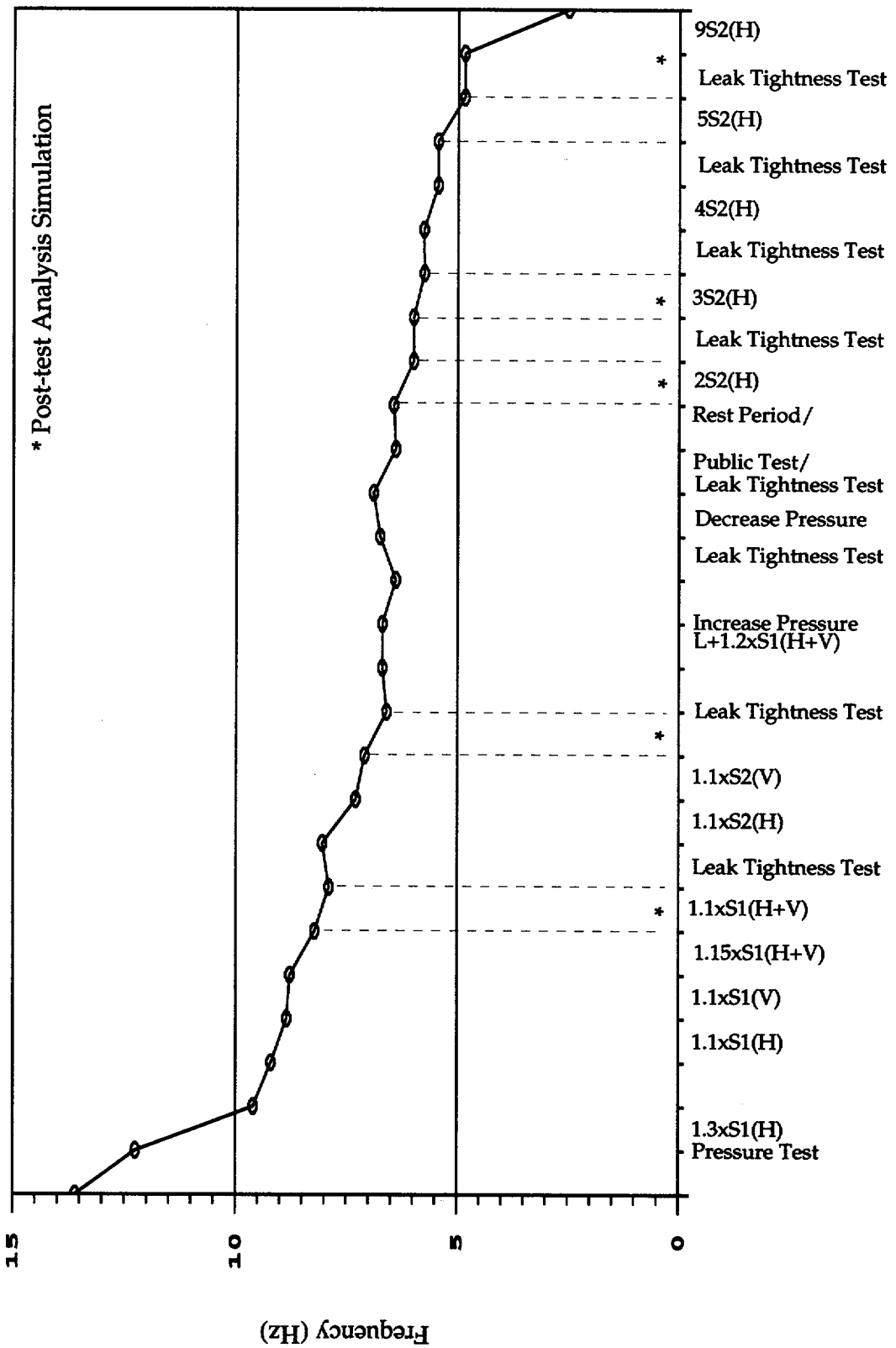

Figure C.1 Frequency shift of fundamental mode during test sequence

NRC FORM 335 (2-89) NRCM 1102, 3201, 3202

U.S. NUCLEAR REGULATORY COMMISSION

BIBLIOGRAPHIC DATA SHEET

(See instructions on the reverse)

1. REPORT NUMBER (Assigned by NRC, Add Vol., Supp., Rev., and Addendum Numbers, if any)
NUREG/CR-6707
SAND 2001/0022P

2. TITLE AND SUBTITLE

Seismic Analysis of a Reinforced Concrete Containment Vessel Model

3. DATE REPORT PUBLISHED

MONTH	YEAR
March	2001

4. FIN OR GRANT NUMBER

W6251

5. AUTHOR(S)

Jeffery L. Cherry/Sandia National Laboratories
R. J. James/ANATECH Corporation
L. Zhang/ANATECH Corporation
Y. R. Rashid/ANATECH Corporation

6. TYPE OF REPORT

Technical

7. PERIOD COVERED *(inclusive Dates)*

8. PERFORMING ORGANIZATION – NAME AND ADDRESS *(If NRC, provide Division, Office or Region, U.S. Nuclear Regulatory Commission, and mailing address; if contractor, provide name and mailing address.)*

Sandia National Laboratories
P. O. Box 5800, MS-0744
Albuquerque, NM 87185-0744

ANATECH Corporation
5435 Oberlin Drive
San Diego, CA 92121 (sub-contractor)

9. SPONSORING ORGANIZATION – NAME AND ADDRESS *(If NRC, type "Same as above", if contractor, provide NRC Division, Office or Region, U.S. Nuclear Regulatory Commission, and mailing address.)*

Division of Engineering Technology
Office of Nuclear Regulatory Research
U. S. Nuclear Regulatory Commission
Washington, D.C. 20555-0001

10. SUPPLEMENTARY NOTES

Dr. Andrew J. Murphy, NRC Project Manager

11. ABSTRACT *(200 words or less)*

A 1:8 scale RCCV model was constructed by NUPEC and subjected to seismic simulation tests using the high-performance shaking table at the Tadotsu Engineering Laboratory. A series of tests representing design-level seismic ground motions, followed by a series of tests in which progressively larger base motions were applied, until structural failure was induced. In collaboration with NUPEC, Sandia National Laboratories and ANATECH Corp. conducted three-dimensional finite element dynamic analyses were performed, first as pretest blind-predictions to evaluate the general capabilities of concrete-structures analytical methods, and second as posttest validation of the methods and interpretation of the test results. Because the pretest analyses had, by necessity, to rely on proposed input motions, which differed significantly from the input motions and because of the interaction between the shake table and the structure during the actual tests, the pretest analyses predict only general trends of the damage and failure regimes of the structure.

12. KEY WORDS/DESCRIPTORS *(List words or phrases that will assist researchers in locating the report.)*

Concrete Constitutive Material Model, Damping, Earthquake, Finite Element Analysis, Failure Prediction, Reinforced Concrete Containment Vessel (RCCV), Scaled Model Test, Seismic

13. AVAILABILITY STATEMENT
Unlimited

14. SECURITY CLASSIFICATION
(This Page)
Unclassified
(This Report)
Unclassified

15. NUMBER OF PAGES

16. PRICE

NRC FORM 335 (2-89)

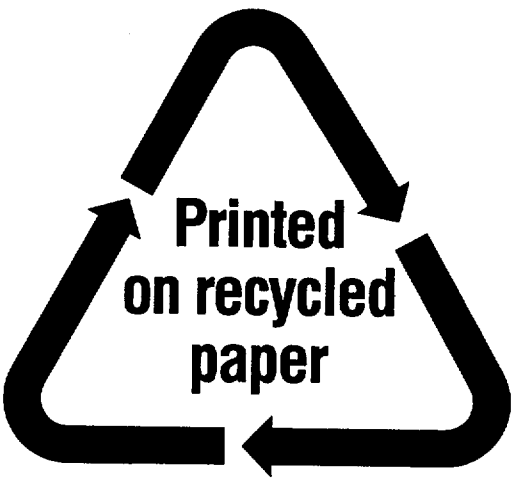

Federal Recycling Program

ISBN 0-16-050775-8

UNITED STATES
NUCLEAR REGULATORY COMMISSION
WASHINGTON, DC 20555-0001